A DUCTILITY AND DISPLACEMENT BASED DESIGN PROCEDURE FOR SEISMIC DESIGN OF REINFORCED CONCRETE FRAMES

by

GEHAD EZ-ELDIN RASHAD

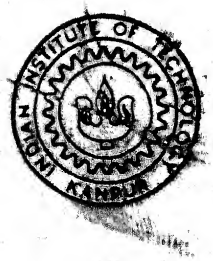

DEPARTMENT OF CIVIL ENGINEERING

INDIAN INSTITUTE OF TECHNOLOGY KANPUR

November, 1993

A DUCTILITY AND DISPLACEMENT BASED DESIGN PROCEDURE FOR SEISMIC DESIGN OF REINFORCED CONCRETE FRAMES

A Thesis Submitted
in Partial Fulfillment of the Requirements
for the Degree of
DOCTOR OF PHILOSOPHY

by

GEHAD EZ-ELDIN RASHAD

to the

DEPARTMENT OF CIVIL ENGINEERING
INDIAN INSTITUTE OF TECHNOLOGY KANPUR

November, 1993

CERTIFICATE

It is certified that the work contained in the thesis entitled "A Ductility and Displacement Based Design Procedure for Seismic Design of Reinforced Concrete Frames" by Gehad Ez-Eldin Rashad, has been carried out under my supervision and that this work has not been submitted elsewhere for a degree.

November, 1993

(Sudhir Kumar Jain)
Associate Professor
Department of Civil Engineering
Indian Institute of Technology
Kanpur

ABSTRACT

A displacement and ductility based design procedure (DDBDP) for reinforced concrete frames has been proposed which explicitly considers strength, stiffness, ductility, and structural configuration. The procedure satisfies the design requirements at two limit states; serviceability limit state (SLS) and ultimate limit state (ULS). To obtain the outer envelope of base shear - roof displacement relationship, a displacement-control non-linear quasi-static analysis has been proposed. The analysis is carried out by imposing a lateral displacement profile on the structure in small increments. The displacement profile is proportional to the first mode shape of the structure, when it is elastic. Under inelastic conditions, the profile is also a function of mode shape of the "yielding" structure at that stage. A computer program has been developed to carry out this quasi-static analysis. The base shear - roof displacement relationship, so obtained is used to assess the suitability of design for stiffness, strength and ductility at the ULS. To account for effect of low initial stiffness modelled by the non-linear analysis procedures on drift requirements at ULS, a correction based on a more realistic linear analysis has been suggested.

A limited parametric study has been conducted to assess the displacement-control quasi-static non-linear procedure with respect to the time-history analysis. The displacement-control quasi-static procedure is seen to give reasonably accurate behaviour and is more consistent than the force-control procedure.

TABLE OF CONTENTS

LIST OF TABLES

LIST OF FIGURES

LIST OF SYMBOLS

Symbols are defined when they first appear in the text. Those symbols which appear frequently are listed below:

A	Peak ground acceleration
A_g	Gross area of concrete section
C_{eu}	Maximum elastic base shear coefficient
C_d	Displacement amplification factor
C_y	Maximum yield strength base shear coefficient
C_w	Code-prescribed unfactored design base shear coefficient
DL	Dead load
E_c	Secant modulus of elasticity of concrete
E_d	Dynamic modulus of elasticity of concrete
EQ	Earthquake load
EQ_x	Earthquake load in x-direction
EQ_y	Earthquake load in y-direction
f'_c	Characteristic strength of concrete cylinder
f_{ck}	Characteristic strength of concrete cube
f_y	Characteristic yield stress of steel
h	Total height of structure
h_x or h_i	Storey height measured from base level
h_{xe}	Height between two adjacent storeys
I	Importance factor
I_{cr}	Moment of inertia of cracked concrete section
I_e	Moment of inertia of concrete section
I_g	Gross moment of inertia of concrete section
I_u	Moment of inertia of the concrete section at ultimate

K	Performance factor
L	Length of a beam or column
LL	Live load
M	Bending moment
M_f	Failure bending moment of a cross section
M_u	Ultimate bending moment of a section
M_y	Yield bending moment of a section
N	Axial force
n	Number of storeys
P - Δ	Geometric non-linearity associated with deformed configuration
P	Maximum linear elastic force at ultimate limit state
P_y	Idealized lateral yield load of the structure
P_s	Lateral load corresponding to first significant yield of the structure
P_w	Unfactored design lateral load
R	Response reduction factor as per NEHRP and ATC codes
R_μ	Ductility reduction factor
R_w	Response reduction factor as per UBC and SEAOC codes
S	Site factor
T	Fundamental time period
T_g	Characteristic period of ground motion
W	Seismic weight of the structure
W_i	Seismic weight of the i^{th} floor
V	Unfactored design base shear force; Peak ground velocity
Z	Zone factor
Δf	Incremental roof displacement
Δp	Incremental lateral load
Δ_{max}	Maximum roof displacement of structure

$\Delta_{max(n.l.)}$ Maximum roof displacement of the structure corresponding to the required displacement ductility (μ_r)

Δ_s Displacement corresponding to the first significant yield of the structure

Δ_w Roof displacement at working load (SLS)

Δ_y Idealized yield roof displacement

δ Curvature ductility of a section

δ_{xe} Elastic floor displacement

Φ Displacement profile along the height of the structure; mode shape

ϕ Curvature at the section

ϕ_d Reinforcement bar diameter

ϕ_f Curvature at the section at failure

ϕ_u Curvature at ultimate strength of the section

ϕ_y Curvature at section at yield of tension steel

μ_r Required displacement ductility

μ_s Structure displacement ductility

$\mu_{s(min)}$ Minimum specified displacement ductility

$\mu_{s(max)}$ Maximum usable displacement ductility

μ_m Maximum storey displacement ductility ratio

Ω Structure overstrength factor

ρ Tension steel ratio

ρ_b Tension steel ratio in a singly-reinforced balanced section

ρ_c Compression steel ratio

θ Rotation at a joint

ξ Viscous damping ratio

LIST OF ABBREVIATIONS

ACI	American Concrete Institute
ATC	Applied Technology Council
BSL	Japan's Building Standard code
COD	Coefficient of Distortion
DDBDP	Ductility and Displacement-Based Design Procedure
DLS	Damageability Limit State
DMRSF	Ductile Moment-Resisting Space Frame
EQRD	Earthquake-Resistant Design
EPP	Elastic-Perfectly Plastic
IS	Indian Standard code
ISD	Inter-Storey Drift
ISD_{max}	maximum Inter-Storey Drift at ULS
ISD_{w}	Inter-Storey Drift at working load (SLS)
MDOF	Multi Degree of Freedom system
MONARCF-DC	MOnotonic Non-Linear Analysis of Reinforced Concrete Frames - Displacement-Control method
MONARCF-FC	MOnotonic Non-Linear Analysis of Reinforced Concrete Frames - Force-Control method
NEHRP	National Earthquake Hazard Reduction Program
NZS	New Zealand Standard code
ODI	Overall Drift Index
OMRSF	Ordinary Moment-Resisting Space Frame
RC	Reinforced concrete
SARCF	Seismic Analysis of Reinforced Concrete Frames
SDOF	Single Degree of Freedom System
SEAOC	Structural Engineers Association of California

SLS	Serviceability Limit State
ULS	Ultimate Limit State
UBC	Uniform Building Code

CHAPTER I
INTRODUCTION

1.1 GENERAL

The earthquake resistant design (EQRD) philosophy expects that in case of a severe, but infrequent, ground shaking a structure may be damaged but should not collapse. In other words, the philosophy relies on the post-yield response of a structure. Ideally, this may mean that a non-linear post-yield analysis of a structure be carried out to ensure adequacy of a design. However, considering numerous uncertainties in design earthquake parameters and in the structural response to a given input motion, and in view of the fact that most civil engineering structures are one-of-a-kind structures, the professional practice consists of designing the structure on the basis of a linear elastic analysis. To account for the post-yield behaviour ("ductility") and the fact that a structure will yield at a much higher force than the design force ("overstrength"), the design force used in the linear elastic analysis is substantially lower than what a structure would experience if it were to sustain a severe ground shaking elastically. In this sense, the present design practice accounts for overstrength and the post-yield behaviour in an implicit manner. The codes endeavour to ensure appropriate post-yield behaviour by imposing requirements on ductile detailing. Therefore, the present design procedures do not account for (a) the enormous variation in the value of overstrength that exists for different buildings, and (b) different ductility demands on different members of a building. In certain buildings these effects may be quite important to consider, in which case non-linear time-history or non-linear quasi-static analysis are usually performed.

In recent years, greater emphasis is being placed on ensuring adequate lateral stiffness in the building structures for a good seismic performance, considering the fact that more flexible structures invariably suffer more damage in case of an earthquake shaking. Suggestions have been made in the literature for adopting a displacement-based design approach (Moehle, 1992a) as an alternative to the present ductility-based design procedures. Also, seismic codes at present are moving towards explicitly considering two levels of design, one level corresponding to a moderate but more frequent shaking and the other level corresponding to severe but infrequent shaking (e.g., Uang, 1993; BSL-1984, Tri-Services Manual, 1986; and draft NZS 4203:1992).

1.2 SCOPE OF THE PRESENT WORK

This thesis presents a procedure for seismic design of reinforced concrete frames which integrates strength, ductility and displacement requirements. The method considers explicitly the overstrength in a structure and it is particularly suitable for buildings with irregular configurations. The procedure considers two limit states, namely serviceability limit state (SLS) for moderate shaking and the ultimate limit state (ULS) for severe shaking. To obtain a realistic base shear - roof displacement relationship of the structure, which is needed for assessing the ductility requirements, a new displacement-control (as against the commonly adopted force-control procedures) non-linear quasi-static monotonic analysis has been proposed. Results from the displacement-control procedure are more realistic than those from the force-control procedures; moreover, the displacement-control procedure is more versatile because it enables one to obtain efficiently the softening part of the base shear - roof displacement relationship.

1.3 THESIS CONTENTS

This thesis has been organized in seven chapters. Chapter II consists of a review of the state-of-the-practice and the state-of-the-art in earthquake-resistant design, followed by a brief discussion on methods used to perform non-linear analysis of reinforced concrete buildings as well as a review of some recent developments in seismic design. In Chapter III, a new Ductility and Displacement-Based Design Procedure (DDBDP) for reinforced concrete frame structures is proposed. In Chapter IV, a displacement-control quasi-static non-linear monotonic analysis is proposed and a computer program, named MONARCF-DC (MOnotonic Non-linear Analysis of Reinforced Concrete Frames - Displacement Control method), has been developed to carry out the proposed analysis. In Chapter V, a parametric study has been carried out on four reinforced concrete frames to compare the non-linear response obtained from the proposed method with that from a time-history analysis. The application of DDBDP is demonstrated through an example in Chapter VI. Finally, a brief summary and conclusions are presented in Chapter VII.

CHAPTER II

LITERATURE REVIEW ON EARTHQUAKE-RESISTANT DESIGN PROCEDURES FOR MULTI-STOREY REINFORCED CONCRETE FRAMES

2.1 INTRODUCTION

The objective of earthquake resistant design is that a structure should be able to: (1) resist minor levels of earthquake ground motion without damage; (2) resist moderate levels of earthquake ground motion without structural damage, but possibly with some non-structural damage; and (3) resist major levels of earthquake ground motion having an intensity equal to the strongest either experienced or forecast at the building site, without collapse, but possibly with some structural as well as non-structural damage. The design seismic codes satisfy the first two requirements by (a) specifying design seismic force which corresponds to service or moderate level of earthquake shaking; (b) limiting the maximum stresses or internal forces in the members; and (c) limiting the storey drift ratio. The third requirement is fulfilled implicitly by ensuring sufficient strength and ductility.

In earlier years, seismic codes specified the seismic design force directly (e.g., UBC-1985, IS:1893-1984, etc.). In recent years, many codes obtain seismic design base shear force by dividing the maximum elastic shear force corresponding to severe ground shaking by a response reduction factor (R). For example, for regular buildings, the design seismic base shear, given in the American codes, ATC 3-06 (1978), UBC-1991, and NEHRP-1991, is evaluated as: $V = C_s W = (C_{eu}/R) W$, where C_s is defined as the design seismic coefficient; W is the weight of the effective reactive mass, C_{eu} is the seismic coefficient equivalent to a

linear elastic design response spectrum for severe shaking, and R is the response reduction factor. The factor R takes into account the reductions in member force levels owing to inelastic deformation capacity (i.e., ductility), to increased damping due to structural damage and soil-foundation response, and to the fact that actual structural strength commonly exceeds that specified in design (i.e., overstrength). Seismic codes expect elastic design with appropriate factors of safety for different combinations of gravity and seismic loads.

The codes provide restrictions on the storey drifts at the specified design load using elastic analysis, while some codes also specify limits on the maximum storey drifts and inter-storey drift (ISD) at the ultimate condition. Finally, seismic codes provide a number of design and detailing requirements regarding member size, grade of concrete, grade of steel, shear reinforcement, beam and column size, etc., with the objective that the structure behaves appropriately in the inelastic range.

Nonetheless, there remain many uncertainties in the seismic design procedure, such as:

1) The codes prescribe the value of response reduction factor (R) as independent of the structure time period (T), the structure overstrength (Ω), and of the structure ductility (μ_s). The fact is that the seismic reduction factor depends directly on T, Ω, and μ_s. Also, the value of overstrength differs from one RC structure to another depending on the overall structure configuration and seismic zone.
2) There is uncertainty that the code-prescribed seismic detailing requirements always ensure adequate inelastic deformation capacity.

3) The actual storey drifts and inter-storey drifts may be quite different from those obtained from analysis. There are many uncertainties regarding the estimation of the elastic stiffness of RC structures due to occurrence of cracks in members, deformation of the foundation, and effects of the non-structural components, etc. (Bertero et al., 1991).

4) Different members of the structure may require different level of ductility, but seismic codes provide same detailing rules for all members which may result in an overall structural ductility less than the anticipated.

This chapter consists of a review of the state-of-the-practice and the state-of-the-art in EQRD, beginning with definition of the seismic reduction factor and how to evaluate it, review on displacement ductility, and evaluation of maximum displacement and drift limits given by seismic codes and by different researchers. This is followed by a brief discussion on methods used to perform non-linear analysis in reinforced concrete buildings and a review of the problems in estimating the initial lateral stiffness. Finally, a review is presented on the recent developments in seismic design approach suggested by many researchers.

2.2 RESPONSE REDUCTION FACTOR

If under a severe earthquake the structure has to remain elastic, it must be designed to sustain large seismic forces, which leads to an expensive and uneconomical design. A ductile structure is able to absorb and dissipate a high amount of energy through hysteresis loops and this reduces the response (i.e., lateral seismic force) of the structure. Based on this fact, the structures are designed for a much less seismic

force than what would be otherwise required. The design base shear is usually established by reducing the elastic base shear demand by a response reduction factor (R) which primarily consists of two factors. One factor is to reduce the elastic demand force to the level of maximum yield strength of the structure; this reduction basically depends on ductility of the structure and hence on its energy dissipation capacity. This factor is called the ductility reduction factor (R_μ). The other factor, called overstrength (Ω), is due to the overstrength inherently introduced in the code-designed structures and is defined as ratio of the maximum lateral strength of the structure and the code prescribed unfactored design base shear force. Hence,

$$R = R_\mu \times \Omega \qquad (2.1)$$

The ductility reduction factor (R_μ) is strongly related to the overall structure ductility (μ_s), time period of the structure (T), ground motion characteristics, etc. (Newmark and Hall, 1973; Briseghella and Zaccaria, 1982; Riddell et al., 1989; and Miranda, 1992). On the other hand, the overstrength factor (Ω) depends on code design procedures for RC structures, seismic zone, structural configuration, number of storeys, and design gravity loads (Zhu et al, 1992; Navin and Jain, 1993).

Fig. 2.1 shows global structural response of a building in terms of base-shear versus roof-displacement relationship, which is idealized by the linearly elastic - perfectly plastic curve. Also shown is the response of the building, if it remains elastic during such a shaking. The maximum base shear that develops in the structure, if it were to remain elastic, is C_{eu} W; where W is total weight of the building. During nonlinear response, the maximum roof displacement of the

structure is Δ_{max}. If the idealized yield roof displacement is Δ_y, then the global ductility demand (μ_s) imposed on the structure can be defined as

$$\mu_s = \frac{\Delta_{max}}{\Delta_y} \qquad (2.2)$$

Seismic design codes express R in different forms. The ATC 3-06 (1978) and NEHRP-1991 use R to reduce the maximum elastic seismic force to the strength design force level ($P_s = C_s W$) (i.e., level of first significant yield); the suggested value of R ranges from 8 for RC-DMRSF (Reinforced Concrete Ductile Moment-Resistance Space Frames) to 2 for RC-OMRSF (Reinforced Concrete Ordinary Moment-Resistance Space Frames). On the other hand, UBC-1991 and SEAOC-1990 have used a force reduction factor (R_w) to reduce the maximum expected seismic force to unfactored design force level (P_w), and its range is from 12 for RC-DMRSF to 5 for RC-OMRSF. UBC-1985 used another factor (K) to consider the effect of structure ductility on energy absorption. The factor K is a multiplier in the base shear equation, and its range is from 0.67 for RC-DMRSF to 1.33 for RC-OMRSF. The value of R_w (in UBC-1991) is roughly related to K (in UBC-1985) as $R_w = 8/K$ (Allan, 1989). The Indian seismic code (IS:1893-1984) uses a performance factor (K) similar to that given by UBC-1985 and it varies from 1.0 for ductile reinforced concrete frame to 1.6 for ordinary frames. The values of R and R_w expressed in codes were set by a combination of experience, judgment, historical precedent, and committee consensus (Allan, 1989). In most of the codes, the value of R, R_w or K is given without explicit consideration to time period of the structure (T), structure ductility (μ_s), and the structure overstrength (Ω).

2.2.1 DUCTILITY REDUCTION FACTOR, R_μ

The ductility reduction factor, R_μ, reduces the elastic force demand to the yield strength level of the structure, and hence, it may be expressed as

$$R_\mu = \frac{C_{eu}\ W}{C_y\ W} = \frac{C_{eu}}{C_y} \qquad (2.3)$$

This factor takes advantage of the energy dissipating capacity of properly-designed and well-detailed structures and hence primarily depends on ductility (μ_s) of the structure.

The first attempt to relate R_μ with μ_s was made by Newmark and Hall (1973, 1982) for single degree of freedom (SDOF) systems with elasto-perfectly plastic (EPP) resistance curve. Based on analytical studies, they concluded that:

- In structures of natural period less than 0.1 sec, the ductility does not help in reducing the response. Hence, for such structures, no ductility reduction factor should be used.
- For moderate period structures, corresponding to acceleration region of elastic response spectrum (T = 0.1 to 0.5 sec), the energy absorbed by an inelastic structure at its maximum displacement approximates that absorbed by an elastic system. This results in the ductility reduction factor as (Fig. 2.2a)

$$R_\mu = (2\mu_s - 1)^{1/2} \qquad (2.4)$$

- For relatively long period structures, corresponding to velocity region (T = 0.5 to 3 sec) and displacement region (T = 3 to 10 sec) of elastic response spectrum, the maximum displacement of elastic and inelastic systems is nearly equal. This gives the value of ductility reduction factor as (Fig. 2.2b)

$$R_{\mu} = \mu_s \tag{2.5}$$

Riddell and Newmark (1979, 1980) conducted a statistical analysis of the response of SDOF systems with elasto-plastic, bilinear, and stiffness degrading resistance curves and obtained empirical formulae for R_{μ} depending on ductility ratio (μ_s) and viscous damping ratio (ζ) for different period ranges. Mahin and Bertero (1981) have computed inelastic response of EPP SDOF systems subjected to 10 recorded ground motions and evaluated the reliability of equations suggested by Newmark and Hall. The results indicate that the inelastic response is particularly sensitive to the actual excitation input as well as to the dynamic and mechanical characteristics of the structure. Murakami and Penzien (1977) carried out non-deterministic response analysis on five SDOF structural models representing RC buildings in which stochastic models were used to represent the expected ground motions. Briseghella et al. (1982) have proposed a relation between structure's ductility and R_{μ} as a function of period based on a study of SDOF systems using artificial time histories compatible with the power spectral density of a recorded motion during the 1976 Friuli earthquake. Lai and Biggs (1980) have investigated the sources of variability of inelastic response spectra, i.e., strong motion duration, ductility ratio, and viscous damping ratio. Pal et al. (1987) have developed yield displacement spectra, constant strength spectra, constant displacement spectra, reduction factor spectra, inelastic acceleration spectra, and inelastic yield displacement spectra for three artificial and two actual earthquake time-histories using different hysteretic models. Miyama et al. (1988) have calculated the inelastic response of SDOF systems by applying artificial earthquake ground motions of which the target spectrum is elastic response spectrum. They have expressed R_{μ} factor as

function of ductility factor, natural frequency of system, and shape of the elastic response spectra. Riddell and Vásquez (1988) have evaluated the dynamic response of SDOF systems subjected to ground motion records during the 1985 Chile earthquake to compare with available recommendations for deriving inelastic response spectrum. Riddell et al. (1989) studied non-linear behaviour of SDOF system, particularly for short period range, using 53 ground motion records, and concluded that reduction factor tends to a value very close to unity for very small periods and to a constant value larger than 1 for periods over 0.4 sec. The idealized bilinear relation between R_μ and T for different values of ductility is shown in Fig. 2.3. Miranda (1992) has reported a statistical study on SDOF systems using 124 ground motion records from different types of site. The study shows that local site conditions significantly affect the ductility reduction factor. Based on an analytical study with recorded and generated soft soil motion, Krawinkler and Rahnama (1992) have shown that ground motion can be significantly amplified in soft soils and thus the strength demand, for which structures have to be designed, is amplified accordingly. Palazzo and Siano (1992) have shown that the reduction factor is influenced significantly by geometrical degrading phenomenon ($P - \Delta$ effect) also.

The above studies were based on SDOF systems. Since most structures are more appropriately multi-degree-of-freedom (MDOF) systems, the application of above formulae to real building structures may be questionable and has been criticized for long (Anagnostopoulous et al., 1978; Lin and Mahin, 1985, etc.). Takada et al. (1988) have established a relation between ductility reduction factor (R_μ) and ductility demand (μ_s) for a MDOF shear-type stick system by means of Monte Carlo simulation techniques. Hwang and Jaw (1989) have statistically evaluated

R_μ factor for MDOF RC structures represented by a stick model. Twelve structural models and ninety synthetic earthquake motions representing different soil conditions were used. They concluded that the R_μ factor depends on structural period (T), dominant period of earthquake motion (T_g) (which depends on the soil conditions), viscous damping ratio (ζ), and maximum storey ductility ratio (μ_m). The design equation suggested by Hwang and Jaw (1989), based on median R_μ value, is given as

$$R_\mu = \left[e^{-0.1857T/T_g} - e^{-2.1673T/T_g} - 0.0276\,\zeta \right] \ln \mu_m \qquad (2.6)$$

Anagnostopoulous and Nikolaou (1992) have investigated the relationship between R_μ and ductility demand depending on natural period of the structure for SDOF systems and for frames designed in accordance with the Uniform Building Code (UBC) provisions. The structural systems were subjected to 10 synthetic accelerograms compatible with UBC design spectrum and 5 historical accelerograms. It was shown that R_μ factor for SDOF systems depends heavily on time period of the structure in the low period range. This dependence becomes weaker for frame structures and disappears completely in the medium and high period ranges.

2.2.2 OVERSTRENGTH

The other component of response reduction factor, called overstrength factor (Ω), is due to the reserve strength that exists between the code-prescribed working load used in design and the maximum lateral strength of the structure. In Fig. 2.1, C_y is the base shear coefficient corresponding to actual yielding of the structure and C_w is the code prescribed unfactored design base shear coefficient. Thus, the total overstrength factor (Ω) may be defined as

$$\Omega = \frac{C_y}{C_w} \tag{2.7}$$

In this study while defining Ω, C_w is taken at the level of unfactored design base shear force. This is because the earthquake force is used in conjunction with gravity load for design specifications and different load factors on earthquake force are used for different load combinations. For example, the ACI-318 (1989) prescribes the load combinations as (1.4 DL + 1.7 LL), (1.05 DL + 1.28 LL ± 1.4 EQ), (0.9 DL ± 1.43 EQ), while the Indian code (IS:456-1978) prescribes the load combinations as 1.5(DL+LL), 1.2(DL+LL+EQ), 1.5(DL+EQ), and (0.9 DL + 1.5 EQ), where DL, LL and EQ are dead, live, and earthquake loads, respectively. On the other hand, the NEHRP-1991 recommended provisions use a strength design approach in which load factor on earthquake load is unity. Hence, the calculated overstrength (Ω) of buildings designed according to NEHRP provisions may appear to have less overstrength compared to buildings designed according to the UBC code.

The inertia force due to earthquake motion at which the first 'significant' yield in the structure starts may be much higher than the prescribed unfactored base shear force. The main reasons being:

(a) A load factor is applied to the code-prescribed design seismic force while designing the structure.

(b) Further, during the actual seismic event, the building has much lower gravity loads than the factored gravity load used in design; this adds to the overstrength for lateral load.

(c) Strength reduction factors on material properties also result in overstrength. Furthermore, the actual strength of materials may be higher than the specified strength. This is particularly true for concrete.

(d) Sometimes, choice of any particular member size is from stability or architectural consideration rather than strength requirements. Also, there are requirements on minimum member sizes and amount of reinforcement.

(e) There is discrete choice in the amount of reinforcement and therefore more reinforcement than required is sometimes provided.

(f) The special ductility requirements specified in design codes may add to overstrength (e.g., the strong column-weak girder provision, the requirement that the area of bottom reinforcement be at least equal to half that of the top reinforcement at beam ends, etc.).

Even after the first 'significant' yield in the structure, after which stiffness of the structure decreases, the structure can take further load due to the following:

(a) Once a member reaches yield, redundancy in structure allows redistribution of internal forces and moments. By this, a local overstress at a member can be passed on to other members resulting in absorption of energy and hence overall yield of the structure may be reached at a load much higher than that at which the first member yielded.

(b) Due to strain hardening of reinforcing steel, the ultimate moment capacity of sections is significantly higher than the yield moment. This will result in overstrength, which is particularly true for under-reinforced beams.

(c) Confinement of concrete also increases the ultimate moment capacity of reinforced concrete sections.

Some other factors, contribution of which is not always evident from analytical studies, give considerable overstrength to the structure. These include:

(a) Materials generally have a higher strength under cyclic conditions over the static conditions.

(b) Non-structural elements and non-seismic structural elements, for example masonry infill walls, partitions, stairways, etc., can take a part of the seismic load.

(c) Due to contribution of floor slab, which acts as a tension flange, the negative moment strength of beams increases significantly.

(d) Common analysis assumptions may neglect secondary stiffening and strengthening effects associated with three-dimensional action (e.g., Bertero et al., 1991).

The importance of overstrength in the survival of buildings during a severe earthquake has been realized for long. Blume (1977) has discussed a number of factors that contribute to overstrength during a severe ground motion. Bertero et al. (1986, 1991) have discussed the fact that the survival of code-designed structures in the event of significantly higher seismic shaking is possible only because of implicitly assumed overstrength. Many experimental studies have demonstrated the role of overstrength in a building surviving severe ground shaking (e.g., Bertero et al., 1984; Uang and Bertero, 1986; Whittaker et al., 1987; Foutch et al., 1987; Whittaker et al., 1989; Bonelli and Tobar, 1992). Shahrooz and Moehle (1990) have made an interesting experimental evaluation of contribution of different sources of overstrength on 1/4 scale model of a six-storey concrete frame structure designed according to UBC and ACI codes. It was shown that the structure designed for the unfactored base shear coefficient of 0.092 could theoretically resist 7.65 times as much.

Miranda and Bertero (1989) have evaluated the performance of low-rise buildings in Mexico City using static and time-history analyses

and noted a high value of overstrength. The base shear versus roof displacement relationship for a four-storey building subjected to monotonically increasing triangular lateral load pattern, without slab contribution, with slab contribution, and with masonry distribution is shown in Fig. 2.4. The overstrength is in the range of 2 to 5, and is significantly higher if slab contribution and masonry distribution are taken into consideration.

Dynamic analysis results by Cassis and Bonelli (1992) on wall, dual wall-frame, and frame systems for three different earthquake records indicated an overstrength value of 3 to 5. It was noted that the frame systems generally have a higher value of overstrength than wall systems. Meli (1992) has shown that the available overstrength varies widely depending on redundancy of structure. It also depends on characteristics of ground motion, viz., higher overstrength is reported if the structure is subjected to a short duration motion with high dominant frequencies and this overstrength is largely impaired with large duration motions with long periods. Assaf (1989) (reported by Uang, 1991) has evaluated the variation of overstrength factor for a typical interior frame of a 1-bay, 3-bay, and 5-bay steel building with 4, 8, and 12 storeys located in a region of high seismic risk using inelastic dynamic analysis.

Zhu et al. (1992), besides noting that the low-rise R.C. frame buildings have a higher overstrength, also demonstrated that a building designed for a lower seismic force with same gravity loading has, in general, a higher value of overstrength since in this case effect of gravity loads in design becomes predominant. The base shear versus roof displacement relationships obtained by them for a 4-storey frame in low, intermediate, and high A/V seismic regions (A: peak ground acceleration, V: peak ground velocity), designated as M4SL, M4SI, and M4SH,

respectively, are shown in Fig. 2.5. It was observed that for 0.1% overall drift, the lateral strength of 4-storey frame in high A/V seismic region is 22% and 42% higher than that of similar frames in intermediate and low A/V regions. The corresponding differences in the seismic design forces are 41% and 100%, respectively. Therefore, the presence of gravity loads in the design tends to reduce the actual difference in strength among these frames.

Navin and Jain (1993) have assessed the seismic overstrength of RC frames by means of non-linear pseudo-static analysis on 4-bay, 3-, 6-, and 9-storey frames designed for seismic zones I to V as per Indian codes. It is seen that the overstrength strongly varies with the seismic zone. The average overstrength of frames in zones V and I was found as 2.84 and 12.7, respectively. The overstrength increases as the number of stories decreases; Ω for the 3-storey frame is higher than that for 9-storey frame by 36% in zone V and by 49% in zone I. Further, overstrength also varies with design gravity load; interior frames have 17% (zone V) to 47% (zone I) higher overstrength as compared to exterior frames of the same building.

2.3 DUCTILITY

The displacement ductility of a structure is defined as ratio of the maximum overall structure displacement (Δ_{max}) to the displacement at the yield point of the structure (Δ_y). Many definitions have been used by researchers to determine Δ_y; these are illustrated in Fig. 2.6 (reported by Park, 1988). These include (a) the displacement when yielding first occurs, (b) the yield displacement of the equivalent elasto-plastic system with the same elastic stiffness and ultimate load as the real system, (c) the yield displacement of the equivalent

elasto-plastic system with the same energy absorption as the real system (Mahin and Bertero, 1976), and (d) the yield displacement of the equivalent elasto-plastic system with reduced stiffness found as the secant stiffness at 75% of the ultimate lateral load of the real system (Priestly and Park, 1987). Δ_{max} has also been defined using various assumptions by researchers (Park, 1988); these are (Fig. 2.7) (a) the displacement corresponding to the peak of the load-displacement relation, and (b) the maximum displacement that the structure may undergo.

The overall structure displacement is usually represented by the roof displacement. Fig. 2.8 shows the cyclic response of a reinforced concrete frame to progressively increasing load cycles. As seen in the figure, the structure possesses some amount of stiffness even after yielding occurs. Beyond the maximum load capacity (P_{max}), the structure looses strength gradually, i.e., it can undergo additional deformation but at reduced load. The additional amount of load capacity, beyond the yield point, in reinforced concrete frames is low. Structures provided with shear walls show capability to sustain high additional load beyond the yield point (Fig. 2.9-a). This is because even when shear wall reaches its flexural yield limits, it can still resist additional lateral load by its shear strength (Midorikawa and Kitagawa, 1984). Although the displacement ductility depends upon the plastic deformability (capability of the structure to deform before rupture), a structure may have significantly greater deformability than another, although its ductility may be smaller. For example, Fig. 2.9-b shows the lateral response of a very flexible RC-DMRSF versus a stiff but very ductile shear wall (Bertero et al., 1991). Though the RC-DMRSF has a higher deformability than the shear wall, its ductility is smaller than

the shear wall ductility.

In a structure which is responding inelastically to earthquake excitation, plastic hinges are formed at critically stressed sections of beams and columns. Hence, these sections must also have adequate ductility. A measure of the ductility of a section, i.e., member ductility, subjected to flexure or combined flexure and axial load is the curvature ductility, which is defined as the ratio of ultimate curvature (ϕ_u) attainable without significant loss of strength, to the curvature corresponding to first yield of the tension reinforcement (ϕ_y). Curvature ductility increases with an increase in compression steel content, concrete compressive strength, and crushing strain of concrete. It decreases with an increase in tension steel content, yield strength of steel, and axial load on the member. Among these factors, the axial load and percentage of tension steel have the maximum influence on curvature ductility. Most building codes impose limits on the maximum tension reinforcement in reinforced concrete flexural members. Confinement of the concrete by closely-spaced hoops significantly increases the ultimate strain in concrete as compared to that for the unconfined concrete. Hence, confinement is an important factor for improvement of the curvature ductility. For instance, consider a section with high yield strength deformed (HYSD) steel with yield stress (f_y) of 415 MPa and concrete with cube strength (f_{ck}) of 28 MPa (f'_c = 3000 psi). Assume the section as a doubly reinforced section with ρ_c/ρ = 0.5 (ρ_c is the ratio of compression steel; and ρ is the ratio of tension steel), and the section is provided with a tension steel equal to 1.0%. If the section is assumed unconfined, the ductility is about 8; with a confinement ratio of 0.5%, 0.75%, and 1.0%, the ductility increases to about 17, 21, and 25, respectively (Rashad and

Jain, 1991), as shown in Fig. 2.10.

Seismic design codes do not explicitly specify the ductility to be provided to RC flexure members. However, specifications are given for detailing of members which endeavour to provide them with adequate ductility. For instance, the ACI specifications in this regard are: (a) the tension steel ratio (ρ) in a singly-reinforced RC section must not exceed 0.75 ρ_b, where ρ_b is the tension steel ratio in a singly-reinforced balanced section; (b) in a doubly reinforced section, the ratio ($\rho - \rho_c$) must not exceed 0.75 ρ_b; (c) for flexural members of frames in highly seismic regions, the tension steel ratio on any face, at any section, shall not exceed 0.025; and (d) the positive moment strength shall not be less than one-half of the negative moment strength provided at that joint face (i.e., $\rho_c/\rho \geq 0.5$). In addition, there are requirements for confinement and shear by specifying the minimum amount of hoops near the joints. The formation of plastic hinges involves large rotations in the members. If the failure of a member in diagonal shear is avoided before formation of plastic hinges, the member will be able to develop full curvature and will behave in a ductile manner.

Plastic hinges are desired at beam ends rather than at column ends because (a) yielding in beam elements does not cause large and undesirable structure deformation and hence the required ductility of beam section is lower and can be easily provided (Park and Paulay, 1975); (b) simultaneous yielding at all beam ends can dissipate substantial hysteretic energy (Park and Paulay, 1975; Otani et al., 1992); and (c) axial load, resulting during the hysteretic behaviour, may reduce ductility of columns. On the other hand, yielding at column ends may lead to a partial yield mechanism, and a significant damage in columns may lead to the collapse (Otani et al., 1992).

Ductility of the structure depends on ductility of the individual members. Priestly and Park (1987), and Moehle (1992a) have established simple relationships between the maximum displacement and the corresponding curvature ductility for a SDOF system (a reinforced concrete bridge pier), but in case of multi-storey structures, there is no explicit way to correlate the two. Typical values of the displacement ductility factor (μ_s) for reinforced concrete ductile structures range from 3 to 5 (SEAOC-1973), 4 to 6 (Fintel, 1973), and 3 to 6 (draft NZS 4203:1992 (IAEE, 1992)). Park and Paulay (1975) recommend that sections at plastic hinges in beams and column bases should be capable of reaching curvature ductility factors of at least four times the required displacement ductility factor (i.e., $\phi_u/\phi_y \geq 4\ \mu_s$). However, reinforced concrete flexural members are sometimes designed for curvature ductility of 5, assuming concrete as unconfined (Park and Paulay, 1975). Confined concrete has a higher value of crushing strain which increases curvature ductility significantly. Since concrete is always confined with transverse reinforcement near the column face where the plastic hinge forms, the actual curvature ductility will be significantly greater than that calculated assuming the concrete as unconfined.

2.4 MAXIMUM DISPLACEMENT AND INTER-STOREY DRIFT

Seismic design codes contain provisions to control the overall displacement and inter-storey displacement of a reinforced concrete structure. These restrictions are important for at least three different reasons (Bertero et al., 1991): (1) to maintain architectural integrity by avoiding unacceptable damage to non-structural components; (2) to limit structural damage and avoid structural instability (P-Δ) problems; and (3) to avoid human discomfort under frequent minor or even

occasional moderate earthquake shaking. The overall displacement ductility of a structure generally provides a good indication of the structure damage, but it does not usually reflect the damage to non-structural elements. For instance, Mahin and Bertero (1976) state that "Non-structural damage estimates based on drift ductilities may be misleading. For example, non-structural damage for relatively rigid structures may be small even for large values of displacement ductility since the yield displacement may be below the non-structural damage threshold. On the other hand, the non-structural damage and lateral displacements for flexible structures may become intolerably large even before significant yielding develops."

Non-structural damage is more dependent on the relative displacement (inter-storey displacement) than on the overall displacement. The overall displacement is usually expressed as overall drift index (ODI) which is the ratio of maximum roof displacement to the height of the structure, and the inter-storey displacement as inter-storey drift (ISD) ratio which is obtained as the maximum difference of the lateral deflections at the top and bottom of the storey under consideration divided by the storey height. Bertero et al. (1991), based on experience of past earthquakes, suggest that under the severe earthquake ground motion the ODI and ISD ratios should not exceed 1.0% - 1.5% depending on the function (occupancy) of the building, type of the non-structural elements, and how these non-structural components are attached to the structure.

According to ATC 3-06 (1978) and NEHRP-1991, the maximum ISD at ultimate limit state should be computed as the difference of the deflections (δ_x) at the top and bottom of the storey under consideration. δ_x is to be evaluated as

$$\delta_x = C_d \, \delta_{xe} \tag{2.8}$$

where C_d is the deflection amplification factor (specified for different types of structure and ranges from 2.0 to 6.5); and δ_{xe} is the deflection determined by an elastic analysis for the seismic forces prescribed by the code considering the building fixed at base. The maximum allowable storey displacement at ultimate limit state by these codes varies from 0.010 h_x to 0.015 h_x; where h_x is height of the storey level from the base level. Also, the ISD limit ranges from 0.010 h_{xe} to 0.015 h_{xe}; where h_{xe} is the height between two adjacent storeys. For certain types of building and limited height, a one-third increase in ISD limitations is allowed if there are no brittle types of non-structural elements. The ATC 3-06 (1978) and the NEHRP-1991 do not specify the maximum inter-storey drift or the maximum storey displacement at the elastic design force level.

On the other hand, UBC-1991 recommends that the calculated storey drift, at working stress level, should not exceed $0.04/R_w$ nor 0.005 times the storey height for buildings with $h \leq 65$ feet (19.81 m), where h is the total building height. For buildings with $h > 65$ feet, the calculated storey drift should not exceed $0.03/R_w$ nor 0.004 times the storey height. The UBC does not specify directly the maximum acceptable drift under the extreme ground motions. However, according to the UBC requirement for deformation compatibility, it is assumed that the maximum displacement (Δ_{max}) should not exceed $3(R_w/8)$ times the displacement resulting from the required forces. Thus, the maximum ISD, for DMRSF structures with height $\leq$ 65 feet, should not exceed (Bertero et al., 1991):

$$\left(\frac{3}{8}\right) R_w \left(\frac{0.04}{R_w}\right) h = 0.015 \, h \tag{2.9}$$

or (for $R_w = 12$)

$$\left(\frac{3}{8}\right) R_w \, (0.005\ h) = 0.0225\ h \qquad (2.10)$$

This means that 0.015 h controls the design, i.e., the maximum storey displacement and ISD should not exceed 0.015 h.

The term C_d, given in the ATC and the NEHRP codes, may be expressed as:

$$C_d = \frac{\Delta_{max}}{\Delta_s} = \frac{\Delta_{max}}{\Delta_y} \times \frac{\Delta_y}{\Delta_s} = \mu_s \frac{\Delta_y}{\Delta_s} = \mu_s \, \Omega \qquad (2.11)$$

Comparing Eq. 2.1 with Eq. 2.11 and the fact that generally $R_\mu \leq \mu_s$, leads to the inference that C_d should be equal to or greater than the response reduction factor (R). However, the values of C_d given in the ATC and the NEHRP are significantly less than R except in case of inverted pendulum structures. This discrepancy has been discussed in detail by Uang (1991). Similarly, the UBC provision which indicates the maximum deflection to be $\frac{3}{8} R_w$ times the elastic deflection is debatable.

The draft NZS 4203:1992 (IAEE, 1992) does not give specific values for drift at serviceability limit state (SLS); the code only states that at SLS "the deflections of the structure shall not be such as to result in damage causing loss of function of the structure or its parts". At ultimate limit state (ULS), the draft NZS code specifies that the ODI and the ISD ratios should not exceed: (a) 0.02 for buildings with $h \leq 15.0$ m; (b) 0.015 for buildings with $h \geq 30$ m; and (c) a linear interpolation is provided for buildings with $15\ m < h < 30$ m. However, in case time-history analysis including when inelastic analysis is done, the allowable value for the ratios is 0.025. In case non-linear time history analysis is not performed, the NZS code recommends that at ULS, the design lateral deflection at each level shall be the larger of:

(a) Structural ductility factor times the deflections obtained from equivalent static method or modal response spectrum method.

(b) Adding (i) deflections obtained by equivalent static method/ response spectrum method, to (ii) each possible sidesway mechanism deflection profile.

Most seismic codes give the same limits for ODI and ISD ratio. Only when the structure deforms as a straight line will the two ratios be the same. In most cases, the ISD in some storeys will be more than the ODI. To consider the difference between the two, Qi and Moehle (1991) define a coefficient of distortion (COD), which is the ratio of maximum ISD in any storey of the building to the overall drift index. They observe that the value of COD depends on stiffness and strength distribution within the structure, and on frequency contents of ground motion together with natural period of the building (T). Its value is larger as the higher modes become more significant. Also, the value of COD is higher in inelastic range as compared to that in the elastic range. They suggest that the maximum value of COD for regular frames may be estimated from static analysis amplified by a factor 1.15 to 1.25. In the absence of COD estimation from static analysis, COD may be taken in the range 1.5 to 2.0. For irregular buildings, the value of COD will obviously be larger than this.

2.5 NON-LINEAR ANALYSIS

The non-linear response of a reinforced concrete structure has usually been obtained in a number of ways. One method is to perform a MDOF non-linear time history analysis of the structure using computer programs such as DRAIN-2D (Kanaan and Powell, 1973), SARCF (Chung et al., 1988), IDARC (Park et al., 1987), etc. Approximate non-linear time

history analysis has also been performed by transforming the structure to an equivalent SDOF system by assuming a displacement shape and a distribution of lateral resistance which are constant during an earthquake (e.g., Saiidi and Sozen, 1979; Kaminosono et al., 1984; Shing and Mahin, 1985; Fajfar and Fischinger, 1987). In another method, a quasi-static non-linear analysis is performed for monotonically increasing lateral forces applied statically on the structure in increments until the point of maximum base shear and the sequence of yielding in members is monitored (e.g., Deshpande and Jain, 1983; Fajfar and Fischinger, 1987; Zhu et al., 1992). The applied static lateral forces are usually chosen to be proportional to the design lateral forces specified by a code.

The inelastic dynamic analysis requires realistic analytical models which can simulate strength, stiffness, and energy dissipation of individual members. Many hysteretic models, based on experimental data, have been proposed for seismic response simulation of a reinforced concrete member. Some of the models are simple to use, viz., Takeda et al. (1970), Saiidi and Sozen (1979), while the others are more sophisticated and involve complicated hysteresis rules, viz., Roufaiel and Meyer (1987), and Chung et al. (1987).

In the inelastic dynamic analysis of RC structures, the geometric non-linearity associated with deformed configuration of the structure, termed as P-Δ effect, may be included. In general, the P-Δ effect increases the storey deformation (drift). But several numerical analyses have indicated that effects are small when maximum inter-storey drift is less than 1% (Montgomery, 1981; Moss and Carr, 1980; and Powell and Row, 1976; reported by Paulay and Priestly, 1992). Anderson and Bertero (1969) (reported by Derecho et al, 1986) have investigated effects of

the associated P-Δ moments and moment-axial load interaction in the columns, on the response of 10- and 20-storey, single-bay, unbraced steel frames, designed to satisfy the strength code requirements only. They concluded that P-Δ moments and moment-axial load interaction in the columns caused yielding to occur much earlier in the response, so that the stiffness of the frame was reduced earlier and more energy was dissipated through inelastic deformation. For these frames, due to the P-Δ effect, the overturning moment was affected by 4% to 8%. They also concluded that when the frames were stiffened to satisfy the drift criterion (i.e., storey drift ratio less than or equal to 0.0025 under working loads), the P-Δ effect became negligible. The same conclusion was arrived at by Goel (1969) (reported by Derecho et al, 1986) in a study of the seismic response of 10- and 25-storey, single-bay symmetrical frames. This study showed that although the maximum lateral displacements were increased by about 10% by the P-Δ effect when the response was elastic, the effect became negligible (around 1%) when the girders were assumed to respond inelastically, with the columns remaining elastic throughout the response.

2.5.1 TIME-HISTORY ANALYSIS OF MDOF SYSTEMS

The structure is idealized as finite number of nodes connected by a finite number of deformable members. The members may be one, two or three dimensional in geometry. Masses are typically lumped at the floor levels, and the mass properties are generally based on the building's dead weight plus a certain amount of live loads. Initially the structure is analyzed for gravity loads, and then a seismic load analysis is conducted. Usually, the technique of constant acceleration method (Bathe, 1982) is used to solve the equations of motion. At each time

step, each member is checked for non-linearities using the element model employed, and then the element stiffness matrix is updated.

The members may be idealized in a number of different ways such as:

1. Single-Component Model (Giberson, 1967, reported by Saatcioglu, 1991): Here, each member is idealized as an elastic line element with inelastic rotational springs at the ends (Fig. 2.11). The springs account for potential flexural hinges at the ends. This model is convenient to use because the inelastic member-end deformation at one end is directly related to the member-end force at the same end. Inelasticities along the member are also assumed to be lumped at the springs. The characteristics of springs are based on assumed deformed shapes for members. For columns and beams, antisymmetric bending can be assumed with a fixed point of contraflexure. The single-component model can also have more springs at each end to represent other deformation components, i.e., at each end, one spring represents the inelastic flexural deformation and another represents the shear deformation. A third spring, which represents the reinforcement slip deformation model, can be also added. The disadvantage of the single-component model is that during seismic response, the point of contraflexure moves continually, and the member-end rotation becomes a function of member-end forces at both ends.

2. Dual-Component Model: This model was suggested by Clough et al. (1965) (reported by Saatcioglu, 1991) for elasto-plastic analysis. In this model, two parallel elements, one representing perfectly elasto-plastic behaviour to mark the yield point, and the other to introduce the strain-hardening of the member, are connected at their ends so that the two elements have the same member-end deformation (Fig. 2.12). Member-end deformations are related to member-end forces at both

ends. However, this dual-component model is applicable to structural members that exhibit elasto-plastic behaviour without stiffness degradation. This model can be extended into a multi-component model where each parallel element represents different characteristic features of hysteretic response.

3. Multiple-Spring Model (Takayanagi and Schnobrich, 1976, reported by Saatcioglu, 1991): In this model, a member is divided into segments along its length. The behaviour of each sub-element can be represented by a pair of inelastic springs. A similar approach was suggested by many researchers, viz., Casciati and Faravelli (1984), Roufaiel and Meyer (1987), Chung et al. (1988), wherein variable lengths of inelastic zones have been considered in segmenting the member. The variation of rigidity along the member length is represented by a continuous function. This method is adopted in IDARC (Park et al., 1987) and SARCF (Chung et al., 1988) programs.

2.5.2 TIME-HISTORY ANALYSIS OF EQUIVALENT SDOF SYSTEM

The equivalent SDOF system has been proposed by many researchers, e.g., Saiidi and Sozen (1979) (named "Q-model"); and Fajfar and Fischinger (1987) (named "N2 procedure"). The Q-model is based on two types of simplification: (1) reduction of a MDOF model of a structure to a SDOF oscillator, and (2) approximation of the incremental stiffness properties of the entire structure by a single nonlinear spring. The mass of the oscillator is equal to that of the MDOF system, adjusted with an appropriate factor, and the oscillator stiffness is derived from the force necessary to deform the MDOF system in a definite shape. The non-linear spring force of the SDOF system is based on the non-linear force-displacement relationship obtained from properties of the actual

structure analyzed, assuming that it is subjected to a set of monotonically increasing external forces. Saiidi and Sozen (1979) carried out experimental tests on eight small-scale reinforced concrete structures and their results were compared analytically using the Q-model. The comparisons showed good agreement between the experimental and the analytical results.

Fajfar and Fischinger (1987) have proposed another procedure (named "N2 procedure") to transform the structure into a SDOF system by assuming a displacement shape $\{\Phi\}$ and a distribution of lateral resistance $\{\Psi\}$ which are constant during the time history analysis. The equation of motion for a planar system subjected to a base acceleration $\ddot{u}_g(t)$ is written in the form

$$[M]\ \{\ddot{U}\} + \{P\} = -\ [M]\ \{1\}\ \ddot{u}_g \qquad (2.12)$$

where [M] is the mass matrix of the structure; and $\{P\}$ represents the restoring force vector (resistance of the structure). The assumed displacement shape $\{\Phi\}$ is taken to be the same as that resulting from static application of the dynamic loads, and the distribution of the lateral resistance $\{\psi\}$ is equal to the distribution of the lateral loads. By introducing $\{U\} = \{\Phi\}\ u$; $\{P\} = \{\psi\}\ p$, and by assuming concentrated masses m_i (a diagonal mass matrix) and by premultiplying by $\{\Phi\}^T$, the equation of motion (Eq. 2.12) can be transformed into the form

$$\sum m_i \Phi_i \cdot \frac{\sum m_i \Phi_i^2}{\sum m_i \Phi_i}\ \ddot{u} + p \sum \Phi_i \psi_i = -\left(\sum m_i \Phi_i \right) \ddot{u}_g \qquad (2.13)$$

or

$$m^*\ \ddot{u}^* + Q^* = -\ m^*\ \ddot{u}_g^* \qquad (2.14)$$

Equation (2.14) represents the equation of motion for an equivalent SDOF

system, where the constants are defined by

$$m^* = \sum m_i \Phi_i \qquad Q^* = \frac{\sum \Phi_i \psi_i}{\sum \psi_i} Q$$

$$Q = p \sum \psi_i \qquad \text{and} \qquad \ddot{u}^* = \frac{\sum m_i \Phi_i^2}{\sum m_i \Phi_i} \ddot{u} \qquad \ldots.(2.15)$$

where Q is the base shear. The viscous damping term can be included directly into Eq. (2.14).

2.5.3 QUASI-STATIC METHOD

Some researchers, viz. Deshpande and Jain (1983), Moazami and Bertero (1987), Miranda and Bertero (1989), Sugano (1989), Zhu et al., (1992), and Navin and Jain (1993) have used a quasi-static method (force-control method) to carry out the non-linear analysis of reinforced concrete frames. In this method, beam and column elements use idealized bilinear moment- curvature curves. The first segment, which represents the elastic region, is upto the yield moment of the section, and the second segment is upto the ultimate curvature of the section and represents the inelastic domain. Static lateral loads, proportional to those specified by a seismic design code, are applied monotonically in small increments. Elastic analysis is carried out for the incremental loads first, and the incremental force vector for each member is determined. The total moment developed at each end of each member is compared with the yield moment capacity of that section to determine whether or not plastic hinge has formed. If no plastic hinge has formed the latest incremental member forces and deformations are added to the respective total values corresponding to new incremental external loads and the check for plastic hinge is applied again in each member. If a

plastic hinge has formed in an element, the stiffness matrix of that element is updated. The process is repeated, until the number of plastic hinges is large enough to transform the structure into a mechanism.

2.5.4 LIMITATIONS OF THE TIME-HISTORY AND QUASI-STATIC ANALYSES

The MDOF time-history analysis is a sophisticated analysis, and can be very sensitive to the structure modelling particularly with regard to initial elastic stiffness and hence time period. Also, it requires a higher computational effort which is time consuming and impractical for many design purposes. While the equivalent SDOF time-history analyses require less computational effort, they loose their accuracy if there are abrupt changes in stiffness or mass along height of the building (Meyer, 1991). Also, the time-history analyses can be quite sensitive to the strong motion record used in analysis. Therefore, considering uncertainties in (a) correctly modelling the structure's initial stiffness, discussed in detail in the next section, and in (b) accurately anticipating ground motion at the site, the non-linear time-history analyses become somewhat less attractive for design-office use.

The quasi-static method is easy to use and gives a good approximation to the upper bound of the base shear - roof displacement relationship. However, its limitations are that it does not provide the load-displacement relationship in the softening region, i.e., beyond the peak in base shear where the structure can undergo further displacement, even though with reduced base shear. Also, the applied load profile is usually based on code-specified design load profile which may not correctly reflect the dynamic characteristics for buildings with unusual configuration. Unlike perfectly elasto-plastic materials, reinforced

concrete shows stiffness degradation under inelastic load cycles, in addition to strength decay under high level cycles of inelastic deformation. These two phenomena result in a significant increase in curvature ductility demand on the structure elements. This curvature ductility may be significantly higher than the same obtained using the quasi-static method; and this is a major limitation of the quasi-static analysis.

2.5.5 LATERAL STIFFNESS OF BUILDINGS

The actual initial lateral stiffness of a building is difficult to assess accurately due to numerous assumptions that are required. Quite often, the modelling for non-linear analysis of RC buildings is based on cracked sections of the bare-frame skeleton, which gives a significantly more flexible structure than the actual building. Assumed stiffness characteristics affect both period (and hence design force) calculations and lateral drift calculations. The main difficulties with accurately assessing structural stiffness are:

1) The non-structural masonry walls, often neglected in analysis, contribute significantly to the structure stiffness. Klingner and Bertero (1976) (reported by Riddell and Newmark, 1979) tested 1/3 scale models representing subassemblages of 11-storey moment resisting RC frame; one bare frame and three infilled frames were subjected to axial loads plus quasi-static cycles of reversed shear and overturning moment simulating the action of gravity and earthquake loads in the prototype structure. It was concluded that the structure stiffness and strength of infilled frames are much higher than those of the bare frames (Fig. 2.13).
2) The moment of inertia (I_e) of a concrete member before the modulus of

rupture is exceeded and after it is exceeded are different. When a reinforced concrete element is subjected to bending, it goes through three predominant stages. The first stage is the uncracked section, herein the gross concrete section (I_g) should be considered in calculating the moment of inertia. The second stage is the cracked section, herein the moment of inertia (I_{cr}; $I_{cr} < I_g$) is calculated by neglecting the concrete in tension zone but considering the tensile steel. The third stage is the ultimate strength stage, where the compression is taken by an assumed concrete stress block and the steel yields in tension; the moment of inertia (I_u) decreases drastically as compared to the first and second stages. Each of these three stages of bending do not occur in all structural elements (or even over the full length of one structural member) at the same time. Some elements never act as uncracked sections due to gravity load effects. All this is difficult to account for in analysis.

3) For monolithic slab-beam construction, the slab contributes to the strength and stiffness of the beam, depending on whether the slab is in tension or compression and on the moment pattern along the beam (Miranda and Bertero, 1989; and Paulay and Priestly, 1992). Although all codes specify effective widths of the slab that contribute to the resistance of the beam when it is subjected to a positive moment (slab in compression), the codes do not generally specify any effective width over which the steel in slab acts as tension reinforcement. Fig. 2.14 (Miranda and Bertero, 1989) shows the influence of different values of effective slab width on moment-curvature relationship for a beam section when subjected to a negative bending moment. From the figure, it is clear that the use of a realistic effective slab width results in a floor system

significantly stiffer and stronger than a system which neglects the slab reinforcement contribution.

4) The modulus of elasticity of concrete (E_c), used for design, is often represented by a secant modulus to account for the effects of creep and shrinkage (Freeman et al., 1980; and Ferguson et al., 1988). Codes give expressions relating E_c to compression strength with the primary aim of obtaining conservative estimate of deflections, i.e., lower stiffness. These expressions have significant variation from one code to another. For instance, the ACI-318 (1989) calculates E_c as $4700\sqrt{f'_c}$ (MPa), while in IS:456-1978 E_c is calculated as $5700\sqrt{f_{ck}}$ (MPa) or $6373\sqrt{f'_c}$ (MPa) (considering $f'_c = 0.8\ f_{ck}$); i.e., E_c given by the IS code is 1.36 times E_c given by the ACI code. On the basis of full-scale tests of concrete structures, it has been observed that cylinders give a low estimate of in-situ modulus of elasticity (Paulay and Priestly, 1992). Also, actual concrete strength in a structure is usually more than the specified 28-day strength and it increases with time. Paulay and Priestly (1992) suggest that the specified design value of E_c, recommended by the ACI, may be as much as 30% to 40% below the actual values. On the other hand, the dynamic modulus of concrete (E_d) refers to almost pure elastic effects and is unaffected by creep, and therefore E_d is approximately equal to the initial tangent modulus determined from a static test and is appreciably higher than the secant modulus (E_c) (Neville, 1981). When the structure is new and subjected to low amplitude of ground motion, the dynamic modulus of elasticity (E_d) is applicable. Long time exposure of the structure to ambient motion and wind pressures overcomes the initial stiffness properties of the structure associated with the initial tangent modulus of elasticity

of the concrete, and the modulus of elasticity of concrete tends to be close to the secant modulus (E_c) (Freeman et al., 1980).

5) Under load reversal, the variations of axial force can influence strength, stiffness, and deformation capacity of reinforced concrete columns (Abrams, 1987).

6) The properties of a reinforced concrete beam in negative bending are usually different from those in positive bending.

7) Architectural elements (e.g., cornices, balconies, lift core, etc.) and non-structural elements (e.g., stairs), which are often neglected in the analysis, may result in considerable stiffness.

8) The common assumption of full fixity at the column base may only be valid for columns supported on rigid raft foundation or on individual foundation pads supported by short stiff piles, or by foundation walls in basements. Foundation pads supported on deformable soil may have considerable rotational flexibility (Paulay and Priestly, 1992); this may result in variation in stiffness calculation.

9) Period determined from analyzing the building using a 2-dimensional model may be slightly higher than what is obtained if the building is analyzed using a 3-dimensional model.

To illustrate the difficulty of estimating lateral stiffness of RC buildings further, consider a 81 feet (24.9 m) high six-storey building studied by Ghosh (1991). He studied four alternative lateral load resisting systems, each having ductile or special moment resisting frames in the E-W direction. The calculated value of fundamental period in this direction for the four schemes ranged from 1.30 sec to 1.94 sec. The fundamental period for this building by the empirical formula in UBC-1991 and NEHRP-1991 is only 0.81 sec. Further, NEHRP recommendations put an upper limit on calculated fundamental time period (Fig. 2.15)

which is 1.2 times the empirical T if the building is located in most severe seismic zone. Thus, in any case, the building should be designed for a period not exceeding 0.97 sec (as against 1.30 sec to 1.94 sec given by the analysis).

Based on experimental data from many actual buildings shaken by underground nuclear explosions or by San Fernando earthquake of 1971, Freeman et al. (1980) show that there are large variations in structural stiffness depending on the amplitude of shaking (and thus on the sectional properties of the RC structure), and on the participation of the structural elements not designed to carry lateral load and of the non-structural elements. For instance, a series of vibration tests on two four-storey structures were conducted in 1965/1966 at the Nevada Test Site. When the structures were new (no partition installed), the measured period for relatively small motion was ranging from 0.36 sec to 0.39 sec. After the test structures were subjected to strong ground motions, the observed periods of the low-level tests lengthened to slightly more than 0.5 sec. After the installation of infilled unreinforced concrete block infills, the measured period for low-level amplitude vibration was 0.2 sec. Freeman et al. (1980) suggest that masonry filler walls can increase the stiffness of a building by a factor of 2 to 8.

Therefore, a conservative design approach is to assume a stiff structure for calculation of lateral force requirements, and to assume a flexible structure for calculating drift (Freeman et al., 1980). They suggest that for evaluation of design seismic force (a) gross concrete sections should be used, moment of inertia of beams be taken as 1.5 times (2.0 times) that for rectangular section for exterior (interior) frames to account for slab contribution, (c) beam-column joints should

be treated as rigid, and (d) the non-seismic structural as well as non-structural elements should be included. For calculation of drift, Freeman et al. (1980) suggest that (a) average of gross section and cracked section (or one half of the gross section) should be considered, (b) beam-column joints should be assumed to have some flexibility (or even no rigidity, i.e., centre to centre beam spans and column heights), and (c) the non-seismic structural and non-structural elements should be ignored.

Paulay and Priestly (1992) suggest that for realistic distribution of member forces, the member stiffness should be close to that at member yield forces. Accordingly, they suggest much lower values of section properties to be used in design than those mentioned above for estimation of design seismic force. For instance, they recommend using 0.40 I_g in rectangular beams and columns having tensile axial force, 0.35 I_g in T and L beams, 0.80 I_g in columns having compression axial force exceeding 0.5 $f_c' A_g$ (f_c' = compressive strength of concrete; and A_g = gross area of section), and 0.60 I_g in columns with axial force equal to 0.2 $f_c' A_g$. Paulay and Priestly (1992) also recommend that column stiffness should be based on an assessment of the axial load that includes permanent gravity load, which may be taken as 1.1 times the dead load on the column, plus the axial load resulting from seismic overturning effects. They also recommend that column base should be modelled by a rotational spring, in case the column foundation pad is supported on deformable soil. Further, they mention that infill panels, even of low-strength masonry, cannot be considered non-structural.

It is thus obvious that a great deal of uncertainties remain in analytical evaluation of lateral stiffness of a RC building. Moreover, non-linear dynamic analyses that calculate the member stiffness for

cracked sections and ignore stiffness contribution of non-structural masonry infills can be grossly unrealistic. Unfortunately, as of now most non-linear analyses on RC buildings do not adequately model the masonry infills.

2.6 DISPLACEMENT-BASED DESIGN APPROACH FOR RC STRUCTURES

In recent years, a "displacement-based design approach" has been proposed (Qi and Moehle, 1991; Moehle, 1992a and 1992b). This design approach focuses on the maximum allowable displacement and inter-storey drift to control the structural and non-structural damage. In the method suggested by Qi and Moehle (1991), the design ground motion is expressed in terms of the elastic displacement response spectrum of a SDOF system. The multi-storey frame structure is modelled by an equivalent SDOF structure, and the characteristic properties for a specified deflection shape are obtained. The displacement response spectrum is modified by an appropriate factor (obtained from the characteristic properties of the equivalent SDOF) so that roof displacement of the multi-storey structure can be read from the modified spectrum. The displacement response is characterized in two period ranges, acceleration and velocity regions, separated by the characteristic period of the ground motion (T_g). When the structure time period (T) is greater than T_g, the maximum displacement response of the structure is largely independent of lateral strength of the structure, and the peak inelastic displacement response can be estimated as being equal to the elastic values. In the period range of $T < T_g$, both stiffness and strength affect the maximum inelastic response. Qi and Moehle have developed a simple method to estimate the peak inelastic displacement for structures having $T < T_g$. The design procedure in this approach may be summarized as below:

a) For a given site, the design displacement response spectrum is constructed on statistical basis of large number of earthquake records in the period range $T > T_g$; and on the procedure developed by Qi and Moehle in the period range $T < T_g$.

b) Structural model of the preliminary design is analyzed, and the characteristic properties of the equivalent SDOF are obtained; the structure stiffness is based on cracked sections of the elements.

c) The design criteria in terms of a maximum allowable ISD is determined. Using coefficient of distortion (COD), where COD relates the maximum ISD with the maximum roof displacement, allowable roof displacement is determined.

d) The design displacement response spectrum is modified so that the modified spectrum can directly give roof displacement of the MDOF structure.

e) For the structure, the maximum allowable fundamental time period (T_{max}) corresponding to the desired drift limit is defined from the modified displacement response spectrum. Fundamental time period of the structure (T) may fall in three different ranges:

   (i) $T_g < T < T_{max}$, then the strength and stiffness requirements are satisfied;

   (ii) $T < T_{max} < T_g$, the stiffness is acceptable only if appropriate strength is selected. In some cases it may be more economical to increase the stiffness because a lower strength is required to meet the displacement requirement;

   (iii) If $T_{max} < T$ then the structure is considered not sufficiently stiff. The stiffness is increased in order to control the maximum displacement response, and the process is repeated from step (b) onwards.

The above procedure provides a new approach to estimate the inelastic displacement spectrum for MDOF short-period structures. It may be noted that: (1) the procedure seems to imply that it is in lieu of the present code-specified procedure; (2) the initial stiffness of the structure is estimated on the properties of cracked elements, which may lead to a very conservative drift design approach; and (3) the method is highly dependent on the dynamic characteristics of ground motion.

Subsequently, Moehle (1992a and 1992b) has elaborated on the displacement-based design procedure. The proposed procedure is summarized in Fig. 2.16 in relation to a reinforced concrete bridge column. Steps 1 and 2 are similar to steps (a-e) given above for the Qi and Moehle procedure. In step 3, the ultimate curvature demand ϕ_u is calculated using empirical formulas in which the displacement ductility is related with the curvature ductility. Lastly in step 4, the sectional curvature capacity is checked for a given set of details using accepted section analysis methods. Moehle indicates that the deflection shape (used in the equivalent SDOF analysis) may be taken proportional to the first mode shape of the structure.

Moehle (1992a) compares the above displacement-approach with the current ductility-based approach to design. In the ductility-based design, the ratio of elastic force demand to structure strength (demand-capacity ratio) is used to obtain the displacement ductility, and subsequently, the section detailing requirements. The procedure is summarized in Fig. 2.17, considering the same example of the concrete bridge column. In step 1, the strength and effective structure period are estimated. In step 2, the displacement ductility demand is obtained as mentioned above. In step 3, the curvature ductility demand is calculated from the displacement ductility demand using empirical

formulas. Finally, in step 4, the cross section is analyzed to determine if the available curvature ductility capacity for a given set of details is sufficient for the calculated curvature ductility.

Moehle (1992a) suggests that though the algorithms of the above two approaches are similar, and the end results "presumably the same", the information that is processed differs. In the ductility-based approach, readily calculated elastic forces define the ductilities but do not provide a clear image of deformations. In the displacement-based approach, displacement is used directly to define element deformations.

In both of the above procedures, the objective is to design the elements to fulfill curvature ductility demands, which ensures that the structure can undergo the required deformations, and provide adequate displacement ductility. Though Moehle (1992a) gave a relationship to relate the displacement ductility to the curvature ductility on individual members for a SDOF RC structure, for a MDOF RC structure it is apparently difficult to establish a relationship for the same.

According to Moehle, the ductility-based approach is suited to cases where inelastic response is distributed uniformly throughout the structure; in such cases the local demand-capacity ratios provide a reasonably accurate picture of ductility distribution and magnitude. Where inelastic response is not uniformly distributed, the local demand capacity-ratios do not provide information on local ductility demands, and the displacement-based approach is preferred. It will be shown in the next chapter how an integrated displacement- and ductility-based design approach can be developed for RC frames; in RC frames the inelastic response is distributed throughout the structure.

2.7 TWO-LEVEL SEISMIC DESIGN PROCEDURE

Since a structure has to resist three levels of earthquake shaking (minor, moderate, and severe) with different performance criteria, it is logical that three limit states should be considered in seismic code provisions (Bertero and Bresler, 1977). These limit states are (Uang, 1993): (1) serviceability limit state (SLS) for minor earthquake; (2) damageability limit state (DLS) for moderate earthquake; and (3) ultimate limit state (ULS) for severe earthquake. Most codes require only one limit state, SLS or DLS, to be considered. However, in recent years, at least three codes, Building Standard Law (BSL-1984; IAEE-1992), Tri-Services Manual (1986), and draft NZS 4203:1992 (IAEE, 1992) require consideration of two limit states for design.

The seismic design procedure of the Building Standard Law (BSL) of Japan considers the SLS (level 1) for moderate earthquakes (which may occur several times during the lifetime of a building), and the ULS (level 2) for severe earthquakes (an earthquake which may possibly occur once in a building lifetime). The elastic design spectrum for the ULS is five times the elastic design spectrum for SLS.

(a) Level 1 Design: The flexural, axial, and shear stiffness of the structure elements are based on the gross uncracked concrete section. Designers have to perform an elastic analysis and proportion the members for the combination of gravity loads with seismic load (C_{es}). For typical buildings, BSL has specified 0.005 as the limit on storey drift ratio to minimize non-structural damage.

(b) Level 2 Design: To satisfy the ULS, the main concern is to provide a structure with sufficient strength to limit the ductility demand; ductility capacity is provided by proper structural detailing. For reinforced concrete buildings, BSL uses a force reduction factor, D_s

(ranges within 0.3 to 0.55), to specify the required ultimate structure strength. Designers have to perform post-elastic analysis to verify that the structure has sufficient strength. The storey drift and ISD are limited to 1/66 (≅ 0.015) for a frame structure and 1/75 (≅ 0.0133%) for a wall-frame structure. A static non-linear analysis under monotonically increasing lateral loads distributed corresponding to the fundamental mode shape is desirable (Otani et al., 1992), in which the flexural stiffness and the shear stiffness of elements are estimated within 0.3-0.5 and 0.3-1.0 of the gross stiffness of uncracked section, respectively, while the axial stiffness remains the same.

The Tri-Services Manual (1986) seeks a two-level (DLS and ULS) seismic design for essential buildings. Design earthquake (EQ-I), in level 1 design (DLS), has a 50% probability of being exceeded in 50 years. The Manual allows limited yielding in members by requiring that "the structure will resist these forces by elastic, or nearly elastic, behaviour". For example, in case of a ductile framing system, "nearly elastic" behaviour is considered to be satisfied by the Manual if (1) less than 20% of the horizontal seismic-resisting elements in the direction of the force in any storey, and (2) less than 10% of the vertical seismic elements in any storey, do not exceed the flexural capacity by 25% (Uang, 1993). The storey drift should not exceed 0.5% of the storey height. The design earthquake (EQ-II), for level 2 design (ULS), has a 10% probability of being exceeded in 100 years. In level 2 design, a post-elastic analysis has to be conducted to evaluate ultimate capacity of the structure. For buildings which are not classified as either essential or high risk, a two-level design approach is still used, except that the intensity of design earthquake in level 1 (EQ-I) is multiplied by 0.7 and the drift limit is increased to 0.7% of the

storey height.

The design procedure developed in the next chapter combines the two-level limit-state design with the displacement- and ductility-based design approach.

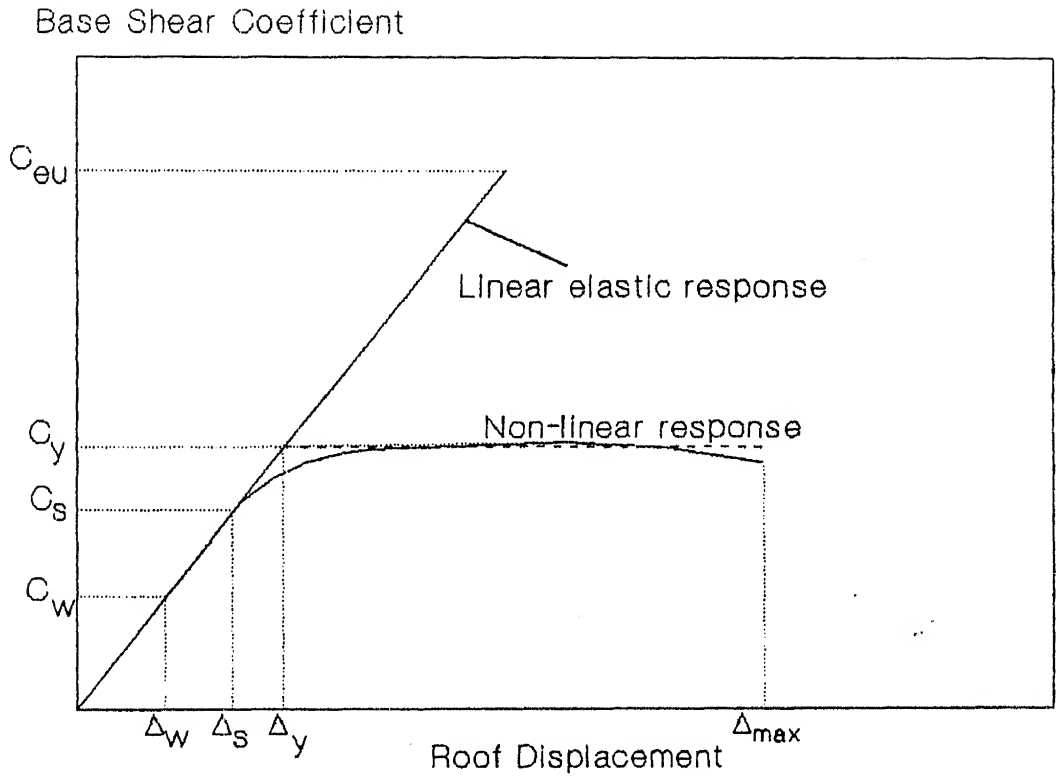

Fig. 2.1 Typical global structural response idealized as linearly elastic - perfectly plastic curve.

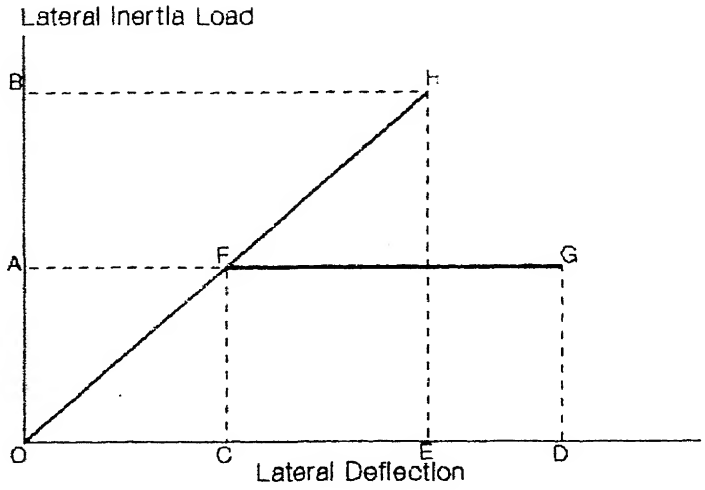

$$R_\mu = \frac{OB}{OA} \; ; \qquad \mu_s = \frac{OD}{OC}$$

area (OHE) = area (OFGDO)

$$\rightarrow \quad R_\mu = (2\,\mu_s - 1)^{0.5}$$

(a)

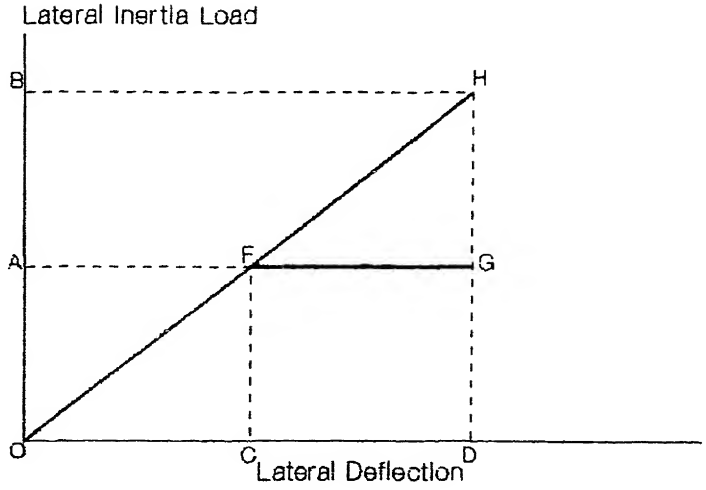

$$R_\mu = \frac{OB}{OA} \; ; \qquad \mu_s = \frac{OD}{OC}$$

$$\rightarrow \quad R_\mu = \mu_s$$

(b)

Fig. 2.2 Response of elastic and elasto-plasto structures.
(a) Equal maximum potential energy response.
(b) Equal maximum deflection response.

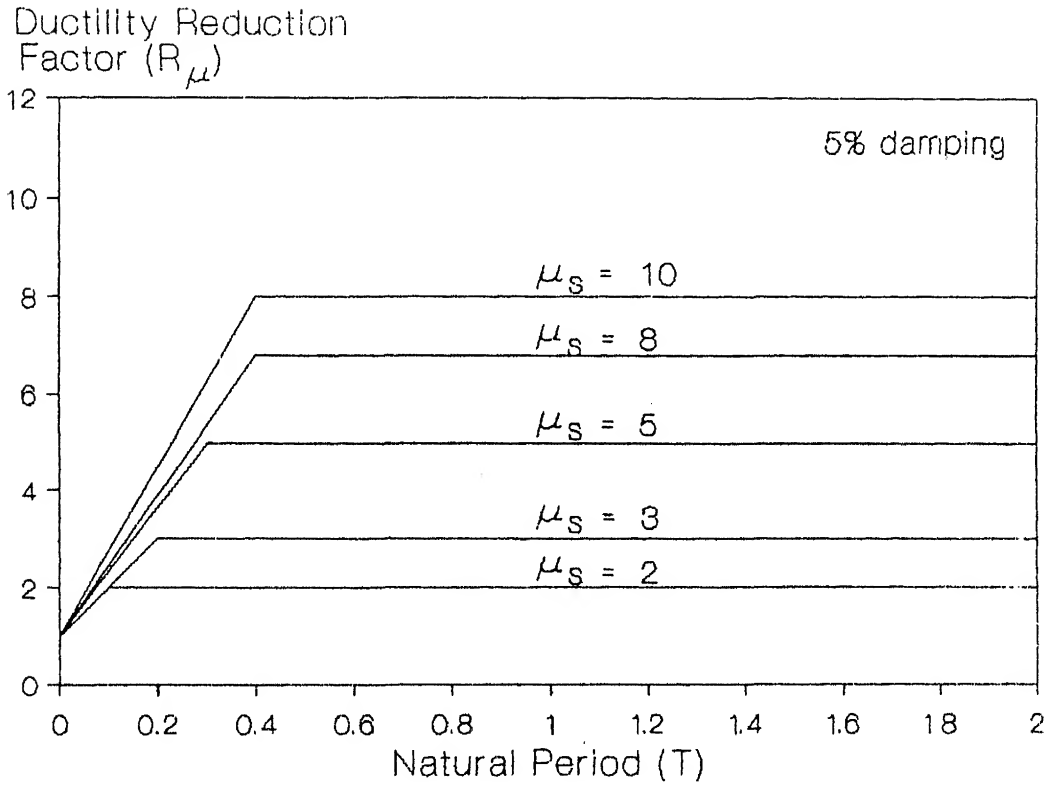

$$R_\mu = 1 + \frac{R_\mu^* - 1}{T^*} T \quad \text{for} \quad 0 < T < T^*$$

$$R_\mu = R_\mu^* \quad \text{for} \quad T \geq T^*$$

μ_s	R_μ^*	T^*
2	2.0	0.1
3	3.0	0.2
4	4.0	0.3
5	5.0	0.4
6	5.6	0.4
7	6.2	0.4
8	6.8	0.4
9	7.4	0.4
10	8.0	0.4

Fig. 2.3 Idealized ductility reduction factor for SDOF systems (Riddell et al. 1989).

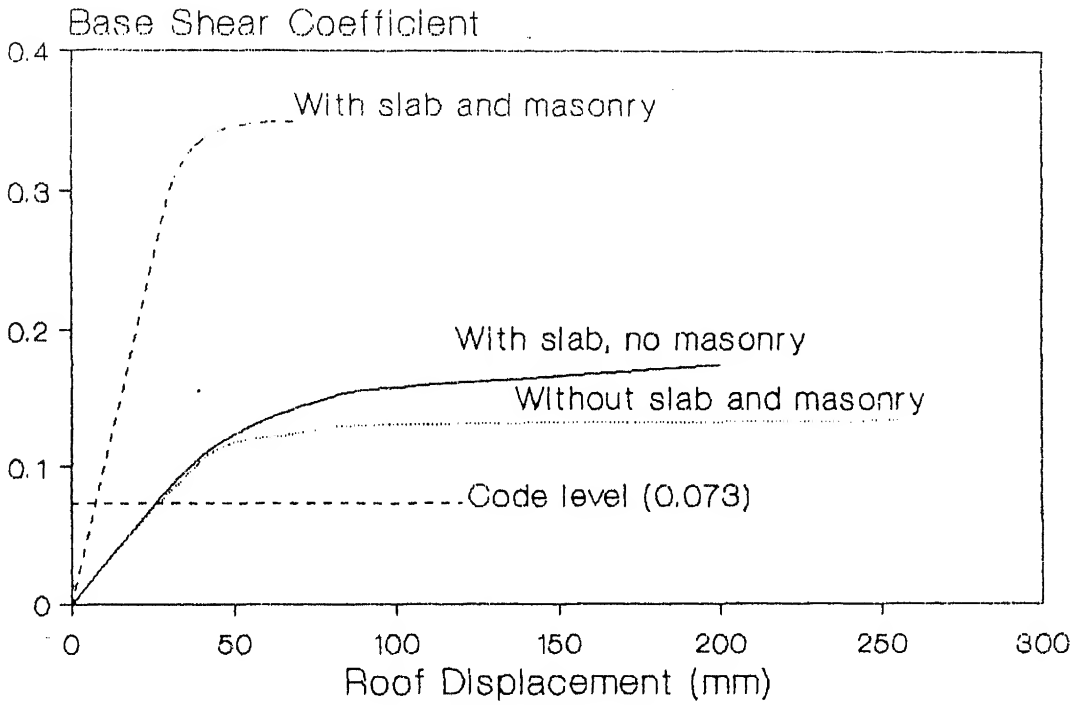

Fig. 2.4 Response of a four-storey building subjected to monotonically increasing lateral load (Miranda and Bertero, 1989).

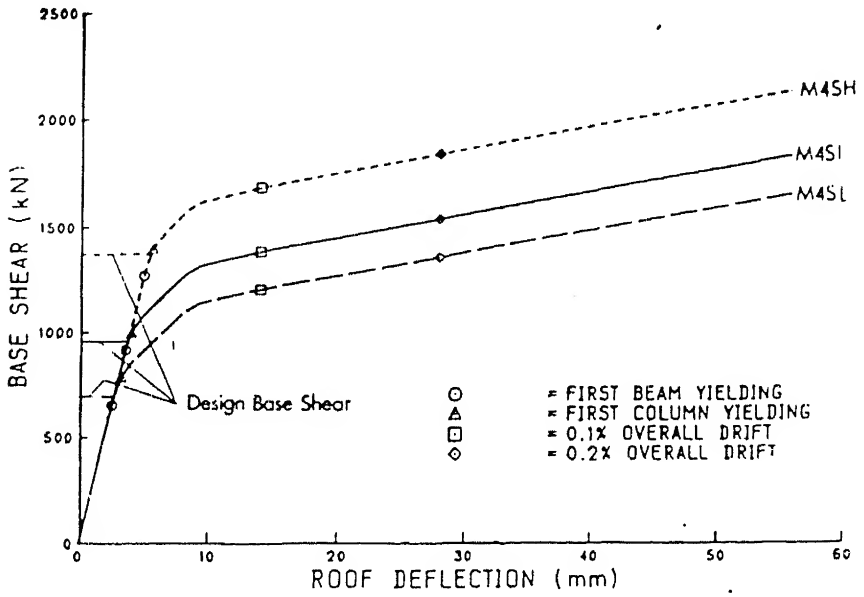

Fig. 2.5 Base shear versus roof displacement response of a four - storey frame in different seismic regions of Canada (Zhu et al., 1992).

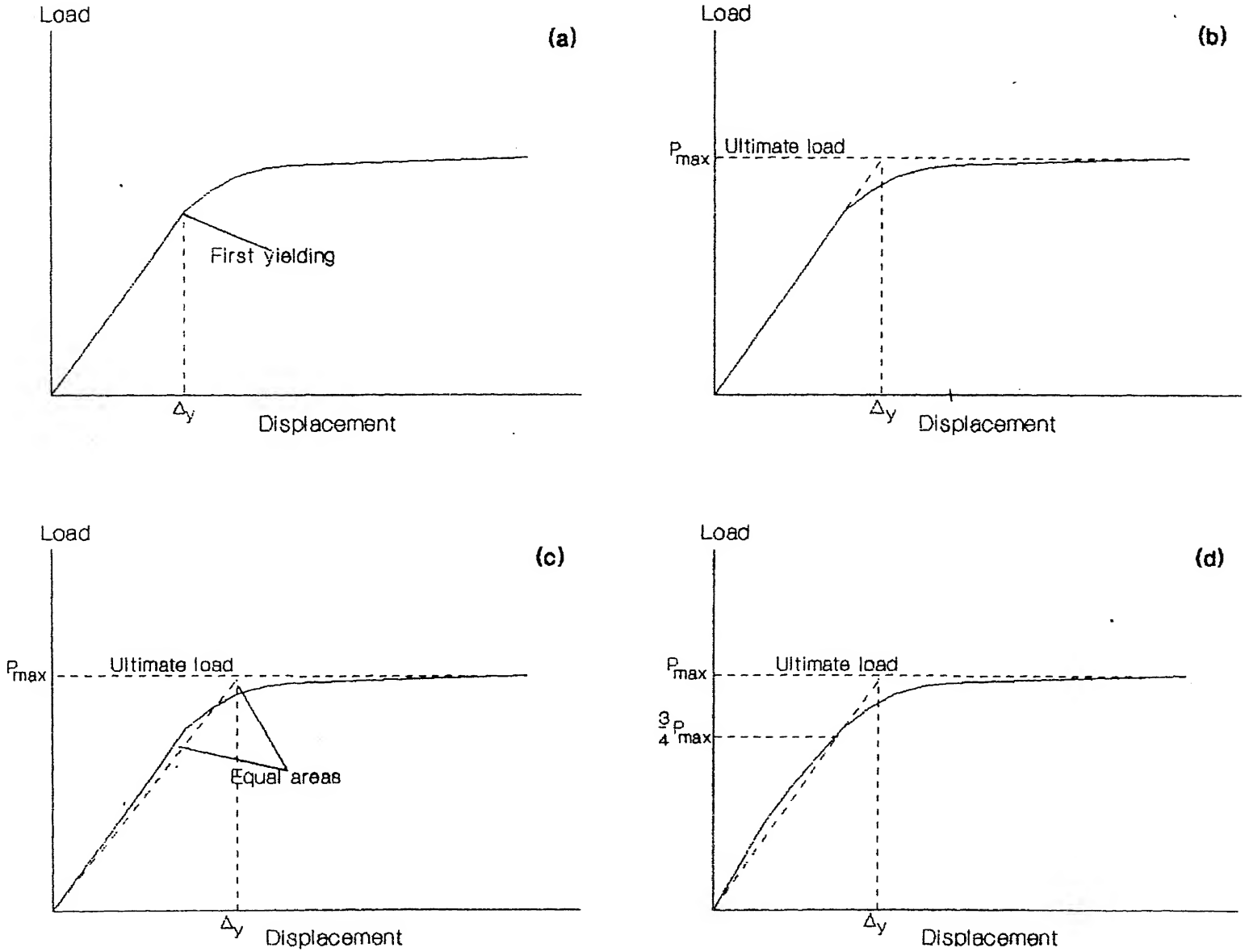

Fig. 2.6 Various definitions for yield displacement (Δ_y) (Park, 1988).

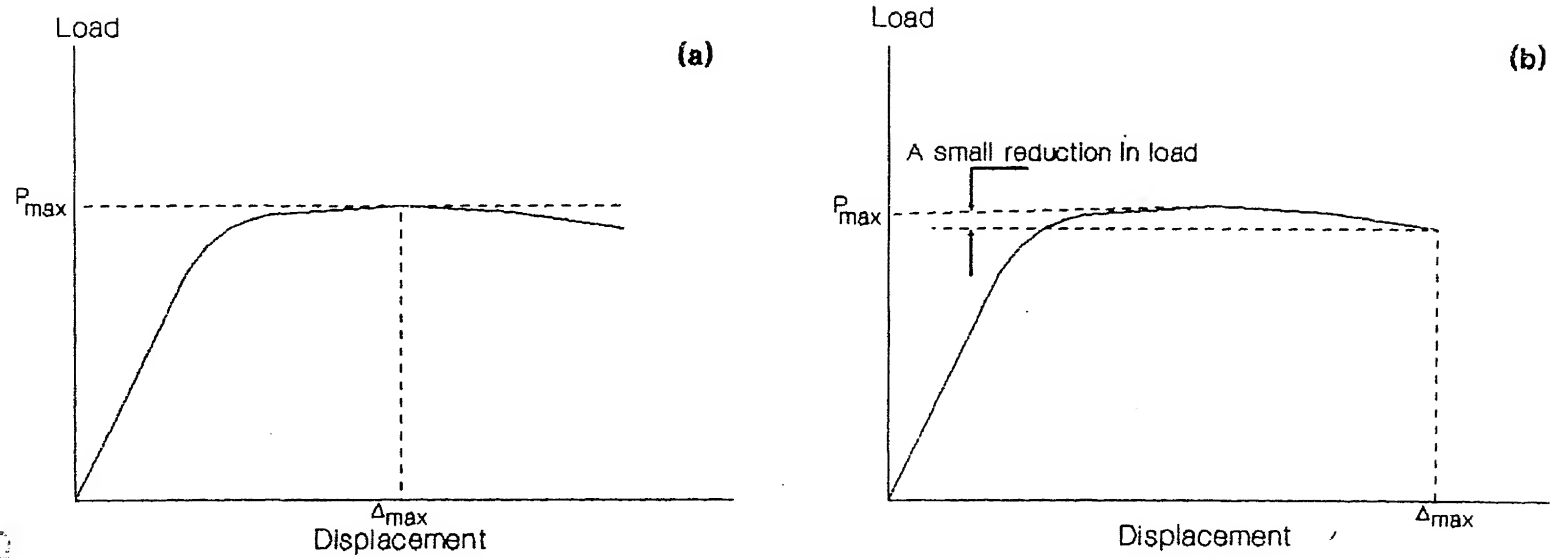

Fig. 2.7 Alternative definitions for ultimate displacement (Δ_{max}) (Park, 1988).

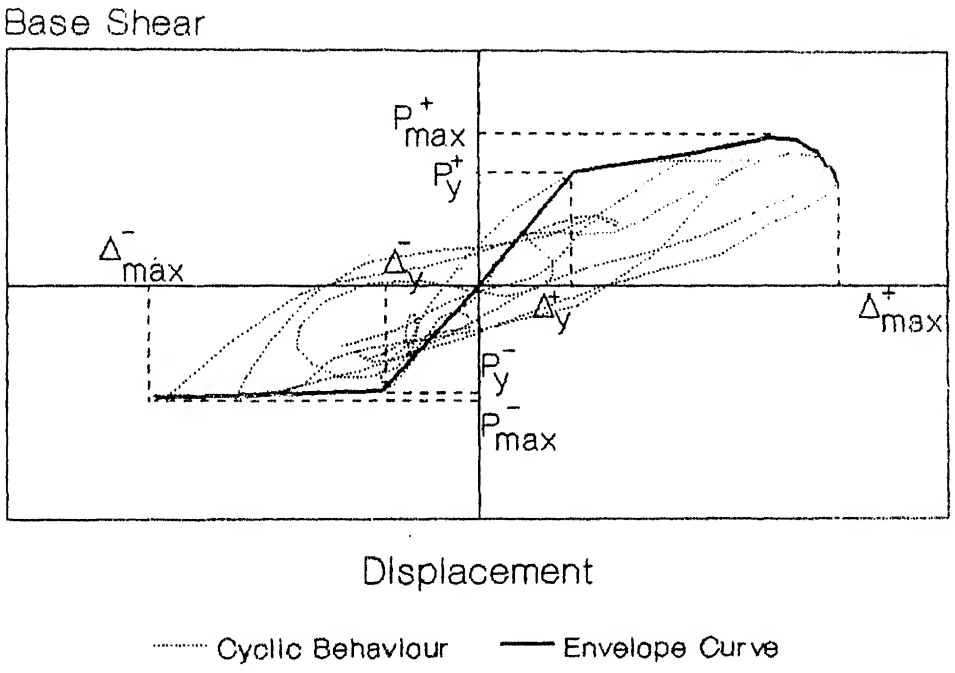

Fig. 2.8 Cyclic behaviour of a RC frame.

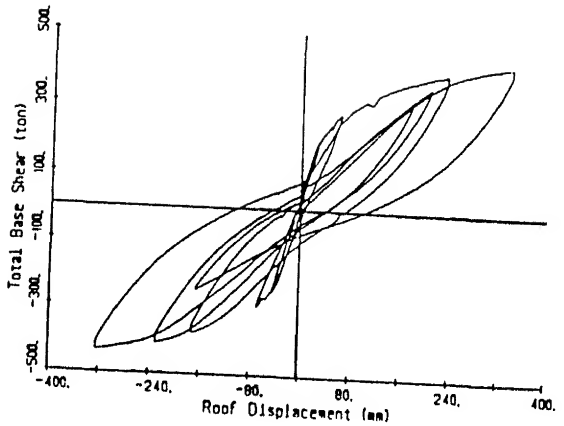

Fig. 2.9-a Force-displacement relationship for 7-storey test structure provided with shear walls (ACI SP-84).

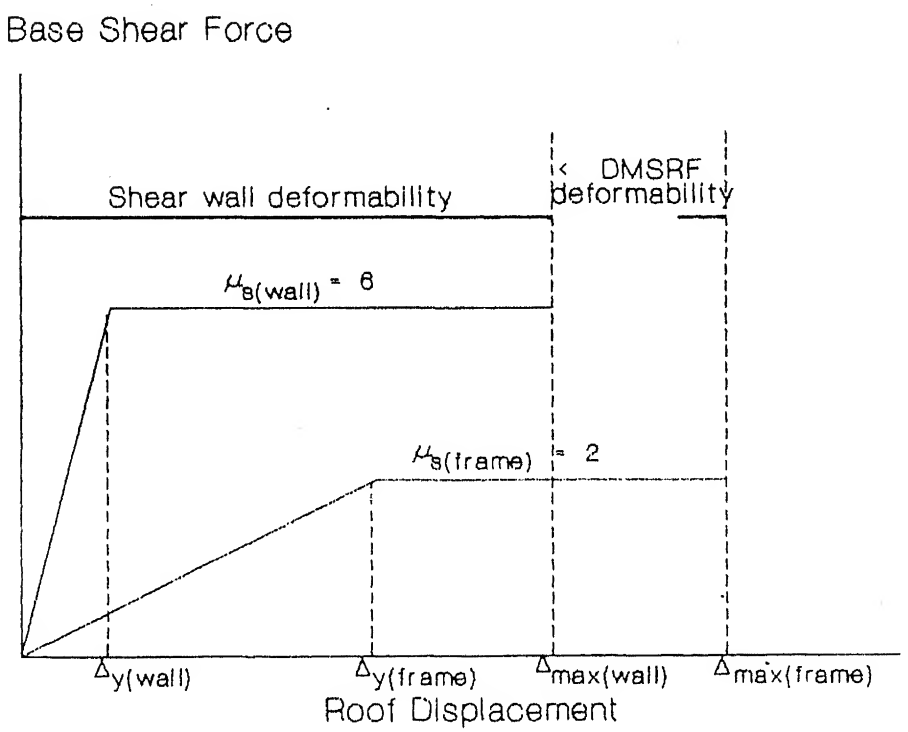

Fig. 2.9-b Deformability and ductility of RC wall and RC-DMRSF (Bertero et al., 1991).

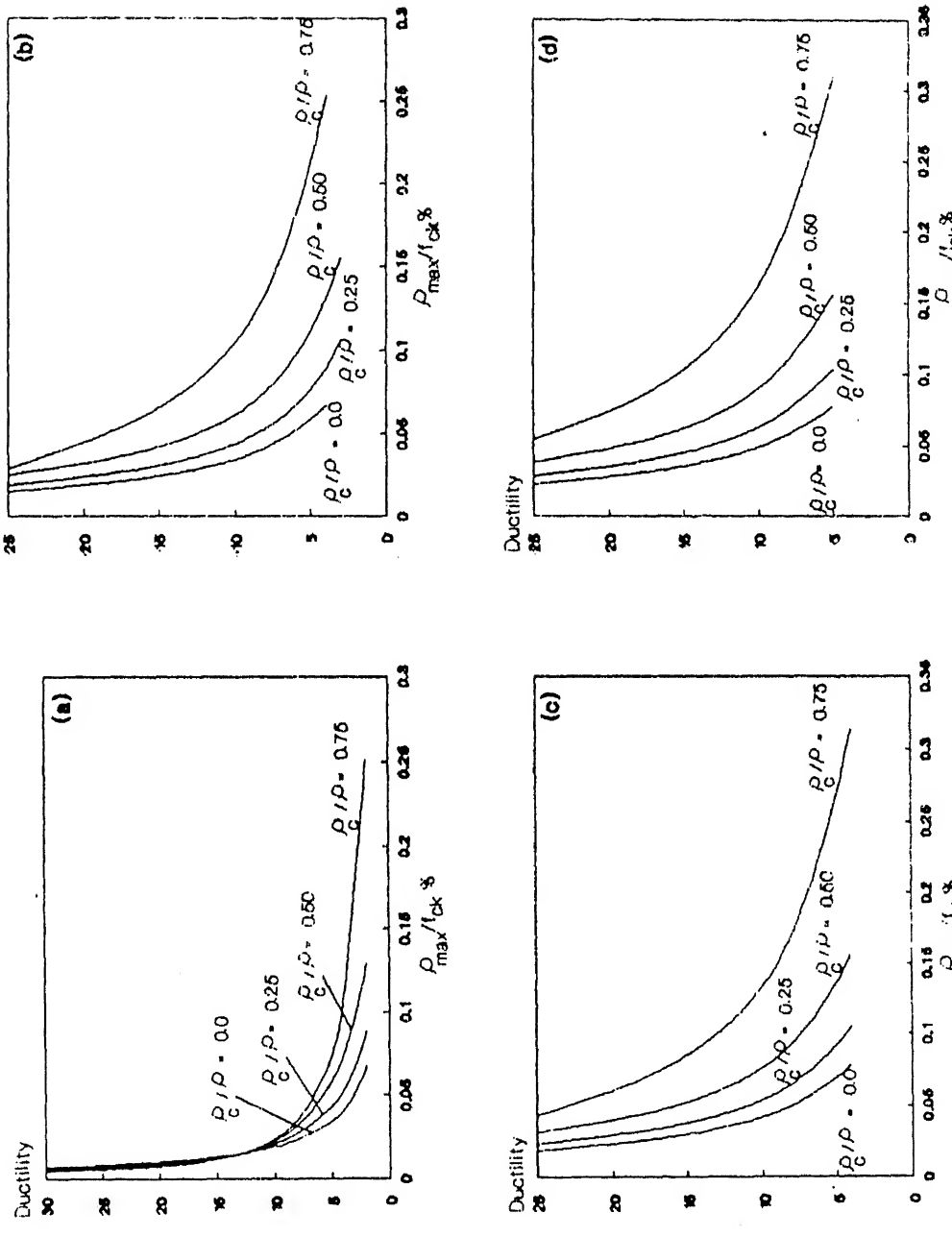

Fig. 2.10 Variation of ductility for beams with HYSD (f_y = 415 MPa.)

(a) ρ'' = 0.0%
(b) ρ'' = 0.50%
(c) ρ'' = 0.75%
(d) ρ'' = 1.00%

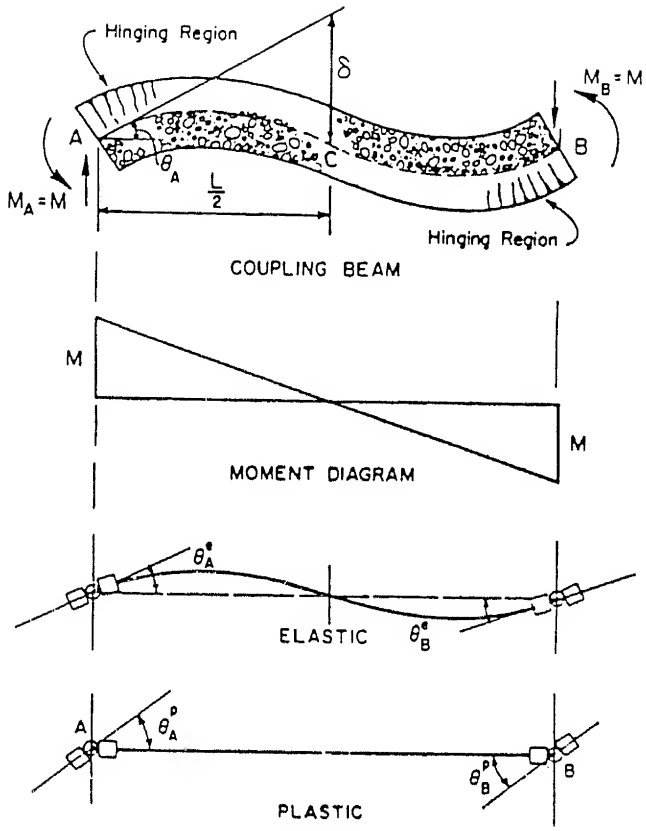

a) Beam element.

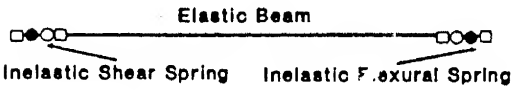

b) Beam element with flexural and shear springs.

Fig. 2.11 Single-component model (Saatcioglu, 1991)

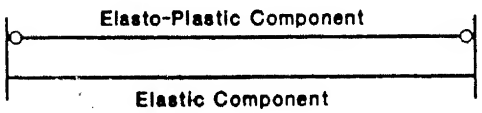

Fig. 2.12 Dual-component model (Clough et al., 1965; reported by Saatcioglu, 1991).

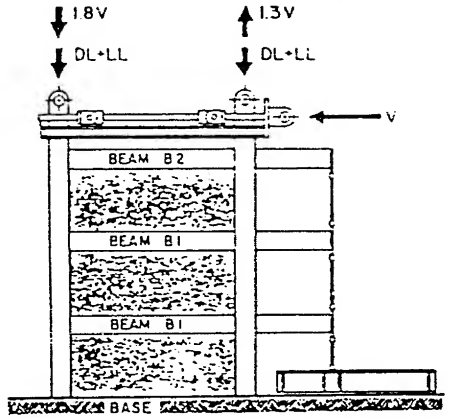

Loading pattern used for infilled frames

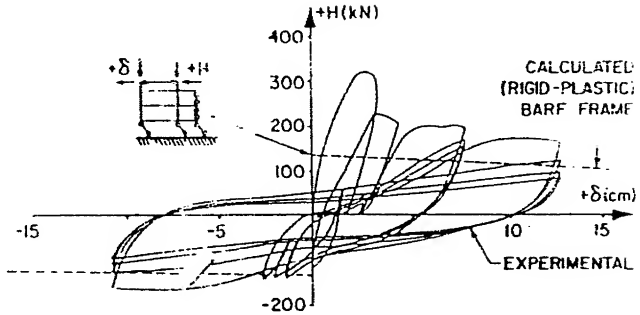

Lateral load-deflection relationship for frame with clay infill

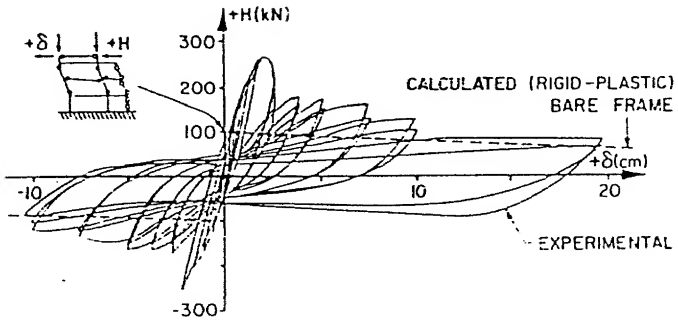

Lateral load-deflection relationship for frame with concrete block infill

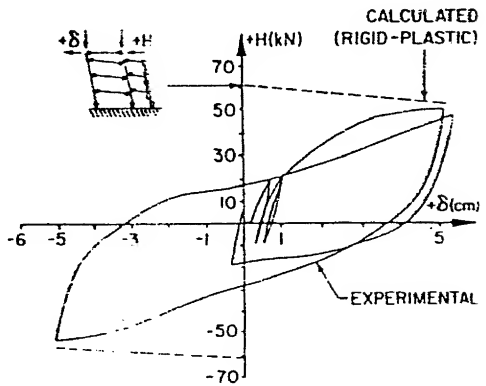

Lateral load-deflection relationship for bare frame

Fig. 2.13 Load-deflection curves for masonry-infilled and bare RC frames (Klingner and Bertero, 1977; reported by Riddell and Newmark, 1979).

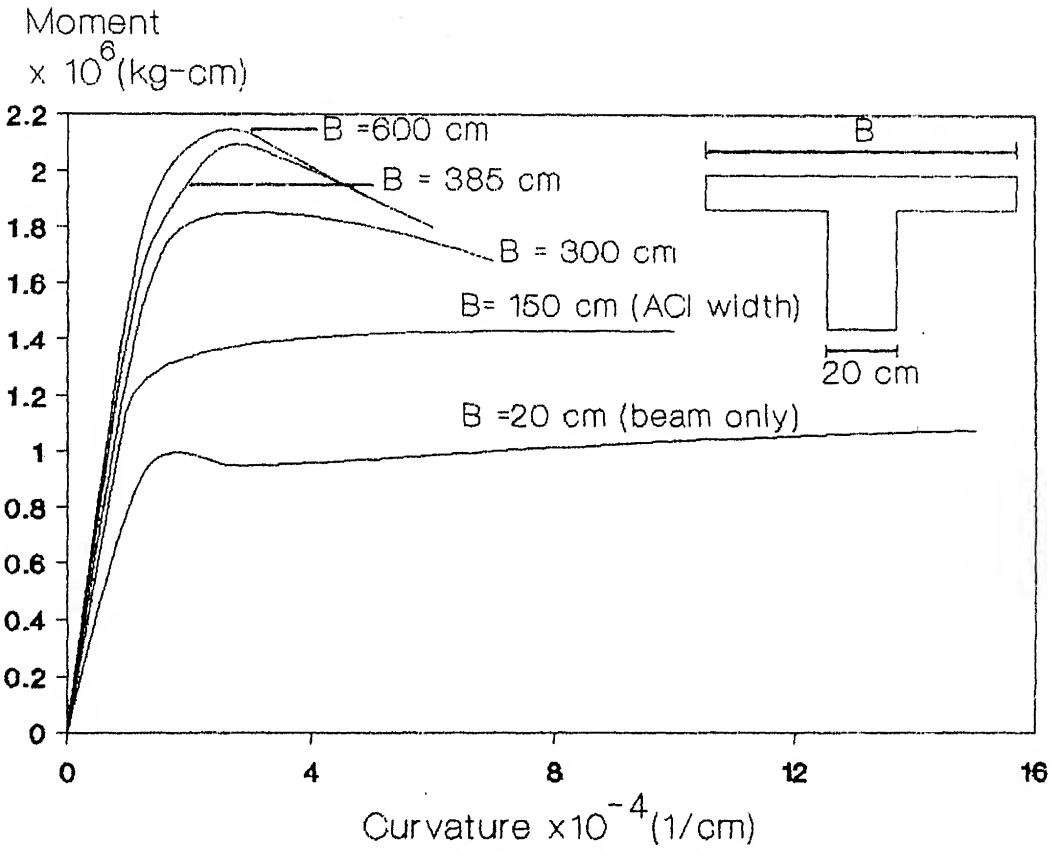

Fig. 2.14 Effect of effective slab width on moment-curvature relationship of a beam section when subjected to negative bending moment (Miranda and Bertero, 1989).

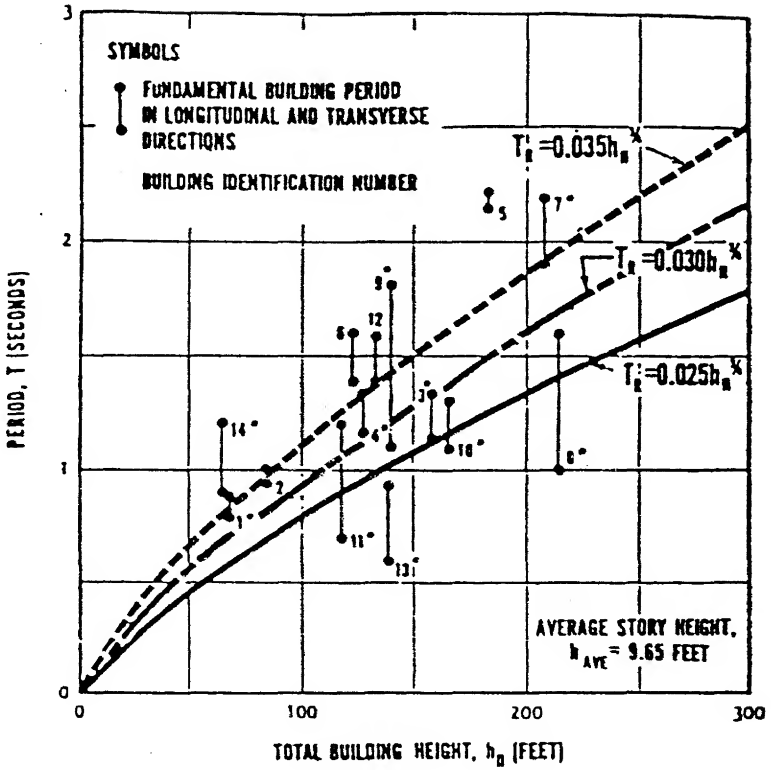

Fundamental period $T \geq C_a T_a$;
where T_a = approximate fundamental period = $C_T h_n^{0.75}$ (NEHRP-1991)

Peak Velocity-Related Acceleration (A_v)	Coefficient C_a
0.4	1.2
0.3	1.3
0.2	1.4
0.15	1.5
0.1	1.7
0.05	1.7

Fig. 2.15 Periods of reinforced concrete frames computed from accelerograph records during the 1971 San Fernando earthquake; and upper limit on calculated period (NEHRP-1991).

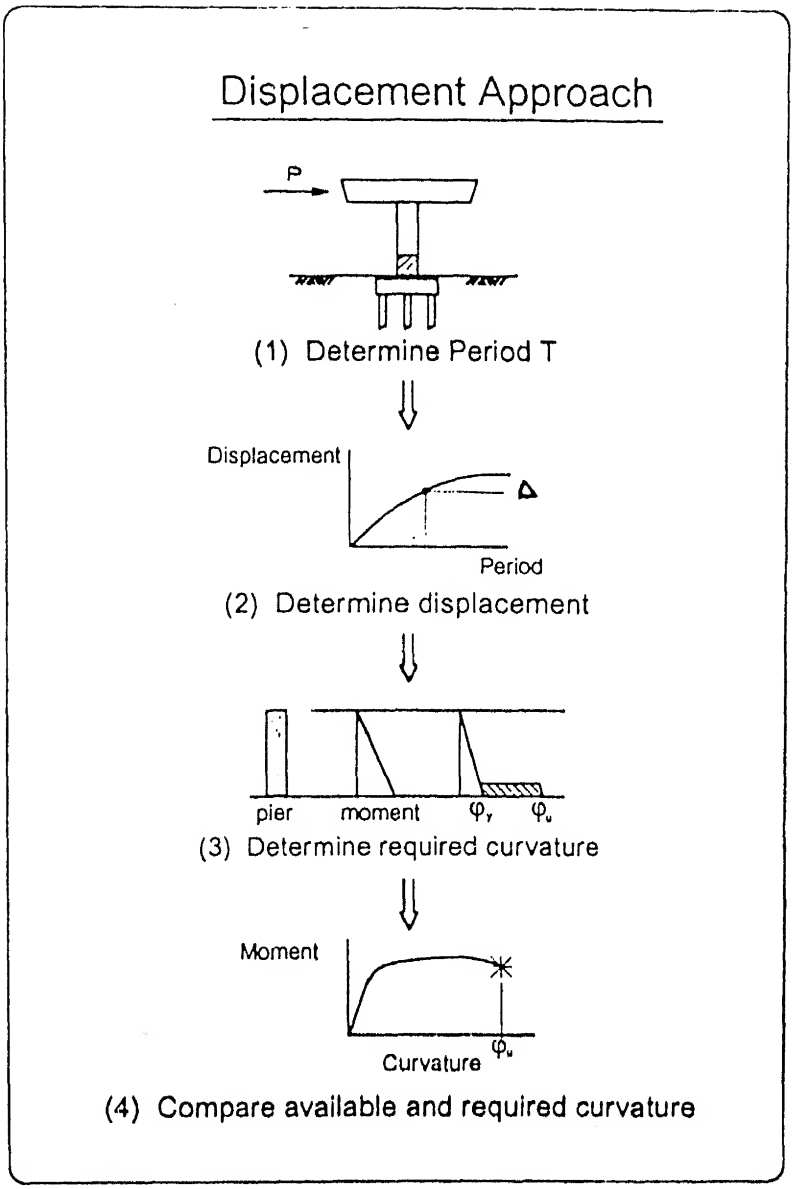

Fig. 2.16 Displacement approach to design (Moehle, 1992a).

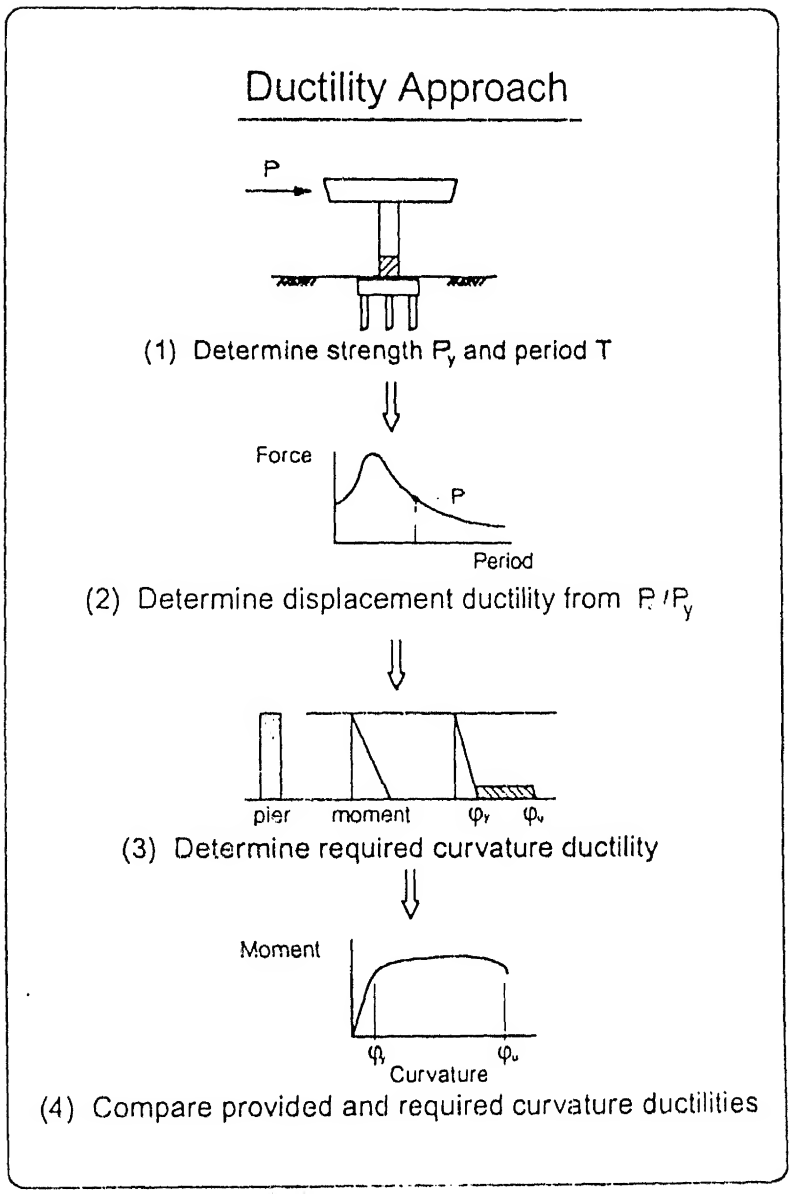

Fig. 2.17 Ductility approach to design (Moehle, 1992a).

CHAPTER III

DUCTILITY AND DISPLACEMENT BASED DESIGN PROCEDURE FOR SEISMIC DESIGN OF REINFORCED CONCRETE FRAMES

3.1 INTRODUCTION

In this chapter, a new Ductility and Displacement Based Design Procedure (DDBDP) is proposed for reinforced concrete frame structures. Ductility, displacement and strength explicitly considered in the proposed procedure. Also, in the method two seismic design levels are considered. The base shear - roof displacement relationship is obtained based on a quasi-static non-linear analysis, and is used to assess the design considering the acceptable displacements, inter-storey drifts, the overall structural ductility, and the resulting requirements on member ductility. If the structure does not satisfy these requirements, it is redesigned to modify its stiffness, strength, or ductility as the need be. This procedure also explicitly accounts for seismic overstrength in the structure. The procedure also indicates approximately the member ductility (curvature ductility) required for different members; this enables the designer to appropriately detail the members requiring high ductility. The latter is particularly useful for irregular building configurations.

3.2 PROPOSED DESIGN METHOD (DDBDP)

Numerical and experimental studies of multi-storey reinforced concrete frames of moderate height have indicated that the seismic response is dominated by response in first mode of vibration (Sozen, 1981; Moehle, 1984; Qi and Moehle, 1991; Moehle, 1992a; Moehle, 1992b;

Otani et al., 1992). In order to obtain the ultimate limit strength of the structure, Otani et al. (1992) indicated that a static non-linear analysis under a monotonically increasing lateral load is desirable, wherein the lateral load profile is proportional to the fundamental mode shape. The limitations of this method are: (1) the method cannot provide the softening part of the force-displacement relationship of the structure; and (2) the force profile in the non-linear range changes as the yielding progresses, and it may differ substantially from that in the linear range.

The proposed DDBDP is based on a displacement-control quasi-static monotonic analysis. First mode shape of the structure is obtained, assuming it to be linear. A lateral displacement profile, proportional to the first mode shape, is forced on the structure. The amplitude of this displacement profile is increased in small increments until yielding starts. During the non-linear response, the increments in the displacement profile are chosen as a function of the normalized incremental displacement profile of the previous stage and first mode shape of the "yielding" structure at that stage, to account for the variation of displacement profile as the yielding progresses. The base shear versus roof displacement relationship thus obtained is used to characterize the overall structure response (Fig. 3.1). This removes both the problems mentioned above in the force-control method.

The DDBDP considers two design levels; serviceability limit state (SLS) and ultimate limit state (ULS). The design ground motions are specified through linear elastic design spectra, one corresponding to each limit state. These spectra are based on the seismic risk and ground motion characteristics of the region. Unlike the usual design spectra, these may not depend on properties of the structure. The design criteria

then consists of specifying strength at SLS, displacement limits (overall drift and inter-story drift) for both the limit states, and the ductility requirements for ULS. For instance, the design requirements would be:

(a) the design capacity of members should be equal to or more than the forces induced by SLS spectrum;

(b) the overall displacement and inter-story drift at SLS and ULS should not exceed the specified values; this is to limit the overall damage to the non-structural elements and structural systems;

(c) the structure should have adequate overstrength and ductility to satisfy the design spectrum at ULS;

(d) the maximum displacement ductility of the structure at ULS should not exceed a specified value ($\mu_{s(max)}$); this is to restrict ductility demand on the structure, and hence on the members, and thereby limiting damage to individual members; it could be different for different usage of buildings and could also depend on frequency of earthquake occurrence;

(e) the members should have adequate curvature ductility consistent with the ductility demand at the ULS; and

(f) in addition, there may be a requirement that the structure should possess, at least, a specified minimum ductility ($\mu_{s(min)}$).

The drift limits at both design levels are to be selected considering the building occupancy and its importance, acceptable damage to the structural and non-structural elements, and human discomfort under frequent minor or even occasional moderate shaking. Based on past earthquake experience, range for these limits suggested in the literature is 0.0025 to 0.005 at SLS (UBC-1991), and 0.01% to 0.015% at ULS (Bertero et al., 1991).

The structure is first designed and detailed for forces induced by SLS spectrum as per usual code design procedures. The requirements for overall displacement and inter-story drift at SLS are checked; if these are not satisfied the lateral stiffness of the structure must be increased. The base shear - roof displacement relationship of the structure is obtained by carrying out the proposed displacement-control quasi-static non-linear monotonic analysis. Using this plot, seismic overstrength (Ω) is obtained as ratio of the actual yield strength of the structure (P_y) to the design seismic force (P_w). Also, the required ductility reduction factor (R_μ) is computed by dividing the elastic design force at ULS (P) by the actual yield strength of the structure (P_y). The required displacement ductility (μ_r) is then obtained using a suitable expression relating R_μ with μ_r. The required displacement ductility (μ_r) should be less than the maximum level of displacement ductility permissible, $\mu_{s(max)}$; if this is not so the structure must be redesigned for higher lateral force. In case the required ductility (μ_r) is less than the minimum specified displacement ductility ($\mu_{s(min)}$), the structure should still be detailed to have a ductility of at least $\mu_{s(min)}$. It is checked whether the structure can provide the required displacement ductility (μ_r), avoiding undesirable yield mechanisms and collapse. In case the structure cannot provide the required ductility, some of the members may be redesigned to have increased ductility. However, if the member ductility cannot be increased adequately to ensure the minimum overall structural ductility (μ_r), the structure has to be redesigned for a higher lateral force to reduce the ductility reduction factor (R_μ) and hence the ductility demand (μ_r) on the structure. At the deformation corresponding to the required displacement ductility (μ_r), the overall displacement and inter-storey drift are

checked to ensure that these are within the permissible limits. In case of unacceptable overall drift or ISD, stiffness of the entire structure or of some storeys must be increased. Then, the curvature ductility demand on individual members is obtained and amplified appropriately to account for the effects of hysteretic behaviour. Finally, the members are redetailed, if required, to ensure that they can fulfill the curvature ductility demand.

The actual overstrength of the building will significantly affect the value of μ_r. Navin and Jain (1993) have carried out a parametric study on seismic overstrength in RC frame by varying the seismic zone, number of storeys, and live load. The same buildings are used here to illustrate some of the design implications of DDBDP. 3-storey and 9-storey frames are designed for seismic zones II, III, and IV as per the Indian codes. Table 3.1 gives the unfactored seismic design force (P_w) which really corresponds to the SLS design. It has been assumed that the ULS level (P) is 12 times the SLS design ($P = 12\ P_w$). Thus, $R_w = 12$ for all the frames. The value of seismic overstrength (Ω), shown in Table 3.1, are as per Navin and Jain (1993). For these values of R_w and Ω, it is obvious that there is a large variation in required R_μ, and hence in μ_r. The displacement ductility demand varies from 1.56 to 4.94. Let the acceptable displacement ductility be in the range 2 - 4 for hospital building and 1.5 - 6 for residential buildings. Thus, the calculated value of ductility requirement for each of these buildings is acceptable, provided the building is a residential one. However, if the building is to be used as a hospital, the 9-storey frame in zone V requires more ductility ($\mu_r = 4.94$) than what can be acceptable ($\mu_{s(max)} = 4$) from damage consideration; in this case the building should be designed for higher seismic force and thus R_w should be reduced. Also,

even though the 3-storey building in zone II requires a ductility of only 1.56, if to be used as a hospital, it should be detailed to have a ductility of at least 2.0.

As discussed in Section 2.5.5, it is difficult to quantify the actual lateral stiffness of a building accurately. If the initial stiffness used in the proposed quasi-static non-linear analysis is less than the realistic stiffness, the fulfillment of drift requirements based on the non-linear analysis will be conservative. In case the analytical model for non-linear analysis gives unduly low stiffness, one could adjust the displacement and drift calculations as shown in 3.4.

The proposed DDBDP requires more computations than the present code-specified design procedures. Hence, a procedure such as this is not meant to be a substitute in the near future to the codal procedures for ordinary buildings of regular configurations. However, for important buildings, buildings with irregular configuration, and to prevent large structures from excessive flexibility, this procedure could be made mandatory.

3.3 THE DDBDP ALGORITHM

The basic steps of the proposed design method (DDBDP) are outlined as follows. A flow chart type algorithm is given in Fig. 3.2.

1. Read the linear elastic design spectrum corresponding to the ultimate limit state (ULS); say the seismic force obtained is P. Also, read the linear elastic design spectrum corresponding to the serviceability limit state (SLS), let the force be P_w.
2. Considering to the type of building, its redundancy, importance, and its occupancy, select the minimum required displacement ductility ($\mu_{s(min)}$) and the maximum usable displacement ductility ($\mu_{s(max)}$).

3. Depending on the building usage, decide the maximum allowable overall displacement and inter-storey drift at the SLS (Δ_w, and ISD_w, respectively) and at ULS the ($\Delta_{max(n.l.)}$ and ISD_{max}, respectively).
4. Design and detail the structure as per usual seismic design code procedures for the design force corresponding to the SLS (P_w).
5. Calculate deformations in the structure due to the lateral loads corresponding to the SLS (P_w) to check if the overall drift and inter-story drift (Δ_w, and ISD_w, respectively) are within acceptable limits. If not, the structure must be redesigned to have higher lateral stiffness.
6. Conduct the proposed quasi-static non-linear analysis to obtain the base shear - roof displacement plot.
7. From the base shear - roof displacement plot, obtain the overstrength factor (Ω) as ratio of the actual yield strength of the structure (P_y) to the design force at SLS (P_w).
8. Calculate the required ductility reduction factor, R_μ ($= \frac{P}{P_w \times \Omega}$). Calculate the required displacement ductility (μ_r) using a suitable empirical expression relating μ_r and R_μ.
9. If μ_r is less than the minimum required displacement ductility $\mu_{s(min)}$, then the structure should still be detailed to have ductility of at least $\mu_{s(min)}$. If μ_r is higher than $\mu_{s(max)}$ then the design is unacceptable. In this case, lateral strength of the structure must be increased by redesigning it for higher lateral force and the process repeated from step 4.
10. Check if the structure can provide the required displacement ductility, μ_r. If not, either a few members may have to be redetailed for increased member ductility, or the structure has to be redesigned for higher lateral force to reduce R_μ and hence the ductility demand

on the structure.

11. Calculate the maximum non-linear displacement ($\Delta_{max(n.l.)}$) as the product of the required displacement ductility (μ_r) and the computed yield displacement of the structure (Δ_y).

12. At $\Delta_{max(n.l.)}$, check if the overall drift and inter-story drift satisfy the acceptable limits. In case of unacceptable overall drift, the structure must be redesigned to have higher lateral stiffness. In case the inter-storey drift for a certain storey transgresses the permissible limit, the stiffness of the storey must be increased.

13. At $\Delta_{max(n.l.)}$, observe the plastic hinge pattern in the structure. It is preferable to have plastic hinges in the beams rather than in columns. Formation of plastic hinges at both ends of column elements may lead to excessive storey drift which is not desirable; in that case, the column strength must be increased. Also, check if any plastic hinge exceeds its failure curvature, if so, redesign the defective element by increasing its curvature ductility.

14. Amplify the curvature ductility demand on individual members appropriately to account for the effects of hysteretic behaviour. Ensure that the members fulfill the enhanced curvature ductility demand.

3.4 STIFFNESS CORRECTION

Lateral stiffness of a building has different implications on seismic design criteria. For calculation of design seismic force, it is unconservative to make a low estimate of the stiffness, which leads to high time period and hence lower design seismic coefficient. This has been recognized by many codes (e.g., NEHRP-1991) which now prescribe a lower bound on the stiffness that can be used for this purpose.

However, for the deflection criteria, it is unconservative to make a higher estimate of the stiffness.

As discussed in section 2.5.5, there remain numerous difficulties in correctly modelling the lateral stiffness of RC buildings. Quite often, the analytical models used for non-linear analysis are very flexible. Therefore, if the design force corresponds to the code-specified lower bound stiffness while the deflection criteria is checked based on such a flexible model, the entire approach will be quite conservative.

For instance, consider the load-displacement relationship for a RC building with brick infills (Fig. 3.3). Curve 1 shows the actual relationship, while curve 2 shows the relationship as is often obtained from a non-linear analysis; the two have a significant difference in initial stiffness. Now, if the deflection criteria in DDBDP is based on curve 2, this may at times be too conservative. For example, the deflection at ULS as obtained by curve 2 (Δ_{u2}) is much higher than the deflection one would expect in the real building (Δ_{u1}). To take care of this difficulty, the following approach could be used.

It may sometimes be possible to carry out a somewhat realistic assessment of stiffness by means of a linear elastic analysis. Such analysis could consider many of the stiffness contributions which are often ignored in non-linear analysis. One could then bench mark the deflection criteria based on the more realistic initial stiffness obtained by the linear analysis. For the example structure of Fig. 3.3, one would then take Δ_{w3} as deflection at SLS and Δ_{u3} as the deflection at ULS. Thus, while the deflection profile at ULS will be given by the quasi-static displacement-control non-linear analysis, the magnitude of deflection at roof in ULS will be based on a somewhat more realistic

assessment of lateral stiffness. Again, to safeguard against unduly large lateral stiffness, the codes could give a conservative empirical relationship for lower bound on natural period for drift calculation; this lower bound will govern only the deflection criteria and not the design force calculation.

Nevertheless, a great deal of uncertainty remains regarding the lateral stiffness calculation for building systems, and extensive experimental and analytical studies focused on this issue are required.

Table 3.1 Overstrength and Ductility of Example 3- and 9-Storey Buildings in Different Seismic Zones in India

		Zone II	Zone III	Zone V
3-storey	P_w	0.02 W	0.04 W	0.08 W
	P	0.24 W	0.48 W	0.96 W
	R_w	12	12	12
	Ω (*)	7.7	4.35	3.3
	R_μ	1.56	2.76	3.64
	μ_r	1.56	2.76	3.64
9-storey	P_w	0.0114 W	0.0228 W	0.0456 W
	P	0.1368 W	0.2736 W	0.5472 W
	R_w	12	12	12
	Ω (*)	5.54	3.33	2.43
	R_μ	2.17	3.60	4.94
	μ_r	2.17	3.60	4.94

W = active seismic weight of the building

(*) from Navin and Jain (1993)

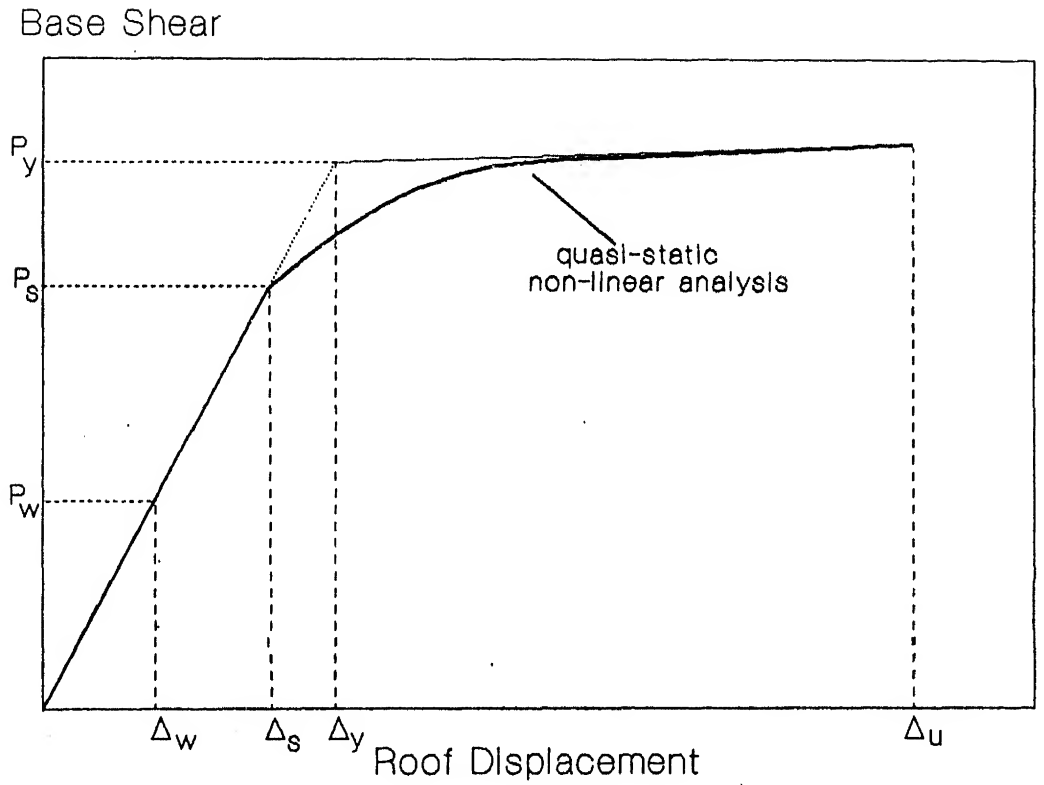

Fig. 3.1 Computed structure response.

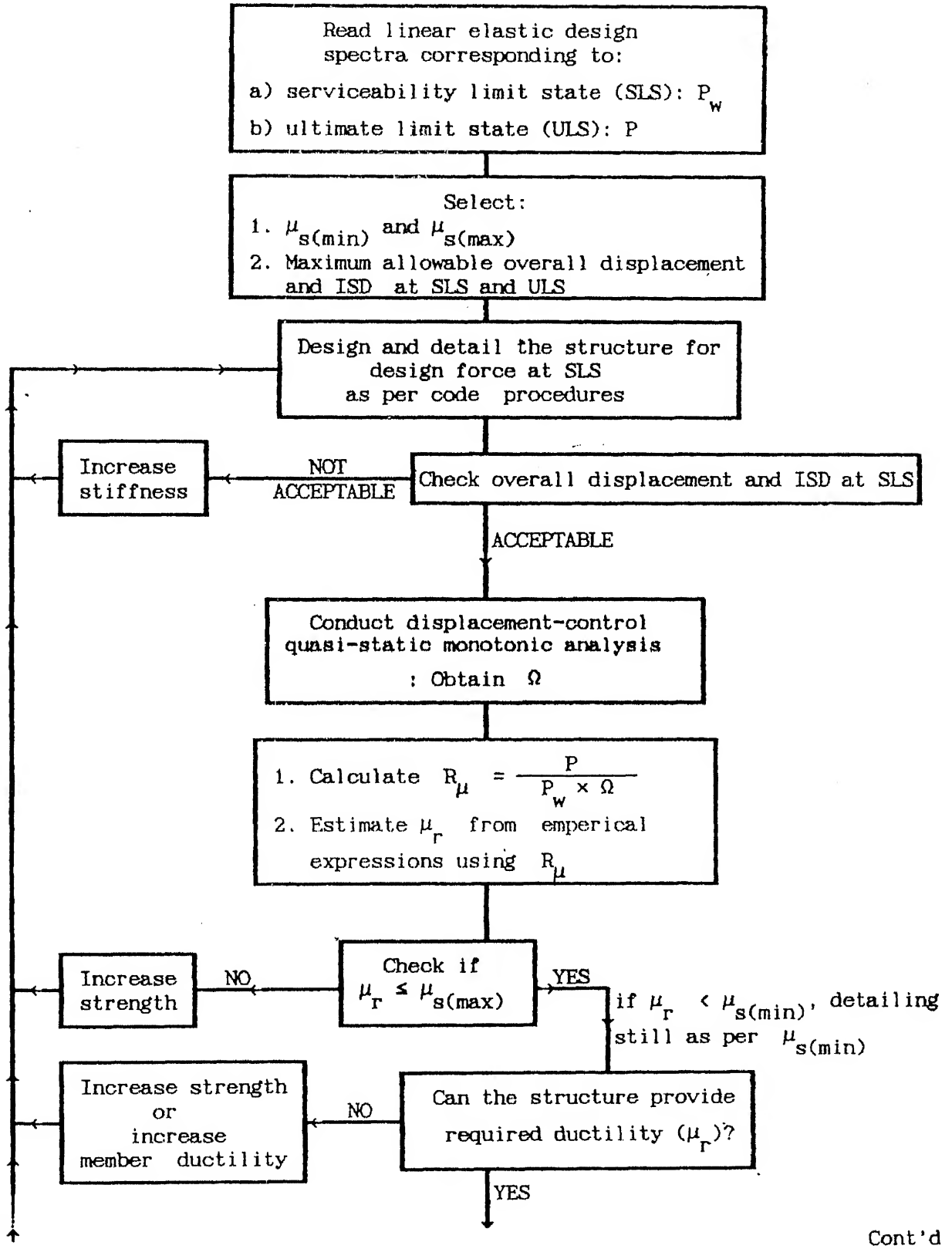
Read linear elastic design spectra corresponding to:
a) serviceability limit state (SLS): P_w
b) ultimate limit state (ULS): P
Select:
1. $\mu_{s(min)}$ and $\mu_{s(max)}$
2. Maximum allowable overall displacement and ISD at SLS and ULS
Design and detail the structure for design force at SLS as per code procedures
Check overall displacement and ISD at SLS
NOT ACCEPTABLE
Increase stiffness
ACCEPTABLE
Conduct displacement-control quasi-static monotonic analysis : Obtain Ω
1. Calculate $R_\mu = \frac{P}{P_w \times \Omega}$
2. Estimate μ_r from emperical expressions using R_μ
Check if $\mu_r \leq \mu_{s(max)}$
NO
Increase strength
YES
if $\mu_r < \mu_{s(min)}$, detailing still as per $\mu_{s(min)}$
Can the structure provide required ductility (μ_r)?
NO
Increase strength or increase member ductility
YES

Cont'd

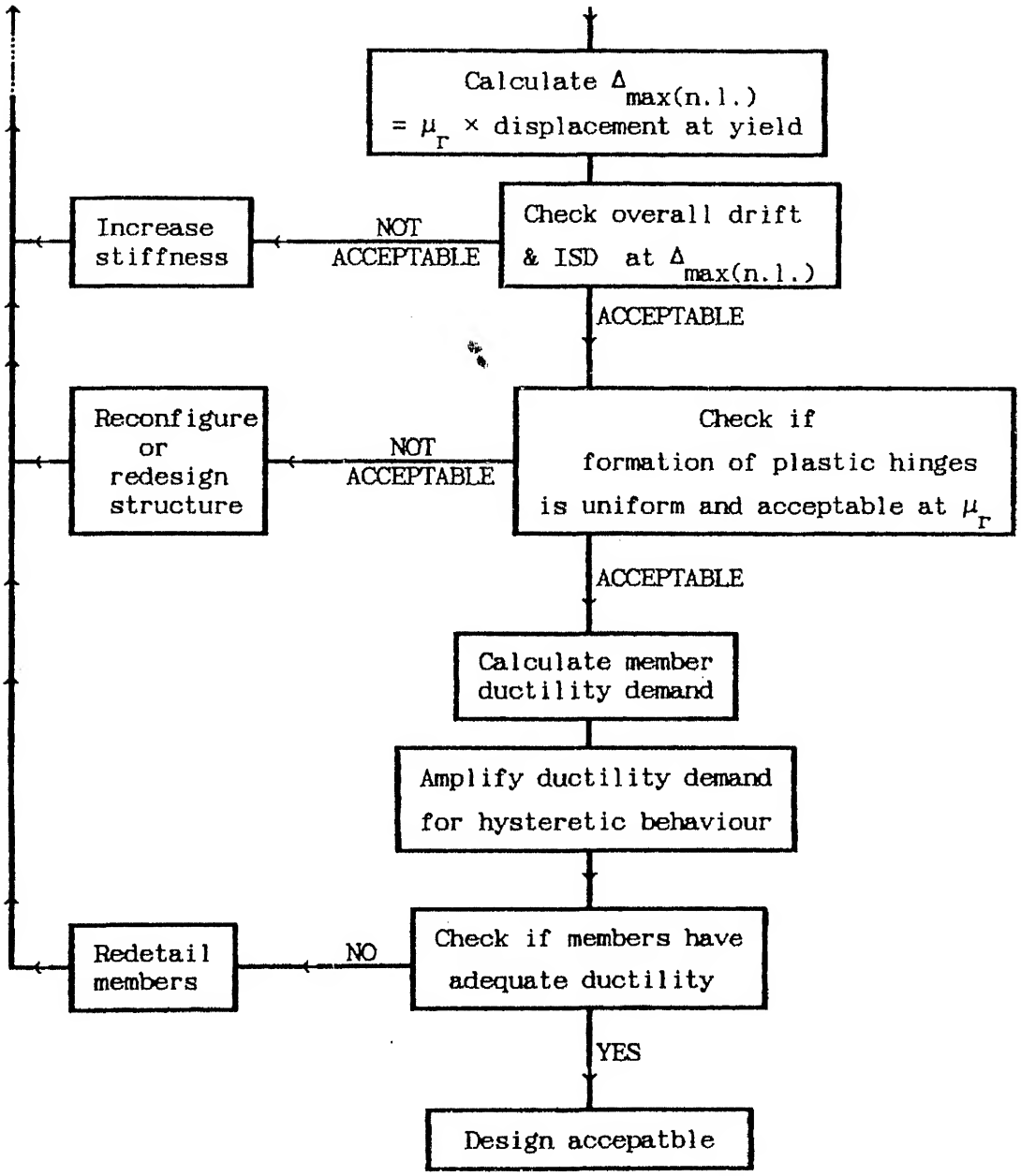

Fig. 3.2 A flow chart of the DDBDP.

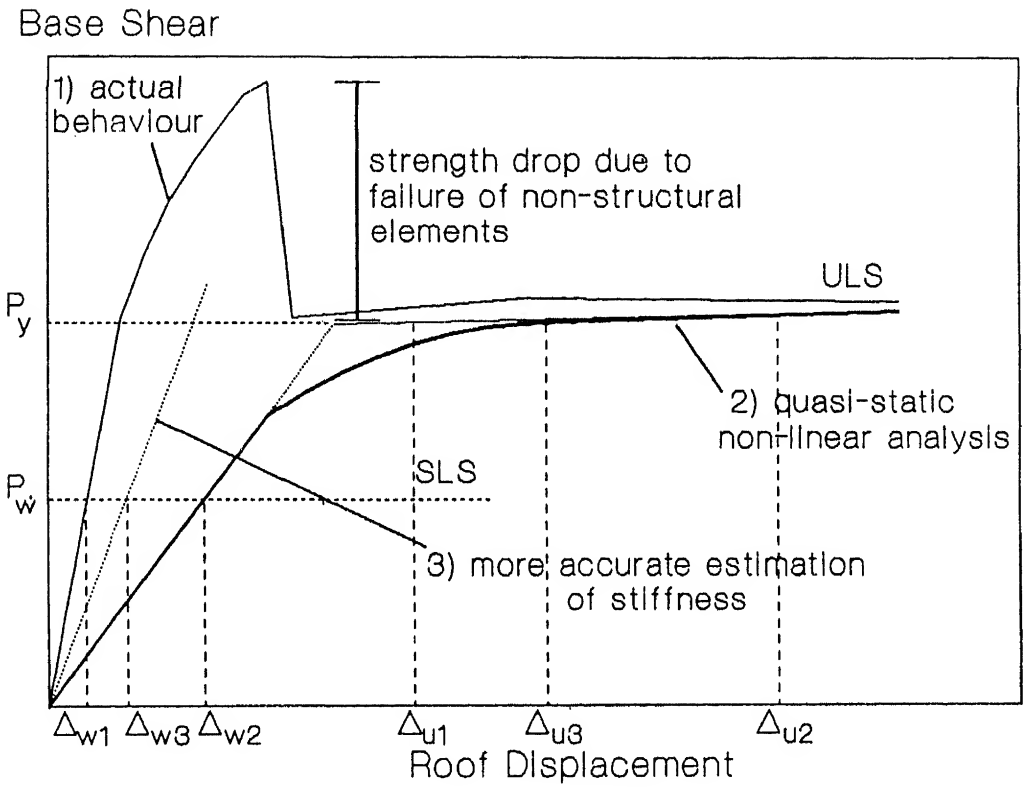

Fig. 3.3 Typical structure response.

CHAPTER IV

DISPLACEMENT-CONTROL QUASI-STATIC NON-LINEAR ANALYSIS

4.1 INTRODUCTION

The seismic behaviour of RC frames depends strongly on the structural configuration, stiffness, strength, and ductility. From design view point, it is important to know the overall inelastic performance of the structure and its displacement ductility. The base shear versus roof displacement relationship is often used to characterize the overall structure response and to determine overall ductility of the structure. This relationship is usually obtained by either a non-linear time-history analysis (MDOF or equivalent SDOF) or a non-linear static analysis (force-control method).

Earlier studies on multi-storey RC frames indicate that the response, in both linear and non-linear ranges, is dominated by the first mode of vibration. In this chapter, this idea is verified by studying four RC frames (1- and 2-bay, 3- and 4-storey frames) under two different earthquake ground motion records using the computer program SARCF (Chung et al., 1988). It is observed that in the loading parts of the linear range and the early stage of non-linear range along the upper bound envelope of the base shear - roof displacement hysteretic curve, the displacement profile along the height is close to the first elastic mode profile. Based on this observation, a displacement-control quasi-static monotonic analysis procedure has been developed to obtain the base shear - roof displacement relationship. A lateral displacement profile, proportional to the first mode shape of the elastic structure treating it as linear, is forced on the structure. The amplitude of this

displacement profile is increased in increments until yielding starts. During the non-linear response, the increments in the displacement profile are chosen as a function of the normalized incremental displacement profile of the previous stage and first mode shape of the "yielding" structure at that stage. The overall structural ductility is then related to the ductility demand on individual members at any deformation stage. Based on this algorithm, a computer program, named MONARCF-DC (MOnotonic Non-linear Analysis of Reinforced Concrete Frames - Displacement Control method) has been developed. For comparison, another version of the program, based on force-control quasi-static monotonic analysis, called MONARCF-FC (MOnotonic Non-linear Analysis of Reinforced Concrete Frames - Force Control method), has also been developed.

4.2 CONTRIBUTION OF FIRST MODE TO THE BUILDING RESPONSE

The contribution of higher modes to seismic response of buildings is small (e.g., Jennings, 1969). Derecho et al. (1986) have stated that "Studies of elastic response of multi-storey frame indicate that for most buildings the fundamental mode contributes about 80% and the second and the third modes contribute about 15%, of the total response". Saiful et al. (1990), through their study on the dynamic response of tall buildings, noted that "In most practical cases the contribution of higher modes, in the elastic range, to the total response is negligible". Many numerical and experimental studies of multi-storey frames of moderate heights have indicated that the displacement response is dominated by response of first mode of vibration (Sozen, 1981; Moehle, 1984; Qi and Moehle, 1991; Moehle, 1992a and 1992b; Otani et al., 1992). In order to carry out an equivalent SDOF non-linear

analysis, a displacement profile and a distribution of lateral resistance are assumed (as discussed in Section 2.5.2). Kaminosono et al. (1984) have discussed the results of a SDOF pseudo-dynamic test for a 7-storey building provided with shear walls. In their experimental study, they have used a displacement profile close to the fundamental mode shape. Based on analytical study of the same building, they also noted that the deflection profile does not change significantly regardless of magnitude of the force and the mode is nearly identical in elastic, inelastic and mechanism ranges. Fajfar and Fischinger (1987) have performed a non-linear equivalent SDOF time-history analysis for the same 7-storey building, using the fundamental mode shape of the building as the displacement profile. Shing and Mahin (1985) state that "for most structures tested by the pseudo-dynamic method, the response is dominated by the fundamental frequency. Spurious higher-mode response can be excited by experimental errors".

It, therefore, appears reasonable to expect that the seismic response of multi-storey buildings, in elastic as well in inelastic ranges is generally governed by the first mode. To confirm this, a limited parametric study has been conducted on four example frames by carrying out a non-linear time-history analysis using the program SARCF.

4.2.1 EXAMPLES

Four reinforced concrete plane frames were analyzed; 1-bay 3-storey frame, 2-bay 3-storey frame, 1-bay 4-storey frame, and 2-bay 4-storey frame. The storey height is 4.40 m for the first storey and 3.20 m for the upper storeys. Details of these frames are given in Fig. 4.1. The cross sections of the columns and beams are 500 × 500 mm and 250 × 600 mm, respectively. The reinforcement details for columns and beams are

presented in Table 4.1. The stirrups at column ends provide confinement of 0.76% and 1.20% for the 3-storey and 4-storey frames, respectively. The stirrups at beam ends provide a confinement of 0.72% for 3-storey frames and 1.14% for 4-storey frames. The calculated fundamental time periods, assuming concrete section is cracked, for the 1-bay 3-storey frame, 2-bay 3-storey frame, 1-bay 4-storey frame, and 2-bay 4-storey frame are 0.967 sec, 0.909 sec, 1.165 sec, and 1.09 sec, respectively.

The frames were analyzed first under gravity load (dead load + 25% live load). Then they were subjected to the first 7.68 seconds of twice the N-S component of El Centro accelerogram (Imperial Valley earthquake of May 18, 1940), and to four times the first 8.40 seconds of the S69E component of Taft Lincoln accelerogram (earthquake of July 21, 1952), one at a time. These accelerograms are shown in Figs. 4.2 and 4.3. The amplification factor and the accelerogram duration for these earthquakes were selected (a) in order to minimize the computational effort; and (b) such that the accelerogram duration contains the most strong records which are sufficient to produce at least four hysteretic non-linear cycles of response. The four examples (1-bay 3-storey, 2-bay 3-storey, 1-bay 4-storey, 2-bay 4-storey) are labelled according to the accelerogram they were subjected to as: EC1, EC2, EC3, and EC4 for El Centro accelerogram, respectively, and ET1, ET2, ET3, and ET4 for Taft accelerogram, respectively. The time increment for integrating the equations of motion for both accelerograms, was taken as 0.01 second.

4.2.2 RESULTS

The time-history plots of base shear and roof displacement, and the base shear versus roof displacement hysteretic response curves and the corresponding outer envelopes for the eight examples are shown in Figs.

4.4 to Figs. 4.11. The time instant of a plastic hinge occurrence and the sequence of plastic hinges, for these examples, are given in Tables 4.2 to 4.5.

a- Structure Response

The base shear - roof displacement hysteretic response is nearly linear upto the formation of the first plastic hinge. The elastic stiffness of the structure may be defined by connecting the first yield points in positive and negative directions. In all the eight examples, plastic hinges occurred first in beam elements. The yielding in beam elements did not change significantly the overall lateral stiffness of the structure. After the formation of plastic hinges in columns, the overall structure stiffness decreased significantly. The outer envelope of the non-linear part of the base shear - roof displacement hysteretic curve characterizes the non-linear load - displacement relationship of the structure under a particular earthquake. From the eight examples, it is observed that the outer envelope curve after yield may show the following trends:

1) An increase in the displacement along with slight increase in the base shear force in both the positive and negative directions, as seen in examples EC1 and EC2 (Figs. 4.4 and 4.6). The positive and negative envelopes, for these two examples, are approximately the same.
2) The outer envelope is not so well defined in one direction as seen in in examples ET1, ET2, ET3, and ET4 (Figs. 4.5, 4.7, 4.9, and 4.11, respectively). It was noted that the outer envelope in the other direction represents the upper bound of the structure response.
3) An increase in the displacement along with slight increase in base

shear upto a point which represents the maximum base shear force the structure can sustain. Beyond this point, as the displacement increases, the base shear force decreases as in examples ET1 and ET2 (Figs. 4.5 and 4.7, respectively).

4) Beyond the yield point of the structure, as the displacement increases the base shear force decreases as seen in examples EC3, ET3, EC4, and ET4 (Figs. 4.8, 4.9, 4.10, and 4.11, respectively).

It was also noticed that the yield point in any given example is almost the same from either of the two time-histories, i.e., the elastic structure stiffness and the base shear at yield condition are about the same, even though different seismic motions were applied. It may be concluded that each structure has a somewhat unique maximum upper bound base shear - roof displacement relationship. This relationship can be idealized by a trilinear curve (Fig. 4.12). The first part of the curve presents the elastic stiffness of the structure. The second part is an ascending curve (the "strain hardening" part). The third part of the curve is a descending curve which presents "softening" of the structure.

b- Plastic Hinge Sequence

Tables 4.2 to 4.5 provide the time instants at which hinges form in the frames. Comparison of these time instants with base shear - time histories in Figs. 4.4 to 4.11 indicate that plastic hinges do not form during the unloading and when the reloading is below the first positive and the first negative yield points of the structure. Plastic hinges are found to form along (or close to) the outer envelope of the base shear - roof displacement hysteretic curve. In examples ET3 and ET4, failure takes place at t = 6.60 sec and t = 7.91 sec, respectively; thereafter, several plastic hinges occurred; these hinges do not form on the outer

envelope. In identical examples, though the frame is subjected to two separate accelerograms, it is observed that the sequence of plastic hinges (in beams and columns), in the first significant non-linear cycle of loading, is somewhat similar and at approximately the same roof displacement.

c- Lateral Displacement Profile Along the Height

Fig. 4.13 shows the vertical displacement profile of the frame at different time instants for example EC1. The following observations about the displacement profile can be made from this figure. These observations were also confirmed on the other seven examples.

1. During the elastic loading and unloading in both directions, the base shear - roof displacement relationship is almost linear (curve 0-1-2). The lateral displacement profile along the height for the loading and reloading parts (a and c) in both directions, is close to the first mode shape of the structure, while in the unloading part (b) the profile may take a different shape.
2. The first plastic hinge occurred in a beam element (point 2). The stiffness of the structure does not change significantly as shown by curve 2-3 in the figure. In this range, the lateral displacement profile (d) is still close to the first mode shape.
3. During the inelastic unloading (curve 3-4), the lateral displacement profile (e) is parabolic and the middle storeys show higher displacement than the roof displacement. From point 4 to point 5, a negative reloading cycle takes place, and during this stage, the displacement profile returns to be close to first mode shape (f).
4. During the unloading part (curve 5-6) and the reloading part (curve 6-7), the displacement profile takes different shapes as shown by g

and h, respectively. In the reloading part, (curve 6-7) the lateral displacement profile (h) is parabolic with a higher displacement at a lower floor than that at the roof. This explains the occurrence of high base shear with less roof displacement.

5. At point 7, a plastic hinge occurs at the base of a column at the foundation level. The stiffness of the structure decreases significantly, as shown by the curve 7-8. Within the non-linear loading (curve 7-8), the lateral displacement profile (i) along the height is close to first mode shape of the structure.
6. During an unloading and subsequently reloading in the opposite direction (curve 8-9-10-11-12-13), the cracks formed at the plastic hinges start to close. This results in the "pinching" characteristics as shown at points 9 and 11. In spite of the occurrence of plastic hinges, a significant amount of strength is observed (curve 12-13). The lateral displacement profile (j) along the curve 12 -13 is close to the first mode shape.
7. After several cycles of loading and unloading, the structure may loose strength gradually, i.e., the structure is tending to collapse. In examples EC1, EC2, and ET2, the structures did not collapse, while in examples ET1, EC3, ET3, EC4, ET4, they did.

It is seen that during the elastic loading (curve 0-1, curve 1-2, and curve 4-5) and inelastic loading (curve 2-3, curve 7-8, and curve 12-13), the lateral displacement profile along the height is close to the fundamental mode shape of the structure.

The lateral displacement profile along the height during linear loading and during the first significant non-linear loading cycle, for the four frames, are given in Tables 4.6 to 4.13. These tables compare the lateral displacement profiles with first elastic mode shapes keeping

the roof displacement same. The percentage difference (ξ) is calculated as

$$\xi = \frac{\left(\frac{\Delta_i}{\Delta_f}\right) - \Phi_i}{\Phi_i} \times 100 \qquad (4.1)$$

where Δ_i is the lateral displacement at floor i; Δ_f is the roof displacement; Φ_i is the value of normalized mode shape at the i^{th} floor. ξ thus obtained gives a somewhat higher indication of deviation from first mode shape. The actual deviation may be quantified by comparing the normalized lateral displacement profile with first mode shape without keeping the same roof displacement; this can be done using regression analysis.

In example EC1 (Table 4.6), five points (time instants) are selected to deduce the difference in the linear range and four points in the non-linear range. In the linear range, ξ at the second floor varies from 0.08% to 3.5%, and at the first floor from 0.4% to 8.2%. In the non-linear range, ξ varies from 1.8% to 3.9% at the second floor and from 1.6% to 9.7% at the first floor. In example ET1 (Table 4.7), displacement profile has been given at four points in the linear range and five points in the non-linear range. In the linear range, ξ ranges from 0.43% to 7.0% at the second floor, and from 2.1% to 12.5% at the first floor. In the non-linear range, ξ varies from 2.2% to 3.1% at the second floor, and from 4.5% to 7.3% at the first floor.

Similarly, Tables 4.8 to 4.13 show that the variation in displacement profile from that for the first mode is small. For the 2-bay 3-storey frame, in the linear range, ξ varies from 0.12% to 5.9% at the second floor, and from 0.43% to 10.0% at the first floor; in the non-linear range, ξ varies from 0.4% to 4.0% at the second floor, and

from 0.55% to 14.9% at the first floor. For the 1-bay 4-storey frame, in the linear range, ξ varies from 1.2% to 4.0% at the third floor, 0.88% to 7.1% at the second floor, and from 1.7% to 10.8% at the first floor; and in the non-linear range, ξ varies from 0.0% to 4.5% at the third floor, 0.46% to 7.8% at the second floor, and from 0.89% to 14.5% at the first floor. For the 2-bay 4-storey frame, in the linear range, ξ varies from 0.47% to 1.5% at the third floor, 0.33% to 7.8% at the second floor, and from 0.03% to 8.4% at the first floor; in the non-linear range, ξ varies from 0.03% to 1.9% at the third floor, 0.12% to 4.5% at the second floor, and from 1.4% to 10.0% at the first floor.

d- Summary of the Results

From the foregoing results, it is seen that:

1. The structure has a maximum upper bound envelope for the base shear - roof displacement relationship. This relationship may be idealized by a trilinear curve (Fig. 4.12); linear part, non-linear hardening part, and non-linear softening part.
2. Plastic hinges form along the upper bound envelope of the structure. In the first significant non-linear cycle of loading, the sequence of plastic hinges may not significantly vary from one ground motion to another.
3. In the linear range, the lateral displacement profile along the height (a) is close to first mode shape during loading and reloading; and (b) takes different shape during unloading.
4. In the non-linear range, along the upper bound envelope, the lateral displacement profile along the height is close to first mode shape.
5. Thus, along the upper bound envelope of the base shear - roof displacement curves, which represents the maximum response of the

structure, the contribution of higher modes, in the linear range and the non-linear range, is small.

4.3 ALGORITHM FOR A PROPOSED DISPLACEMENT-CONTROL QUASI-STATIC ANALYSIS

To overcome the difficulties of the conventional force-control quasi-static analysis, an algorithm has been developed for quasi-static analysis based on displacement control. The procedure consists of forcing on the structure, in small increments, a lateral displacement profile which is proportional to first mode shape of the structure. To account for change in mode shape after yielding in the structure, particularly for buildings with unusual configuration, the displacement profile to be imposed on the structure after yield may be based on the mode shape of structure at that stage of yielding. This could be done in a number of ways. For instance, after yielding, the increments in the displacement profile may be chosen as proportional to the first mode shape of the "yielding structure" at that stage. A limited parametric study was conducted on the eight examples to attempt an algorithm which will give a base shear - roof displacement relationship that is closest to that obtained by the time history analysis using SARCF. The algorithm that was found to be most appropriate consists of applying increments in lateral displacement profile, in the post-yield range, which are a function of the weighted average of incremental lateral displacement profile of the previous step and the mode shape of the structure at that stage of yielding.

The proposed displacement-control quasi-static monotonic analysis is discussed here in greater detail. To begin with, first mode shape $\{\Phi\}$ is obtained assuming the structure to be linear. A lateral displacement profile, proportional to first mode shape, is forced on the structure in

small increments until yielding starts. At each step in the post-yield range, the stiffness matrix of the elements which have yielded is modified as per the moment-curvature relationship of the sections, and consequently the global stiffness matrix is updated. The eigen value problem, at the current step "j", is then solved to obtain the first mode shape of the yielded structure $\{\Phi\}_j$ at that step. The normalized incremental displacement profile $\{S\}_j$, at this step, is computed as $\frac{\left[R_{j-1}\ \{S\}_{j-1} + \Delta f\ \{\Phi\}_j\right]}{R_{j-1} + \Delta f}$; where R_{j-1} is the total roof displacement at the previous step; $\{S\}_{j-1}$ is the normalized incremental displacement profile of the previous step; and Δf is the incremental roof displacement. The incremental displacement profile is calculated as Δf times $\{S\}_j$. From the incremental displacement profile, the incremental nodal rotations are calculated. The total nodal deformations are obtained by adding the incremental deformations to the previous nodal deformations. The incremental nodal forces are computed and added to the total nodal forces obtained from previous steps. At each incremental step beyond yield, the curvature ductility on individual members is also calculated. The process is continued till the structure fails. The steps for the proposed method are as follows:

1. Calculate the positive and negative moment-curvature relationship for the cross-section at each end of all the members. If a plastic hinge is expected to form in the middle of a beam, then the beam is to be sub-divided into two sub-elements.
2. Assuming the structure to be linear elastic, the global stiffness matrix is assembled from beam and column element stiffness matrices. The global stiffness matrix is condensed, using the static condensation technique. Mass matrix is developed and the eigen value

problem is solved to obtain first mode shape.

3. A displacement profile proportional to the first mode shape $\{\Phi\}$, with a small roof displacement (Δf), is imposed on the structure.
4. Rotation at the nodes and the total base shear force are obtained.
5. Moment at each node for each element is calculated. These moments are checked against the yield criteria. If no yielding occurs anywhere, then the imposed lateral displacement on the structure is increased by ($\Delta f\ \{\Phi\}$) and steps 4 and 5 are repeated.
6. At the occurrence of plastic hinge at the end of an element at step "j-1", the stiffness matrix of that element in step "j" is modified by incorporating the inelastic stiffness of the yielded end. A revised global stiffness matrix is assembled. The eigen value problem is again solved to get first mode shape $\{\Phi\}_j$ corresponding to that stage of yielding in structure.
7. The normalized incremental displacement profile, $\{S\}_j$, in the current step (j), is calculated as $\dfrac{\left[R_{j-1}\ \{S\}_{j-1} + \Delta f\ \{\Phi\}_j\right]}{R_{j-1} + \Delta f}$. Hence, the incremental lateral displacement profile is calculated as $\Delta f \times \{S\}_j$ and the incremental joint rotations are then calculated. The total nodal deformations are obtained by adding the incremental deformations to the previous deformations.
8. The incremental nodal forces are calculated using the incremental nodal deformations. The total nodal forces are obtained by adding the incremental nodal forces to the total nodal forces from the previous step. The curvature ductility for the yielded sections is computed and the total base shear is calculated.
9. The incremental procedure is repeated from step 6 until the structure collapses.

4.4 MONARCF-DC PROGRAM

Based on the above algorithm, a computer program named MONARCF-DC (MOnotonic Non-linear Analysis of Reinforced Concrete Frames - Displacement Control method) is developed. MONARCF-DC provides the upper bound envelope of the base shear - roof displacement relationship of a RC frame, the nodal displacement and forces as well as the curvature ductility in individual members at a given roof displacement. The computer program is based on the following assumptions:

1. The structure is idealized as a plane frame.
2. Each member is treated as a massless prismatic line member represented by its centroidal axis. Total mass of the structure is concentrated at the floors levels.
3. Shear deformation in the elements is ignored.
4. The axial deformation in beams and columns is neglected.
5. The P-Δ effect is neglected.
6. The frame is assumed to be fixed at its base.

4.4.1 PRIMARY MOMENT-CURVATURE RELATIONSHIP

The primary moment-curvature relation of the section at the end of an element relating bending moment to curvature under monotonic loading, is idealized by three linear branches, as illustrated in Fig. 4.14. The first branch is for the elastic loading. The second branch is for the inelastic (strain hardening) loading and the third branch is for the inelastic loading beyond the ultimate.

The yield moment (M_y) is defined as the moment at which the steel strain reaches the yield value. The ultimate moment (M_u) and the failure moment (M_f) and the corresponding curvatures ϕ_u and ϕ_f, respectively, depend on the controlling failure mode. The calculation of moments and

curvatures and the definitions of the controlling failure modes are same as those in SARCF.

4.4.2 ELEMENT STIFFNESS MATRIX

The members are modelled in the same manner as by Chung et al. (1988). When the moment at end of a member exceeds the yield moment (M_y), the section yields. Thus, if yielding occurs at both the ends, the member of length L consists of three segments; one segment each at either end (i and j) of the element where yielding has taken place, and an elastic segment in between. The length of inelastic segment at either end is such that moment everywhere in this segment exceeds M_y. Flexural stiffness (EI) of the inelastic segment is obtained corresponding to the maximum moment in the segment and from the moment-curvature relationship. Fig. 4.15 shows the three segments of a member which are:

1. an inelastic segment of length x_i at node i, having a constant stiffness $(EI)^i$;
2. an inelastic segment of length x_j at node j, having a constant stiffness $(EI)^j$;
3. an elastic segment of length $L-x_i-x_j$ with the initial stiffness $(EI)_e$.

For the six planar degrees of freedom identified in Fig. 4.15, the tangent stiffness matrix of this frame element is of the form

$$[K_e] = \begin{bmatrix} K_{11} & 0 & 0 & K_{14} & 0 & 0 \\ & K_{22} & K_{23} & 0 & K_{25} & K_{26} \\ & & K_{33} & 0 & K_{35} & K_{36} \\ & & & K_{44} & K_{45} & K_{46} \\ & & & & K_{55} & K_{56} \\ \text{Sym.} & & & & & K_{66} \end{bmatrix} \qquad (4.2)$$

The coefficients, $K_{11} = K_{44} = -K_{14} = \frac{E A}{L}$, where E is the modulus of

elasticity for concrete, and A is the cross section area. Since the axial deformation in beam and column elements is neglected, therefore these coefficients are eliminated from the element stiffness matrix. K_{33}, K_{36} and K_{66} are obtained from their flexibility counterparts, which are computed as follows (Chung et al., 1988):

Denoting by

$$Q_i = \frac{(EI)_e}{(EI)^i} \qquad \& \qquad Q_j = \frac{(EI)_e}{(EI)^j} \tag{4.3}$$

which are the stiffness ratios for the end segments i and j. The flexibility coefficients are computed as:

$$f_{ii} = \frac{1}{3(EI)_e L^2}\left[(Q_j - 1)x_j^3 - (Q_i - 1)(L-x_i)^3 + Q_i L^3\right] \tag{4.4}$$

$$f_{jj} = \frac{1}{3(EI)_e L^2}\left[(Q_i - 1)x_i^3 - (Q_j - 1)(L-x_j)^3 + Q_j L^3\right] \tag{4.5}$$

$$f_{ij} = -\frac{1}{3(EI)_e L^2}\left[(Q_j - 1)x_j^2 (1.5\,L - x_j) + (Q_i - 1)\, x_i^2 (1.5\,L - x_i) + \frac{L^3}{2}\right] \tag{4.6}$$

The corresponding stiffness coefficients are:

$$K_{33} = \frac{f_{jj}}{f_{ii} f_{jj} - f_{ij}^2} \tag{4.7}$$

$$K_{66} = \frac{f_{ii}}{f_{ii} f_{jj} - f_{ij}^2} \tag{4.8}$$

$$K_{36} = -\frac{f_{ij}}{f_{ii} f_{jj} - f_{ij}^2} \tag{4.9}$$

$$K_{23} = -K_{35} = \frac{(K_{33} + K_{36})}{L} \tag{4.10}$$

$$K_{26} = -K_{56} = \frac{(K_{36} + K_{66})}{L} \tag{4.11}$$

$$K_{22} = K_{55} = -K_{25} = \frac{(K_{33} + 2 \times K_{36} + K_{66})}{L^2} \tag{4.12}$$

Using Fig. 4.14, the values of EI for the three loading segments are computed as:

a. For elastic loading

$$(EI)_e = \frac{M_y}{\phi_y} \tag{4.13}$$

$$x_i = 0.0, \qquad x_j = 0.0$$

$$Q_i = 1.0 \quad \text{and} \quad Q_j = 1.0 \tag{4.14}$$

b. For inelastic loading after yield and upto ultimate

$$(EI)_1 = \frac{M_u - M_y}{\phi_u - \phi_y} \tag{4.15}$$

$$x_i = \frac{M_i - M_y}{M_i + M_y} L \quad \text{and} \quad Q_i = \frac{(EI)_e}{(EI)_1}$$

or

$$x_j = \frac{M_j - M_y}{M_j + M_y} L \quad \text{and} \quad Q_j = \frac{(EI)_e}{(EI)_1} \tag{4.16}$$

c. For inelastic loading beyond ultimate

$$(EI)_2 = \frac{M_f - M_u}{\phi_f - \phi_u} \tag{4.17}$$

$$x_i = x_i(\text{ultimate stage}), \qquad Q_i = c \left(\frac{(EI)_e}{(EI)_2} - 1 \right) + 1$$

$$x_j = x_j(\text{ultimate stage}), \qquad Q_j = c \left(\frac{(EI)_e}{(EI)_2} - 1 \right) + 1 \tag{4.18}$$

where c is an empirical constant. Equation 4.18 is adopted from SARCF

program. Chung et al. (1988) suggest the value of c in the range 0.5 to 0.75. In the present analysis the value of c equal to 0.5 was used.

4.4.3 BEAM ELEMENTS

The beam elements are modelled as simple flexural springs. The axial and shear deformations are neglected. A typical beam element and its degrees-of-freedom are shown in Fig. 4.16.

The incremental equation relating incremental moments to incremental rotations is

$$\begin{Bmatrix} \Delta M_i \\ \Delta M_j \end{Bmatrix} = [K] \begin{Bmatrix} \Delta\theta_i \\ \Delta\theta_j \end{Bmatrix} \tag{4.19}$$

where

$$[K] = \begin{bmatrix} K_{33} & K_{36} \\ K_{63} & K_{66} \end{bmatrix} \tag{4.20}$$

The terms K_{33}, K_{36} and K_{66} are as given by Eqs.(4.7), (4.8), and (4.9), respectively, and K_{63} is equal to K_{36}.

4.4.4 COLUMN ELEMENTS

Column elements are modelled similar to beam elements, i.e., as flexural springs, in which the axial and shear deformations are neglected. A typical column element that forms part of a reinforced concrete plane frame is shown in Fig. 4.17.

The incremental deformations and incremental forces in the column element are related as:

$$\begin{Bmatrix} \Delta X_i \\ \Delta M_i \\ \Delta X_j \\ \Delta M_j \end{Bmatrix} = \begin{bmatrix} K_{22} & -K_{23} & K_{25} & -K_{26} \\ & K_{33} & -K_{35} & K_{36} \\ & & K_{55} & K_{56} \\ & & & K_{66} \end{bmatrix} \begin{Bmatrix} \Delta U_i \\ \Delta \theta_i \\ \Delta U_j \\ \Delta \theta_j \end{Bmatrix} \qquad (4.21)$$

The terms of the stiffness matrix are obtained using Eqs. (4.7) to (4.12).

4.4.5 SOLUTION OF EIGENVALUE PROBLEM

The incremental load - deformation relationship for the frame may be written as:

$$\{\Delta F\} = [K]\ \{\Delta U\} \qquad (4.22)$$

$$\begin{Bmatrix} \Delta X_1 \\ \vdots \\ \Delta X_n \\ \hdashline \Delta M_1 \\ \vdots \\ \Delta M_m \end{Bmatrix} = \left[\begin{array}{ccc} & K_{aa} & \\ & & \\ \hdashline & K_{ba} & \end{array}\right. \left.\begin{array}{c} \\ K_{ab} \\ \\ \hdashline \\ K_{bb} \\ \\ \end{array}\right] \begin{Bmatrix} \Delta U_1 \\ \vdots \\ \Delta U_n \\ \hdashline \Delta \theta_1 \\ \vdots \\ \Delta \theta_m \end{Bmatrix} \qquad (4.23)$$

where n is the number of lateral floor degrees of freedom and m is the remaining degrees of freedom. Also, the mass matrix is written as:

$$[\bar{M}] = \begin{bmatrix} m_1 & & & \\ & m_2 & & \\ & & m_i & \\ & & & \ddots \\ & & & & m_n \end{bmatrix}_{n \times n} \qquad (4.24)$$

where m_i is the mass at the i^{th} storey level. In order to obtain the eigenvalues, the stiffness matrix [K] is condensed to $(n \times n)$ matrix using the static condensation technique as:

$$[\bar{K}] = [K_{aa}] - [K_{ab}]\ [K_{bb}]^{-1}\ [K_{ba}] \qquad (4.25)$$

Therefore, the natural frequencies and mode shapes are computed by

solving the eigen problem as:

$$[\bar{K}] - \omega^2 [\bar{M}] = 0 \tag{4.26}$$

4.4.6 CALCULATION OF FRAME DISPLACEMENTS

Initially, the structure is analyzed under vertical loads (dead plus live loads). Also, first mode shape $\{\Phi\}$ (normalized by equating roof displacement to 1.0) is calculated. The incremental lateral horizontal displacement profile, at step k, for the structure is

$$\{\Delta X\}_k = \Delta f \times \{S\}_k \tag{4.27}$$

where Δf is the increment in roof displacement, and $\{S\}_k$ is the normalized incremental lateral displacement profile. In the linear range, $\{S\}_k$ is same as first mode shape of the structure $\{\Phi\}$. Then, the total lateral displacement profile $\{X\}_k$ for the structure is calculated by

$$\{X\}_k = \{X\}_{k-1} + \{\Delta X\}_k \tag{4.28}$$

where $\{X\}_k$ is current horizontal displacement profile; and $\{X\}_{k-1}$ is displacement profile at the previous step.

Then, the additional rotational displacements are computed by

$$\{\Delta\theta\}_k = \left[- [K_{bb}]^{-1} [K_{ba}] \{\Delta X\}_k \right] \tag{4.29}$$

and the total rotational displacements are

$$\{\theta\}_k = \{\theta\}_{k-1} + \{\Delta\theta\}_k \tag{4.30}$$

where $\{\theta\}_k$ is rotational deformation in the current step; and $\{\theta\}_{k-1}$ is rotational deformation in the previous step.

Beyond the yielding stage, at incremental step j, the first mode

shape of the yielded structure $(\Phi)_j$ is calculated and the normalized incremental lateral displacement profile $\{S\}_j$ is calculated as:

$$\{S\}_j = \frac{\left[R_{j-1} \{S\}_{j-1} + \Delta f \{\Phi\}_j \right]}{R_{j-1} + \Delta f} \qquad (4.31)$$

where $\{S\}_{j-1}$ is the normalized incremental displacement profile in the previous step; and R_{j-1} is the total roof displacement in the previous step. Hence, the incremental and the total lateral displacements are calculated as per Eqs. 4.27 and 4.28, respectively. Also, the calculation of the additional and total rotational displacements are as per Eqs. 4.29 and 4.30, respectively.

4.4.7 CALCULATION OF ELEMENT FORCES AND CURVATURE DUCTILITY

At step j, knowing the incremental element deformations $\{\Delta U\}_j$, the updated internal forces in the element are determined by

$$\{F\}_j = \{F\}_{j-1} + [K]_j \{\Delta U\}_j \qquad (4.32)$$

where $\{F\}_j$ are total element forces at the current step; $\{F\}_{j-1}$ are element internal forces in the previous step; $[K]_j$ is element stiffness matrix for the current step; and $\{\Delta U\}_j$ is incremental displacement at current step. In order to properly account for the sudden change in stiffness at different stages of inelasticity, very small increment must be chosen. The displacement increment used has to be arrived basing on a number of trials.

Once the element internal forces are obtained, the bending moment at each end of each element is checked with its moment-curvature curve. In the non-linear range, curvature ductility (δ) for each plastic hinge is computed by

$$\delta = \frac{\phi}{\phi_y} \tag{4.33}$$

where ϕ is curvature at the current step of a section; and ϕ_y is the yield curvature of the section.

4.5 MONARCF-FC PROGRAM

To compare the results of the proposed displacement-control analysis with those of the force-control analysis, a computer program named MONARCF-FC (MOnotonic Non-linear Analysis of Reinforced Concrete Frames - Force Control method) has also been developed. MONARCF-FC provides the linear and non-linear structure response of reinforced concrete frames, as well as the element ductility. The moment-curvature relationship for beam and column elements is first calculated as given in MONARCF-DC. The structure is first solved under the gravity load. The lateral load profile at floor levels is specified. The base shear force is applied in small increments and is distributed along the height as per the specified load profile. At each incremental step, the structure is analyzed for the applied lateral load, and the incremental nodal deformations and forces are then calculated and added to the total nodal deformations and forces, respectively, obtained from the previous step. The moment at each node is checked against the yield criteria. If no plastic hinge occurs anywhere, the base shear force is increased. At the occurrence of a plastic hinge in an element, the stiffness matrix of that element is modified. The incremental procedure is continued till the structure is unable to sustain more additional force. In the non-linear range, the curvature ductility for the yielded elements is obtained. Finally, the base shear - roof displacement plot in the linear and non-linear ranges is obtained.

Table 4.1 Details of Beam and Column Elements

Example	Material	Beams	Columns
3-storey frames Examples (EC1, ET1, EC2 and ET2)	Steel • Modulus of elasticity, E_s = 210000 MPa • Yield stress, f_y = 415 MPa • Modulus of elasticity at strain Hardening, E_{sh} = 693 MPa • Max. elongation = 15% Concrete • Prism strength, f'_c = 28.0 MPa • Strain at Max. stress, ε_{co} (for unconfined concrete) = 0.0020	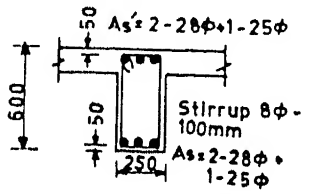 Cross-Section • Confinement stirrup ratio, ρ'' = 0.72%	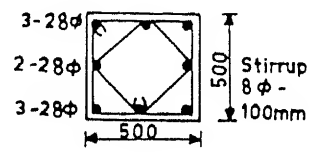 Cross-Section • Confinement stirrup ratio, ρ'' = 0.76%
4-storey frames Examples (EC3, ET3, EC4 and ET4)		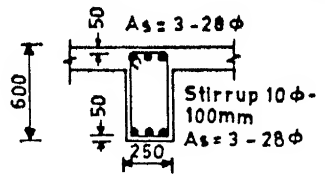 Cross-Section • Confinement stirrup ratio, ρ'' = 1.14%	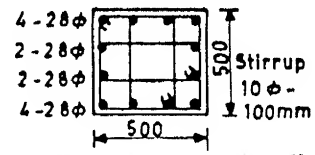 Cross-Section • Confinement stirrup ratio, ρ'' = 1.20%

Table 4.2 Sequence of Plastic Hinge Formation for the 3-Storey 1-Bay Frame

a- EC1 (El Centro)

Time (sec)	Δ (mm)	P (kN)	P. Hinge Location
1.17	-45.90	-213.87	3-b1
1.88	46.34	241.03	4-b1
1.89	54.76	258.23	2-c2
1.90	67.36	267.76	1-c1
1.92	79.65	267.43	6-b2
2.95	109.51	270.60	4-c2
3.00	136.70	306.21	3-c1
3.11	178.40	292.20	5-c3
			6-c4
			8-c6
3.14	183.80	267.70	8-b3
3.16	184.80	261.54	7-b3

b- ET1 (Taft Lincoln)

Time (sec)	Δ (mm)	P (kN)	P. Hinge Location
3.25	46.57	216.11	4-b1
3.29	60.54	253.93	2-c2
3.32	70.78	261.02	6-b2
			1-c1
3.40	95.55	265.60	3-b1
3.83	-57.68	-206.68	5-b2
3.91	-124.13	-215.97	7-c5
3.92	-129.81	-219.12	7-b3
3.93	-134.84	-222.69	5-c3
4.05	-151.59	-284.19	6-c4
			3-c1
6.82	167.72	186.66	8-c6
6.83	171.60	186.60	8-b3

Δ : Roof displacement
P : Base shear force

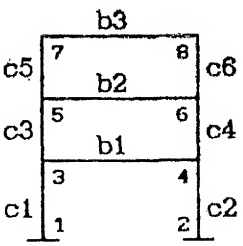

Table 4.3 Sequence of Plastic Hinge Formation for the 3-Storey 2-Bay Frame

a- EC2 (El Centro)

Time (sec)	Δ (mm)	P (kN)	P. Hinge Location
1.89	56.46	412.76	5-b1
			6-b2
			2-c2
			3-c3
1.90	64.62	423.13	1-c1
1.91	72.57	423.31	8-b3
			9-b4
1.92	80.24	424.37	8-c5
1.97	111.74	429.31	4-b1
2.03	128.80	450.47	5-c2
2.04	129.09	451.80	5-b2
2.31	-67.57	-275.17	7-b3
2.34	-84.09	-277.61	7-c4
2.51	-140.32	-457.27	9-c6
2.52	-141.24	-416.57	8-b4
2.53	-141.24	-393.49	11-c8

b- ET2 (Taft Lincoln)

Time (sec)	Δ (mm)	P (kN)	P. Hinge Location
3.25	53.48	406.63	5-b1
			6-b2
			2-c2
3.27	59.28	421.83	3-c3
			1-c1
3.36	72.83	425.88	8-b3
3.37	84.42	532.03	4-b1
3.80	-54.78	-367.75	5-b2
			5-c2
3.81	-65.60	-378.27	8-c5
3.82	-75.88	-388.48	7-b3
			8-b4
			4-c1
3.85	-102.94	-409.20	7-c4
3.86	-110.73	-397.91	9-b4
3.89	-130.66	-430.60	9-c6

Δ : Roof displacement
P : Base shear force

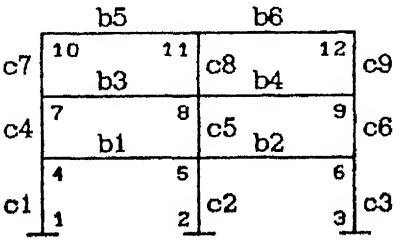

Table 4.4 Sequence of Plastic Hinge Formation for the 4-Storey 1-Bay Frame

a- EC3 (El Centro)

Time (sec)	Δ (mm)	P (kN)	P. Hinge Location
1.19	-61.30	-237.51	3-b1
1.25	-70.46	-235.80	5-b2
1.90	77.84	290.06	4-b1
1.91	88.24	297.34	6-b2
			2-c2
1.92	98.44	302.63	1-c1
1.93	108.38	302.22	8-b3
2.01	172.35	282.61	7-b3
3.12	257.30	196.19	10-b4
3.13	262.81	206.89	9-b4

b- ET3 (Taft Lincoln)

Time (sec)	Δ (mm)	P (kN)	P. Hinge Location
3.23	56.52	274.00	4-b1
3.33	75.44	279.65	6-b2
3.39	92.48	300.19	2-c2
3.41	97.18	301.76	1-c1
3.47	106.66	297.07	8-b3
			3-b1
3.49	108.73	297.71	5-b2
3.89	-130.49	-249.74	7-b3
6.60	-228.40	33.28	9-b4
6.61	-225.90	63.53	10-b4

Δ : Roof displacement
P : Base shear force

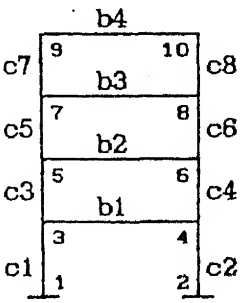

Table 4.5 Sequence of Plastic Hinge Formation for the 4-Storey 2-Bay Frame

a-EC4 (El Centro)

Time (sec)	Δ (mm)	P (kN)	P. Hinge Location
1.22	-61.65	-417.70	4-b1
1.88	60.86	471.00	6-b2
1.89	70.10	507.00	5-b1
			2-c2
			3-c3
1.90	79.48	519.40	1-c1
1.91	88.27	519.70	8-b3
			9-b4
1.95	121.30	522.30	7-b5
			12-b6
1.96	128.50	521.74	8-b4
			11-b5
			8-c5
2.00	151.40	515.10	11-c8
2.06	165.94	523.29	5-c5
			5-b2
2.45	-105.70	-398.14	10-b5
2.47	-112.82	-413.08	7-c4
3.24	239.18	331.87	10-c7
			12-c9
4.55	-118.79	-206.93	8-c8

b- ET1 (Taft Lincoln)

Time (sec)	Δ (mm)	P (kN)	P. Hinge Location
3.32	61.62	431.80	6-b2
3.33	65.05	446.91	5-b1
3.35	71.95	472.15	2-c2
3.38	81.90	495.37	9-b4
			3-c3
3.39	84.96	498.80	8-b3
			1-c1
3.49	104.34	505.52	4-b1
3.82	-56.65	-460.14	5-b2
3.86	-100.06	-474.74	7-b3
			8-b4
3.89	-127.19	-456.28	8-c5
3.90	-135.03	-451.80	10-b5
3.91	-142.33	-436.84	11-b6
			11-c8
3.96	-168.05	-408.34	12-b6
6.92	194.85	439.86	11-b5
7.91	-235.61	-205.98	12-c9
7.95	-272.58	-123.19	14-c11
7.98	-280.49	-107.88	10-c7
7.99	-300.45	-79.65	15-b8
8.01	-310.97	-84.88	13-b7

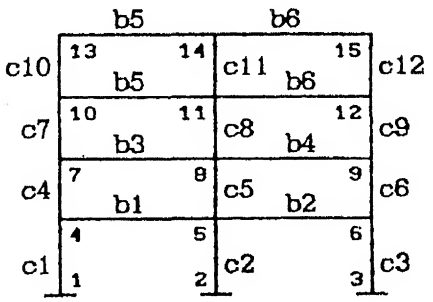

Δ : Roof displacement
P : Base shear force

Table 4.6 Comparison of Displacement Profile with the First Linear Mode of Vibration (Example EC1)

i	1st mode shape Φ_i	Δ_i (mm)	Time (sec)								
			0.38	0.505	1.03	1.09	1.14	1 1.17	2 1.88	3 1.89	3 1.90
3	1.000	Δ_3	10.04	12.82	-20.23	-30.37	-39.80	-45.92	54.77	58.98	67.37
2	.7933	Δ_2	8.230	10.20	-10.64	-24.32	-32.69	-37.81	45.16	48.24	54.41
		$\frac{\Delta_2}{\Delta_3}$	0.819	0.796	0.793	0.800	0.822	0.823	0.824	0.818	0.808
		ξ %	+3.300	+0.317	-0.083	+0.890	+3.520	+3.790	+3.930	+3.110	+1.808
1	.4606	Δ_1	4.950	5.960	-9.350	-14.46	-19.84	-22.83	27.67	29.16	32.14
		$\frac{\Delta_1}{\Delta_3}$	0.493	0.493	0.462	0.476	0.498	0.497	0.505	0.494	0.477
		ξ %	+6.900	-0.400	-0.365	+3.340	+8.200	+7.950	+9.680	+7.340	+1.650
Base Shear (kN)			46.16	54.39	-85.34	-134.5	-186.8	-213.9	258.23	262.12	267.76

i :storey level; Δ_i : displacement at the i^{th} floor

$$\xi\ \% = \frac{\left(\frac{\Delta_i}{\Delta_3}\right) - \Phi_i}{\Phi_i} \times 100$$

1. Plastic hinge occurred at node 3-b1 due to force in -X direction.
2. Plastic hinges occurred at nodes 4-b1 and 2-c2 due to load in +X direction.
3. Plastic hinge occurred at node 1-c1.

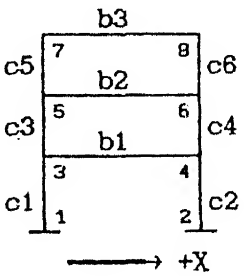

Table 4.7 Comparison of Displacement Profile with the First Linear Mode of Vibration (Example ET1)

i	1st mode shape Φ_i	Δ_i (mm)	Time (sec)								
			1.49	1.61	2.02	3.23	1 3.25	1 3.26	2 3.29	3 3.32	3 3.35
3	1.000	Δ_3	10.10	20.33	-30.85	39.68	46.55	50.05	60.54	70.76	80.58
2	.7933	Δ_2	8.580	16.06	-23.89	32.52	37.87	40.64	49.09	57.57	65.91
		$\frac{\Delta_2}{\Delta_3}$	0.8491	0.7898	0.7743	0.8196	0.8135	0.8119	0.8108	0.8134	0.8179
		ξ %	+7.030	-0.432	+2.390	+3.310	+2.546	+2.347	+2.206	+2.538	+3.108
1	.4606	Δ_1	5.240	9.170	-13.27	20.04	23.00	24.52	29.13	33.89	39.12
		$\frac{\Delta_1}{\Delta_3}$	0.5180	0.4508	0.4302	0.5050	0.4940	0.4898	0.4811	0.4789	0.4855
		ξ %	+12.46	-2.100	-6.580	+9.650	+7.260	+6.350	+4.469	+3.977	+5.405
Base Shear (kN)			49.49	81.91	-115.9	191.77	217.58	227.93	255.74	262.63	263.55

i :storey level; Δ_i : displacement at the i^{th} floor

$$\xi\ \% = \frac{\left(\frac{\Delta_i}{\Delta_3}\right) - \Phi_i}{\Phi_i} \times 100$$

1. Platic hinge occurred at node 4-b1 under a (+ve) loading.
2. Plastic hinge occurred at node 2-c2.
3. Plastic hinges occurred at nodes 6-b2 and 1-c1.

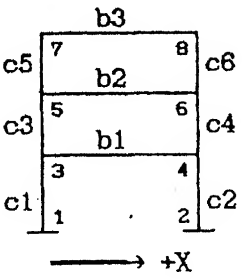

Table 4.8 Comparison of Displacement Profile with the First Linear Mode of Vibration (Example EC2)

i	1st mode shape Φ_i	Δ_i (mm)	Time (sec) 0.98	1.04	1.10	1.16	1.22	1 1.89	2 1.90	3 1.91	4 1.92
3	1.000	Δ_3	-11.20	-20.87	-30.69	-40.27	-45.89	56.46	64.62	72.57	80.24
2	.8089	Δ_2	-9.420	-16.91	-25.31	-33.71	-37.20	45.96	52.06	58.07	63.96
		$\frac{\Delta_2}{\Delta_3}$	0.8407	0.8099	0.8248	0.8370	0.8107	0.8139	0.8057	0.8001	0.7971
		ξ %	+3.900	+0.123	+1.973	+3.470	+0.230	+0.625	-0.396	-1.070	-1.458
1	.4866	Δ_1	-5.970	-10.25	-15.75	-21.06	-22.23	28.09	31.27	34.52	37.86
		$\frac{\Delta_1}{\Delta_3}$	0.5329	0.4909	0.5131	0.5229	0.4845	0.4974	0.4839	0.4756	0.4718
		ξ %	+9.500	+0.893	+5.450	+7.470	-0.428	+2.236	-0.553	-2.250	-3.040
Base Shear (kN)			-91.63	-152.5	-238.8	-319.9	-327.1	412.76	423.13	423.31	424.38

i :storey level; Δ_i : displacement at the i^{th} floor

$$\xi\ \% = \frac{(\frac{\Delta_i}{\Delta_3}) - \Phi_i}{\Phi_i} \times 100$$

1. Plastic hinges occurred at nodes 5-b1, 6-b2, 2-c2 and 3-c2, under a (+ve) loading.
2. Plastic hinge occurred at node 1-c1.
3. Plastic hinges occurred at nodes 8-b3 and 9-b4.
4. Plastic hinge occurred at node 5-c8.

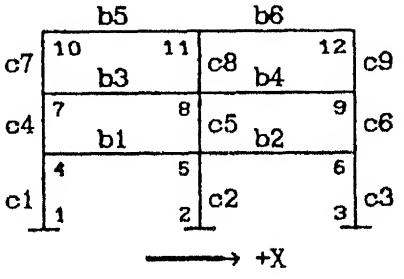

Table 4.9 Comparison of Displacement Profile with the First Linear Mode of Vibration (Example ET2)

i	1st mode shape Φ_i	Δ_i (mm)	Time (sec)							
			1.50	1.64	3.23	3.24	1 3.25	2 3.27	2 3.31	3 3.32
3	1.000	Δ_3	9.920	18.96	47.58	50.54	53.48	59.28	70.25	72.83
2	.8089	Δ_2	8.500	15.19	38.84	41.35	43.91	49.01	58.72	61.29
		$\frac{\Delta_2}{\Delta_3}$	0.8568	0.8103	0.8162	0.8183	0.8209	0.8266	0.8357	0.8416
		ξ %	+5.930	-0.936	+0.907	+1.162	+1.480	+2.193	+3.313	+4.040
1	.4866	Δ_1	5.310	8.850	23.99	25.56	27.15	30.33	36.94	40.72
		$\frac{\Delta_1}{\Delta_3}$	0.5355	0.4665	0.5041	0.5057	0.5075	0.5115	0.5257	0.5591
		ξ %	+10.05	-4.120	+3.606	+3.924	+4.290	+5.117	+8.050	+14.89
Base Shear (kN)			80.48	127.52	361.42	385.89	404.63	421.83	425.02	429.23

i :storey level; Δ_i : displacement at the i^{th} floor

$$\xi\ \% = \frac{\left(\frac{\Delta_i}{\Delta_3}\right) - \Phi_i}{\Phi_i} \times 100$$

1. Plastic hinges occurred at nodes 5-b1, 6-b2 and 2-c2, under a (+ve) loading.
2. Plastic hinges occurred at nodes 1-c1 and 3-c3.
3. Plastic hinge occurred at node 8-b3

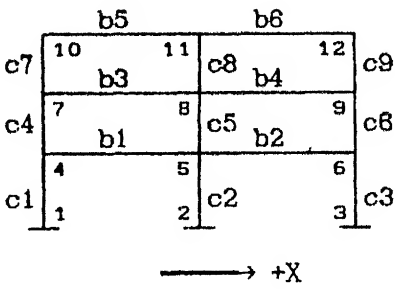

Table 4.10 Comparison of Displacement Profile with the First Linear Mode of Vibration (Example EC3)

i	1st mode shape Φ_i	Δ_i (mm)	Time (sec)								
			0.35	1.05	1.17	1.18	1 1.19	2 1.25	3 1.90	4 1.91	5 1.92
4	1.000	Δ_4	10.29	-22.05	-56.32	-58.88	-61.29	-70.48	77.84	88.24	98.44
3	.8649	Δ_3	9.030	-19.56	-49.30	-51.69	-53.93	-61.43	68.07	76.59	85.08
		$\frac{\Delta_3}{\Delta_4}$	0.8776	0.8872	0.8755	0.8780	0.8798	0.8718	0.8745	0.8680	0.8643
		ξ %	+1.470	+2.580	+1.228	+1.310	+1.730	+0.800	+1.116	+0.359	-0.069
2	.6430	Δ_2	6.930	-15.08	-37.33	-39.19	-40.91	-45.79	52.84	58.64	64.46
		$\frac{\Delta_2}{\Delta_4}$	0.6389	0.6839	0.6628	0.6655	0.6673	0.6499	0.6788	0.6645	0.6548
		ξ %	+4.800	+6.360	+3.088	+3.510	+3.786	+1.080	+5.568	+3.350	+1.842
1	.3547	Δ_1	3.970	-8.670	-20.97	-21.95	-22.85	-24.54	30.22	32.98	35.69
		$\frac{\Delta_1}{\Delta_4}$	0.3861	0.3931	0.3723	0.3728	0.3727	0.3482	0.3882	0.3738	0.3625
		ξ %	+8.870	+10.82	+4.968	+5.120	+5.080	-1.800	+9.467	+5.390	+2.211
Base Shear (kN)			42.41	-92.69	-220.5	-229.3	-237.5	-239.3	297.32	302.64	302.22

i :storey level; Δ_i : displacement at the i^{th} floor

$$\xi\ \% = \frac{\left(\frac{\Delta_i}{\Delta_3}\right) - \Phi_i}{\Phi_i} \times 100$$

1. Plastic hinge occurred at node 3-b1 under (-ve) loading.
2. Plastic hinge occurred at node 5-b2.
3. Under reversal (+ve) loading, plastic hinge occurred at node 4-b1.
4. Plastic hinges occurred at nodes 6-b2 and 2-c2.
5. Plastic hinge occurred at node 1-c1.

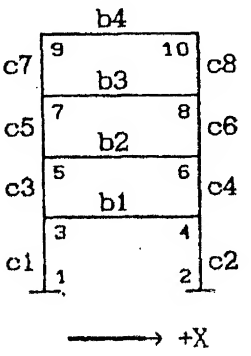

Table 4.11 Comparison of Displacement Profile with the First Linear Mode of Vibration (Example ET3)

i	1st mode shape Φ_i	Δ_i (mm)	Time (sec)								
			0.96	1.57	1.68	1 3.23	2 3.33	2 3.36	3 3.39	4 3.41	4 3.46
4	1.000	Δ_4	-10.29	20.80	30.58	56.52	75.43	84.28	92.48	97.18	105.51
3	.8649	Δ_3	-9.190	17.27	26.77	46.68	66.34	73.10	79.98	84.35	93.24
		$\frac{\Delta_3}{\Delta_4}$	0.8938	0.8303	0.8754	0.8260	0.8794	0.8674	0.8649	0.8680	0.8838
		ξ %	+3.346	-4.000	+1.215	-4.490	+1.455	+0.288	+0.000	+0.310	+2.178
2	.6430	Δ_2	-7.090	12.45	19.84	39.19	50.74	54.94	59.74	62.99	70.08
		$\frac{\Delta_2}{\Delta_4}$	0.6889	0.5983	0.6486	0.6934	0.6726	0.6518	0.6459	0.6482	0.6641
		ξ %	+7.142	-6.950	+0.882	+7.820	+4.603	+1.360	+0.462	+0.808	+3.294
1	.3547	Δ_1	-3.960	+6.880	+10.69	+22.96	+28.47	+30.30	+32.51	+33.88	+36.65
		$\frac{\Delta_1}{\Delta_4}$	0.3851	0.3309	0.3488	0.4063	0.3774	0.3597	0.3516	0.3486	0.3474
		ξ %	+8.583	-6.700	-1.650	+14.54	+6.409	+1.428	-0.887	-1.699	-2.058
Base Shear (kN)			-41.35	71.65	106.89	274.00	279.64	289.03	300.18	301.80	297.27

i :storey level; Δ_i : displacement at the i^{th} floor

$$\xi\ \% = \frac{\left(\frac{\Delta_i}{\Delta_3}\right) - \Phi_i}{\Phi_i} \times 100$$

1. Plastic hinge started at node 4-b1 under (+ve) loading.
2. Plastic hinge occurred at node 6-b2.
3. Plastic hinge occured at node 2-c2.
4. Plastic hinge occured at node 1-c1.

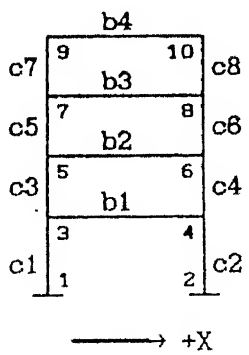

Table 4.12 Comparison of Displacement Profile with the First Linear Mode of Vibration (Example EC4)

i	1st mode shape Φ_i	Δ_i (mm)	time (sec)								
			0.36	1.04	1.11	1 1.22	2 1.89	3 1.90	4 1.91	4 1.92	4 1.93
4	1.000	Δ_4	10.31	-21.72	-39.17	-61.64	70.10	79.25	88.27	97.03	105.51
3	.8763	Δ_3	9.160	-19.23	-34.06	-55.04	62.00	69.65	77.24	84.71	92.02
		$\frac{\Delta_3}{\Delta_4}$	0.8891	0.8853	0.8696	0.8929	0.8844	0.8788	0.8751	0.8730	0.8722
		ξ %	+1.467	+1.030	-0.760	+1.892	+0.926	+0.032	-0.136	-0.372	-0.468
2	.6650	Δ_2	7.390	-14.86	-25.96	-42.64	48.72	54.07	59.44	64.77	70.09
		$\frac{\Delta_2}{\Delta_4}$	0.7167	0.6842	0.6627	0.6918	0.6949	0.6824	0.6733	0.6675	0.6642
		ξ %	+7.780	+2.889	-0.334	+4.034	+4.502	+2.611	+1.260	+0.382	-0.123
1	.3808	Δ_1	4.190	-8.790	-15.21	-24.56	29.39	32.23	35.08	37.89	40.74
		$\frac{\Delta_1}{\Delta_4}$	0.4064	0.4046	0.3884	0.3984	0.4192	0.4067	0.3974	0.3905	0.3861
		ξ %	+6.720	+6.265	+2.006	+4.633	+10.08	+6.807	+4.360	+2.547	+1.399
Base Shear (kN)			72.53	-152.6	-264.0	-417.7	506.98	519.38	519.70	520.54	520.91

i :storey level; Δ_i : displacement at the i^{th} floor

$$\xi\ \% = \frac{(\frac{\Delta_i}{\Delta_3}). - \Phi_i}{\Phi_i} \times 100$$

1. Plastic hinge occurred at node 4-b1 undder (-ve) loading.
2. Plastic hinges occurred at nodes 5-b1, 6-b2, 2-c2 and 3-c3 under reversal (+ve) loading.
3. Plastic hinge occurred at node 1-c1.
4. Plastic hinges occurred at nodes 8-b3 and 9-b4.

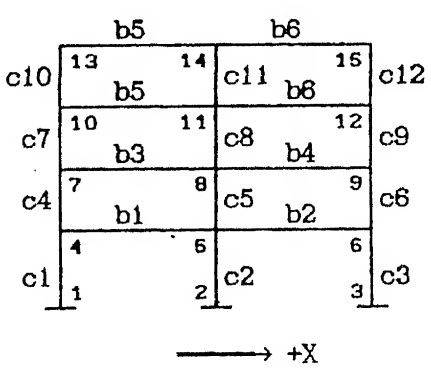

Table 4.13 Comparison of Displacement Profile with the First Linear Mode of Vibration (Example ET4)

i	1st mode shape Φ_i	Δ_i (mm)	Time (sec)								
			0.38	3.32	1.58	1 3.32	2 3.33	3 3.35	4 3.38	5 3.39	5 3.40
4	1.000	Δ_4	8.712	-10.77	21.82	61.62	65.05	71.96	81.89	84.96	87.835
3	.8763	Δ_3	7.670	-9.296	18.95	54.76	57.58	63.25	71.70	74.39	77.041
		$\frac{\Delta_3}{\Delta_4}$	0.8804	0.8631	0.8684	0.8887	0.8852	0.8789	0.8756	0.8756	0.87703
		ξ %	+0.467	-1.501	-0.895	+1.415	+1.016	+0.300	-0.080	-0.080	+0.0916
2	.6650	Δ_2	5.765	-7.188	14.37	42.49	44.40	48.41	54.89	57.10	59.230
		$\frac{\Delta_2}{\Delta_4}$	0.6617	0.6674	0.6589	0.6896	0.6825	0.6728	0.6702	0.6720	0.67446
		ξ %	-0.491	+0.362	-0.916	+3.701	+2.638	+1.170	+0.795	+1.059	+1.4105
1	.3808	Δ_1	3.200	-4.445	8.300	24.97	25.96	28.12	31.62	32.79	33.966
		$\frac{\Delta_1}{\Delta_4}$	0.3673	0.4127	0.3807	0.4051	0.3990	0.3907	0.3861	0.3859	0.38669
		ξ %	-3.545	+8.377	-0.027	+6.405	+4.797	+2.610	+1.409	+1.350	+1.5303
Base Shear (kN)			52.77	-79.92	142.37	431.87	446.99	472.62	495.37	498.80	499.441

i :storey level; Δ_i : displacement at the i^{th} floor

$$\xi\ \% = \frac{\left(\frac{\Delta_i}{\Delta_3}\right) - \Phi_i}{\Phi_i} \times 100$$

1. Plastic hinge started at node 6-b21 under (+ve) loading.
2. Plastic hinge occurred at node 5-b1.
3. Platic hinge occurred at node 2-c2.
4 Plastic hinges occurred at nodes 9-b4 and 3-c3.
5. Plastic hinge occurred at node 8-b3.

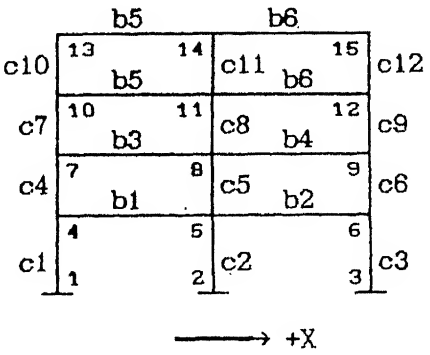

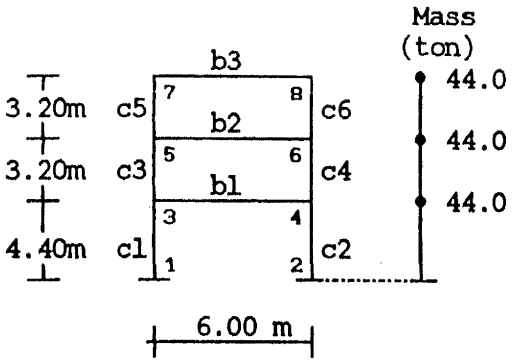

3-storey 1-bay frame
(Examples EC1 & ET1)

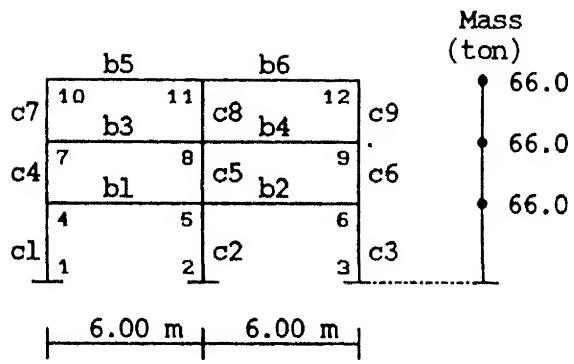

3-storey 2-bay frame
(Examples EC2 & ET2)

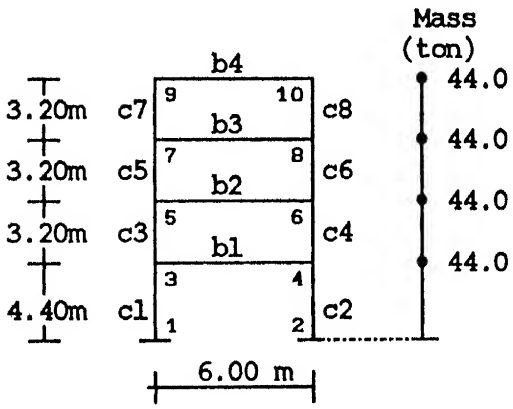

4-storey 1-bay frame
(Examples EC3 & ET3)

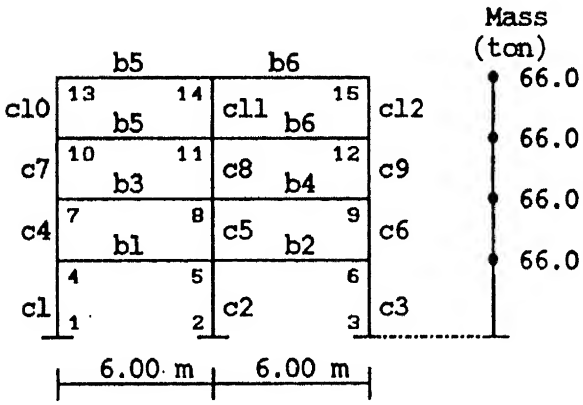

4-storey 2-bay frame
(Examples EC4 & ET4)

N.B : 1. Damping has been taken as 5%.
2. All the beams are loaded with permanent unit load equal to 40 kN/m′.

Fig. 4.1 Details of the four reinforced concrete plane frames.

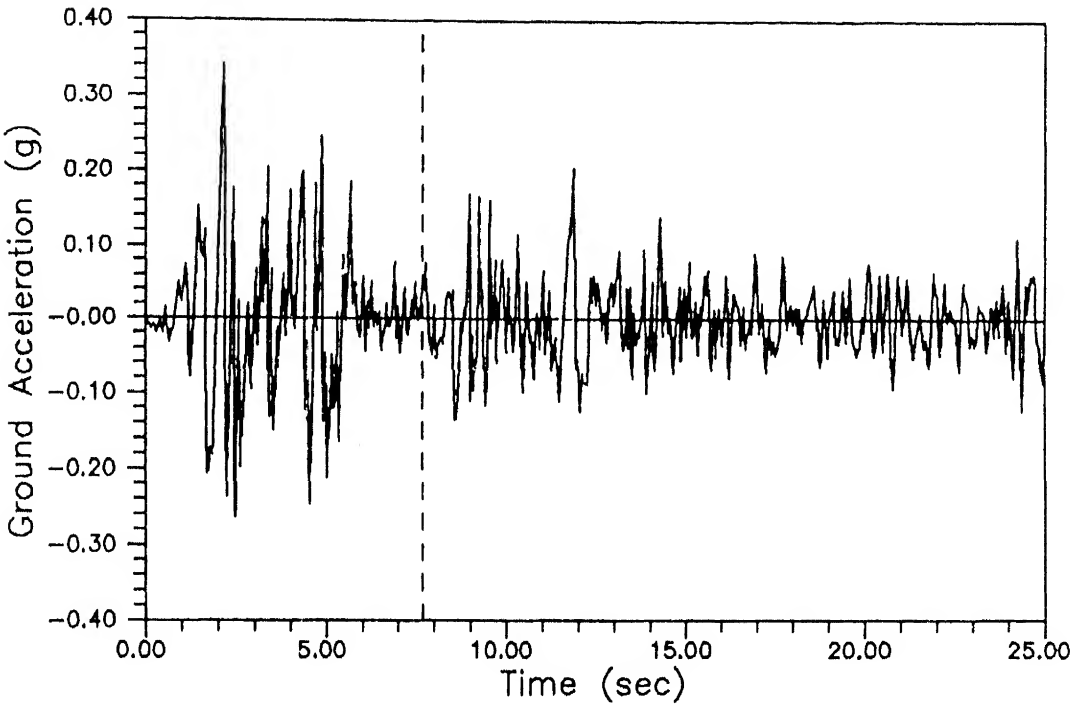

Fig. 4.2 Time-history plot of N-S component of May 18, 1940 El Centro earthquake.

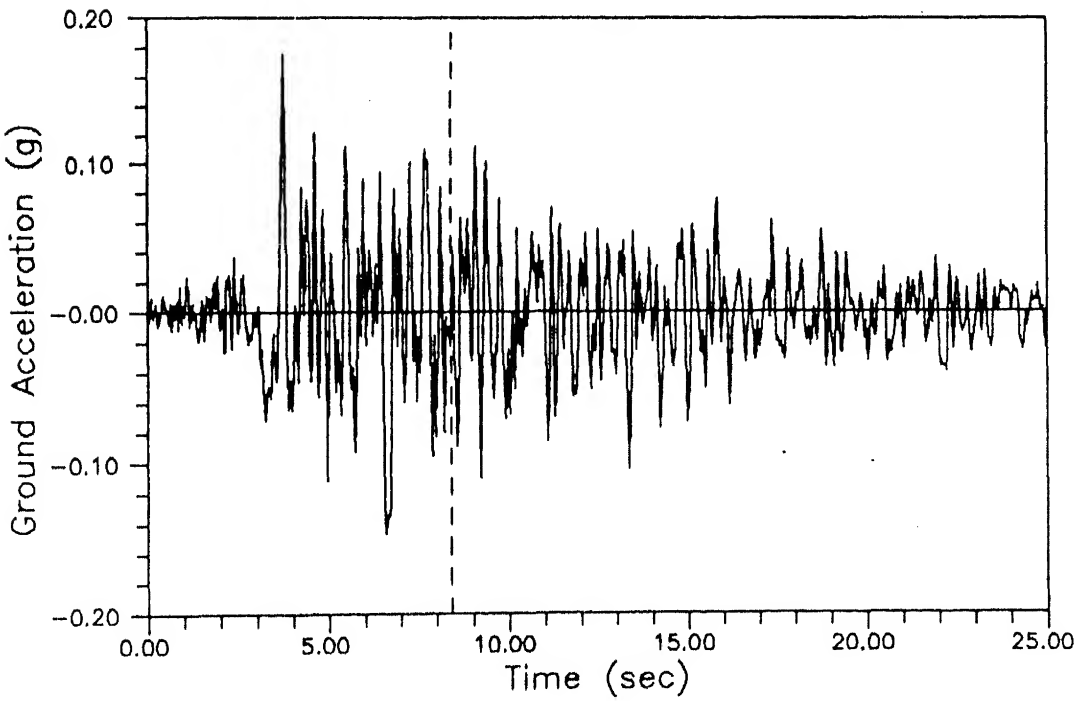

Fig. 4.3 Time-history plot of S69E component of July 21, 1952 Taft Lincoln earthquake.

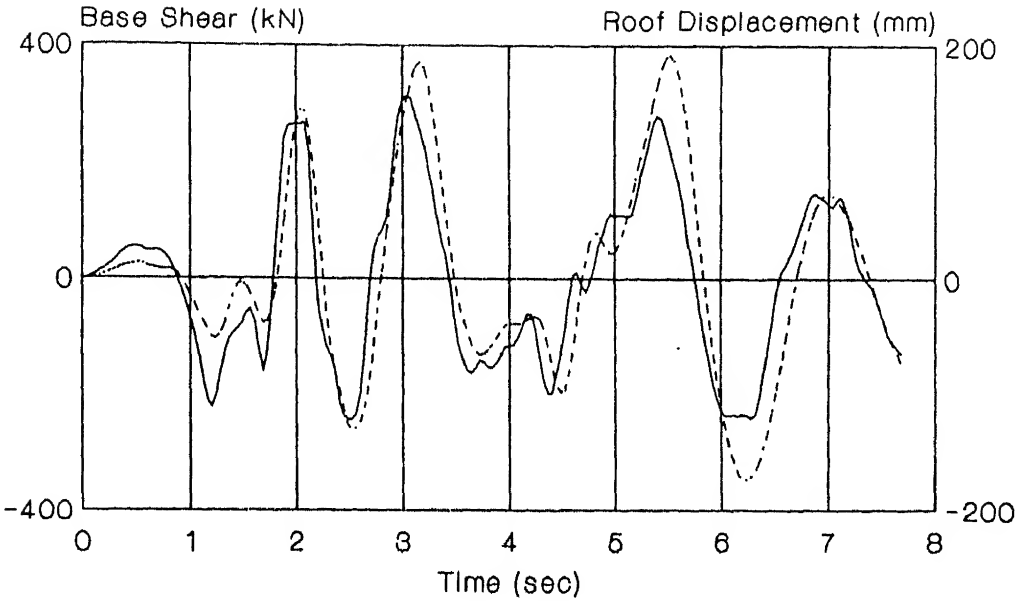

a- Base shear and roof displacement time-histories

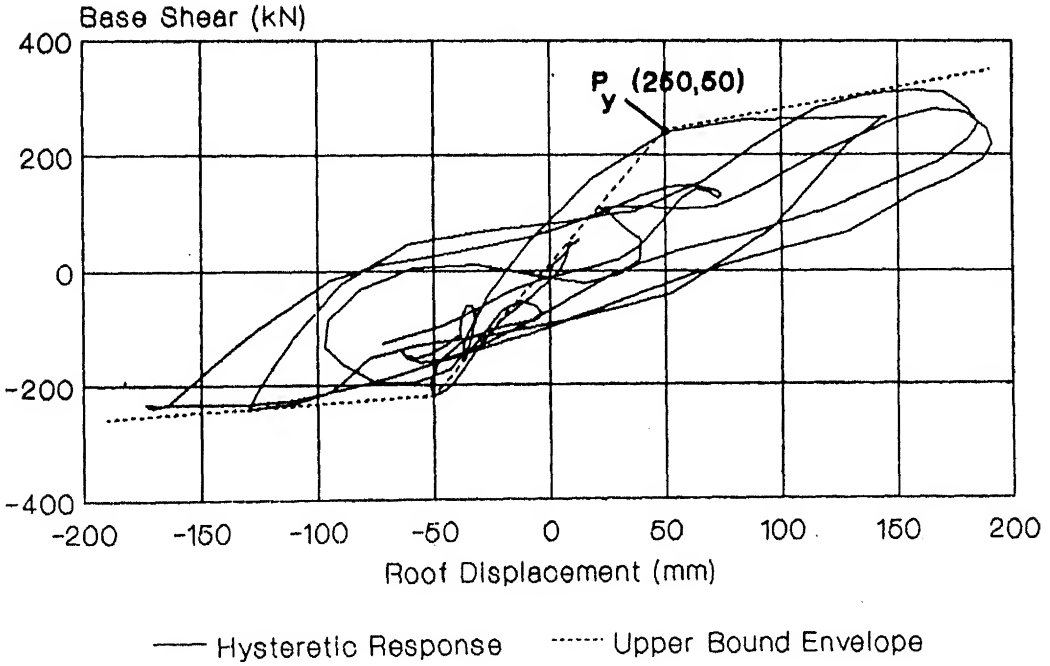

b- Base shear - roof displacement relationship

Fig. 4.4 Response of example EC1.

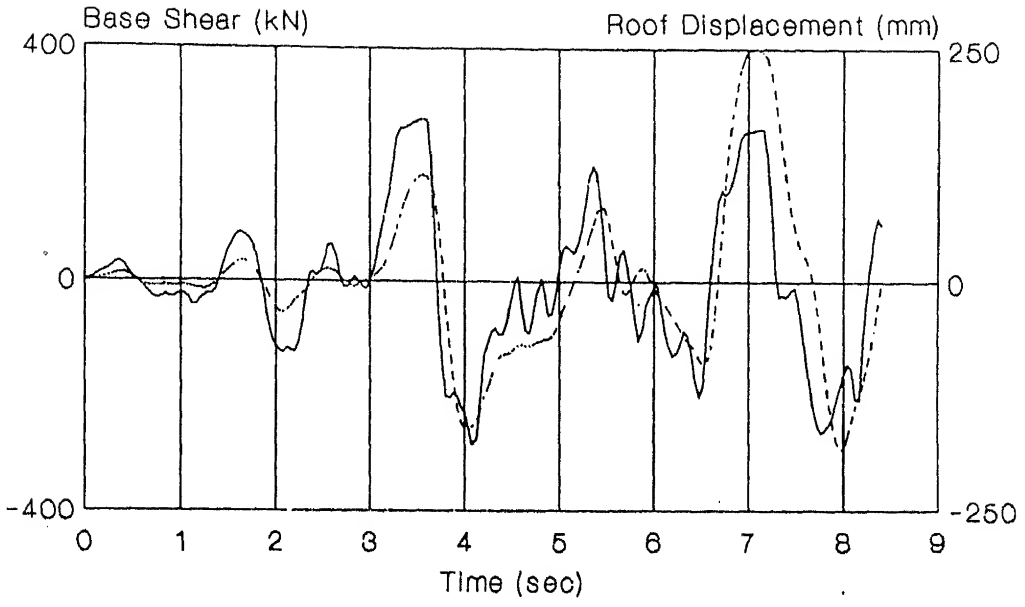

a- Base shear and roof displacement time-histories

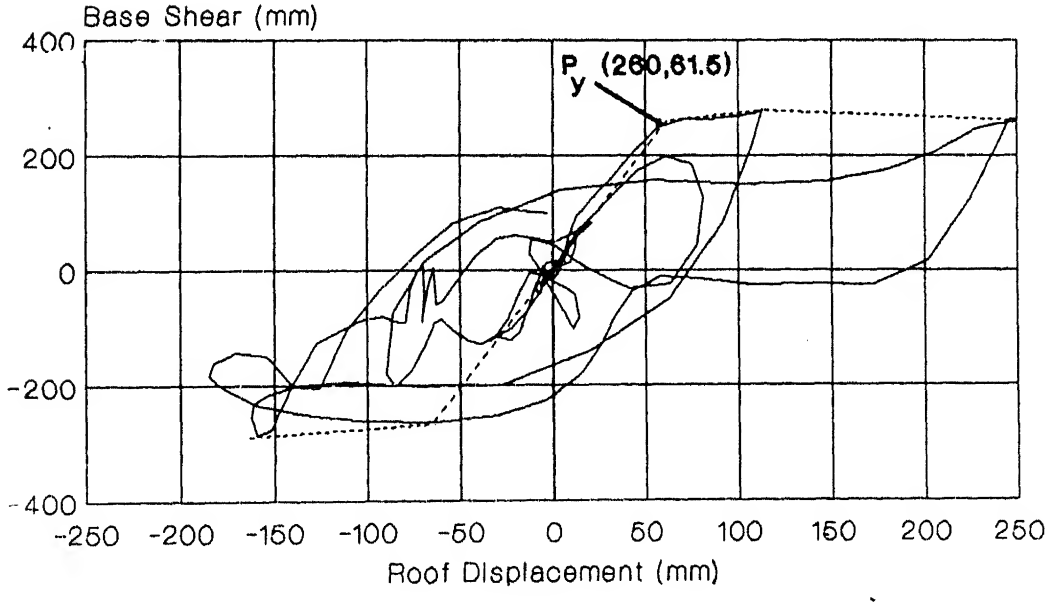

b- Base shear - roof displacement relationship

Fig. 4.5 Response of example ET1.

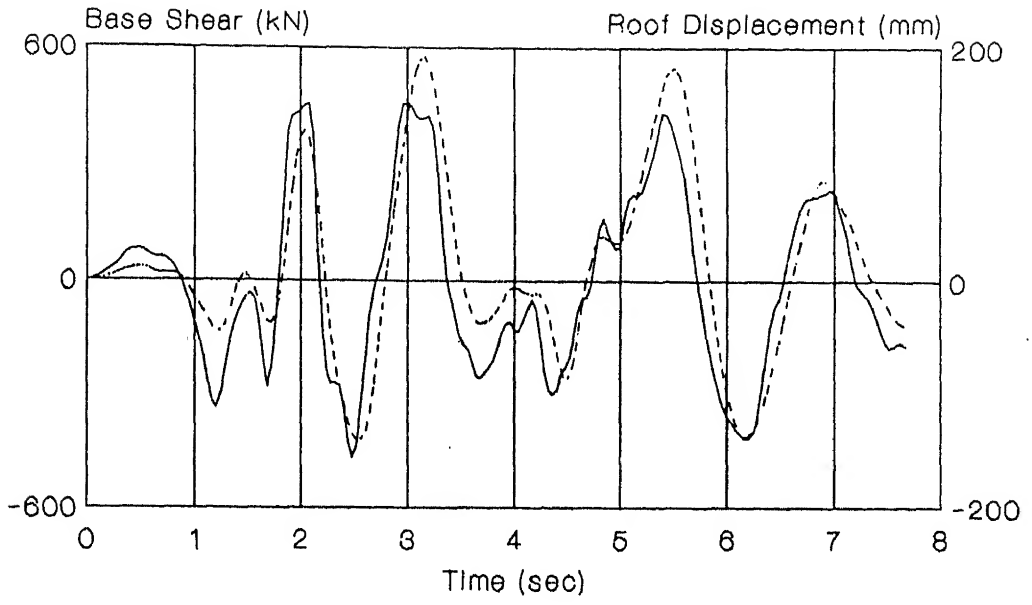

a- Base shear and roof displacement time-histories

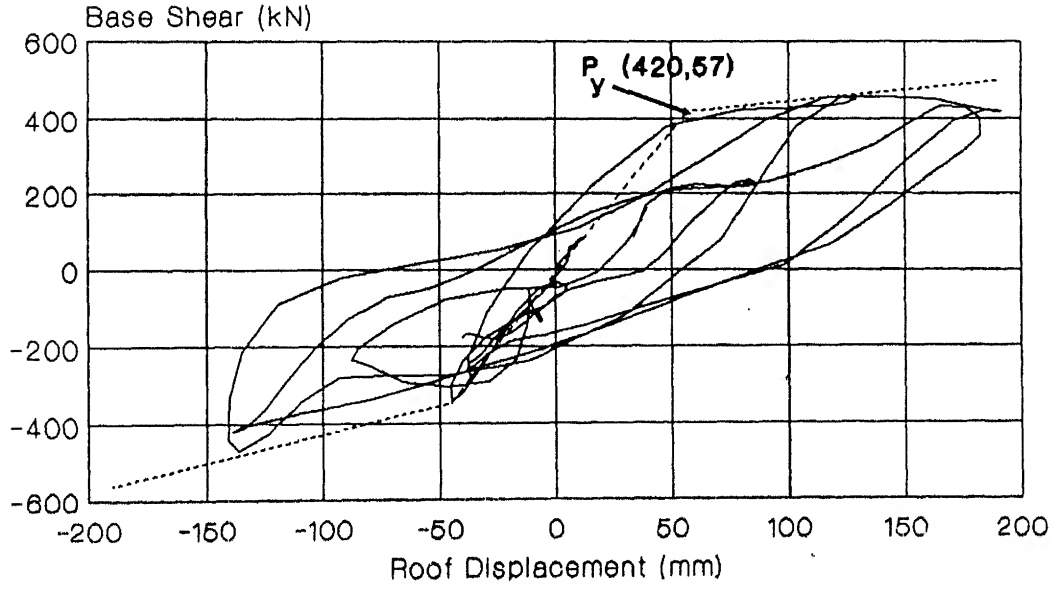

b- Base shear - roof displacement relationship

Fig. 4.6 Response of example EC2.

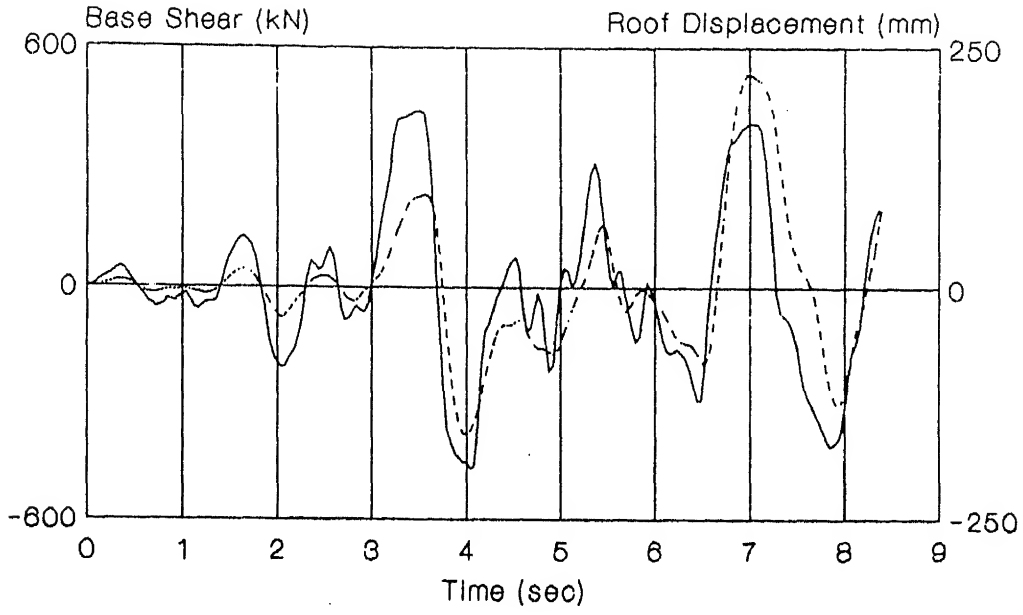

a- Base shear and roof displacement time-histories

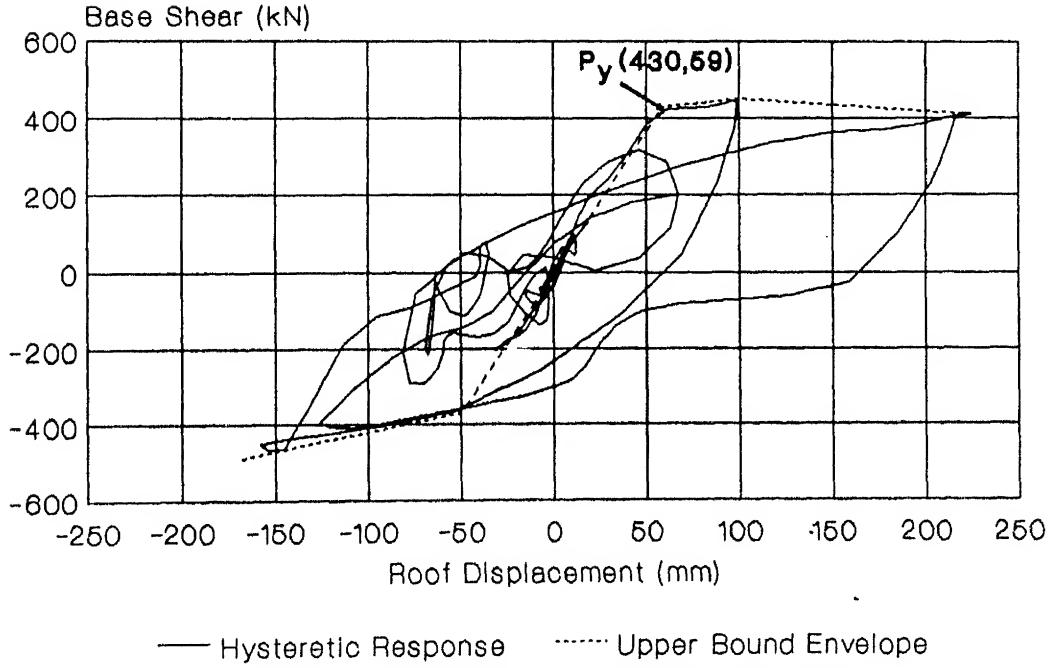

b- Base shear - roof displacement relationship

Fig. 4.7 Response of example ET2.

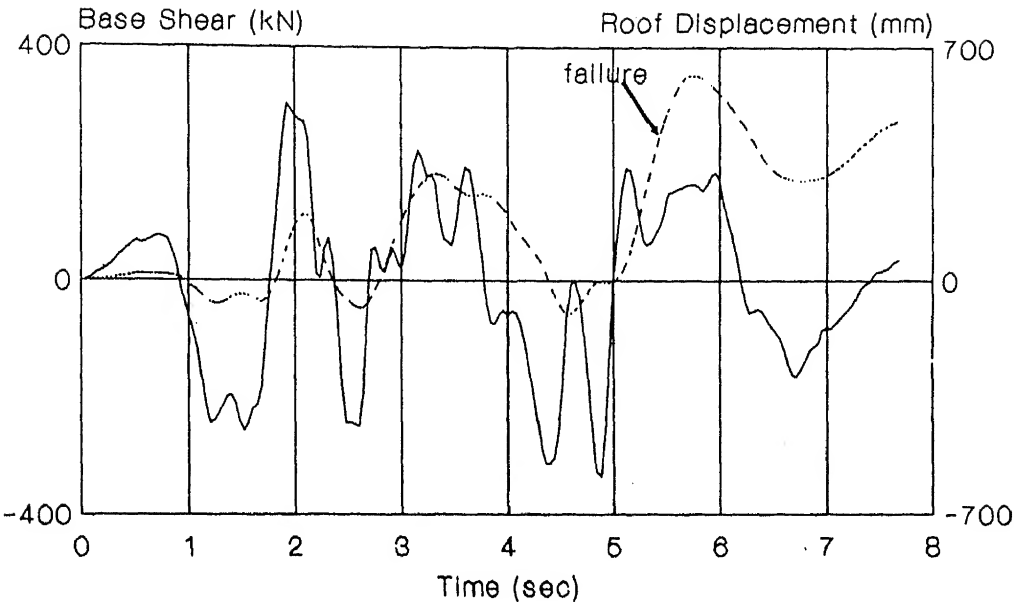

a- Base shear and roof displacement time-histories

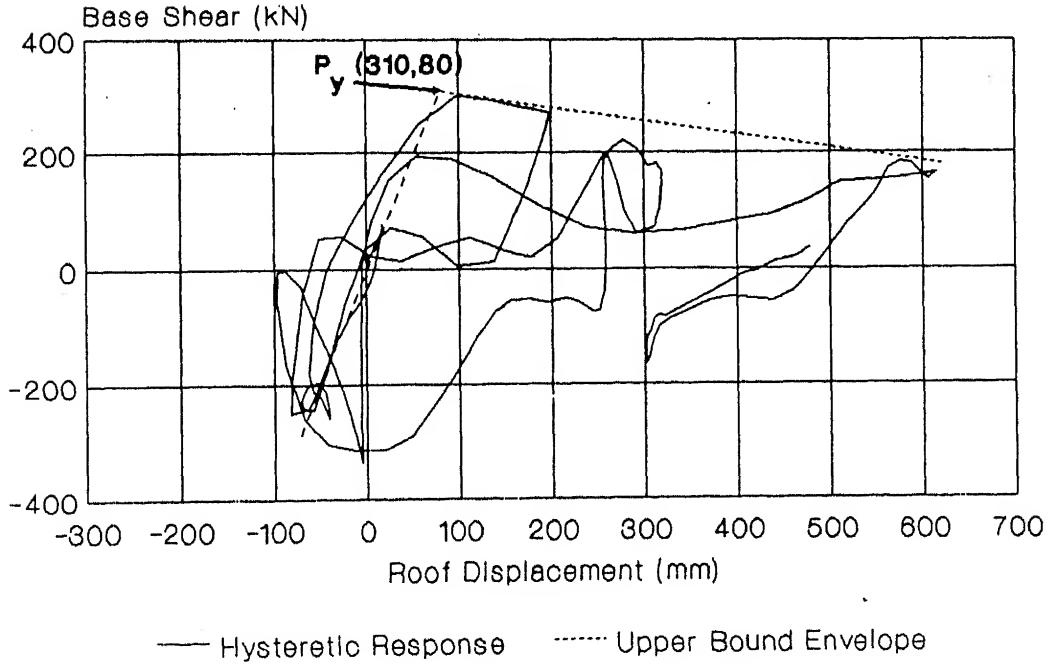

b- Base shear - roof displacement relationship

Fig. 4.8 Response of example EC3.

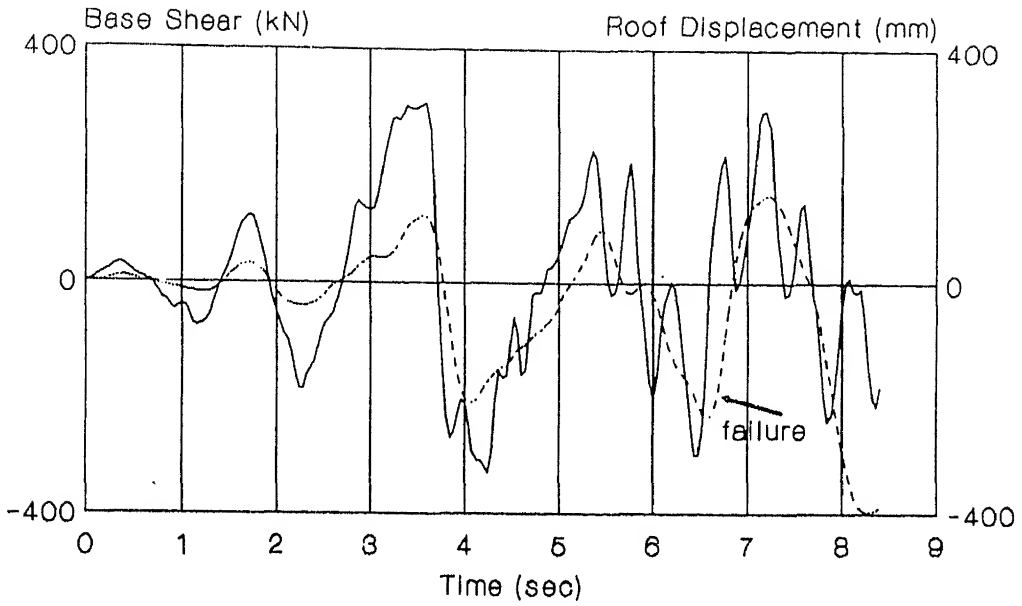

a- Base shear and roof displacement time-histories

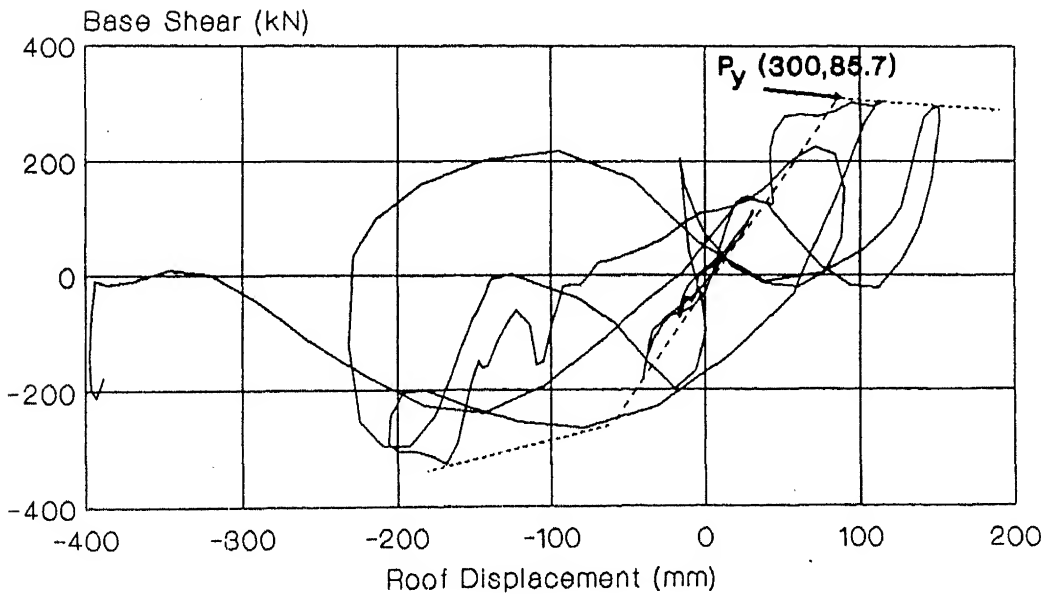

b- Base shear - roof displacement relationship

Fig. 4.9 Response of example ET3.

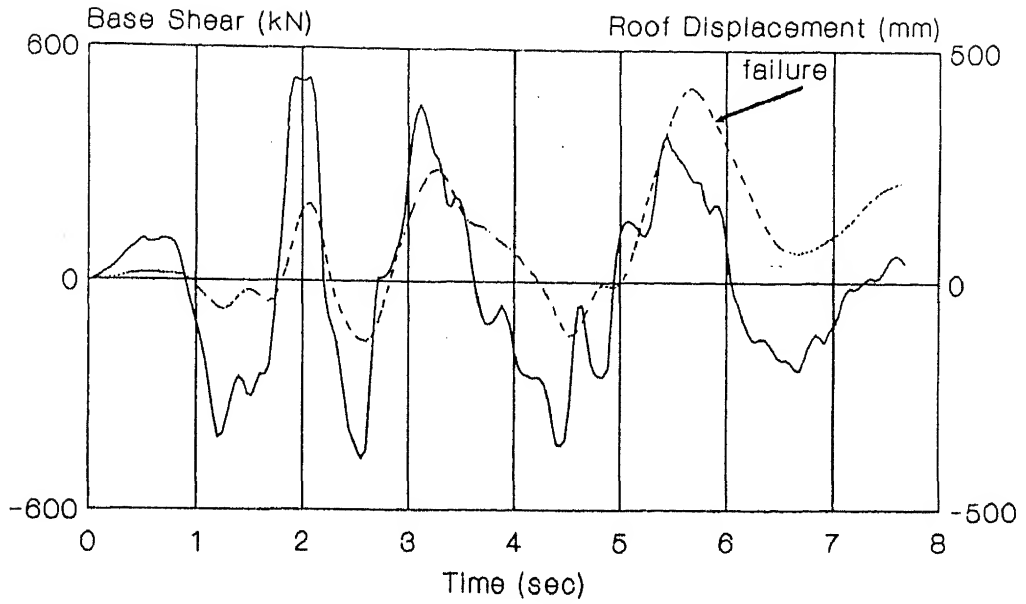

a- Base shear and roof displacement time-histories

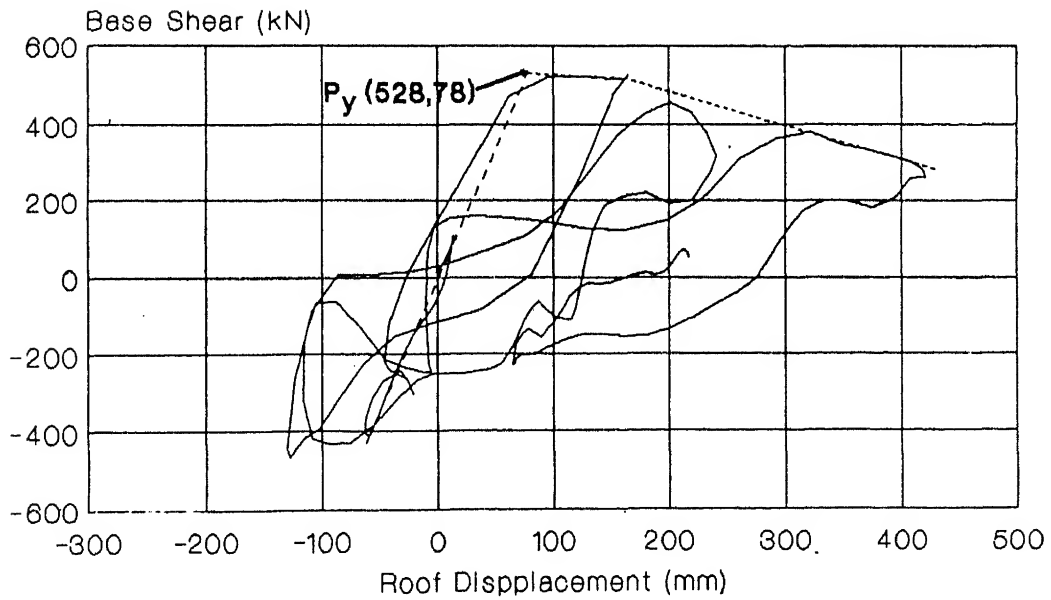

b- Base shear - roof displacement relationship

Fig. 4.10 Response of example EC4.

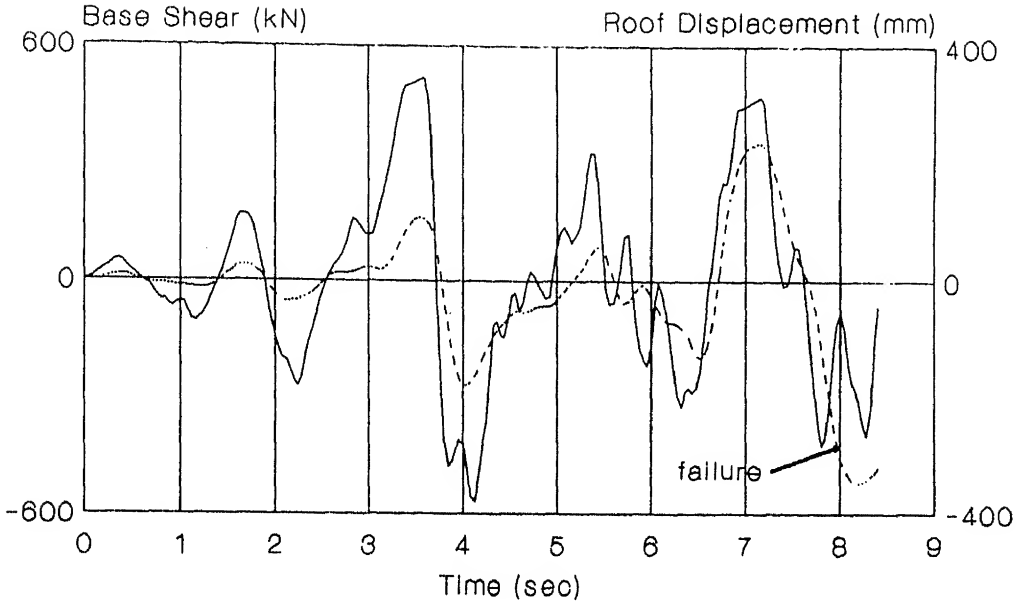

a- Base shear and roof displacement time-histories

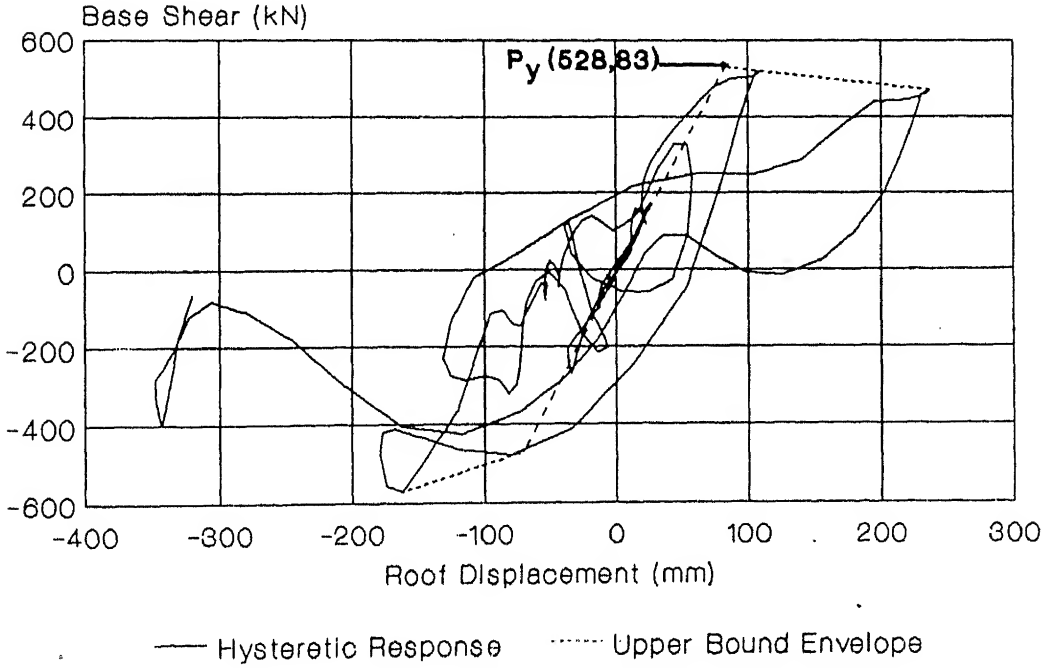

b- Base shear - roof displacement relationship

Fig. 4.11 Response of example ET4.

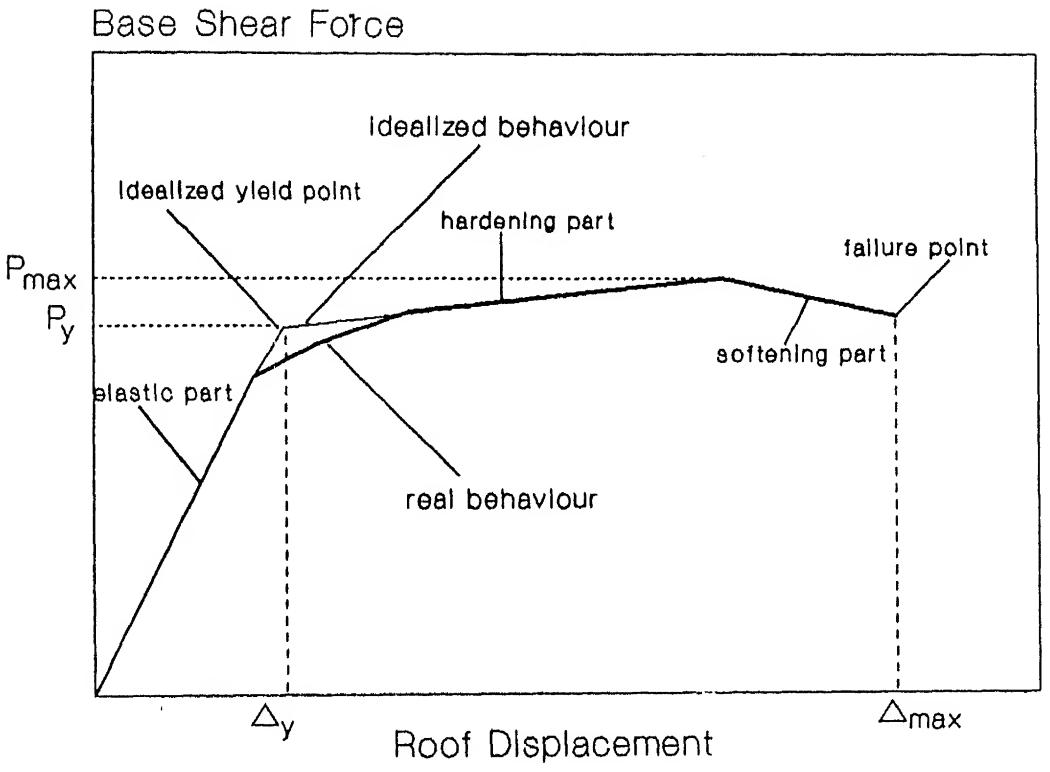

Fig. 4.12 Idealized base shear - roof displacement relationship.

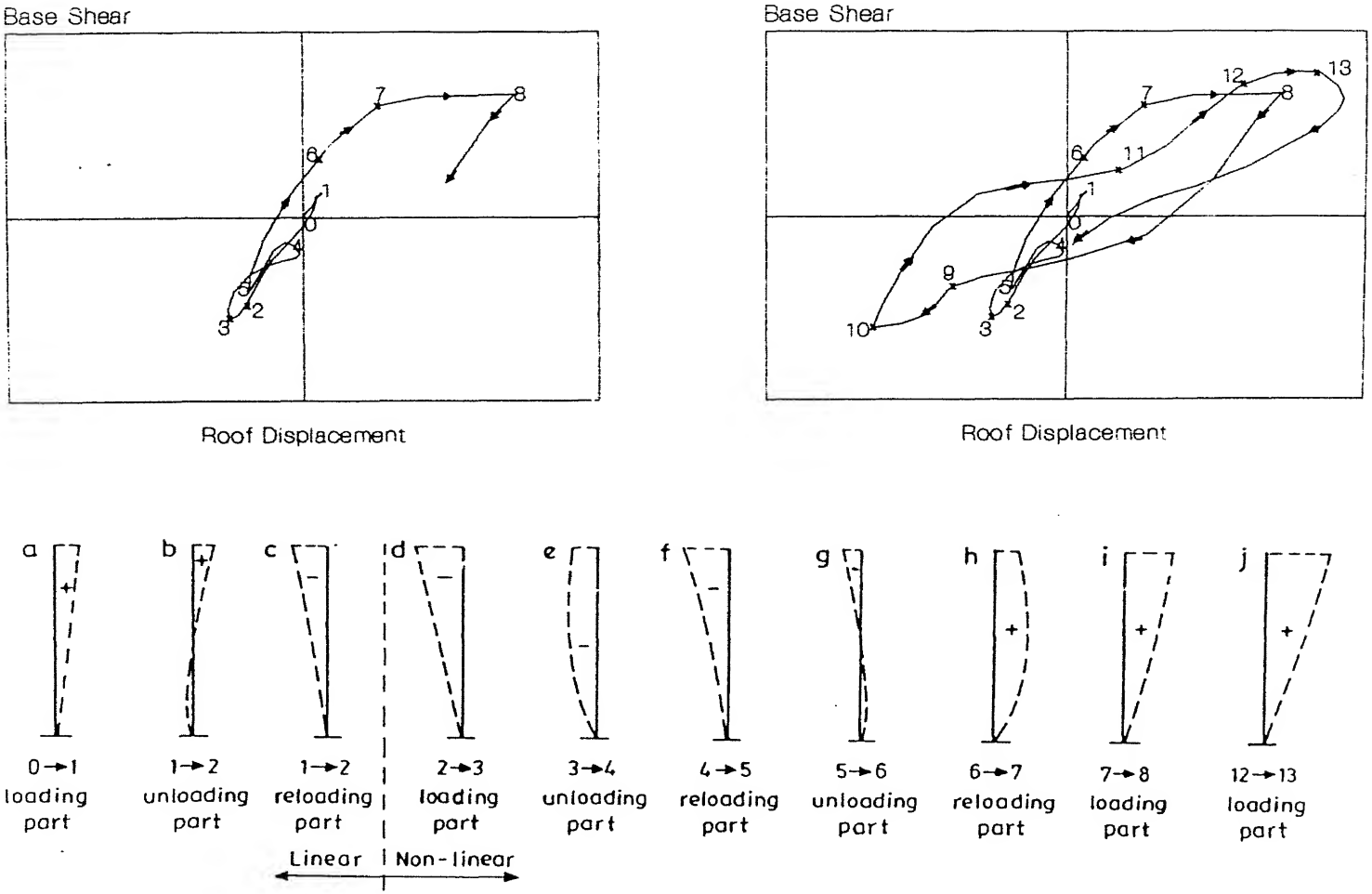

Fig. 4.13 Displacement profile along height during loading and unloading cycles.

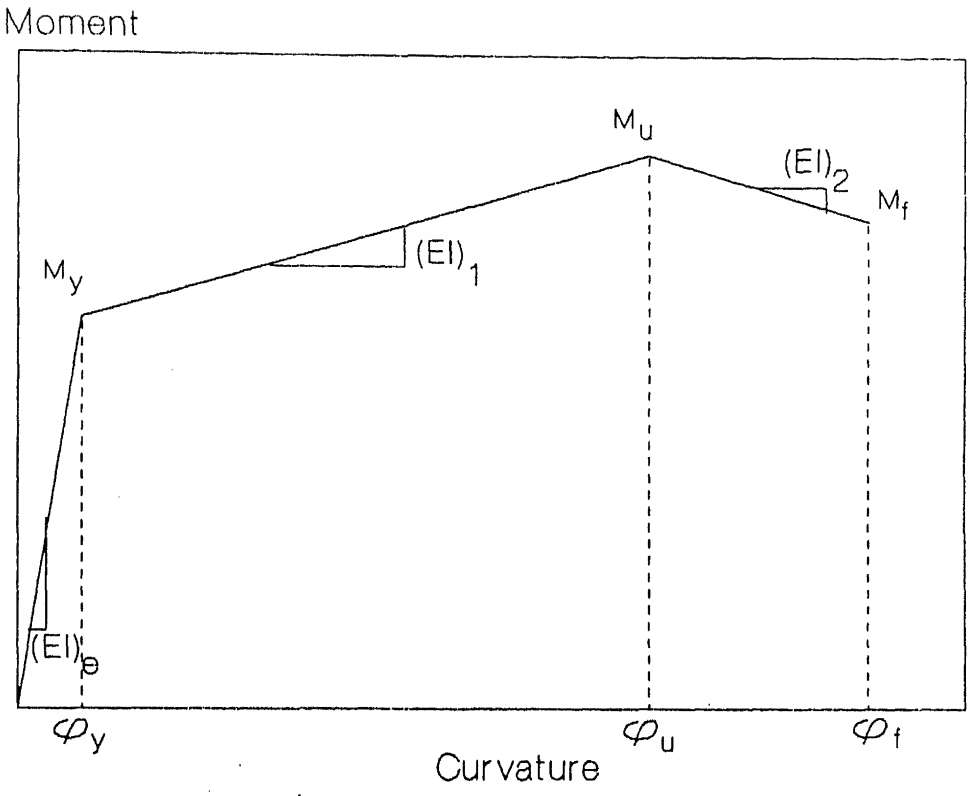

Fig. 4.14 Moment-curvature relationship at cross section in a RC element.

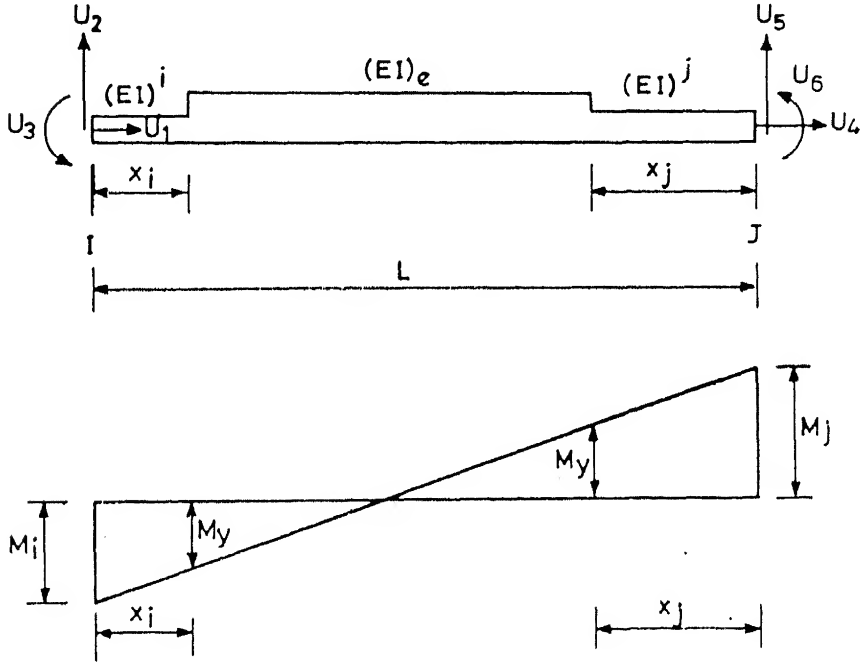

Fig. 4.15 RC element model (from Chung et al., 1988).

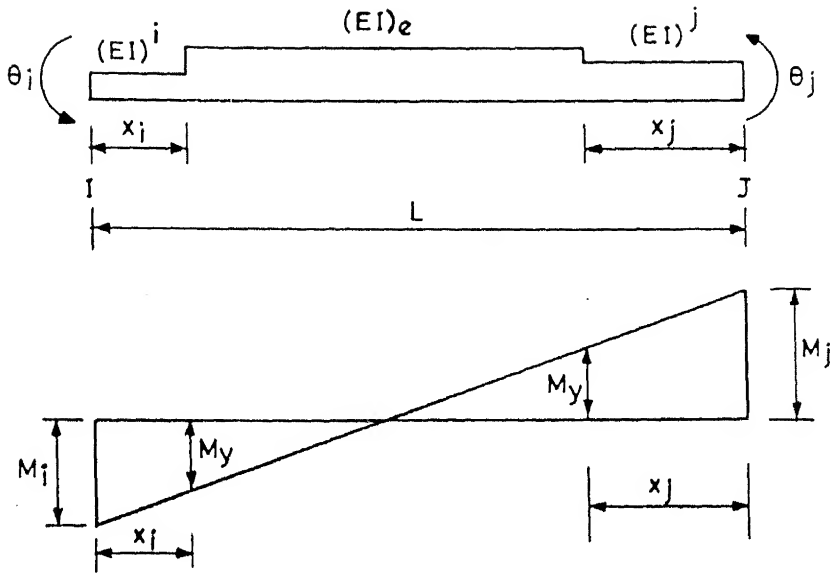

Fig. 4.16 Beam element model.

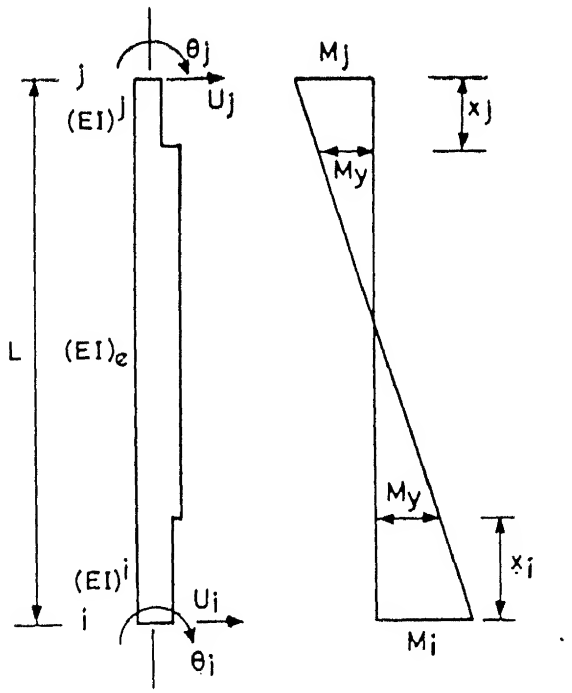

Fig. 4.17 Column element model.

CHAPTER V

PARAMETRIC STUDY AND COMPARISONS

5.1 INTRODUCTION

In this chapter, a parametric study has been carried out to assess effectiveness of the proposed displacement-control quasi-static analysis in: a) evaluating the upper bound envelope of the base shear - roof displacement hysteretic curve in an accurate manner; b) defining the yield point of the structure; c) providing sequence of plastic hinge formation; d) giving realistic values of joint rotation in the linear and non-linear ranges; and e) evaluating the curvature ductility demand on individual members. A good assessment of the overall structural response (upper bound envelope and yield point) of the frame is needed for estimation of the main parameters incorporated in the proposed DDBDP method (e.g., strength, stiffness, overstrength factor, overall structure ductility, etc.). Estimation of plastic hinge sequence provides an overall view of the failure mechanism, this is needed to avoid undesirable failure mechanisms. Comparisons for joint rotation and curvature ductility have been made to see the effect of cyclic loads.

The four example frames (discussed in Chapter IV) have been analyzed using SARCF for the two time-histories (the first 7.68 seconds of twice the N-S component of El Centro accelerogram of May 18, 1940 earthquake; and four times the first 8.40 seconds of the S69E component of Taft Lincoln accelerogram of July 21, 1952 earthquake) and the results are compared with those from the proposed displacement-control quasi-static monotonic analysis, using the program MONARCF-DC. The increment (Δf) in roof displacement for the MONARCF-DC analysis was

taken as 1.0 mm. The results on upper bound envelope, yield point, and sequence of plastic hinges are also compared with those from the force-control quasi-static monotonic non-linear analysis (MONARCF-FC program). In the MONARCF-FC analysis, the profile of imposed lateral loads was taken as parabolic (Eq. 5.1), same as that recommended in IS:1893-1984:

$$V_i = \Delta p \frac{W_i h_i^2}{\sum_{j=1}^{j=n} W_i h_i^2} \qquad (5.1)$$

where V_i is the incremental lateral force at the i^{th} floor; Δp is the incremental base shear force; W_i is the seismic weight of the i^{th} floor; h_i is the height of the i^{th} floor from base of the building; and n is total number of storeys in the structure. The amplitude of Δp was taken as 4.0 kN. In view of the fact that fundamental period of the four frames ranged from 0.91 to 1.16 seconds, the above profile was considered reasonable.

5.2 UPPER BOUND ENVELOPE

For the four example frames, the base shear - roof displacement hysteretic curves from the SARCF analysis and the upper bound envelope of the base shear - roof displacement relationship obtained by the MONARCF-DC and MONARCF-FC programs are shown in Figs. 5.1 to 5.8. The structure yield point (Δ_y, P_y) is determined from the hysteretic response (SARCF results) by extending the hysteretic curve in the linear range till it intersects with the tangent passing along the upper bound of the hysteretic curve in the non-linear range. In the MONARCF-DC and MONARCF-FC analyses, the structure yield point is obtained by extending the elastic stiffness line till it intersects with the tangent of the

strain hardening part of the non-linear response.

In general, the quasi-static procedures provide a reasonable estimate of the upper bound envelope of the time-history response. Only in case of example EC1, the time-history response goes beyond the envelope curves obtained by the two methods; in example ET4 the response goes beyond the MONARCF-DC but remains within MONARCF-FC curve. In general, the displacement control analysis allows one to obtain the envelope curve for upto a larger roof displacement than does the force-control method (examples EC3, ET3, EC4, and ET4). The maximum roof displacement obtained by the MONARCF-DC is a much better indication of the maximum roof displacement capacity of the structure than that by the MONARCF-FC.

The yield points obtained by the three programs are compared in Table 5.1. The table also gives the elastic stiffness modulus of the structure (K_e), obtained by the three programs. K_e is calculated as the base shear force at yield (P_y) divided by the yield displacement (Δ_y). P_y obtained by MONARCF-DC and MONARCF-FC is approximately the same, and its difference from the SARCF values is within 9%. The yield displacement (Δ_y) obtained by MONARCF-DC differs from the average yield displacement of SARCF within the range of 0.43% to 14.7%. On the other hand, Δ_y obtained by MONARCF-FC is consistently higher than that obtained by SARCF by 7.7% to 27.2%. Considering the variation in P_y and Δ_y by SARCF using two different time-histories of ground motion, the estimation of P_y by either of the two quasi-static methods, and Δ_y by the displacement-control method may be considered accurate. However, the force-control method gives somewhat higher values of Δ_y; this is because the force-control method is quite sensitive to the imposed lateral load profile. The imposed profile (Eq. 5.1) gives lateral loads which are

somewhat too large towards the roof; this reduces the slope of base shear - roof displacement curve. Table 5.1 also shows that the elastic lateral stiffness (base shear divided by roof displacement) is estimated by the MONARCF-DC more accurately (within 0.4% to 8.2%) than that by the MONARCF-FC (within 9% to 17%). Again, this is because of the assumed profile for force-control analysis.

In the non-linear range, the strain hardening stiffness obtained by MONARCF-DC program seems to match same from SARCf better than does the strain hardening stiffness by MONARCF-FC. The strain hardening stiffness by MONARCF-FC is slightly higher than that obtained by SARCF.

Table 5.2 compares the maximum base shear and roof displacement obtained by MONARCF-DC and MONARCF-FC. As is expected, the force-control method does not provide the base shear - roof displacement relationship after a certain limit wherein the base shear force decreases with an increase in the roof displacement (third stage of loading, Fig. 4.12). Thus, force-control method gives incomplete information about the overall structure displacement. The maximum displacement at failure resulted from MONARCF-DC is higher than that from MONARCF-FC by 2% to 38%. On the other hand, the displacement-control method is able to provide the third stage of the trilinear base shear - roof displacement relationship (for example, as in case of 4-storey 1-bay and 4-storey 2-bay frames).

From the foregoing discussion, it is obvious that the quasi-static method based on displacement-control monotonic analysis (i.e., MONARCF-DC program) offers itself as a good approach to estimate the main parameters which describe the upper bound envelope of the base shear - roof displacement relationship of a reinforced concrete frame.

5.3 PLASTIC HINGE FORMATION

The sequence of plastic hinge formation and corresponding values of base shear and roof displacement, for the four examples analyzed using MONARCF-DC and MONARCF-FC, are presented in Tables 5.3 to 5.6. Tables 5.7 to 5.10 give the sequence of plastic hinge obtained using SARCF, and compare the values of roof displacement and base shear corresponding to a hinge formation at a particular location have by the MONARCF-DC and MONARCF-FC analyses with those by SARCF. The percentage differences are expressed as

$$\Delta_e = \frac{\Delta_2 - \Delta_1}{\Delta_1} \times 100 \quad \text{and} \quad P_e = \frac{P_2 - P_1}{P_1} \times 100 \qquad (5.2)$$

where, for a particular hinge formation, Δ_e is the percentage difference in roof displacement; Δ_1 is the roof displacement obtained by SARCF program; Δ_2 is the roof displacement obtained by MONARCF-DC or MONARCF-FC program; P_e is the percentage difference in base shear force; P_1 is the base shear force obtained by SARCF program; and P_2 is the base shear force obtained by MONARCF-DC or MONARCF-FC program.

In general, the quasi-static procedures provide a reasonable estimate for the plastic hinge formation. The plastic hinge sequence and the number of plastic hinges estimated by the displacement-control method are generally better than those using the force-control method. The sequence of plastic hinge formation and the roof displacement and base shear values at the occurrence of a plastic hinge are discussed separately for (a) those hinges which occur during first significant inelastic excursion of loading; and (b) those which occur in subsequent excursions of loading. For the former, the following observations can be made from Tables 5.7 to 5.10:

1. In all the examples, the sequences of plastic hinge formation

obtained by MONARCF-DC and MONARCF-FC are somewhat similar, even though the sequence of plastic hinge formation by MONARCF-DC shows a better agreement with that from SARCF analysis.

2. The percentage difference, between SARCF and MONARCF-DC results, for roof displacement and base shear values at the occurrence of a plastic hinge is small for all the examples, except example EC3. In these examples, Δ_e varies from -11.5% to +15.1%, except at the end of the excursion where the percentage difference is high (ranges -17.1% to 46.6%). P_e varies from -13.1% to 7.8%, except for the first plastic hinge where P_e ranges from -8.7% to -21.5%. In example EC3, the percentage difference in roof displacement and base shear is high at the occurrence of first two hinges (Δ_e ranges from -19.5% to -24.3%, and P_e ranges from -14.3% to -23.7%). With the progress of plastic hinge formation in example EC3, Δ_e and P_e decrease to smaller values.
3. When the results of SARCF and MONARCF-FC are compared, Δ_e and P_e, range from -23.1% to 35.6% and from -26.9% to 11.1%, respectively, except in example ET3, where Δ_e is high at the last hinge formed at the end of the excursion (52.4%).

For the hinges formed in subsequent inelastic excursions, the following observations are made:

1. Several plastic hinges which are formed in the SARCF analysis do not form in the MONARCF-DC and MONARCF-FC analyses. Most of these hinges are located on the top of the columns. Also, a few plastic hinges form by SARCF and MONARCF-DC analyses, but do not occur in MONARCF-FC analysis.
2. For plastic hinges formed in beam elements, analysis by SARCF and MONARCF-DC give the percentage difference in roof displacement (Δ_e)

in the range of -34.3% to +21.1% (except for the hinge at node 8-b4, in example EC2, where Δ_e is -41.9%), and in the base shear (P_e) in the range of -18.0% to 55.8%. However, for these hinges, comparison of MONARCF-FC and SARCF results shows that the percentage difference in roof displacement (Δ_e) and base shear (P_e) ranges from -49.6% to +21.9% and -24.6% to 52.6%, respectively.

3. For plastic hinges which form in column elements, the percentage difference in roof displacement (Δ_e), between SARCF and MONARCF-DC, ranges from -15.3% to +55.6%, except for a few hinges in examples EC2 and ET2 for which Δ_e ranges from 74.9% to 131.8%. P_e ranges from -4.5% to 49.9%, except for examples EC4 and ET4 where the structures fail (P_e varies from 63.4% to 402.7%) and for the plastic hinge at node 7-c4 in example EC2 (P_e is equal to 88.5%). It must be noted that many of the plastic hinges of columns did not form while using MONARCF-FC; however for the plastic hinges which form by MONARCF-FC, Δ_e and P_e range from -23.9% to 100.7% and from -24.6% to 28.4%, respectively.

Thus, it is seen that for the first significant inelastic load excursion, the sequence of plastic hinge formation obtained by MONARCF-DC is close to that obtained by SARCF. The values of Δ_e and P_e from MONARCF-DC are lower than those obtained from MONARCF-FC. During the subsequent hysteretic loading, most of the plastic hinges which formed in the SARCF analysis also form by MONARCF-DC analysis. However, a number of hinges which form in SARCF, particularly those located at the top of columns, do not form in MONARCF-DC. As against this, in analysis by MONARCF-FC, many more hinges of the SARCF analysis are not formed. For the hinges that form in all the three programs, MONARCF-DC gives less percentage difference in roof displacement and base shear at

the occurrence of a plastic hinge than what is given by MONARCF-FC.

5.4 JOINT ROTATION

A comparison of joint rotation by the SARCF and MONARCF-DC results for the eight examples is presented in Tables 5.11 to 5.18. In the SARCF analysis, a few instants have been chosen when the roof displacement (Δ) is on the upper bound envelope; at these instants the values of rotation (θ) at different joints have been obtained. These are then compared with the joint rotations obtained from MONARCF-DC corresponding to the same value of roof displacement. Also, a few points have been chosen in the linear, loading part of the base shear - roof displacement curve. The percentage difference (ε) between SARCF and MONARCF-DC results is calculated as

$$\varepsilon = \frac{\theta^S - \theta^M}{\theta^S} \times 100 \quad (5.3)$$

where θ^S = rotation of a joint obtained by SARCF at a particular roof displacement; θ^M = rotation of the same joint obtained by MONARCF-DC at the same roof displacement. When no yielding takes place at a joint, leaving it as linear, the value of joint rotation at some nodes (e.g., node 7 at t = 1.09 and t = 1.14 sec, Table 5.11) obtained from both the programs may be very small, and even the small difference between such joint rotation values will appear as large percentage difference (ε). Hence, the percentage difference for joints with low rotation (rotation less than 0.001 radians) has not been shown in the tables.

In the linear range of base shear - roof displacement curve, the joint rotation obtained by both the programs is approximately the same for the eight examples. For the first floor joints, ε ranges from -3.9% to +6.9%, except in example ET3 where ε ranges from -14.5% to +7.5%. For

the upper floor joints, the maximum ε varies from -7.60% to +5.0%, except for examples ET2 and ET3 where the maximum ε ranges from -19.9% to +12.1%.

In the non-linear range of response, the joint rotation obtained by SARCF and MONARCF-DC, for the eight examples, are described as follows:

Example EC1: During the first inelastic excursion of loading (t = 1.17 sec to t = 1.22 sec), the rotations at elastic and inelastic joints show good agreement with those of MONARCF-DC with maximum ε equal to +5.0% in the inelastic joints and -7.9% in the elastic joints. At the beginning of the next excursion of loading (t = 1.88 sec to t = 2.06 sec), ε for the inelastic joints is within 4.9% and for the other elastic joints ε is ranging from -19.2% to -14.8%. With further increase of loading, more joints yield and the percentage difference in the linear joints decreases to values less than +9.0% (except for θ_8, wherein ε ranges from -3.3% to +17.9%). For the inelastic joints, ε is small and ranges from -5.4% to +8.8%. During a second positive post-elastic excursion (t = 2.96 sec to 3.15 sec) there is a significant difference between SARCF and MONARCF-DC results. The rotation values of inelastic joints, obtained by SARCF, are greater from those of MONARCF-DC with ε varying from +16.3% to +24.3% in the first floor joints and from +2.9% to +14.7% in the second floor joints. For the third floor joints, rotations from MONARCF-DC are higher from those from SARCF with ε ranging from +8.0% to +47.6%.

Example ET1: During the first inelastic excursion of loading (t = 3.25 sec to t = 3.42 sec), the rotation of inelastic joints obtained by the two methods shows good agreement with ε ranging from -3.6% to +4.0% (except at the end of the excursion where ε may go upto -15.4%). After the first inelastic excursion, the response in SARCF does not lie on

the upper bound envelope of the base shear - roof displacement curve; hence joint rotations for subsequent excursions cannot be compared.

Example EC2: During the first inelastic excursion of loading (t = 1.89 sec to t = 2.04 sec), many plastic hinges formed. The elastic and inelastic joint rotations, obtained by SARCF during this excursion, are approximately same as those obtained by MONARCF-DC. ε ranges from -8.5% to +10.7% in the inelastic joints and from -4.9% to +7.6% in the elastic joints (except for the third floor where the rotations at joints 11 and 12 show ε of around +21.0%). At the end of this excursion, ε increases and it ranges from -18.5% to +15.0% in the inelastic joints and from -19.9% to 0.1% in the elastic joints. During the next non-linear positive excursion (t = 3.02 sec to t = 3.15 sec), rotations of the second and third floor joints obtained by MONARCF-DC are significantly higher than those of SARCF (maximum ε = -68.6%). For the first floor joints, ε in the two outer joints (θ_4 and θ_6) is small (-5.3% to +7.3%), but at the middle joint (θ_5), ε is high and ranges from -14.3% to +20.9%.

Example ET2: During the first inelastic excursion (from t = 3.25 sec to t = 3.34 sec), ε for both elastic and inelastic joints ranges from -14.0% to +1.7%, except for θ_{12} where the rotations obtained by MONARCF-DC are higher than those of SARCF (maximum ε = -32.3%). From t = 3.35 sec to t = 3.56 sec, the roof displacement as well as the base shear continue to increase, however the joint rotation values obtained by SARCF decrease; hence MONARCF-DC joint rotation values are significantly higher than those of SARCF (ε ranges from -93.4% to -7.0%) during this period.

Example EC3: During the first inelastic excursion of loading (from t = 1.19 sec to t = 1.25 sec) plastic hinges occurred in beams only (nodes

3 and 5 in beams b1 and b2, respectively). ε is very small and ranges from -0.34% to +4.9% for the inelastic joints, and from -5.5% to 0.0% for the elastic joints. A significant non-linear positive excursion of load started at t = 1.89 sec and lasted till t = 2.08 sec. From t = 1.89 sec to t = 1.97 sec, the inelastic rotation θ_3 obtained by SARCF is higher than that from MONARCF-DC by 12.1% to 17.5%; for the remaining elastic and inelastic joints (except for θ_{10}) the average ε is small and does not exceed ±10%. From t = 1.98 to t = 2.08 sec, the rotation at the elastic and inelastic joints obtained by SARCF is higher from that by MONARCF-DC with ε ranging from +6.0% to +17.3%. Finally, at t = 3.00 sec, the structure started to fail.

Example ET3: At the beginning of the first significant inelastic excursion of loading (t = 3.28 sec to 3.51 sec), the inelastic joint rotation obtained by SARCF, at nodes 3 and 4, is higher than that from MONARCF-DC by upto 11.7% and 17.0%, respectively. With further increase in loading, ε becomes small and ranges from -0.83% to +5.0%. As for the remaining joints (except for θ_{10}), the ε is small and ranges from -15.4% to +7.4%. In the negative excursion of loading (from t = 3.88 sec to t = 4.06 sec), the joint rotation values obtained by SARCF are higher than those by MONARCF-DC with maximum ε of 25%.

Example EC4: At t = 1.22 sec, a plastic hinge occurred at joint 4 of beam b1. At this joint ε is equal to +4.0% while in the remaining joints ε ranges from -11.2% to +4.1%. For the positive inelastic excursion (t = 1.88 sec to t = 2.05 sec), ε in the inelastic joints ranges from -12.9% to +11.2%. Later, at the beginning of next excursion of load (t = 3.00 sec), the structure started to fail and the joint rotations obtained by SARCF are significantly higher than

those obtained by MONARCF-DC.

Example ET4: During a positive excursion of loads (from t = 3.32 sec to t = 3.50 sec), ε in the inelastic joints is small and ranges from -10.6% to +3.8%. At the elastic joints, ε is slightly higher and ranges from -13.4% to +8.2%. During another positive excursion of load (from t = 6.80 sec to t = 7.06 sec), the rotation values at joints 7, 10, and 12 are higher than those of MONARCF-DC with maximum ε equal to +20%, and ε at joints 4, 5, and 8 is equal to ±10%. In the other remaining joints, ε ranges from -56.3% to +5.4%.

Summary of the Results

From the foregoing comparisons of joint rotation, the following observations are made:

1. In the linear range of response, the joint rotations obtained by SARCF and MONARCF-DC are nearly the same. The maximum ε in the linear range is within ±12.0%.
2. During the first non-linear excursion of loading, in case the plastic hinges occur in beam elements only (e.g., examples EC1 and EC3), the rotations in elastic and inelastic joints obtained by MONARCF-DC show good agreement to the same obtained by SARCF with ε in the range of -0.34% to 5.0% at inelastic joints, and -8.0% to +4.0% at elastic joints.
3. During the first significant non-linear excursion of load, ε in rotations by SARCF and MONARCF-DC at the inelastic joints is slightly higher at the beginning and end of the non-linear loop with a range of ±17.0%. This is because the upper bound of base shear - roof displacement curve obtained by MONARCF-DC does not coincide with the beginning and ending parts of the non-linear loading hysteretic curve

obtained by SARCF. In the middle of the non-linear loading excursion, both curves coincide, and ε at the inelastic joints is very small and generally does not exceed ±5.0%.

4. In case, after a number of excursions the structure experiences high damage (for instance, frames EC3 and EC4 suffer high damage because the global damage index, e.g., Chung et al., 1987, exceeds 1.0), the joint rotations obtained by SARCF are significantly higher than those from MONARCF-DC.

5. If the structure does not experience high damage, the maximum percentage difference at the inelastic joints is around +25.0% (i.e., SARCF results may be about 33.0% higher than MONARCF-DC results).

5.5 CURVATURE DUCTILITY

A comparison of SARCF and MONARCF-DC results on the curvature ductility demand in individual members is illustrated in Figs. 5.10 to 5.17, with notation explained in Fig. 5.9. These figures give the ductility demand at each plastic hinge after the end of the first significant inelastic excursion of load (first case) and after the complete hysteretic seismic loading (second case). In the first case, the comparison between SARCF and MONARCF-DC results is done for the same roof displacement which is obtained at the end of the first significant inelastic excursion by SARCF. In the second case, the curvature ductility demand by SARCF is the maximum ductility obtained during the hysteretic loading; in this case, the absolute value of maximum roof displacement obtained by SARCF during the hysteretic loading is considered as the roof displacement at which MONARCF-DC results are obtained and compared to those of SARCF. The global damage index (Chung et al., 1987) computed by SARCF in the first four examples (EC1, ET1,

EC2, and ET2) ranges from 0.13 to 0.5. In examples ET1 and ET2, the maximum displacement obtained during the hysteresis is higher than what roof displacement can be obtained by MONARCF-DC (Figs. 5.2 and 5.4, respectively). Therefore, for examples ET1 and ET2, the accelerogram duration was decreased from 8.40 sec to 6.88 sec. For examples EC3, ET3, EC4, and ET4, the global damage index was higher than 1.0. Hence, the accelerogram duration was reduced in these examples to 5.36 sec, 7.80 sec, 5.30 sec, and 7.80 sec, respectively, such that the global damage index does not exceed 1.0.

In SARCF and MONARCF-DC analyses, the ductility demand in some beams and columns exceeded the maximum available ductility. However, for the sake of this comparison, the third branch of the moment-curvature (M - ϕ) relationship (Fig. 4.14) was allowed to go beyond the failure point but with the same degrading slope.

In the eight examples, the ductility demand obtained by SARCF on beams at the end of the first significant inelastic excursion is close to that obtained by MONARCF-DC. However, the ductility demand for columns obtained by SARCF is significantly less than that obtained by MONARCF-DC. It may be concluded that if the earthquake ground motion is such that it causes only one significant inelastic excursion, then MONARCF-DC gives reasonable estimates of the curvature ductility demand for beams but overestimates the ductility demand for columns.

For case two, the ratio of ductility demand by SARCF analysis to that by MONARCF-DC analysis in the beams and columns is summarized in Table 5.19. The following observations are made from Figs. 5.10 to 5.17 and Table 5.19:

1. MONARCF-DC generally underestimates the ductility demand for beams but overestimates the same for columns.

2. The ductility demand in beams at the roof level is relatively small as compared to that for beams in the middle storeys. This is because the same reinforcement has been provided in beams of all the floors, even though the reinforcement could have been lower for the roof beams.
3. It appears that the underestimation of beam ductility by MONARCF-DC is more for hinges with sagging curvature than it is for hinges with hogging curvature. Particularly for examples having global damage index less than 0.5 (EC1, ET1, EC2, and ET2), the difference in the ductility demand for hogging curvatures in beams, obtained from both analyses, is generally small (except for a few plastic hinges, e.g., node 4-b1 in example EC1). In most cases, at a given beam section (a) the ductility demand in hogging moment is higher than that in sagging moment, and (b) the ductility available in hogging moment is lower than that in sagging moment due to the presence of more reinforcement on the upper face. In view of this, for design situations, it will be adequate if the demand for hogging ductility can be estimated reasonably.
4. The ductility demand for columns obtained by MONARCF-DC tends to be higher than that by SARCF (except the plastic hinge at node 8-c5 in example EC4); however, there are some plastic hinges which form in columns by using SARCF but not by MONARCF-DC.

Table 5.20 shows the range and the average values of the ratio of member ductility demand by SARCF and the overall structure displacement ductility, μ_s ($\mu_s = \Delta_u/\Delta_y$; Δ_y has been taken same as obtained by MONARCF-DC). From Table 5.20, it is observed that:

1. For examples EC1, ET1, EC2, and ET2, having overall damage index less than 0.5, ductility demand for beams ranges from 3.1 μ_s to 16.2 μ_s

for hogging curvatures, and 0.37 μ_s to 14.4 μ_s for sagging curvatures, with an average statistical value varying from 6.2 μ_s to 9.4 μ_s and 5.0 μ_s to 7.6 μ_s, respectively. For the remaining examples (with global damage index ranging within 0.5 to 1), ductility demand for beams ranges from 0.33 μ_s to 25.2 μ_s with an average statistical value varies from 8.5 μ_s to 11.6 μ_s.

2. The ductility demand for column sections ranges from 0.31 μ_s to 5.70 μ_s (except for two high values, 8.57 μ_s and 11.22 μ_s in example EC4) with an average statistical value varying from 1.77 μ_s to 2.78 μ_s.
3. Thus, the ductility demand for columns as a multiple of overall structural ductility is less than the ductility demand for beams.

Both accelerograms used in these analyses have high peak ground acceleration due to the scaling (0.7g in case of twice El Centro accelerogram, and 0.72g in case of four times Taft Lincoln accelerogram) and have therefore caused severe damage to the members and the overall structure. Hence, it may be useful to look at the ductility demand for the members, if the structures are subjected to a ground motion with somewhat moderate intensity. Hence, the four frames have been analyzed by SARCF and subjected to the first 7.68 seconds of 1 × El Centro accelerogram. SARCF and MONARCF-DC results for these examples, termed as EC1*, EC2*, EC3*, and EC4*, are presented in Figs. 5.18 to 5.22. The analysis for unfactored El Centro accelerogram requires the frames to have overall displacement ductility of 2.34, 1.84, 1.31, and 1.89, respectively. And the global damage index in none of these frames exceeds 0.50. Table 5.21 shows the range of values for the ratio of ductility demand by SARCF analysis to MONARCF-DC analysis. Interestingly, now the ductility demand estimates by the two methods are somewhat more comparable. For instance, MONARCF-DC gives ductility

demand for beams (hogging curvature) which ranges from 0.44 to 1.48 times that from SARCF, with average value ranging from 0.62 to 1.04. Similarly, the ductility demand ratios for columns average from 0.75 to 1.03.

Table 5.22 gives the range of member ductility demand as a ratio of overall structural ductility demand. Again, it is seen that a more moderate time history leads to overall moderation in this ratio. For instance, now the demand in curvature ductility for beams and columns become somewhat comparable; i.e., the ratio increases for columns and slightly decreases for beams over what was seen with scaled-up time histories.

It is thus obvious that curvature ductility is a difficult parameter to generalize from parametric studies. The very limited study here indicates that for moderate damage situations, the ductility demand estimates from MONARCF-DC may not be very much different from those by sophisticated dynamic analyses. However, in case of severe damage situations, the hysteretic behaviour becomes more significant and hence the quasi-static analysis procedures may not be very appropriate.

Table 5.1 Comparison of Load and Displacement at the Yield Points Obtained by SARCF, MONARCF-DC and MONARCF-FC.

Example	SARCF			MONARCF-DC			MONARCF-FC		
	P_y (kN)	Δ_y (mm)	K_e (kN/mm)	P_y (kN)	Δ_y (mm)	K_e (kN/mm)	P_y (kN)	Δ_y (mm)	K_e (kN/mm)
EC1	250.0	50.0							
ET1	260.0	61.5							
average	255.0	55.75	4.57	268.6	63.97	4.20	269.9	70.94	3.81
dif. %				5.3	14.7	-8.2	5.8	27.2	-16.8
EC2	420.0	57.0							
ET2	430.0	59.0							
average	425.0	58.0	7.33	450.8	62.93	7.16	457.4	70.59	6.48
dif. %				5.9	7.8	-2.3	7.6	21.7	-11.6
EC3	310.0	80.0							
ET3	300.0	85.7							
average	305.0	82.85	3.68	312.2	83.21	3.75	298.2	89.22	3.34
dif. %				9.0	0.43	1.9	-2.2	7.7	-9.2
EC4	528.0	78.0							
ET4	528.0	83.0							
average	528.0	80.5	6.56	530.3	81.16	6.53	550.0	94.75	5.81
dif. %				0.43	0.82	-0.38	4.2	17.7	-11.5

K_e = elastic stiffness

$$\text{dif. \%} = \frac{\text{MONARCF} - \text{SARCF}}{\text{SARCF}} \times 100\ \%$$

Table 5.2 Maximum Base Shear and Roof Displacement Obtained by MONARCF-DC AND MONARCF-FC.

Example	MONARCF-DC				MONARCF-FC	
	Max. Base Shear		Failure Point		Max. Base Shear	
	P (kN)	Δ (mm)	P (kN)	Δ (mm)	P (kN)	Δ (mm)
3-S. 1-Bay	283	208	283	208	206	204
3-S. 2-Bay	474	199	474	199	500	180
4-S. 1-Bay	322	185	305	289	332	210
4-S. 2-Bay	544	225	542	321	576	238

Table 5.3 Plastic Hinge Sequence by the Quasi-static Analyses for the 3-Storey 1-Bay Frame.

MONARCF-DC		
Δ (mm)	P (kN)	P.HINGE LOCATION
47.0	197.34	4-b1
63.0	247.48	2-c2
66.0	253.31	6-b2
68.0	257.28	1-c1
110.0	277.05	3-b1
165.0	279.39	5-c3
166.0	279.53	5-b2
171.0	279.93	8-c6
173.0	280.12	8-b3
202.0	282.87	6-c4

MONARCF-FC		
Δ (mm)	P (kN)	P.HINGE LOCATION
49.4	188.00	4-b1
61.2	220.00	6-b2
70.9	240.00	2-c2
77.8	252.00	1-c1
110.9	280.00	3-b1
180.2	300.00	5-c3
206.2	304.00	5-b2
		6-c4
		8-c6

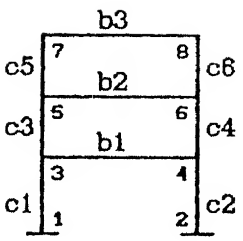

Table 5.4 Plastic Hinge Sequence by the Quasi-static Analyses for the 3-Storey 2-Bay Frame.

MONARCF-DC		
Δ (mm)	P (kN)	P.HINGE LOCATION
51.0	365.32	5-b1
53.0	378.39	6-b2
54.0	383.83	2-c2
59.0	403.95	3-c3
64.0	416.64	1-c1
75.0	426.85	8-b3
77.0	428.74	9-b4
87.0	439.31	8-c5
111.0	462.28	4-b1
114.0	463.76	5-c2
142.0	467.31	5-c5
146.0	467.88	11-c8
152.0	468.75	5-b2
180.0	472.08	7-c4
195.0	473.19	9-c6

MONARCF-FC		
Δ (mm)	P (kN)	P.HINGE LOCATION
52.4	340.00	5-b1
53.8	348.00	6-b2
59.6	376.00	2-c2
64.5	396.00	3-c3
69.2	412.00	1-c1
71.2	416.00	8-b3
73.3	420.00	9-b4
93.0	452.00	8-c5
109.8	472.00	5-c2
114.8	476.00	4-b1
160.2	496.00	5-c5
179.6	500.00	4-c1
		6-c3

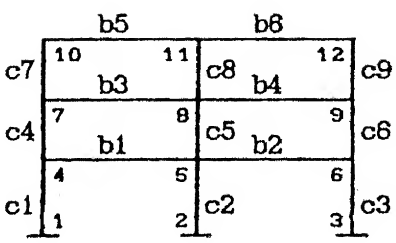

Table 5.5 Plastic Hinge Sequence by the Quasi-static Analyses for the 4-Storey 1-Bay Frame.

MONARCF-DC			MONARCF-FC		
Δ (mm)	P (kN)	P.HINGE LOCATION	Δ (mm)	P (kN)	P.HINGE LOCATION
59.0	221.36	4-b1	63.5	212.13	4-b1
71.0	254.87	6-b2	69.7	228.14	6-b2
88.0	303.03	2-c2	98.9	284.17	8-b3
95.0	311.26	1-c1	103.9	292.18	2-c2
107.0	314.73	8-b3	107.0	296.18	1-c1
129.0	318.65	3-b1	135.1	316.89	3-b1
158.0	320.87	5-b2	165.7	328.20	5-b2

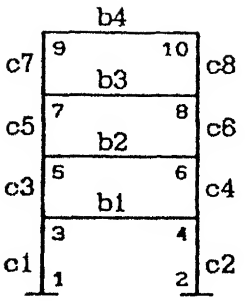

Table 5.6 Plastic Hinge Sequence by the Quasi-static Analyses for the 4-Storey 2-Bay Frame.

MONARCF-DC			MONARCF-FC		
Δ (mm)	P (kN)	P.HINGE LOCATION	Δ (mm)	P (kN)	P.HINGE LOCATION
64.0	418.18	5-b1	67.6	392.23	5-b1
		6-b2	68.2	396.23	6-b2
73.0	462.54	2-c2	76.2	432.26	8-b3
79.0	483.56	8-b3	78.1	440.26	9-b4
80.0	487.04	9-b4	81.5	452.27	2-c2
81.0	490.61	3-c3	85.4	464.28	3-c3
85.0	499.92	1-c1	93.6	486.29	1-c1
123.0	529.07	8-c5	128.9	544.32	4-b1
127.0	532.36	4-b1			11-b5
128.0	533.14	11-b5			12-b6
		12-b6			8-c5
159.0	542.44	5-b2	158.1	564.34	5-b1
164.0	542.50	11-c8	170.1	568.34	5-c2
169.0	542.48	7-b3	186.9	572.34	7-b3
239.0	542.45	10-c7			11-c8
241.0	542.45	12-c9			
279.0	542.42	14-c11			

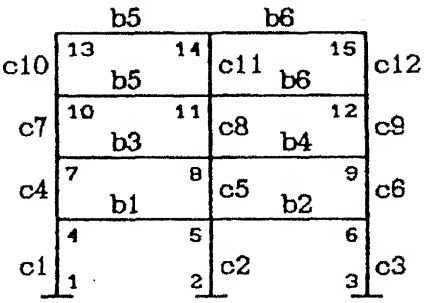

Table 5.7 Comparison of Plastic Hinge Sequence for the 3-Storey 1-Bay Frame

a- EC1 (El Centro)

SARCF				MONARCF-DC					MONARCF-FC				
P. H.L.	Δ (mm)	P (kN)	S	Δ (mm)	P (kN)	S	Δ_e%	P_e%	Δ (mm)	P (kN)	S	Δ_e%	P_e%
3-b1	-45.9	-213.9	1	-47	-197.3	1	2.4	-7.7	49.40	188	1	7.6	-12.1
4-b1	46.3	241.0	1	47	197.3	1	1.4	-18.1	49.4	180	1	6.6	-25.3
2-c2	54.8	258.2	2	63	247.5	2	15.0	-4.1	70.9	240	3	29.5	-7.0
1-c1	67.4	267.8	3	68	257.3	4	0.94	-0.3	77.8	252	4	15.5	-5.9
6-b2	79.7	267.4	4	66	253.3	3	-17.1	-5.3	61.2	220	2	-23.1	-17.7
4-c2	109.5	270.6	5										
3-c1	136.7	306.2	6										
5-c3	178.4	292.2	7	165	279.4	6	-7.5	-4.5	180.2	300	6	1.0	2.6
6-c4	178.4	292.2	7	202	282.9	10	13.2	-3.3	206.2	304	7	15.6	3.8
8-c6	178.4	292.2	7	171	279.9	8	-4.1	-4.2	206.2	304	7	15.6	3.8
8-b3	183.8	287.7	10	173	280.1	9	-6.2	4.4					
7-b3	184.8	281.5	11										

b- ET1 (Taft Lincoln)

SARCF				MONARCF-DC					MONARCF-FC				
P. H.L.	Δ (mm)	P (kN)	S	Δ (mm)	P (kN)	S	Δ_e%	P_e%	Δ (mm)	P (kN)	S	Δ_e%	P_e%
4-b1	46.6	216.1	1	47	197.3	1	0.97	-8.7	49.4	188	1	6.1	-13.0
2-c2	60.6	253.9	2	63	247.5	2	4.1	-2.5	70.9	240	3	17.1	-5.5
6-b2	70.8	261.0	3	66	253.3	3	6.6	-2.9	61.2	220	2	-13.4	-15.7
1-c1	70.8	261.0	3	68	258.3	4	3.8	-1.0	77.8	252	4	10.1	-3.5
3-b1	95.6	265.6	5	110	277.0	5	15.1	4.3	110.9	280	5	16.0	5.4
5-b2	-57.7	-206.7		-66	-253.3		14.4	22.5	-81.2	-220		6.1	6.0
7-c5	-124.1	-216.0		-171	-279.9		37.8	29.6	-206.2	-304		66.2	40.7
5-c3	-129.8	-219.0		-202	-282.9		55.6	27.0	-206.2	-304		58.9	38.8
6-c4	-134.8	-222.7		-165	-279.5		22.4	25.5	-180.3	-300		33.8	34.7
3-c1	-134.8	-222.7											
8-c6	167.7	186.7		171	279.9		1.96	49.9	206.2	304		55.2	62.8
8-b3	171.6	186.6		173	280.1		0.81	50.1					

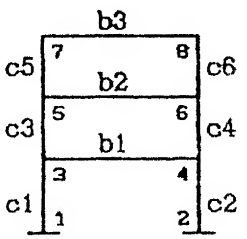

Δ : Roof displacement

P : Base shear force

$$\Delta_e\% = \frac{\Delta_2 - \Delta_1}{\Delta_1} \times 100$$

$$p_e\% = \frac{P_2 - P_1}{P_1} \times 100$$

Δ_1 : Roof displacement recorded by SARCF

Δ_2 : Roof displacement recorded by MONARCF-DC or MONARCF-FC

P_1 : Base shear force recorded by SARCF

P_2 : Base shear force recorded by MONARCF-DC or MONARCF-FC

Table 5.8 Comparison of Plastic Hinge Sequence for the 3-Storey 2-Bay Frame

a- EC2 (El Centro)

SARCF				MONARCF-DC					MONARCF-FC				
P. H.L.	Δ (mm)	P (kN)	S	Δ (mm)	P (kN)	S	Δ_e%	P_e%	Δ (mm)	P (kN)	S	Δ_e%	P_e%
5-b1	56.5	412.8	1	51	365.3	1	-9.7	-11.5	52.4	340	1	-7.2	-17.6
6-b2	56.5	412.8	1	53	378.4	2	-6.1	-8.4	53.8	348	2	-4.6	-15.7
2-c2	56.5	412.8	1	54	383.8	3	-4.4	-7.0	59.6	376	3	5.6	-8.9
3-c3	56.5	412.8	1	59	403.9	4	4.5	-2.1	64.5	396	4	14.3	-4.1
1-c1	64.6	423.1	5	64	416.6	5	-0.96	-1.5	69.2	412	5	7.1	-2.6
8-b3	72.6	423.3	6	75	426.9	6	3.3	0.84	71.2	416	6	-1.9	-1.7
9-b4	72.6	423.3	6	77	428.7	7	6.1	1.3	73.3	420	7	1.0	-0.78
8-c5	80.2	424.4	8	87	439.3	8	8.4	3.5	93.0	452	8	15.9	6.5
4-b1	111.7	429.3	9	111	462.3	9	-0.62	7.7	114.8	476	10	2.7	10.9
5-c2	128.8	450.5	10	114	463.7	10	-11.5	3.0	109.8	472	9	-14.8	4.8
5-b2	129.1	451.8	11	152	468.8	13	-17.7	3.7					
7-b3	-67.6	-275.2		-77	-428.7		13.9	55.8	-73.3	-420		8.4	52.6
7-c4	-84.1	-277.6		-195	-473.2		131.8	88.5					
9-c6	-140.3	-455.3		-180	-472.1		28.3	3.7					
8-b4	-141.2	-416.6		-75	-428.7		-41.9	2.9	-71.2	-416		-49.6	2.9
11-c8	-141.2	-393.5		-146	-467.9		3.4	18.9					

b- ET2 (Taft Lincoln)

SARCF				MONARCF-DC					MONARCF-FC				
P. H.L.	Δ (mm)	P (kN)	S	Δ (mm)	P (kN)	S	Δ_e%	P_e%	Δ (mm)	P (kN)	S	Δ_e%	P_e%
5-b1	53.5	404.6	1	51	365.3	1	-4.64	-9.7	52.4	340	1	-2.0	-16.0
6-b2	53.5	404.6	1	53	378.4	2	-0.89	-6.5	53.8	348	2	0.65	-14.0
2-c2	53.5	404.6	1	54	383.8	3	0.97	-5.1	59.6	376	3	11.5	-7.1
3-c3	59.3	421.8	4	59	403.9	4	-0.48	-4.2	64.5	396	4	8.9	-6.1
1-c1	59.3	421.8	4	64	416.6	5	8.0	-1.2	69.2	412	5	16.7	-2.3
8-b3	72.8	425.9	6	75	426.9	6	3.0	0.23	71.2	416	6	-2.2	-2.3
4-b1	84.4	532.0	7	111	462.3	9	31.0	-13.1	114.8	476	10	35.6	-10.5
5-b2	-54.8	-367.8		-51	-365.3		-6.9	-0.68	-52.4	-340		-4.3	-7.6
5-c2	-54.8	-367.8		-114	-463.7		108.0	26.1	-109.8	-472		100.4	28.4
8-c5	-65.6	-378.3		-87	-439.3		32.6	16.1	-93.0	-452		41.7	19.5
7-b3	-75.9	-388.5		-77	-428.7		1.4	10.3	-73.3	-420		-3.4	8.1
8-b4	-75.9	-388.5		-75	-428.7		-1.2	10.3	-71.2	-416		-8.2	7.1
4-c1	-75.9	-388.5											
7-c4	-102.9	-409.2		-180	-472.1		74.9	15.4					
9-b4	-110.7	-397.9											
9-c6	-130.7	-430.6		-146	-467.9		11.7	8.7					

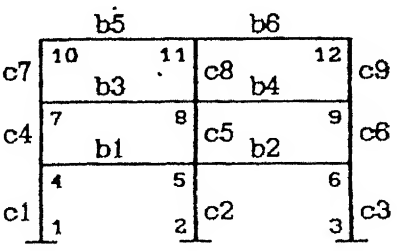

Table 5.9 Comparison of Plastic Hinge Sequence for the 4-Storey 1-Bay Frame

a- EC3 (El Centro)

SARCF				MONARCF-DC					MONARCF-FC				
P. H.L.	Δ (mm)	P (kN)	S	Δ (mm)	P (kN)	S	Δ_e%	P_e%	Δ (mm)	P (kN)	S	Δ_e%	P_e%
3-b1	-61.3	-237.5	1	-59	-221.4	1	-3.7	-6.8	-63.4	-212.1	1	3.4	-10.7
5-b2	-70.5	-235.8	2	-71	-254.9	2	0.77	8.1	-69.7	-228.1	2	-1.1	-3.3
4-b1	77.9	290.1	1	59	221.4	1	-24.3	-23.7	63.4	212.1	1	-14.5	-26.9
6-b2	88.2	297.3	2	71	254.9	2	-19.5	-14.3	69.7	228.1	2	-20.1	-23.3
2-c2	88.2	297.9	2	88	303.0	3	13.1	4.5	103.9	292.2	4	33.6	-0.79
1-c1	98.4	302.6	4	95	311.3	4	-3.5	2.9	107.0	296.2	5	-8.7	-2.1
8-b3	108.4	302.2	5	107	314.7	5	-1.3	4.1	98.9	284.2	3	-8.7	-6.0
7-b3	172.4	282.6	6										
10-b4	257.3	196.2											
9-b4	262.8	206.9											

b- ET3 (Taft Lincoln)

SARCF				MONARCF-DC					MONARCF-FC				
P. H.L.	Δ (mm)	P (kN)	S	Δ (mm)	P (kN)	S	Δ_e%	P_e%	Δ (mm)	P (kN)	S	Δ_e%	P_e%
4-b1	61.2	282.1	1	59	221.4	1	-3.6	-21.5	63.4	212.1	1	3.6	-24.8
6-b2	75.4	279.7	2	71	254.9	2	-5.9	-8.9	69.7	228.1	2	-7.6	-18.4
2-c2	92.5	300.2	3	88	303.0	3	-4.9	0.95	103.9	292.2	4	12.4	-2.7
1-c1	97.2	301.8	4	95	311.3	4	-2.2	3.2	107.0	296.2	5	10.2	-1.9
8-b3	106.7	297.1	5	107	314.7	5	0.28	5.9	98.9	284.2	3	7.3	-4.3
3-b1	108.7	297.1	5	129	318.7	6	20.9	7.3	135.1	316.9	6	26.6	6.8
5-b2	108.7	297.7	7	158	320.9	7	46.6	7.8	165.7	328.2	7	52.4	10.2
7-b3	-130.5	-249.7		-107	-314.7		-18.0	26.0	98.9	284.2		-24.2	13.8
9-b4	-228.4	33.3											
10-b4	-225.9	63.5											

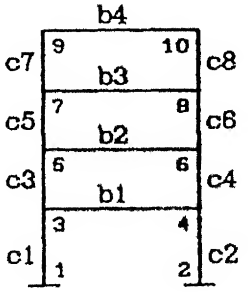

Table 5.10 Comparison of Plastic Hinge Sequence for the 4-Storey 2-Bay Frame

a- EC4 (El Centro)

SARCF				MONARCF-DC					MONARCF-FC				
P. H.L.	Δ (mm)	P (kN)	S	Δ (mm)	P (kN)	S	Δ_e%	P_e%	Δ (mm)	P (kN)	S	Δ_e%	P_e%
4-b1	61.7	417.7	1	-64	-418.2	1	3.8	0.12	-68.2	396	2	10.7	-5.1
6-b2	60.9	471.0	1	64	418.2	1	5.2	-11.2	68.2	396	2	12.1	-15.9
5-b1	70.1	507.0	2	64	462.5	1	-8.7	-17.5	67.6	392	1	-3.6	-22.6
2-c2	70.1	507.0	2	73	490.6	3	4.1	-8.8	81.5	452	5	16.3	-10.8
3-c3	70.1	507.0	2	81	499.9	5	15.5	-3.2	85.4	464	6	21.8	-8.4
1-c1	79.5	519.4	6	85	483.6	7	6.9	-3.8	93.6	486	7	17.8	-6.4
8-b3	88.2	519.7	6	79	487.0	4	-10.5	-7.0	76.2	432	3	-13.7	-16.8
9-b4	88.2	519.7	7	80	533.1	6	-9.4	-6.3	78.1	440	4	-11.5	-15.3
12-b6	121.3	522.3	8	128	533.1	10	5.5	2.1	128.9	544	8	6.3	4.2
8-b4	128.5	521.7	9										
11-b5	128.5	521.7	9	128	533.1	10	-0.3	2.2	128.9	544	8	0.35	4.3
8-c5	128.5	521.7	9	123	529.0	8	-4.2	1.4	128.9	544	8	0.35	4.3
11-c8	151.4	515.1	12	164	542.5	13	6.6	5.3	187.0	572	13	23.5	11.1
5-c5	165.9	523.3	13										
5-b2	165.9	523.3	13	159	542.4	12	-4.2	3.6					
10-b5	-105.7	-398.1		-128	-533.1		21.1	33.9	-128.9	-544		21.9	36.7
7-c4	-112.8	-413.1											
10-c7	239.2	331.9		239	542.4		-0.08	63.4					
12-c9	239.2	331.9		241	542.4		0.75	63.4					
8-c8	-116.8	-206.9											

cont'd

b- ET4 (Taft Lincoln)

SARCF				MONARCF-DC					MONARCF-FC				
P. H.L.	Δ (mm)	P (kN)	S.	Δ (mm)	P (kN)	S	Δ_e%	P_e%	Δ (mm)	P (kN)	S	Δ_e%	P_e%
6-b2	61.6	431.9	1	64	418.2	1	3.9	-3.2	68.2	396	2	10.7	-8.3
5-b1	65.1	446.9	2	64	418.2	1	-1.6	-6.4	67.6	392	1	3.9	-12.3
2-c2	72.0	472.2	3	73	462.5	3	1.5	-2.0	81.5	452	5	13.3	4.2
9-b4	81.9	495.4	4	80	487.0	5	-2.3	-1.7	78.1	440	4	-4.6	-11.1
3-c3	81.9	495.4	4	81	490.6	6	-1.1	-0.9	85.4	464	6	4.2	-6.3
8-b3	85.0	498.8	6	79	483.0	4	-7.0	-3.1	76.2	432	3	-10.3	-13.3
1-c1	85.0	498.8	6	85	499.9	7	0.47	0.22	93.6	486	7	10.2	-2.5
4-b1	104.3	505.5	8										
5-b2	-56.7	-400.1		-64	-418.2		12.9	4.6	-67.6	-392		19.2	-2.0
7-b3	-100.1	-474.7		-80	-487.0		-20.0	2.6	-78.1	-440		-22.0	-7.2
8-b4	-100.1	-474.7		-79	483.0		-21.0	1.7	-76.2	-432		-23.9	-8.9
8-c5	-127.2	-456.3		-123	-529.1		-3.3	15.9	-128.9	-544		1.3	19.3
10-b5	-135.0	-451.8		-128	-533.1		-5.2	-18.0	-128.9	-544		-4.5	-20.5
11-b6	-142.3	-436.8		-128	-533.1		-10.0	22.0	-128.9	-544		-9.4	-24.6
11-c8	-142.3	-436.8		-164	-542.5		-15.3	24.2	-186.9	-572		-31.3	31.0
12-b6	-168.1	-408.3											
11-b5	194.8	439.9		128	533.1		-34.3	21.2	128.9	544		-33.8	23.7
12-c9	-235.6	-206.0		-239	-542.4		1.4	163.3					
14-c11	-272.6	-123.2		-288	-542.4		5.6	340.3					
10-c7	-280.5	-107.9		-241	-542.4		14.1	402.7					
15-b8	-300.5	-79.7											
13-b7	-311.0	-84.9											

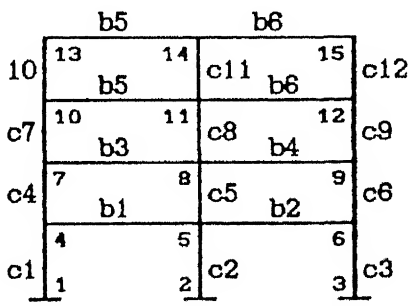

Table 5.11 Comparison of Joint Rotations Obtained by SARCF and MONARCF-DC for Example EC1.

Time sec	Δ (mm)		θ_3 $\times 10^{-4}$	θ_4 $\times 10^{-4}$	θ_5 $\times 10^{-4}$	θ_6 $\times 10^{-4}$	θ_7 $\times 10^{-4}$	θ_8 $\times 10^{-4}$
1.09	-30.4	S	20.5	35.3	16.4	22.6	-1.50	21.9
	(1.)	M	20.2	35.2	16.7	22.8	-1.67	21.7
		ε%	1.40	0.19	-1.72	-0.94	.....	0.71
1.14	-39.8	S	30.2	45.2	21.2	27.3	0.00	23.4
	(1.)	M	28.8	43.8	22.8	28.9	1.45	24.8
		ε%	4.57	3.01	-7.60	-6.01	.....	-6.21
1.17	-45.9	S	36.2	51.1	25.0	31.1	1.50	24.9
		M	34.4	49.4	26.8	32.9	3.46	26.8
		ε%	4.95	3.27	-7.15	-5.85	.....	-7.93
1.20	-50.1	S	41.3	55.2	28.3	34.7	3.80	27.1
		M	39.4	53.7	29.3	35.6	4.90	28.3
		ε%	4.57	2.69	-3.47	-2.54	.....	-4.27
1.22	-51.6	S	42.5	56.2	30.6	37.1	5.40	28.7
		M	41.5	55.4	30.1	36.5	5.44	28.8
		ε%	2.39	1.48	1.51	1.50	.....	-0.21
1.88	46.3	S	-52.4	-36.3	-28.9	-22.7	-23.6	-2.00
		M	-49.8	-34.8	-33.2	-27.0	-27.0	-3.60
		ε%	4.94	4.16	-14.84	-19.21	-14.46	.....
1.89	58.9	S	-65.0	-50.4	-39.1	-32.5	-29.5	-6.30
		M	-63.4	-51.5	-41.1	-34.2	-31.1	-7.98
		ε%	2.45	-2.27	-5.19	-5.36	-5.44	.....
1.90	67.3	S	-73.6	-61.5	-45.9	-38.6	-33.3	-10.3
		M	-72.6	-62.3	-46.5	-39.4	-33.7	-10.6
		ε%	1.30	-1.27	-1.19	-2.07	-1.22	-3.34
1.91	79.6	S	-86.1	-77.2	-56.0	-49.5	-38.6	-15.3
		M	-83.9	-75.9	-55.5	-49.8	-37.0	-13.5
		ε%	2.57	1.69	0.88	-0.63	3.97	11.9
1.92	91.4	S	-98.2	-92.3	-66.5	-61.4	-43.0	-19.2
		M	-94.1	-89.1	-63.9	-59.4	-40.1	-16.0
		ε%	4.10	3.48	3.85	3.30	6.78	16.33
1.93	102.4	S	-110.4	-105.8	-75.8	-72.2	-46.8	-22.4
		M	-103.7	-101.4	-71.6	-68.0	-42.7	-18.4
		ε%	6.05	4.13	5.54	5.77	8.56	17.94
1.96	112.4	S	-122.4	-121.9	-84.0	-81.9	-49.3	-24.9
		M	-112.9	-112.7	-78.3	-75.7	-45.2	-20.4
		ε%	7.68	7.55	6.76	7.49	8.24	17.96
1.98	121.4	S	-135.0	-130.5	-90.4	-90.6	-52.0	-26.1
		M	-123.0	-122.6	-83.7	-82.6	-47.5	-22.1
		ε%	8.86	6.02	7.33	8.79	8.65	15.14
2.00	131.4	S	-147.5	-143.0	-97.9	-98.8	-53.8	-27.6
		M	-134.2	-133.5	-89.6	-90.3	-49.9	-23.9
		ε%	8.97	6.59	8.39	8.61	7.09	13.21

cont'd

2.02	140.5	S	-157.3	-153.1	-103.9	-105.1	-54.9	-28.6
		M	-144.5	-143.5	-94.9	-97.1	-52.2	-25.5
		ε%	8.15	6.29	8.66	7.63	4.97	10.73
2.05	145.2	S	-160.1	-155.9	-105.7	-107.0	-55.5	-29.1
		M	-149.7	-148.5	-97.5	-100.5	-53.3	-26.3
		ε%	6.48	4.71	7.71	6.06	4.02	9.54
2.06	145.6	S	-159.1	-154.6	-104.8	-106.1	-55.5	-29.2
		M	-150.2	-149.0	-97.8	-100.8	-53.4	-26.4
		ε%	5.60	3.62	6.70	4.97	3.84	9.60
2.43	-102.2	S	111.0	132.5	75.7	86.7	17.5	39.0
		M	101.2	103.5	67.8	71.5	18.4	42.7
		ε%	8.83	21.85	10.34	17.58	-4.78	-9.60
2.45	-110.0	S	112.6	134.2	74.4	85.4	15.8	37.3
		M	110.0	110.4	73.9	76.8	19.9	44.6
		ε%	2.25	17.73	0.58	10.02	-26.36	-19.67
2.48	-120.5	S	109.2	130.7	71.3	82.4	15.6	37.1
		M	121.7	122.1	81.9	83.3	21.9	47.3
		ε%	-11.46	6.59	-14.97	-1.05	-40.96	-27.45
2.53	-123.9	S	104.0	125.1	66.5	77.7	14.8	36.3
		M	125.4	125.9	84.6	85.3	22.6	48.1
		ε%	-20.62	-0.65	-27.26	-9.79	-52.83	-32.64
2.96	117.2	S	-156.4	-155.8	-89.3	-85.4	-41.4	-17.1
		M	-118.4	-118.0	-81.2	-79.4	-46.4	-21.4
		ε%	24.32	24.22	9.00	7.03	-12.18	-24.98
2.98	130.3	S	-172.7	-172.1	-93.6	-89.8	-40.4	-16.1
		M	-133.0	-132.4	-89.0	-89.4	-49.7	-23.7
		ε%	22.95	23.07	4.85	0.36	-23.06	-47.59
3.00	140.4	S	-185.3	-181.8	-97.4	-94.4	-41.3	-16.7
		M	-143.9	-142.9	-94.6	-96.7	-52.0	-25.4
		ε%	22.33	21.38	2.85	-2.45	-26.03	-52.38
3.03	150.7	S	-194.4	-190.9	-104.0	-101.3	-44.4	-19.7
		M	-155.9	-154.6	-100.7	-104.5	-54.5	-27.2
		ε%	19.75	19.00	3.20	-3.23	-22.8	-38.3
3.05	159.3	S	-201.4	-197.7	-111.4	-108.8	-48.9	-24.1
		M	-166.2	-164.5	-105.6	-111.1	-56.6	-28.7
		ε%	17.45	16.80	5.15	-2.11	-15.82	-19.25
3.15	178.7	S	-226.4	-221.4	-135.5	-130.0	-58.7	-33.1
		M	-186.8	-185.2	-115.6	-124.2	-61.2	-30.7
		ε%	17.48	16.34	14.68	4.41	-8.00	7.23

Δ : Roof displacement

(l.): Linear state

S : SARCF results

M : MONARCF-DC results

ε% : $\frac{\theta^S - \theta^M}{\theta^S} \times 100$ θ^S = rotation obtained by SARCF;

θ^M = rotation obtained by MONARCF-DC

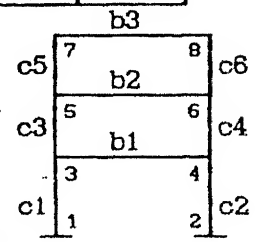

Table 5.12 Comparison of Joint Rotations Obtained by SARCF and MONARCF-DC for Example ET1.

Time sec	Δ (mm)		θ_3 $\times 10^{-4}$	θ_4 $\times 10^{-4}$	θ_5 $\times 10^{-4}$	θ_6 $\times 10^{-4}$	θ_7 $\times 10^{-4}$	θ_8 $\times 10^{-4}$
3.20	30.1	S	-36.6	-21.5	-19.9	-13.8	-19.6	4.00
	(l.)	M	-35.0	-20.0	-22.6	-16.5	-21.7	1.75
		ε%	4.31	6.93	-13.88	-19.88	-11.68	.....
3.23	39.7	S	-44.4	-29.9	-26.8	-20.5	-23.7	-0.30
	(l.)	M	-43.7	-28.7	-28.8	-22.7	-24.8	-1.40
		ε%	1.51	3.98	-7.69	-10.87	-4.72	.....
3.25	46.5	S	-50.6	-36.2	-31.7	-25.4	-26.3	-2.90
		M	-50.0	-34.9	-33.3	-27.2	-27.0	-3.67
		ε%	1.18	3.36	-5.14	-7.08	-2.98	.....
3.26	50.0	S	-53.8	-39.3	-34.1	-28.1	-27.4	-4.00
		M	-53.6	-39.3	-35.5	-29.3	-28.2	-4.88
		ε%	0.29	0.00	-4.22	-4.08	-3.05	.....
3.29	60.5	S	-65.5	-54.5	-41.3	-34.2	-30.6	-7.70
		M	-65.1	-53.7	-42.1	-35.1	-31.6	-8.51
		ε%	0.58	1.46	-1.95	-2.67	-3.26	.....
3.32	70.7	S	-77.4	-70.6	-47.9	-39.9	-33.3	-10.5
		M	-75.9	-66.0	-48.9	-42.3	-34.6	-11.4
		ε%	1.95	6.14	-2.20	-6.02	-4.09	-9.08
3.35	80.6	S	-86.9	-78.5	-54.0	-47.8	-35.5	-12.1
		M	-84.7	-76.9	-56.1	-50.6	-37.3	-13.7
		ε%	2.51	2.02	-4.02	-5.81	-5.09	-13.11
3.38	89.8	S	-92.4	-84.3	-58.3	-53.3	-37.8	-14.0
		M	-92.8	-87.3	-62.8	-58.1	-39.7	-15.7
		ε%	-0.42	-3.57	-7.75	-9.01	-4.98	-12.30
3.42	99.9	S	-94.1	-88.1	-60.6	-55.9	-39.9	-15.8
		M	-101.6	-98.7	-69.9	-66.1	-42.2	-17.8
		ε%	-7.98	-14.65	-15.39	-18.33	-5.779	-13.19

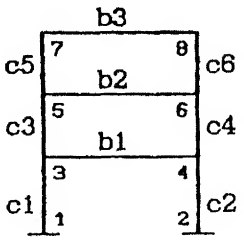

Δ : Roof displacement

(l.): Linear state

S : SARCF results

M : MONARCF-DC results

ε% : $\frac{\theta^S - \theta^M}{\theta^S} \times 100$ θ^S = rotation obtained by SARCF;

θ^M = rotation obtained by MONARCF-DC

Table 5.13 Comparison of Joint Rotations Obtained by SARCF and MONARCF-DC for Example EC2.

Time sec	Δ (mm)		θ_4 $\times 10^{-4}$	θ_5 $\times 10^{-4}$	θ_6 $\times 10^{-4}$	θ_7 $\times 10^{-4}$	θ_8 $\times 10^{-4}$	θ_9 $\times 10^{-4}$	θ_{10} $\times 10^{-4}$	θ_{11} $\times 10^{-4}$	θ_{12} $\times 10^{-4}$
1.10	-30.7	S	23.3	20.7	36.5	14.4	14.8	21.5	-0.74	5.90	19.3
	(1.)	M	22.8	20.1	35.9	15.5	15.4	22.3	0.30	6.21	19.5
		ε%	2.34	2.87	1.40	-7.74	-4.00	-4.16	.....	.....	-1.34
1.16	-40.2	S	32.3	27.6	46.4	19.4	19.0	26.6	1.00	7.10	21.1
	(1.)	M	31.9	26.4	45.1	21.4	20.2	28.3	3.46	8.15	22.6
		ε%	1.06	4.39	2.66	-10.5	-6.28	-6.45	.....	.....	-7.38
1.22	-45.9	S	37.6	30.6	51.0	25.4	23.7	32.5	5.10	9.70	25.4
	(1.)	M	37.3	30.0	50.5	24.9	23.0	31.8	5.22	9.28	24.5
		ε%	0.71	1.74	0.89	1.93	2.89	2.18	.....	.....	1.93
1.89	56.4	S	-60.7	-37.7	-47.2	-38.2	-28.2	-30.8	-28.3	-12.2	-8.30
		M	-61.4	-38.7	-48.8	-38.2	-28.0	-31.2	-27.9	-11.4	-8.69
		ε%	-1.22	-2.67	-3.52	0.00	0.43	-1.21	1.38	6.04	-4.78
1.90	64.6	S	-68.2	-43.5	-54.2	-44.5	-33.1	-37.2	-32.0	-14.7	-11.9
		M	-70.4	-46.3	-59.1	-42.9	-31.8	-35.7	-30.5	-13.0	-11.3
		ε%	-3.27	-6.38	-9.03	3.50	3.90	4.09	4.81	11.10	4.83
1.91	72.5	S	-75.9	-51.1	-65.9	-50.4	-37.5	-42.3	-35.5	-17.0	-15.7
		M	-77.7	-53.7	-68.5	-47.6	-35.2	-39.9	-32.6	-14.5	-13.7
		ε%	-2.48	-5.07	-3.96	5.41	6.02	5.49	7.93	14.28	12.83
1.92	80.2	S	-82.2	-57.0	-76.9	-55.9	-41.8	-47.2	-38.6	-19.2	-19.1
		M	-84.7	-60.6	-77.4	-52.4	-39.4	-44.5	-34.6	-15.7	-15.6
		ε%	-3.02	-6.25	-0.59	6.20	5.69	5.64	10.34	18.07	17.96
1.93	87.5	S	-89.0	-63.0	-84.3	-61.2	-46.7	-53.2	-41.7	-20.9	-21.5
		M	-91.1	-66.8	-85.4	-57.0	-44.0	-49.7	-36.3	-16.7	-17.2
		ε%	-2.44	-6.14	-1.38	6.77	5.68	6.50	12.89	20.22	19.98
1.94	94.3	S	-94.0	-66.1	-89.7	-66.4	-49.9	-59.2	-43.3	-22.7	-23.2
		M	-97.2	-72.1	-93.2	-61.4	-47.2	-54.5	-37.8	-17.8	-18.5
		ε%	-3.42	-9.07	-3.92	7.57	5.40	7.84	12.64	21.57	20.04
1.95	100.7	S	-100.0	-69.8	-95.3	-70.3	-53.5	-62.7	-45.2	-22.5	-25.2
		M	-102.7	-76.9	-100.4	-65.3	-49.9	-58.9	-39.1	-18.8	-19.7
		ε%	-2.44	-8.88	-5.36	7.07	8.70	5.93	13.36	16.16	21.67
1.96	106.5	S	-104.6	-73.8	-98.6	-73.7	-55.6	-69.5	-45.5	-24.0	-23.7
		M	-107.8	-81.2	-106.9	-68.9	-52.3	-62.9	-40.3	-19.8	-20.8
		ε%	-3.07	-10.13	-8.49	8.52	5.91	9.42	11.35	17.2	12.28
1.97	111.7	S	-111.3	-84.3	-107.5	-74.2	-60.9	-70.0	-48.8	-23.1	-26.8
		M	-112.3	-85.1	-112.7	-72.7	-54.4	-66.5	-41.3	-20.7	-21.6
		ε%	-0.90	-1.04	-4.84	2.87	10.65	4.97	13.09	10.53	18.47

cont'd

1.98	116.3	S	-113.5	-89.2	-110.2	-76.9	-62.0	-71.8	-47.2	-23.4	-26.5
		M	-112.3	-88.3	-117.7	-74.6	-56.2	-69.6	-42.3	-21.3	-22.4
		ε%	-3.28	0.97	-6.87	2.97	9.30	3.02	10.36	8.58	15.23
1.99	120.2	S	-115.9	-89.4	-112.5	-77.2	-61.9	-72.3	-46.9	-23.3	-26.2
		M	-121.5	-90.6	-122.1	-76.7	-57.7	-72.2	-43.1	-22.0	-23.1
		ε%	-4.88	-1.41	-8.54	0.58	6.68	0.06	8.07	5.58	11.81
2.04	128.8	S	-117.4	-95.6	-144.4	-72.5	-51.5	-67.1	-41.1	-21.8	-20.4
		M	-131.0	-95.5	-131.5	-81.2	-61.0	-77.8	-44.8	-23.3	-24.4
		ε%	-11.66	0.10	14.99	-12.11	-18.46	-16.03	-8.99	-6.80	-19.87
3.01	147.6	S	-155.1	-84.5	-144.0	-50.9	-39.4	-35.5	-26.1	-9.90	-8.80
		M	-152.1	-104.3	-152.3	-90.7	-67.6	-89.6	-48.3	-25.7	-27.2
		ε%	1.87	-23.43	-5.78	-78.4	-71.5	.....	-85.0	.....	.....
3.02	153.0	S	-162.5	-92.2	-150.4	-55.9	-42.7	-41.1	-28.7	-11.6	-11.0
		M	-158.3	-105.3	-158.2	-93.4	-68.7	-92.9	-49.4	-25.5	-28.1
		ε%	2.56	-14.29	-5.28	-67.1	-60.8	.....	-72.2	.....	.....
3.03	158.1	S	-168.9	-98.8	-155.3	-61.0	-46.7	-46.7	-31.3	-13.1	-13.5
		M	-164.1	-107.4	-164.0	-95.9	-69.8	-96.0	-50.5	-25.2	-29.0
		ε%	2.83	-8.75	-5.61	-57.19	-49.44	.....	-61.4	-92.9	.....
3.06	171.6	S	-187.9	-119.4	-174.1	-75.5	-56.5	-61.8	-38.0	-17.9	-20.1
		M	-179.6	-114.9	-178.9	-102.1	-72.4	-104.1	-53.4	-24.3	-31.3
		ε%	4.38	3.75	-2.78	-35.25	-28.27	-68.55	-40.51	-36.07	-55.88
3.09	182.2	S	-201.5	-130.3	-189.8	-86.8	-65.0	-73.4	-42.3	-20.5	-24.3
		M	-191.8	-121.4	-190.7	-106.7	-74.5	-110.4	-55.7	-23.5	-33.1
		ε%	4.82	6.81	-0.49	-22.91	-14.66	-50.49	-31.89	-14.98	-36.22
3.12	189.2	S	-212.3	-145.5	-204.2	-93.1	-68.1	-79.7	-43.6	-22.1	-25.6
		M	-199.3	-119.9	-198.5	-108.7	-75.8	-114.6	-57.5	-22.9	-34.2
		ε%	6.09	17.54	2.75	-16.84	-11.39	-43.79	-31.89	-3.95	-33.80
3.15	191.9	S	-218.2	-150.5	-207.5	-93.6	-68.3	-81.2	-43.2	-22.0	-24.9
		M	-202.3	-119.0	-201.6	-109.5	-76.3	-116.2	-58.2	-22.7	-34.7
		ε%	7.28	20.89	2.82	-17.04	-11.80	-43.11	-34.73	-3.38	-39.36

Δ : Roof displacement

(l.): Linear state

S : SARCF results

M : MONARCF-DC results

ε% : $\frac{\theta^S - \theta^M}{\theta^S} \times 100$ θ^S = rotation obtained by SARCF;

θ^M = rotation obtained by MONARCF-DC

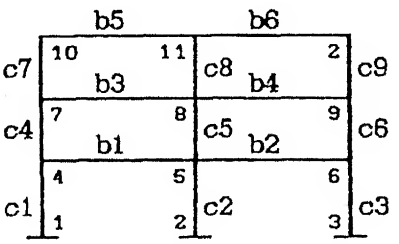

Table 5.14 Comparison of Joint Rotations Obtained by SARCF and MONARCF-DC for Example ET2.

Time sec	Δ (mm)		θ_4 $\times 10^{-4}$	θ_5 $\times 10^{-4}$	θ_6 $\times 10^{-4}$	θ_7 $\times 10^{-4}$	θ_8 $\times 10^{-4}$	θ_9 $\times 10^{-4}$	θ_{10} $\times 10^{-4}$	θ_{11} $\times 10^{-4}$	θ_{12} $\times 10^{-4}$
3.23	47.6	S	-52.7	-31.5	-39.3	-32.0	-23.5	-24.9	-25.4	-9.70	-5.40
	(1.)	M	-52.1	-31.1	-38.9	-32.8	-23.8	-25.9	-25.0	-9.63	-5.77
		ε%	1.01	1.02	0.87	-2.60	-1.53	-4.23	1.47	.....	.....
3.24	50.5	S	-55.6	-33.8	-42.2	-33.7	-24.7	-26.7	-26.1	-10.3	-6.00
	(1.)	M	-54.9	-33.1	-41.7	-34.6	-25.3	-27.7	-25.9	-10.2	-6.72
		ε%	1.08	2.02	0.98	-2.86	-2.63	-4.03	0.45	0.65	.....
3.25	53.4	S	-58.8	-35.7	-45.4	-35.2	-26.2	-28.2	-26.7	-10.6	-6.70
		M	-58.1	-35.7	-44.7	-36.4	-26.7	-29.6	-26.9	-10.8	-7.68
		ε%	1.09	0.00	1.45	-3.49	-1.96	-4.91	-0.91	-2.37	.....
3.26	56.4	S	-61.8	-38.6	-48.9	-36.9	-27.3	-29.8	-27.2	-11.0	-7.10
		M	-61.4	-38.6	-48.8	-38.1	-28.0	-31.1	-27.9	-11.4	-8.68
		ε%	0.66	0.00	0.21	-3.42	-2.76	-4.52	-2.54	-4.11	.....
3.27	59.2	S	-65.2	-39.3	-55.7	-38.2	-29.0	-30.4	-27.8	-11.2	-7.90
		M	-64.5	-41.3	-52.7	-39.8	-29.4	-32.6	-28.8	-12.0	-9.65
		ε%	0.95	-5.12	5.30	-4.30	-1.34	-7.49	-3.63	-7.35	.....
3.28	62.1	S	-67.5	-43.1	-60.1	-40.0	-29.8	-31.6	-28.1	-11.8	-8.40
		M	-67.7	-43.9	-56.1	-41.4	-30.7	-34.3	-29.7	-12.5	-10.5
		ε%	-0.36	-1.99	6.58	-3.73	-2.98	-8.48	-5.69	-8.49	.....
3.29	64.9	S	-70.3	-45.2	-63.7	-41.2	-31.0	-32.8	-28.6	-11.9	-8.90
		M	-70.7	-46.5	-59.4	-43.1	-31.9	-35.8	-30.5	-13.1	-11.4
		ε%	-0.57	-2.95	6.70	-4.63	-3.01	-9.24	-6.78	-10.25	.....
3.30	67.6	S	-72.1	-47.5	-64.2	-42.7	-31.8	-34.5	-29.0	-12.3	-9.20
		M	-73.2	-49.0	-62.6	-44.7	-33.1	-37.3	-31.3	-13.6	-12.2
		ε%	-1.56	-3.30	2.42	-4.80	-4.15	-8.18	-7.99	-10.95	.....
3.31	70.2	S	-73.9	-48.9	-66.9	-43.7	-32.8	-35.3	-29.6	-12.6	-9.90
		M	-75.6	-51.5	-65.7	-46.3	-34.2	-38.7	-32.0	-14.1	-13.0
		ε%	-2.37	-5.37	1.69	-5.97	-4.41	-9.76	-8.28	-12.26	.....
3.32	72.8	S	-74.9	-50.3	-68.5	-44.8	-33.4	-36.3	-30.1	-13.0	-10.4
		M	-78.0	-53.9	-68.8	-47.8	-35.3	-40.1	-32.7	-14.6	-13.7
		ε%	-4.14	-7.20	-0.43	-6.73	-5.82	-10.49	-8.81	-12.44	-32.29
3.33	75.3	S	-75.8	-51.0	-69.6	-45.5	-34.0	-36.9	-30.8	-13.4	-11.2
		M	-80.3	-56.2	-71.7	-49.2	-36.4	-41.4	-33.4	-15.0	-14.4
		ε%	-5.94	-10.29	-3.11	-8.31	-7.16	-12.21	-8.48	-12.39	-29.17

cont'd

3.34	77.7	S	-76.1	-51.5	-70.1	-46.0	-34.4	-37.5	-31.3	-13.8	-11.7
		M	-82.4	-58.4	-74.5	-50.8	-37.8	-42.7	-34.0	-15.4	-15.1
		ε%	-8.36	-13.39	-6.39	-10.52	-9.97	-14.03	-8.62	-11.63	-29.25
3.35	80.1	S	-76.2	-51.5	-70.2	-46.3	-34.6	-37.7	-31.9	-14.0	-12.3
		M	-84.5	-60.4	-77.2	-52.3	-39.3	-44.4	-34.5	-15.7	-15.8
		ε%	-10.96	-17.36	-9.69	-13.05	-13.67	-17.87	-8.38	-12.23	-27.15
3.36	82.3	S	-76.0	-51.3	-69.8	-46.3	-34.7	-37.8	-32.8	-14.3	-12.6
		M	-86.5	-62.4	-79.6	-53.7	-40.7	-46.0	-35.1	-16.0	-16.1
		ε%	-13.87	-21.59	-14.15	-16.11	-17.48	-21.77	-7.02	-11.90	-27.91
3.37	84.4	S	-75.4	-51.7	-68.5	-46.1	-34.4	-37.7	-32.5	-14.4	-12.8
		M	-88.4	-64.2	-82.0	-55.1	-42.1	-47.5	-35.6	-16.2	-16.5
		ε%	-17.27	-24.21	-19.73	-19.52	-22.42	-26.09	-9.54	-13.02	-29.37
3.38	86.6	S	-75.4	-51.3	-69.1	-45.6	-34.1	-37.1	-32.4	-14.3	-12.7
		M	-90.1	-65.9	-84.1	-56.3	-43.3	-48.9	-36.0	-16.5	-16.9
		ε%	-19.55	-28.44	-21.79	-23.51	-27.12	-31.84	-11.28	-15.50	-33.58
3.39	88.1	S	-74.9	-51.1	-68.5	-45.0	-33.5	-36.5	-32.0	-14.0	-12.3
		M	-91.7	-67.3	-86.1	-57.4	-44.3	-50.1	-36.4	-16.7	-17.3
		ε%	-22.43	-31.77	-25.73	-27.62	-32.43	-37.42	-13.92	-19.70	-40.83
3.40	89.7	S	-74.3	-50.1	-68.3	-44.1	-33.0	-35.5	-31.4	-13.6	-11.7
		M	-93.0	-68.5	-87.9	-58.4	-45.1	-51.2	-36.8	-17.0	-17.6
		ε%	-25.29	-36.85	-28.69	-32.47	-36.69	-44.41	-17.23	-25.14	-50.74
3.56	98.8	S	-69.4	-45.5	-63.5	-34.1	-25.4	-25.5	-23.7	-8.80	-9.10
		M	-101.1	-75.5	-98.3	-64.1	-49.1	-57.6	-38.7	-18.5	-19.3
		ε%	-45.69	-66.02	-54.79	-88.18	-93.42	.....	-63.59	.....	.....

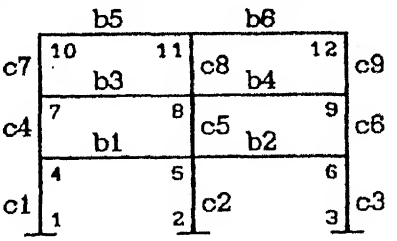

Δ : Roof Displacement

(1.): Linear state

S : SARCF results

M : MONARCF-DC results

$\varepsilon\% : \dfrac{\theta^S - \theta^M}{\theta^S} \times 100$

θ^S = rotation btained by SARCF;

θ^M = rotation btained by MONARCF-DC

Table 5.15 Comparison of Joint Rotations Obtained by SARCF and MONARCF-DC for Example EC3.

Time sec	Δ (mm)		θ_3 $\times 10^{-4}$	θ_4 $\times 10^{-4}$	θ_5 $\times 10^{-4}$	θ_6 $\times 10^{-4}$	θ_7 $\times 10^{-4}$	θ_8 $\times 10^{-4}$	θ_9 $\times 10^{-4}$	θ_{10} $\times 10^{-4}$
1.17	-56.3 (1.)	S	38.5	49.6	31.5	40.0	20.6	26.6	2.70	22.0
		M	37.3	49.0	31.9	40.1	21.3	27.4	2.66	22.0
		ε%	3.09	1.10	-1.40	-0.37	-3.66	-3.04	.....	0.00
1.18	-58.8 (1.)	S	40.5	52.5	33.5	41.6	21.4	27.5	2.90	22.3
		M	39.2	51.0	33.5	41.7	22.4	28.5	3.22	22.5
		ε%	3.02	2.82	0.00	-0.46	-4.94	-3.69	.....	-1.22
1.19	-61.3	S	42.4	54.4	35.1	43.5	22.3	28.3	3.20	22.5
		M	41.7	53.1	35.0	43.3	23.5	29.5	3.73	23.1
		ε%	1.40	2.33	0.27	0.45	-5.52	-4.48	.....	-2.68
1.25	-70.4	S	51.8	61.6	42.3	51.0	27.7	33.6	6.10	25.5
		M	51.9	61.4	40.2	48.9	27.5	33.4	5.65	25.1
		ε%	-0.34	0.22	4.87	3.95	0.61	0.41	.....	1.74
1.89	67.3	S	-71.0	-52.0	-43.3	-35.9	-28.1	-21.7	-23.5	-4.30
		M	-58.6	-48.4	-47.0	-38.4	-32.1	-26.1	-24.4	-5.01
		ε%	17.47	6.81	-8.67	-7.13	-14.39	-20.63	-3.83	.....
1.90	77.8	S	-79.5	-60.2	-50.4	-43.5	-34.1	-27.8	-27.3	-8.10
		M	-68.1	-59.9	-54.2	-46.0	-36.4	-30.4	-26.6	-7.25
		ε%	14.39	0.43	-7.54	-5.83	-6.87	-9.27	2.54	.....
1.91	88.2	S	-88.6	-70.4	-57.7	-49.8	-40.0	-33.7	-30.7	-11.4
		M	-77.5	-71.1	-61.8	-54.6	-40.6	-34.2	-28.7	-9.46
		ε%	12.48	-1.01	-7.11	-9.77	-1.55	-1.73	6.49	17.02
1.92	98.4	S	-97.9	-80.5	-65.2	-59.0	-45.5	-38.6	-33.7	-14.7
		M	-86.0	-80.6	-69.4	-63.6	-44.5	-37.9	-30.7	-11.5
		ε%	12.10	-0.21	-6.54	-7.79	2.07	1.72	8.92	21.37
1.93	108.4	S	-107.0	-92.4	-73.9	-67.7	-50.4	-43.5	-36.4	-17.4
		M	-93.9	-90.3	-76.8	-72.0	-48.3	-41.4	-32.5	-13.4
		ε%	12.19	2.27	-3.99	-6.38	4.23	4.73	10.70	22.66
1.94	117.9	S	-116.2	-102.4	-82.9	-78.2	-54.7	-47.5	-38.6	-19.8
		M	-101.7	-99.9	-83.7	-79.6	-52.2	-45.9	-34.1	-14.8
		ε%	12.48	2.43	-1.01	-1.82	4.58	3.32	11.64	25.11
1.95	127.1	S	-125.9	-112.8	-91.7	-87.7	-59.1	-52.6	-40.2	-21.1
		M	-109.1	-109.1	-90.2	-86.8	-55.9	-50.2	-35.6	-16.1
		ε%	13.32	3.28	1.55	0.94	5.42	4.60	11.46	23.71
1.96	135.9	S	-135.2	-122.8	-101.0	-97.5	-63.2	-55.9	-41.0	-23.5
		M	-117.1	-117.7	-98.2	-93.8	-59.4	-54.1	-36.9	-17.2
		ε%	13.35	4.09	4.66	3.71	6.02	3.15	9.87	28.45

cont'd

1.97	144.2	S	-144.1	-133.0	-110.5	-106.3	-66.4	-62.3	-42.5	-21.7
		M	-125.3	-126.0	-101.8	-100.4	-62.6	-57.8	-38.2	-18.4
		ε%	13.02	5.26	7.87	5.51	5.60	7.19	10.10	15.29
1.98	152.0	S	-152.5	-142.3	-119.6	-115.4	-69.8	-65.7	-42.2	-22.1
		M	-133.1	-133.7	-106.9	-106.5	-65.7	-61.2	-39.3	-19.4
		ε%	12.70	5.99	10.58	7.65	5.84	6.81	6.73	12.27
1.99	159.3	S	-160.3	-154.0	-128.4	-123.3	-72.7	-69.3	-42.3	-21.9
		M	-140.4	-141.0	-111.7	-112.2	-68.5	-64.3	-40.4	-20.3
		ε%	12.40	8.39	12.94	8.97	5.76	7.11	4.46	7.29
2.02	178.0	S	-180.7	-175.8	-150.7	-146.8	-80.4	-77.7	-42.6	-21.9
		M	-158.2	-159.5	-126.0	-126.6	-75.0	-72.2	-43.2	-22.5
		ε%	12.41	9.27	16.35	13.73	6.65	6.98	-1.36	-2.87
2.08	197.7	S	-200.2	-194.3	-170.7	-166.7	-94.0	-92.5	-48.0	-26.9
		M	-177.1	-178.9	-141.1	-141.6	-81.7	-80.4	-45.9	-24.7
		ε%	11.51	7.93	17.31	15.01	13.06	13.11	4.20	7.93

Δ : Roof displacement

(1.): Linear state

S : SARCF results

M : MONARCF-DC results

$$\varepsilon\% : \frac{\theta^S - \theta^M}{\theta^S} \times 100$$

θ^S = rotation obtained by SARCF;

θ^M = rotation obtained by MONARCF-DC

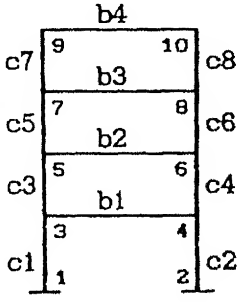

Table 5.16 Comparison of Joint Rotations Obtained by SARCF and MONARCF-DC for Example ET3.

Time sec	Δ (mm)		θ_3 $\times 10^{-4}$	θ_4 $\times 10^{-4}$	θ_5 $\times 10^{-4}$	θ_6 $\times 10^{-4}$	θ_7 $\times 10^{-4}$	θ_8 $\times 10^{-4}$	θ_9 $\times 10^{-4}$	θ_{10} $\times 10^{-4}$
1.57	20.8	S	-20.5	-8.80	-17.2	-9.00	-13.7	-7.60	-16.2	5.20
	(1.)	M	-21.8	-10.0	-17.4	-9.21	-12.0	-5.97	-14.2	5.12
		ε%	-6.44	-14.52	-1.30	-2.37	12.15	.....	12.12	.....
1.68	30.5	S	-29.5	-17.8	-24.7	-16.5	-16.4	-10.3	-16.2	3.10
	(1.)	M	-29.3	-17.5	-23.7	-15.4	-16.2	-10.2	-16.3	2.98
		ε%	0.60	1.25	4.12	6.23	0.79	0.87	-1.09	.....
3.23	56.5	S	-52.3	-40.5	-38.6	-29.4	-24.9	-19.8	-19.1	-2.50
	(1.)	M	-49.2	-37.4	-40.3	-32.0	-27.5	-21.4	-22.0	-2.70
		ε%	5.91	7.50	-4.35	-9.08	-10.42	-8.29	-15.46	.....
3.28	61.2	S	-60.1	-50.2	-40.4	-31.6	-29.6	-22.7	-20.0	-5.00
		M	-53.0	-41.6	-43.2	-34.9	-29.5	-23.5	-23.0	-3.71
		ε%	11.72	16.98	-7.06	-10.61	0.23	-3.49	-15.42	.....
3.33	75.4	S	-68.4	-60.4	-51.4	-42.4	-33.6	-27.6	-25.8	-6.40
		M	-65.9	-57.4	-52.4	-44.0	-35.4	-29.4	-26.1	-6.74
		ε%	3.56	5.03	-2.09	-3.97	-5.61	-6.76	-1.19	.....
3.36	84.2	S	-74.0	-67.1	-58.4	-50.3	-39.5	-33.4	-29.7	-10.2
		M	-74.0	-66.8	-58.8	-51.3	-39.0	-32.8	-27.9	-8.63
		ε%	0.00	0.34	-0.84	-2.09	1.21	1.78	6.00	.....
3.39	92.4	S	-80.7	-74.8	-65.2	-58.4	-43.7	-37.2	-31.9	-12.7
		M	-81.3	-75.1	-64.9	-58.4	-42.3	-35.8	-29.5	-10.3
		ε%	-0.83	-0.41	0.39	0.00	3.25	3.70	7.39	18.53
3.41	97.2	S	-85.5	-82.7	-69.7	-63.0	-45.2	-38.8	-32.4	-13.2
		M	-85.0	-79.5	-68.5	-62.5	-44.0	-37.4	-30.4	-11.3
		ε%	0.50	3.88	1.71	0.78	2.48	3.37	6.00	14.34
3.46	105.5	S	-98.0	-95.5	-79.0	-73.9	-46.0	-39.2	-30.7	-11.7
		M	-91.6	-87.4	-74.7	-69.6	-47.1	-40.3	-32.0	-12.9
		ε%	6.48	8.42	5.38	5.76	-2.57	-2.99	-4.24	-10.57
3.51	110.6	S	-100.4	-97.3	-81.6	-77.2	-45.7	-38.8	-29.4	-10.4
		M	-95.7	-92.5	-78.4	-73.8	-49.2	-42.4	-32.8	-13.8
		ε%	4.62	4.90	3.84	4.38	-7.62	-9.47	-11.85	-32.56
3.88	-121.0	S	124.0	140.8	88.0	99.6	48.6	43.6	14.4	34.2
		M	103.0	104.2	82.0	85.9	47.4	53.4	15.2	34.6
		ε%	16.93	25.99	13.72	5.26	-22.57	2.53	-5.98	-1.18
3.89	-130.5	S	131.1	147.5	97.8	110.3	49.5	54.5	17.7	37.5
		M	112.4	111.9	89.5	92.6	51.7	57.2	18.5	36.1
		ε%	14.27	24.15	8.44	16.03	-4.42	-4.97	6.49	3.69

cont'd

3.90	-139.4	S	137.7	154.1	108.6	120.7	56.1	61.0	20.1	44.0
		M	121.1	120.5	96.6	98.5	55.6	60.7	17.7	37.4
		ε%	12.04	21.80	11.05	18.33	0.79	0.40	11.75	14.83
3.92	-155.4	S	149.9	166.1	128.6	142.2	70.4	73.8	23.1	43.5
		M	137.1	136.4	109.1	109.1	62.6	67.0	19.8	39.8
		ε%	17.85	8.54	15.12	22.18	10.99	9.20	14.26	8.42
3.94	-169.0	S	160.2	176.3	146.3	157.3	82.4	84.8	25.1	45.4
		M	150.7	149.7	119.7	119.1	68.5	71.9	19.8	39.8
		ε%	8.54	17.85	15.12	22.18	10.99	9.20	14.26	8.42
3.96	-180.3	S	169.4	184.7	160.1	170.8	92.5	94.2	27.1	98.2
		M	150.7	149.7	127.8	128.4	73.2	75.8	22.8	43.5
		ε%	4.53	13.15	19.81	25.17	20.85	19.50	15.87	55.69
3.98	-189.2	S	177.6	191.5	171.2	180.0	98.5	101.8	30.2	50.7
		M	170.5	168.9	135.2	134.7	76.9	78.8	23.8	44.8
		ε%	3.99	11.79	21.01	25.19	21.92	22.52	21.14	11.65
4.00	-196.0	S	183.3	196.2	175.7	185.4	106.1	106.1	32.2	52.9
		M	177.2	175.5	140.4	139.9	79.7	81.1	24.5	45.7
		ε%	3.31	10.56	20.09	24.56	24.89	23.51	23.66	13.51
4.02	-201.0	S	187.7	200.7	173.0	187.4	109.5	109.2	33.7	55.5
		M	182.1	180.4	144.1	143.6	81.7	82.8	25.1	46.4
		ε%	2.96	10.11	16.66	23.36	25.39	24.16	25.43	16.32
4.04	-204.3	S	192.4	205.9	175.0	185.1	110.0	110.8	34.7	56.1
		M	183.6	185.4	146.7	146.1	83.0	83.9	25.5	46.9
		ε%	3.63	10.79	16.17	21.05	24.51	24.25	26.53	16.41
4.06	-205.9	S	197.1	210.4	172.7	183.0	107.3	108.3	34.2	55.5
		M	186.9	185.2	147.9	147.3	83.6	84.4	25.6	47.1
		ε%	5.13	11.95	14.36	19.48	22.01	22.02	24.96	15.12

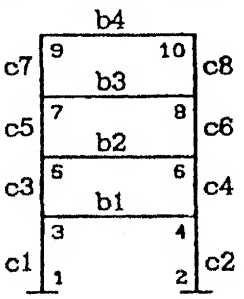

Δ : Roof displacement

(l.): Linear state

S : SARCF results

M : MONARCF-DC results

$\varepsilon\% : \dfrac{\theta^S - \theta^M}{\theta^S} \times 100$ θ^S = rotation obtained by SARCF;

θ^M = rotation obtained by MONARCF-DC

Table 5.17 Comparison of Joint Rotations Obtained by SARCF and MONARCF-DC for Example EC4.

Time sec	Δ (mm)		θ_4 $\times 10^{-4}$	θ_5 $\times 10^{-4}$	θ_6 $\times 10^{-4}$	θ_7 $\times 10^{-4}$	θ_8 $\times 10^{-4}$	θ_9 $\times 10^{-4}$	θ_{10} $\times 10^{-4}$	θ_{11} $\times 10^{-4}$	θ_{12} $\times 10^{-4}$	θ_{13} $\times 10^{-4}$	θ_{14} $\times 10^{-4}$	θ_{15} $\times 10^{-4}$
1.09	-21.7	S	12.5	12.9	23.4	8.90	10.4	17.1	5.30	6.90	12.0	-4.30	3.10	13.3
	(l.)	M	12.3	12.5	22.8	9.75	10.9	17.3	5.89	7.19	12.1	-3.38	3.07	12.5
		ε%	1.73	2.74	2.56	-9.6	-4.9	-1.25	.....	.....	-1.00	.....	.....	5.41
1.11	-39.1	S	25.7	22.4	36.5	19.6	19.0	27.7	13.3	13.5	20.1	0.50	6.30	18.1
	(l.)	M	26.4	22.6	36.9	20.6	19.7	28.2	13.1	13.0	19.4	0.33	5.54	16.2
		ε%	-2.65	-1.00	-1.08	-5.23	-3.59	-1.78	1.27	3.89	3.69	.....	.....	10.0
1.22	-61.6	S	46.4	37.1	57.4	34.4	31.2	42.5	20.2	19.0	27.0	2.70	8.90	20.3
		M	44.5	35.6	55.0	34.6	30.9	42.2	22.4	20.4	28.6	5.08	8.72	21.0
		ε%	4.01	4.03	4.09	-0.69	0.73	0.69	-11.2	-7.47	-6.20	.....	.....	-3.62
1.88	60.8	S	-58.7	-37.4	-45.8	-38.3	-28.2	-30.5	-25.2	-17.3	-18.3	-20.4	-8.20	-2.90
		M	-54.4	-35.1	-43.9	-41.7	-30.5	-34.1	-28.3	-20.1	-22.1	-20.8	-8.61	-4.92
		ε%	7.30	6.02	4.14	-8.91	-8.44	-11.9	-12.5	-16.5	-20.9	-2.30	.....	.....
1.89	70.1	S	-65.2	-42.1	-52.4	-44.2	-33.0	-36.4	-30.2	-21.6	-23.3	-23.6	-9.50	-6.10
		M	-62.5	-42.5	-53.1	-47.3	-34.9	-39.5	-32.1	-23.2	-25.9	-22.8	-9.90	-6.84
		ε%	4.02	-1.08	-1.48	-7.18	-5.84	-8.73	-6.53	-7.61	-11.5	3.34	.....	.....
1.90	79.2	S	-71.7	-48.5	-59.4	-50.4	-37.6	-42.6	-35.1	-25.6	-25.6	-26.3	-11.5	-8.90
		M	-71.2	-50.4	-63.7	-52.9	-39.2	-44.6	-35.8	-26.2	-29.7	-24.6	-11.1	-8.67
		ε%	0.75	-3.92	-7.29	-4.94	-4.24	-4.86	-2.15	-2.35	-16.3	6.19	3.09	.....
1.91	88.2	S	-78.7	-53.2	-69.6	-56.3	-42.6	-47.9	-39.8	-29.3	-32.8	-28.9	-13.4	-11.4
		M	-79.0	-57.2	-72.6	-59.0	-45.5	-51.5	-39.2	-28.7	-33.0	-26.4	-12.3	-10.5
		ε%	-0.50	-7.65	-4.32	-4.93	-6.78	-7.55	1.41	2.00	-0.64	8.46	7.65	7.86
1.92	97.0	S	-84.8	-61.0	-78.9	-62.5	-47.5	-54.4	-44.2	-32.8	-37.1	-31.2	-15.0	-13.8
		M	-85.9	-63.9	-80.8	-65.2	-51.6	-58.4	-42.3	-31.0	-35.9	-28.0	-13.4	-12.2
		ε%	-1.38	-4.87	-2.50	-4.29	-8.75	-7.43	4.23	5.37	3.12	9.95	10.0	11.6
1.93	105.5	S	-91.9	-67.0	-87.3	-68.8	-54.4	-60.6	-48.1	-35.6	-41.0	-33.3	-16.6	-15.8
		M	-92.6	-70.4	-88.9	-70.9	-57.5	-65.0	-45.2	-33.1	-38.6	-29.6	-14.5	-13.7
		ε%	-0.81	-5.21	-1.88	-3.16	-5.75	-7.29	6.00	6.80	5.73	11.1	12.5	12.9

cont'd

1.95	121.3	S	-106.4	-87.0	-104.8	-81.0	-66.5	-74.7	-54.4	-39.9	-46.9	-36.5	-19.0	-19.1
		M	-105.3	-83.2	-104.5	-81.4	-68.0	-76.8	-50.3	-36.9	-43.4	-32.2	-16.3	-16.4
		ε%	1.01	4.31	0.23	-0.53	-2.37	-2.83	7.53	7.30	7.34	11.9	14.0	13.9
1.96	128.4	S	-114.0	-95.5	-114.1	-87.3	-71.5	-82.5	-56.3	-43.2	-48.1	-37.7	-19.3	-20.6
		M	-111.2	-89.0	-111.8	-86.0	-72.1	-82.0	-52.5	-38.7	-45.5	-33.3	-17.0	-17.6
		ε%	2.40	6.82	2.00	1.40	-0.90	0.56	6.71	10.2	5.34	11.6	11.6	14.6
1.97	135.0	S	-122.3	-99.8	-122.5	-92.9	-78.5	-87.8	-58.3	-43.3	-53.0	-37.6	-21.4	-18.8
		M	-117.8	-93.9	-118.6	-90.0	-75.2	-86.6	-54.7	-41.1	-48.0	-34.2	-17.5	-18.4
		ε%	3.66	5.86	3.17	3.10	4.20	1.31	6.06	4.99	9.43	8.91	17.8	1.77
2.00	151.4	S	-143.6	-124.0	-144.8	-109.5	-86.5	-103.7	-60.6	-48.4	-55.7	-37.9	-19.3	-19.7
		M	-134.2	-106.2	-135.2	-99.7	-82.6	-98.0	-60.2	-47.0	-54.0	-36.4	-18.7	-20.4
		ε%	6.51	14.33	6.58	8.96	4.43	5.45	0.64	2.69	2.98	3.83	3.25	-3.92
2.01	155.5	S	-152.9	-116.5	-150.4	-112.7	-90.8	-108.2	-61.6	-48.2	-55.7	-37.2	-19.1	-19.1
		M	-138.4	-109.4	-139.4	-102.1	-84.6	-100.9	-61.5	-48.5	-55.5	-36.9	-18.9	-20.9
		ε%	9.45	6.10	7.25	9.36	6.81	6.65	-0.75	-0.80	0.29	0.56	0.82	-9.82
2.02	159.0	S	-159.8	-118.4	-152.5	-116.0	-92.5	-112.7	-61.0	-48.0	-55.7	-36.4	-18.7	-18.4
		M	-141.9	-112.0	-143.0	-104.2	-86.2	-103.4	-62.6	-49.8	-56.7	-37.4	-19.1	-21.4
		ε%	11.15	5.36	6.20	10.17	6.78	8.20	-2.75	-3.79	-1.93	-2.87	-2.53	-16.2
2.05	165.3	S	-166.1	-98.2	-164.1	-123.2	-94.8	-118.8	-60.0	-46.0	-59.7	-34.0	-17.6	-16.0
		M	-148.3	-117.8	-149.3	-107.8	-89.0	-107.8	-64.6	-51.9	-58.9	-38.2	-19.5	-22.1
		ε%	10.70	-19.98	8.97	12.45	6.11	9.23	-7.76	-12.9	1.24	-12.5	-11.3	-38.2

Δ : Roof displacement

(l.): Linear state

S : SARCF results

M : MONARCF-DC results

$\varepsilon\% : \dfrac{\theta^S - \theta^M}{\theta^S} \times 100$

θ^S = rotation obtained by SARCF;

θ^M = rotation obtained by MONARCF-DC

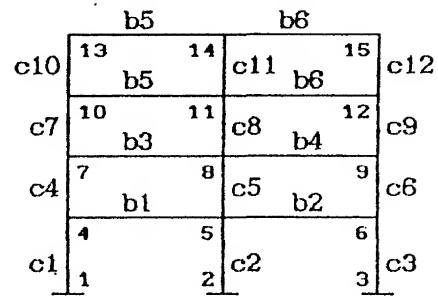

Table 5.18 Comparison of Joint Rotations Obtained by SARCF and MONARCF-DC for Example ET4.

Time sec	Δ (mm)		θ_4 $\times 10^{-4}$	θ_5 $\times 10^{-4}$	θ_6 $\times 10^{-4}$	θ_7 $\times 10^{-4}$	θ_8 $\times 10^{-4}$	θ_9 $\times 10^{-4}$	θ_{10} $\times 10^{-4}$	θ_{11} $\times 10^{-4}$	θ_{12} $\times 10^{-4}$	θ_{13} $\times 10^{-4}$	θ_{14} $\times 10^{-4}$	θ_{15} $\times 10^{-4}$
1.58	21.8	S	-22.8	-12.4	-11.9	-17.4	-10.8	-9.30	-12.8	-7.60	-6.00	-14.0	-3.60	3.50
	(1.)	M	-22.6	-12.6	-12.3	-17.4	-10.9	-9.81	-12.1	-7.23	-5.94	-12.6	-3.08	3.35
		ε%	0.363	-1.65	-3.90	0.00	-1.47	-5.56	4.97	.....	.....	9.98	.....	.....
3.32	61.6	S	-56.9	-36.8	-45.9	-41.2	-30.3	-33.4	-27.2	-19.3	-20.4	-20.8	-8.30	-3.40
		M	-55.0	-35.6	-44.5	-42.2	-30.9	-34.6	-28.6	-20.4	-22.4	-21.0	-8.71	-5.08
		ε%	3.28	3.28	3.01	-2.40	-2.18	-3.66	-5.38	-5.75	-10.0	-1.10	.....	.....
3.33	65.0	S	-59.3	-38.3	-48.3	-43.4	-32.4	-35.5	-29.3	-20.7	-22.5	-22.0	-9.20	-4.40
		M	-57.9	-37.9	-47.5	-44.3	-32.6	-36.7	-30.0	-21.5	-23.8	-21.7	-9.20	-5.80
		ε%	2.35	1.08	1.62	-2.09	-0.75	-3.43	-2.69	-4.09	-6.09	1.09	0.00	.....
3.35	71.9	S	-64.2	-43.2	-55.3	-48.2	-35.7	-39.6	-33.0	-23.7	-26.3	-24.3	-10.7	-6.70
		M	-64.3	-44.3	-55.3	-48.4	-35.7	-40.6	-32.9	-23.8	-26.7	-23.2	-10.1	-7.22
		ε%	-0.15	-2.54	0.00	-0.61	0.00	-2.56	0.20	-0.66	-1.79	4.56	5.10	.....
3.38	81.9	S	-76.5	-54.1	-66.5	-54.3	-39.8	-45.4	-37.2	-27.5	-30.6	-27.3	-12.5	-9.70
		M	-73.6	-52.4	-66.5	-54.6	-40.9	-46.4	-36.8	-26.9	-30.8	-25.2	-11.5	-9.20
		ε%	3.75	3.09	-0.14	-0.69	-2.92	-2.30	0.91	1.96	-0.59	7.70	7.96	.....
3.39	84.9	S	-76.8	-55.2	-72.0	-56.0	-41.7	-46.8	-38.3	-28.1	-31.8	-27.9	-13.0	-10.3
		M	-76.5	-54.7	-69.5	-56.7	-43.1	-48.9	-38.0	-27.8	-31.8	-25.8	-11.9	-9.83
		ε%	0.38	0.79	3.47	-1.33	-3.46	-4.44	0.71	1.03	0.00	7.48	8.19	4.54
3.40	87.8	S	-78.9	-58.1	-75.7	-58.1	-43.4	-49.5	-39.1	-28.9	-32.4	-28.5	-13.3	-10.9
		M	-78.7	-56.9	-72.2	-58.7	-45.1	-51.1	-39.1	-28.6	-32.8	-26.4	-12.3	-10.4
		ε%	0.17	1.99	4.62	-1.16	-4.10	-3.38	0.00	1.05	-1.42	7.48	7.39	4.43
3.44	97.1	S	-86.9	-64.9	-83.1	-65.0	-50.8	-57.8	-41.0	-30.1	-34.0	-27.9	-13.2	-10.4
		M	-86.0	-64.0	-80.9	-65.2	-51.7	-58.5	-42.3	-31.0	-35.9	-28.1	-13.5	-12.2
		ε%	0.95	1.28	2.53	-0.41	-1.86	-1.28	-3.35	-3.21	-5.82	-0.78	-2.35	-17.6
3.50	105.4	S	-88.6	-65.5	-85.7	-65.8	-52.3	-58.7	-40.7	-29.7	-33.7	-27.1	-12.8	-9.60
		M	-92.5	-70.4	-88.8	-70.9	-57.4	-64.8	-45.1	-33.1	-38.6	-29.5	-14.5	-13.7
		ε%	-4.47	-7.50	-3.67	-7.75	-9.86	-10.63	-11.0	-11.6	-14.5	-9.15	-13.4	.....
6.80	105.3	S	-81.9	-74.0	-75.0	-80.1	-54.8	-59.0	-41.4	-35.6	-34.4	-25.6	-10.4	-8.20
		M	-92.5	-70.4	-88.7	-70.8	-57.4	-64.8	-45.1	-33.1	-38.6	-29.5	-14.5	-13.7
		ε%	-12.9	4.94	-18.33	11.58	-4.72	-9.94	-9.04	6.95	12.16	-15.4	-39.5	.....

cont'd

6.84	140.4	S	-113.8	-102.6	-105.1	-112.2	--64.2	-93.0	-63.1	-52.1	-52.9	-32.6	-15.6	-16.2
		M	-123.2	-97.9	-124.1	-93.1	-77.5	-90.3	-56.5	-43.1	-50.0	-34.9	-17.9	-19.1
		ε%	-8.31	4.50	-18.1	16.95	-20.8	2.87	10.3	17.2	5.43	-7.31	-14.9	-18.1
6.88	170.5	S	-142.8	-129.2	-132.1	-132.5	-87.7	-113.7	-78.7	-63.7	-68.4	-39.5	-20.6	-23.1
		M	-153.5	-122.7	-154.6	-110.9	-91.0	-111.4	-66.2	-53.2	-60.7	-38.8	-20.0	-22.6
		ε%	-7.55	4.97	-17.06	16.28	-3.81	1.99	15.8	16.4	11.1	1.63	2.82	1.86
6.90	183.5	S	-158.1	-143.2	-145.9	-140.3	-95.2	-123.5	-82.8	-70.2	-72.0	-40.9	-20.7	-24.5
		M	-166.4	-135.2	-167.8	-119.7	-95.8	-120.4	-69.9	-56.2	-65.1	-40.4	-21.1	-24.0
		ε%	-5.28	5.53	-15.05	14.67	-0.71	2.05	15.5	19.9	9.51	1.13	-2.07	1.98
6.92	194.8	S	-172.6	-156.8	-159.7	-148.4	-102.6	-131.9	-84.2	-71.0	-73.5	-40.9	-20.6	-24.2
		M	-177.9	-146.2	-179.4	-127.4	-100.0	-128.1	-73.0	-58.7	-68.8	-41.7	-22.0	-25.1
		ε%	-3.05	6.73	-12.35	14.15	2.55	2.82	13.22	17.34	6.29	-2.05	-7.17	-3.78
6.96	211.6	S	-187.4	-182.1	-182.2	-163.7	-116.3	-148.2	-82.8	-63.7	-71.1	-35.5	-18.1	-19.7
		M	-195.1	-162.7	-196.7	-138.7	-105.9	-139.7	-77.5	-62.1	-74.3	-43.5	-23.4	-26.6
		ε%	-4.15	10.62	-7.96	15.22	8.87	5.73	6.30	2.44	-4.49	-22.7	-29.5	-35.4
7.00	221.5	S	-212.4	-194.3	-194.6	-171.5	-124.8	-157.5	-80.9	-66.3	-68.9	-30.9	-15.5	-15.0
		M	-205.3	-172.2	-206.9	-145.4	-109.2	-146.4	-80.1	-64.0	-77.4	-44.6	-24.2	-27.5
		ε%	3.30	11.35	-6.31	15.18	12.51	7.01	0.91	3.33	-12.3	-44.4	-56.3	-83.5
7.03	226.4	S	-212.1	-192.9	-195.1	-172.3	-126.1	-156.9	-80.6	-66.6	-69.4	-31.6	-15.0	-15.5
		M	-210.4	-177.0	-211.9	-148.7	-110.7	-149.8	-81.4	-65.0	-78.9	-45.1	-24.6	-27.9
		ε%	0.77	8.22	-8.64	13.64	12.19	4.51	-1.04	2.34	-13.7	-42.7	-63.9	-80.3
7.06	230.4	S	-207.3	-191.6	-189.6	-167.8	-120.5	-152.8	-81.8	-67.8	-70.6	-34.6	-17.6	-18.5
		M	-214.6	-181.0	-216.1	-151.5	-111.9	-152.5	-82.4	-65.8	-80.1	-45.5	-24.9	-28.3
		ε%	-3.54	5.48	-14.00	9.70	7.06	0.14	-0.82	2.94	-13.5	-31.5	-41.5	-52.9

Δ : Roof displacement

(l.): Linear state

S : SARCF results

M : MONARCF-DC results

$$\varepsilon\% : \frac{\theta^S - \theta^M}{\theta^S} \times 100$$

θ^S = rotation obtained by SARCF;

θ^M = rotation obtained by MONARCF-DC

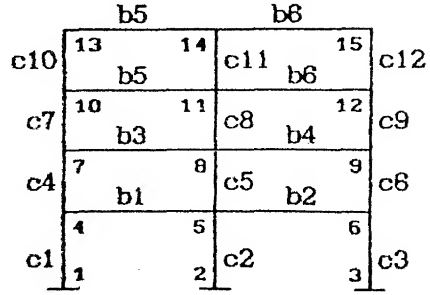

Table 5.19 Ratio of SARCF Curvature Ductility Demand to MONARCF-DC Curvature Ductility Demand.

Example	Beams				Columns	
	Hogging		Sagging			
	Range	Average	Range	Average	Range	Average
EC1	0.74 - 2.95	1.51	1.03 - 3.59	2.60	0.29 - 2.12	0.77
ET1	0.51 - 2.50	1.32	0.69 - 2.59	1.46	0.16 - 2.00	0.57
EC2	0.58 - 1.56	1.32	1.32 - 3.89	2.52	0.10 - 1.54	0.62
ET2	0.54 - 1.90	1.04	0.63 - 1.98[1]	1.49	0.20 - 1.33	0.59
EC3	0.94 - 4.01	2.43	1.78 - 3.58	2.39	0.28 - 0.38	0.34
ET3	1.03 - 3.86	2.13	0.90 - 2.23	1.56	0.29 - 0.39	0.33
EC4	0.21 - 4.09	1.24	1.30 - 3.55[2]	2.36	0.16 - 2.05	0.68
ET4	0.95 - 3.44	1.92	1.20 - 5.60[3]	3.12	0.10 - 0.77	0.40

1 : one high value (6.12) is excluded.
2 : two high values (6.38 and 13.96) are excluded.
3 : one high value (19.56) is excluded.

Table 5.20 Ratio of Curvature Ductility Demand to the Structure Displacement Ductility (μ_s); by SARCF Analysis.

Example	μ_s	Ductility Demand for Beams				Ductility Demad for Columns	
		Hogging		Sagging			
		Range	Average	Range	Average	Range	Average
EC1	2.95	3.70 - 16.2	9.39	0.37 - 13.8	6.56	0.37 - 5.73	2.78
ET1	3.25	3.70 - 9.75	6.15	2.04 - 8.15	4.99	0.31 - 4.24	1.92
EC2	3.05	3.08 - 11.7	8.75	2.85 - 9.54	7.55	0.39 - 8.39	2.62
ET2	3.12	3.10 - 16.0	8.24	0.61 - 14.4	7.10	0.39 - 4.23	2.67
EC3	3.40	4.41 - 21.2	11.59	0.33 - 17.5	8.53	1.58 - 2.03	1.77
ET3	2.78	6.00 - 21.4	11.41	5.29 - 21.2	10.51	1.54 - 2.41	1.97
EC4	2.93	0.98 - 25.2	10.98	0.65 - 19.8	9.07	0.34 - 5.70[1]	2.64
ET4	2.88	4.69 - 20.5	10.61	4.00 - 18.7	9.79	0.38 - 4.62	2.43

1 : two high values (8.57 and 11.22) are excluded.

Table 5.21 Ratio of SARCF Curvature Ductility Demand to MONARCF-DC Curvature Ductility Demand for the Four Frames Subjected to 1 × El Centro Accelerogram.

Example	Beams				Columns	
	Hogging		Sagging			
	Range	Average	Range	Average	Range	Average
EC1*	0.44 - 0.77	0.62	1.05 - 1.19	1.12	0.81 - 1.25	1.03
EC2*	0.58 - 1.48	0.68	2.26 - 2.35	2.31	0.16 - 1.93	0.75
EC3*	0.43 - 1.37	1.04	-	-	0.67 - 1.10	0.90
EC4*	0.46 - 1.15	0.84	1.17 - 1.47	1.32	0.67 - 1.21	1.00

Table 5.22 Ratio of Curvature Ductility Demand to the Structure Displacement Ductility (μ_s) for the Four Frames Subjected to 1 × El Centro Accelerogram.

Example	μ_s	Ductility Demand for Beams				Ductility Demand for Columns	
		Hogging		Sagging			
		Range	Average	Range	Average	Range	Average
EC1*	2.36	5.21 - 9.57	7.52	4.02 - 7.33	6.20	5.80 - 9.07	7.51
EC2*	1.87	1.77 - 10.4	7.74	1.34 - 9.25	6.62	0.70 - 11.8	4.80
EC3*	1.47	4.42 - 14.7	11.0	3.88 - 12.7	9.60	4.76 - 7.83	6.24
EC4*	1.94	3.09 - 9.53	6.86	2.68 - 8.56	5.72	3.55 - 10.0	7.48

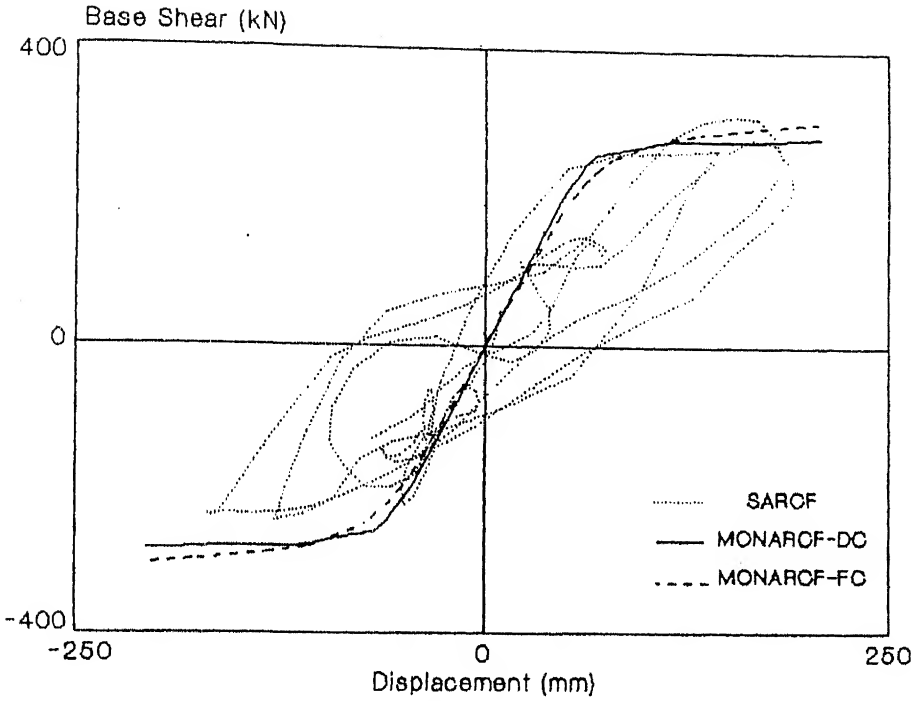

Fig. 5.1 Comaparison of the upper bound envelopes for example EC1.

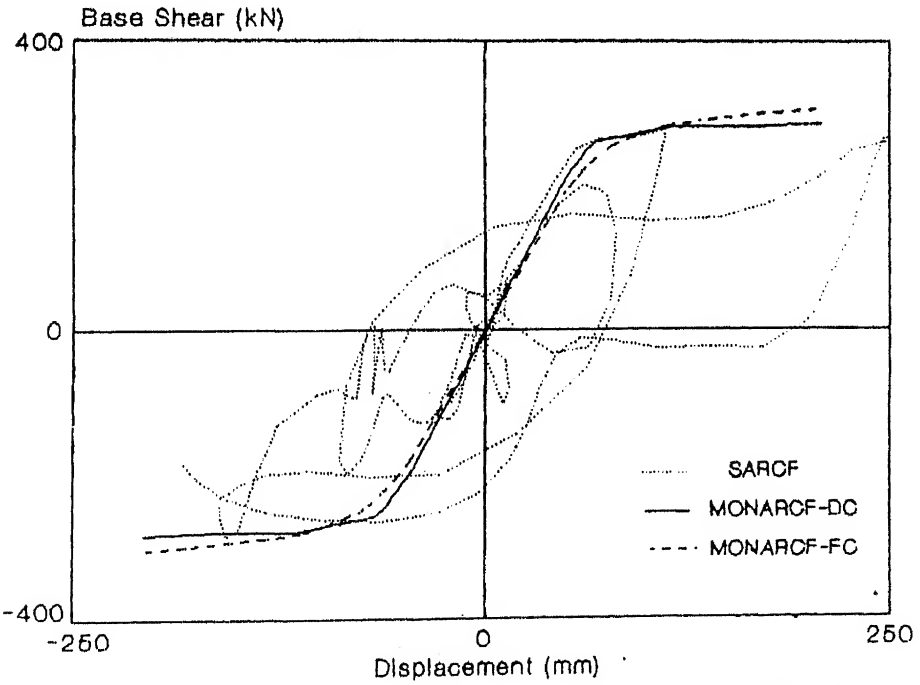

Fig. 5.2 Comaparison of the upper bound envelopes for example ET1.

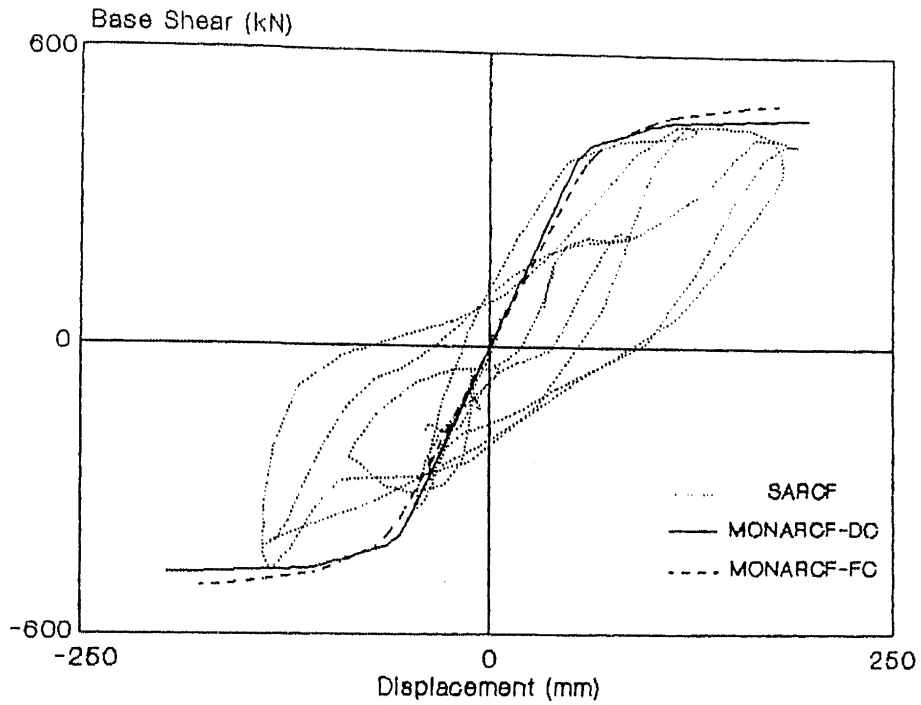

Fig. 5.3 Comaparison of the upper bound envelopes for example EC2.

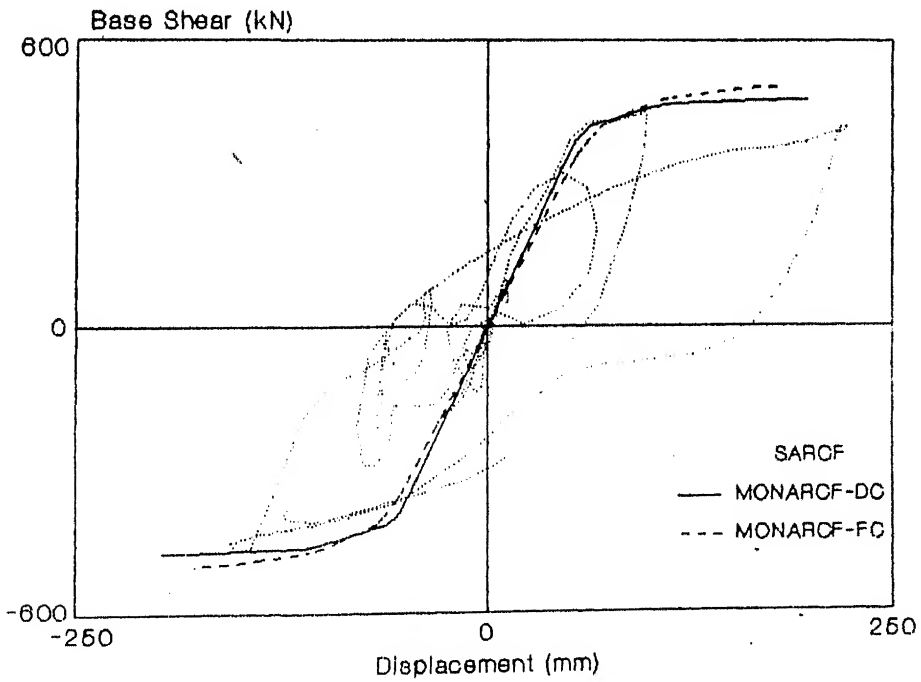

Fig. 5.4 Comaparison of the upper bound envelopes for example ET2.

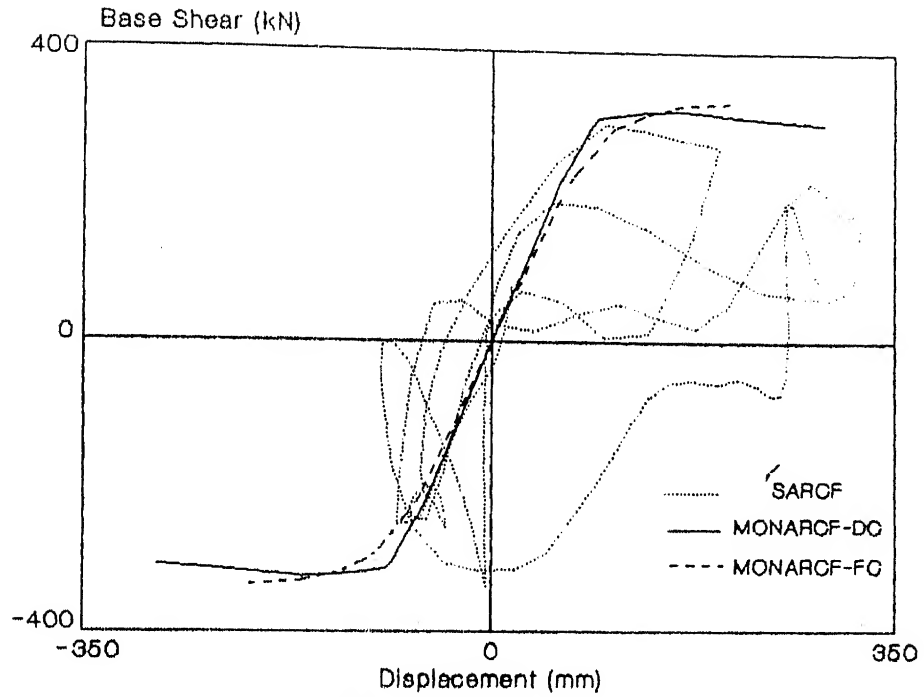

Fig. 5.5 Comaparison of the upper bound envelopes for example EC3.

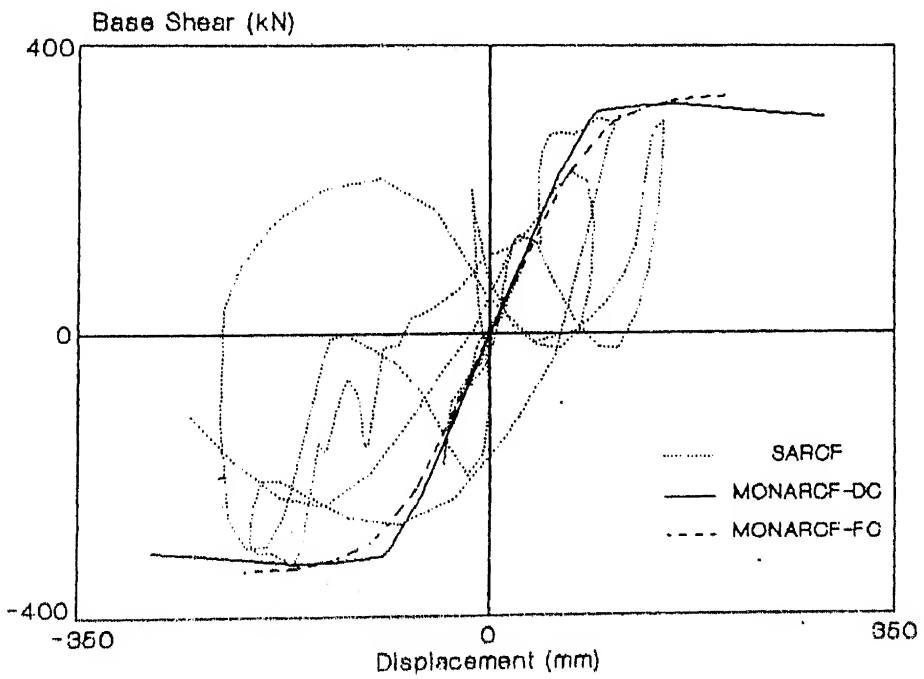

Fig. 5.6 Comaparison of the upper bound envelopes for example ET3.

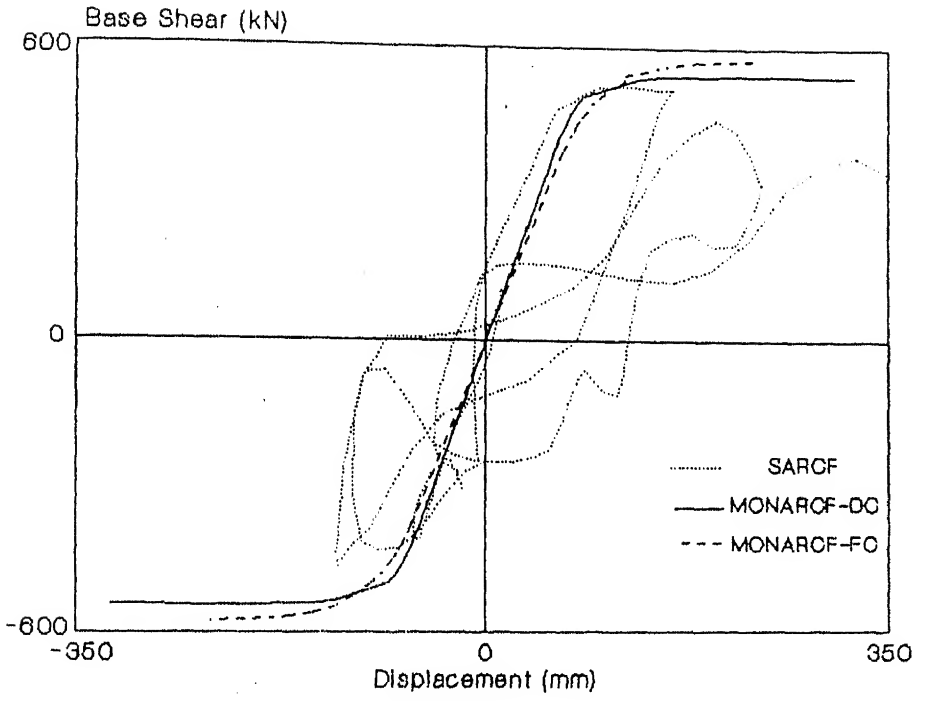

Fig. 5.7 Comaparison of the upper bound envelopes for example EC4.

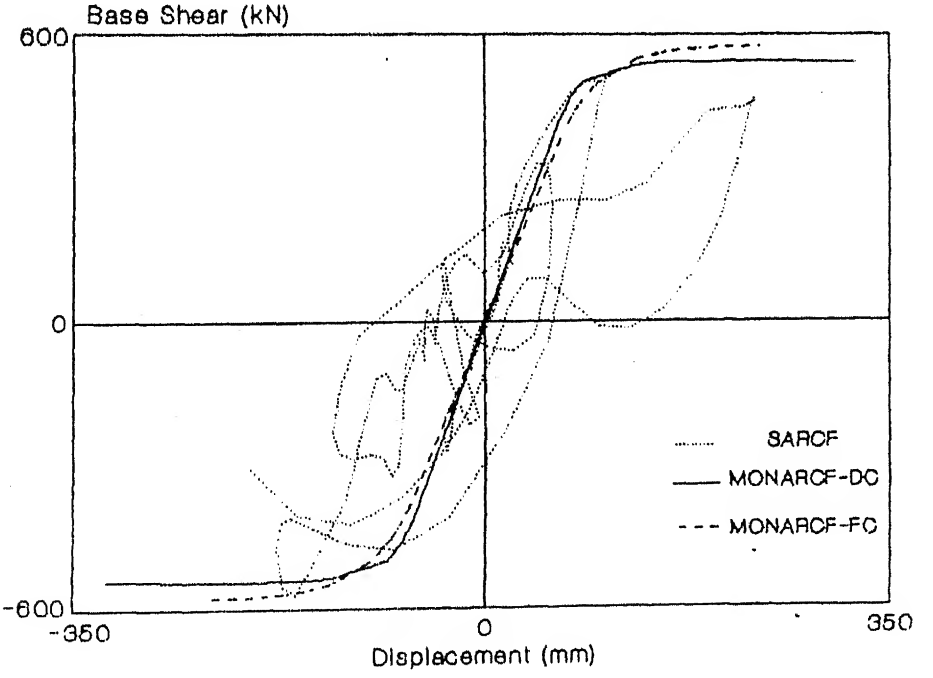

Fig. 5.8 Comaparison of the upper bound envelopes for example ET4.

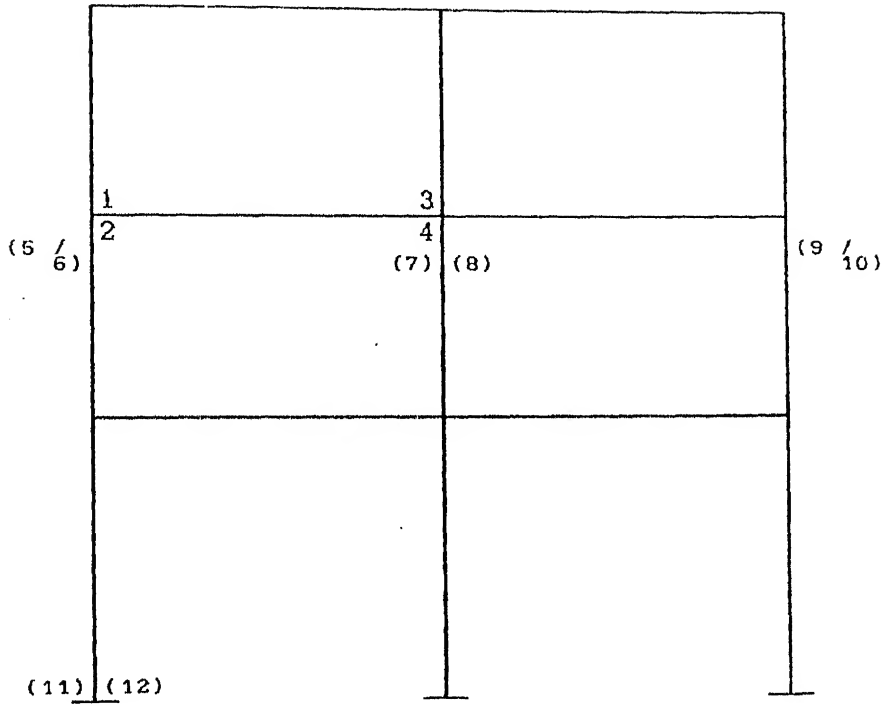

1 & 3: (value written in standard character) indicates ductility in hogging curvature (tension on upper face of the section) of beam element at this end.

2 & 4: (value written in standard character) indicates ductility in sagging curvature (tension on lower face of the section) of beam element at this end.

(5 / 6): (value written in small character); the first value (5) indicates ductility of the left face(i.e., moment with tension on the left face) of this column end; and the second value (6) indicates ductility of the right face of this column end.

(7) : (value written in small character) indicates ductility at the left face of this column end.

(8) : (value written in small character) indicates ductility at the right face of this column end.

(9/10): (value written in small character); the first value (9) indicates ductility of the left face of this column end; and the second value (10) indicates ductility of the right face of this column end.

(11) : (value written in small character) indicates ductility at the left face at base of the column.

(12) : (value written in small character) indicates ductility at the right face at base of the column.

Fig. 5.9 Template for reading the curvature ductilities at different sections from Figs. 5.10 to 5.21.

a. Curvature ductility at the end of 1st significant inelastic excursion

Δ_{roof} = 134.0 mm

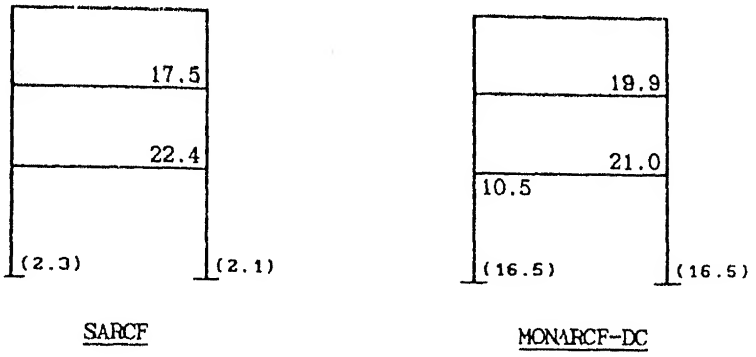

b. Curvature ductility after complete hysteretic loading

duration = 7.68 sec. Max. Δ_{roof} = 189.2 mm

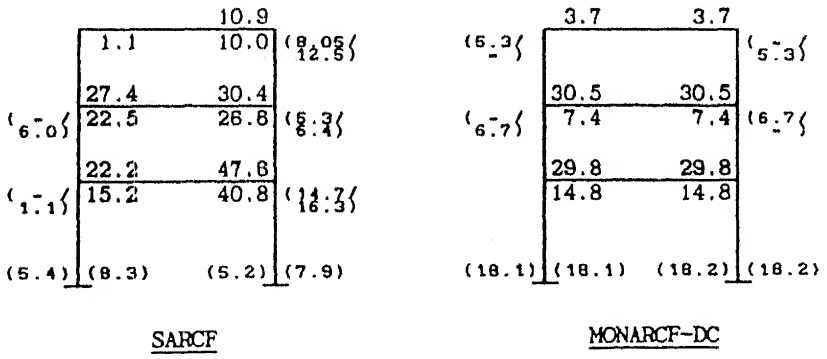

Fig 5.10 Comparison of curvature ductility for example EC1 subjected to 2 × El Centro accelerogram.

a. Curvature ductility at the end of 1st significant inelastic excursion

Δ_{roof} = 103.9 mm

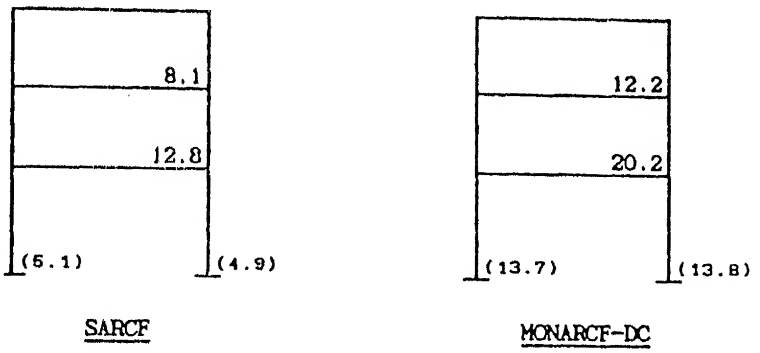

b. Curvature ductility after complete hysteretic loading

duration = 6.88 sec. Max. Δ_{roof} = 207.6 mm

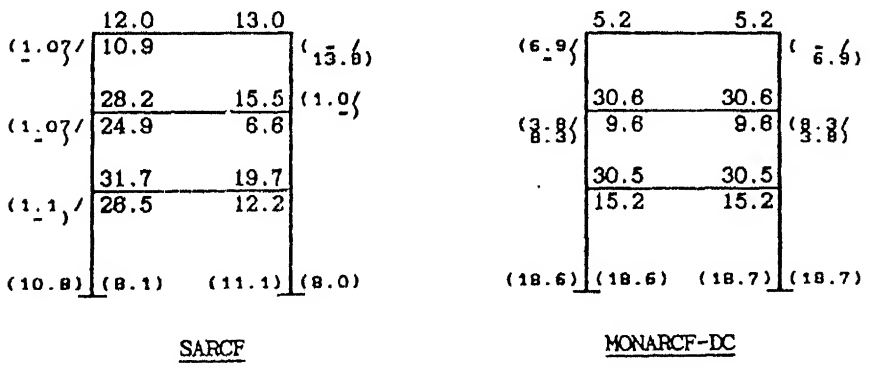

Fig 5.11 Comparison of curvature ductility for example ET1 subjected to 4 × Taft Lincoln accelerogram.

a. Curvature ductility at the end of 1st significant inelastic excursion

Δ_{roof} = 124.4 mm

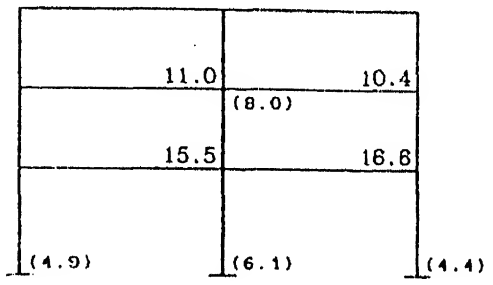

SARCF

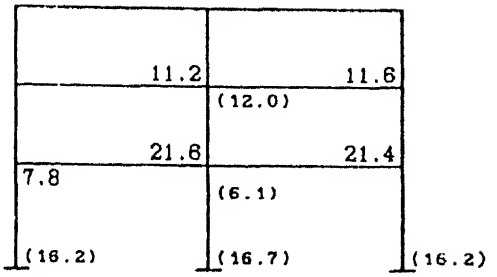

MONARCF-DC

b. Curvature ductility after complete hysteretic loading

duration = 7.68 sec. Max. Δ_{roof} = 191.9 mm

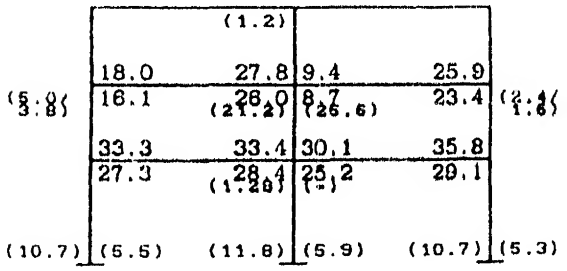

SARCF

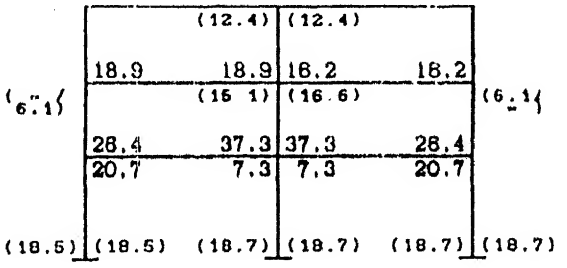

MONARCF-DC

Fig 5.12 Comparison of curvature ductility for example EC2 subjected to 2 × El Centro accelerogram.

a. Curvature ductility at the end of 1st significant inelastic excursion

Δ_{roof} = 84.60 mm

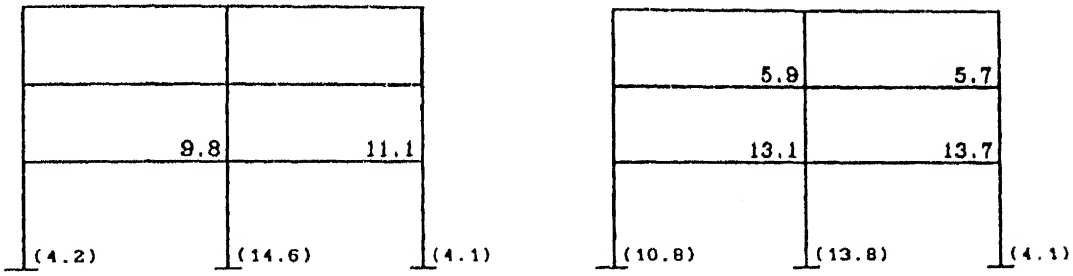

SARCF MONARCF-DC

b. Curvature ductility after complete hysteretic loading

duration = 6.88 sec. Max. Δ_{roof} = 198.8 mm

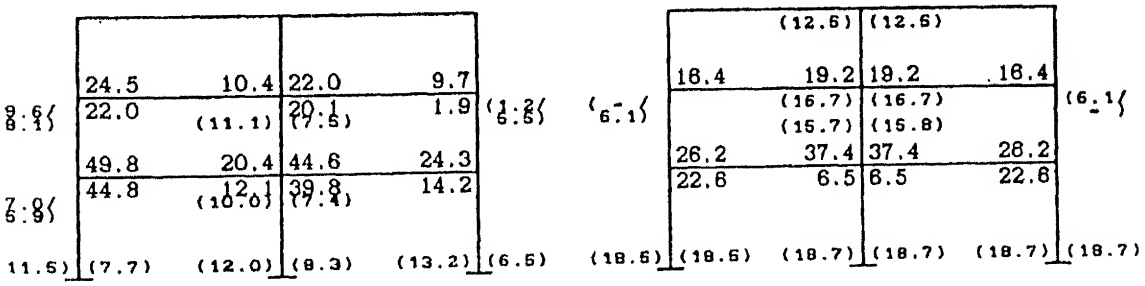

SARCF MONARCF-DC

Fig 5.13 Comparison of curvature ductility for example ET2 subjected to 4 × Taft Lincoln accelerogram.

a. Curvature ductility at the end of 1st significant inelastic excursion

Δ_{roof} = 185.1 mm

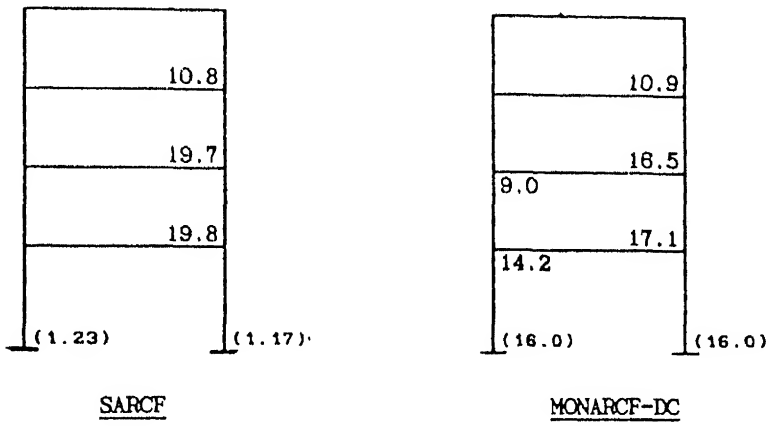

b. Curvature ductility after complete hysteretic loading

duration = 5.36 sec. Max. Δ_{roof} = 283.4 mm

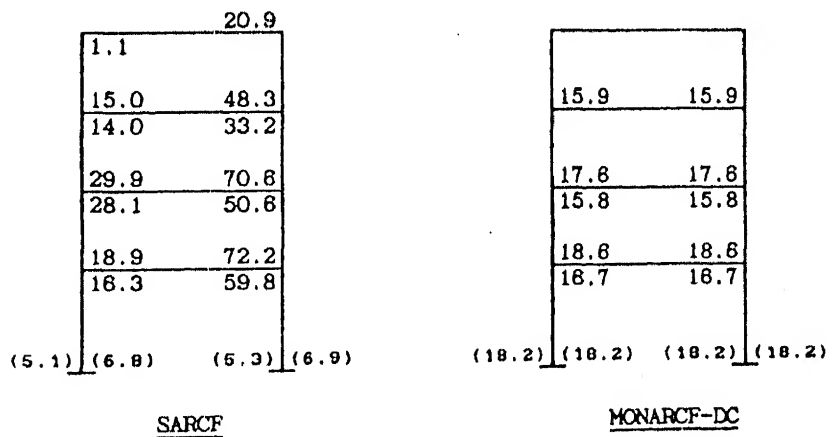

Fig 5.14 Comparison of curvature ductility for example EC3 subjected to 2 × El Centro accelerogram.

a. Curvature ductility at the end of 1 st significant inelastic excursion

Δ_{roof} = 106.0 mm

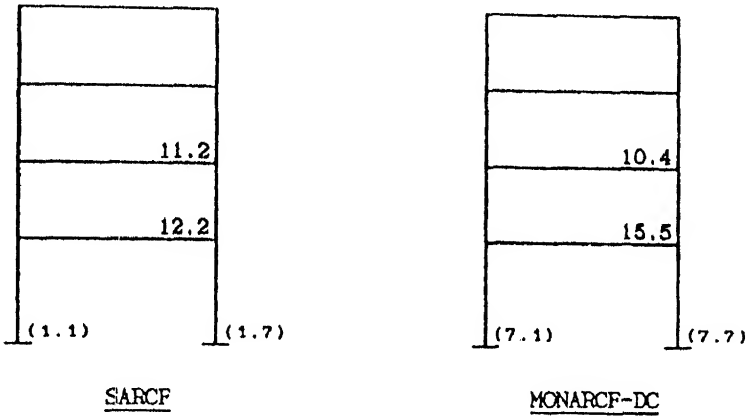

b. Curvature ductility after complete hysteretic loading

duration = 7.80 sec. Max. Δ_{roof} = 231.2 mm

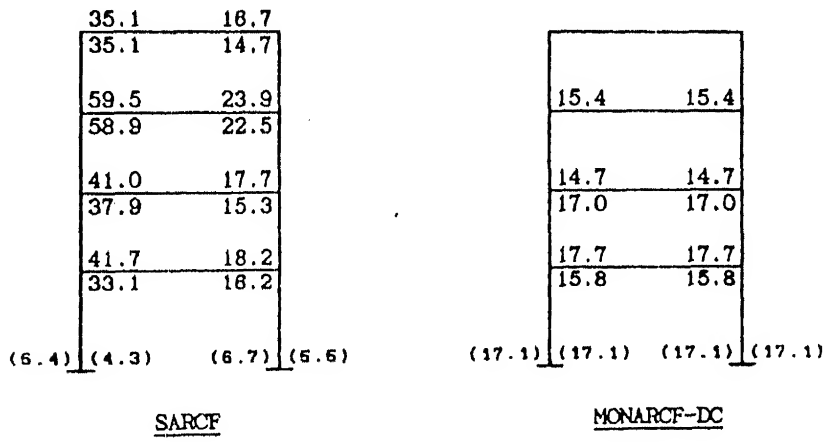

Fig 5.15 Comparison of curvature ductility for example ET3 subjected to 4 × Taft Lincoln accelerogram.

a. Curvature ductility at the end of 1st significant inelastic excursion

Δ_{roof} = 160.0 mm

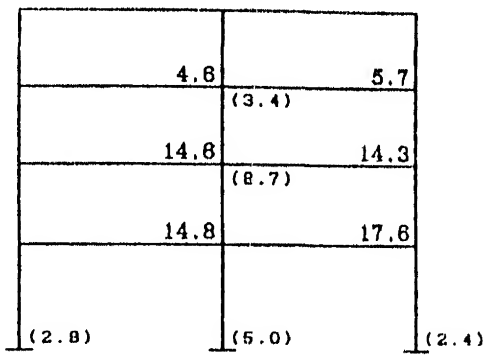

SARCF

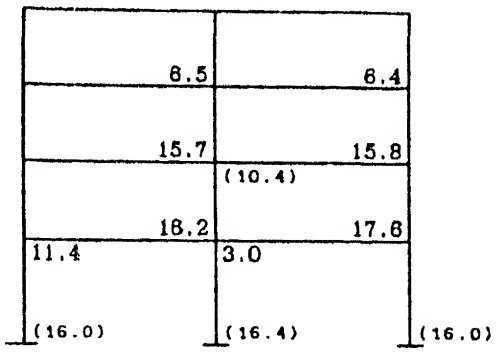

MONARCF-DC

b. Curvature ductility after complete hysteretic loading

duration = 5.30 sec. Max. Δ_{roof} = 238.1 mm

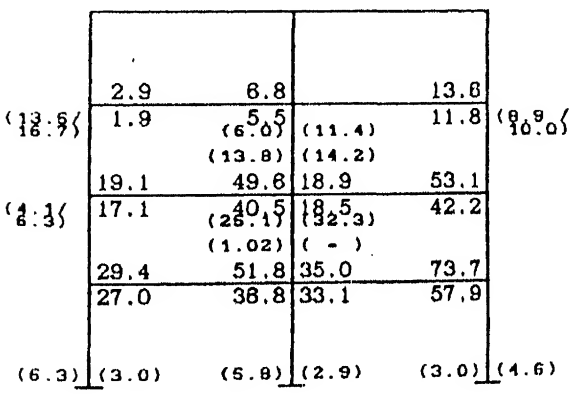

SARCF

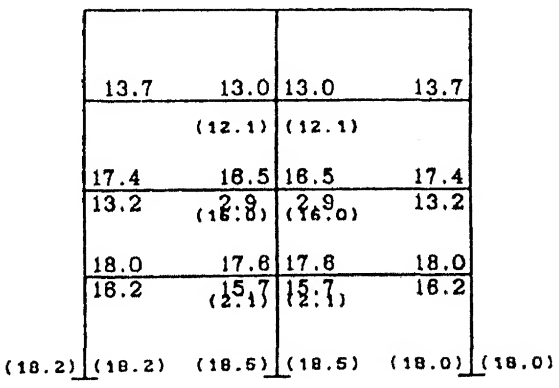

MONARCF-DC

Fig 5.16 Comparison of curvature ductility for example EC4 subjected to 2 × El Centro accelerogram.

a. Curvature ductility at the end of 1st significant inelastic excursion

Δ_{roof} = 103.2 mm

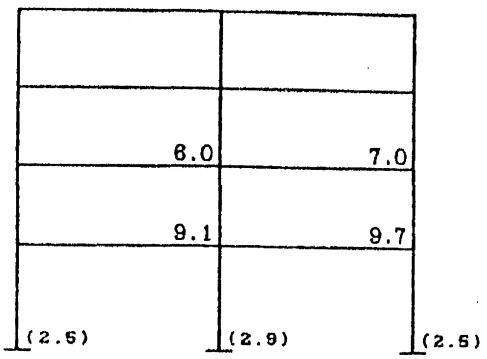

SARCF

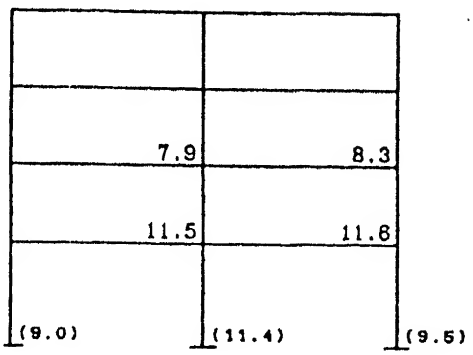

RDARCF

b. Curvature ductility after complete hysteretic loading

duration = 7.80 sec. Max. Δ_{roof} = 234.1 mm

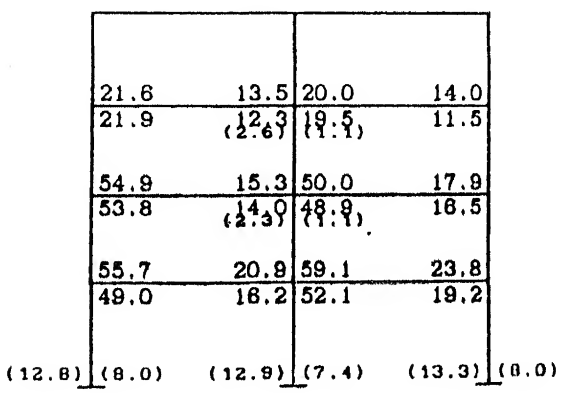

SARCF

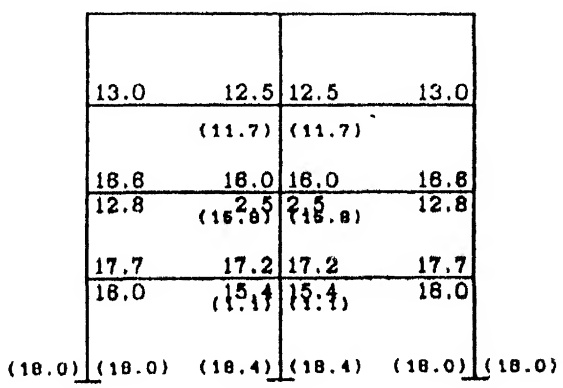

MONARCF-DC

Fig 5.17 Comparison of curvature ductility for example ET4 subjected to 4 × Taft Lincoln accelerogram.

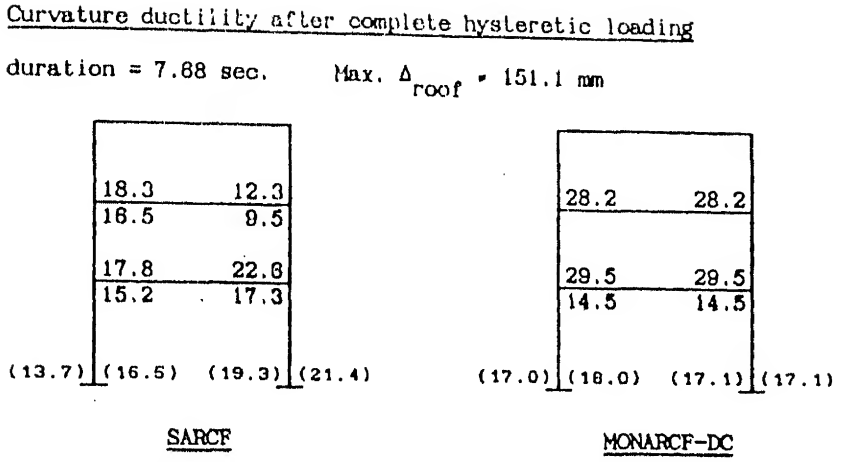

Fig 5.18 Comparison of curvature ductility for example EC1* subjected to 1 × El Centro accelerogram.

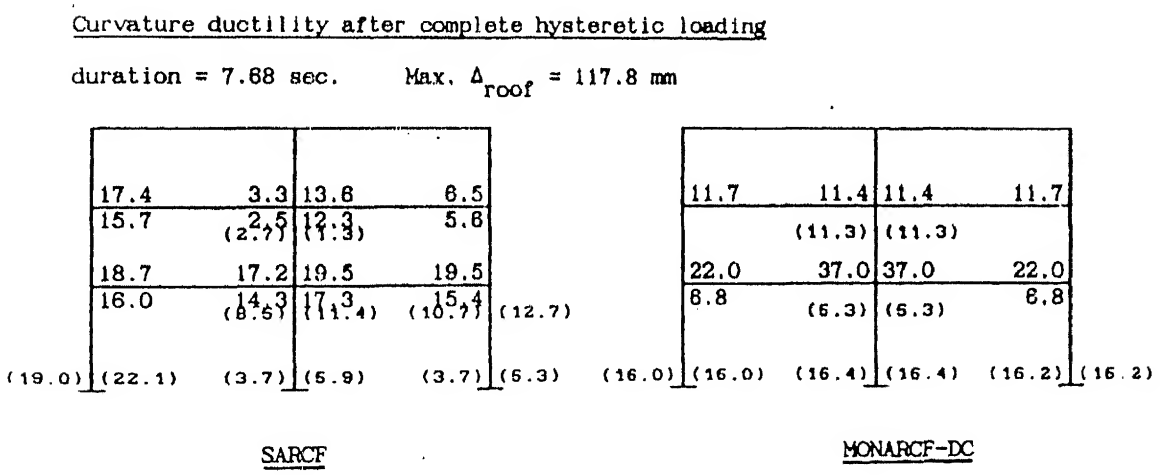

Fig 5.19 Comparison of curvature ductility for example EC2* subjected to 1 × El Centro accelerogram.

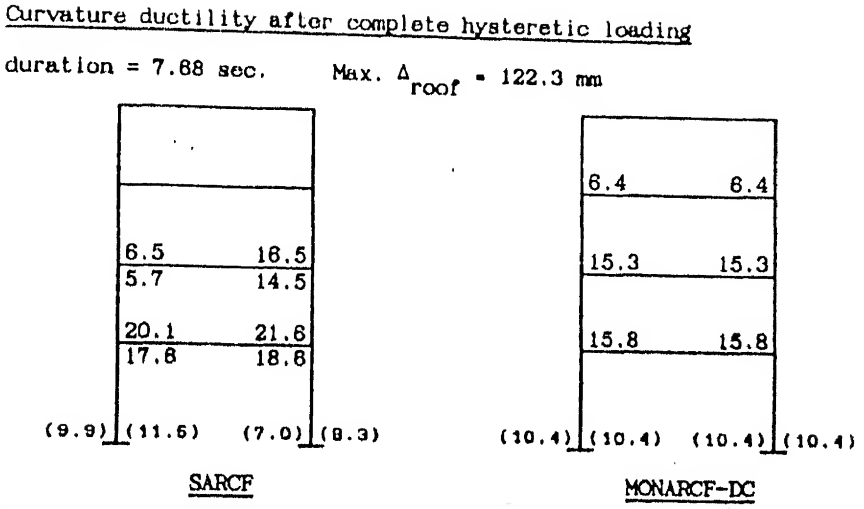

Fig 5.20 Comparison of curvature ductility for example EC3* subjected to 1 × El Centro accelerogram.

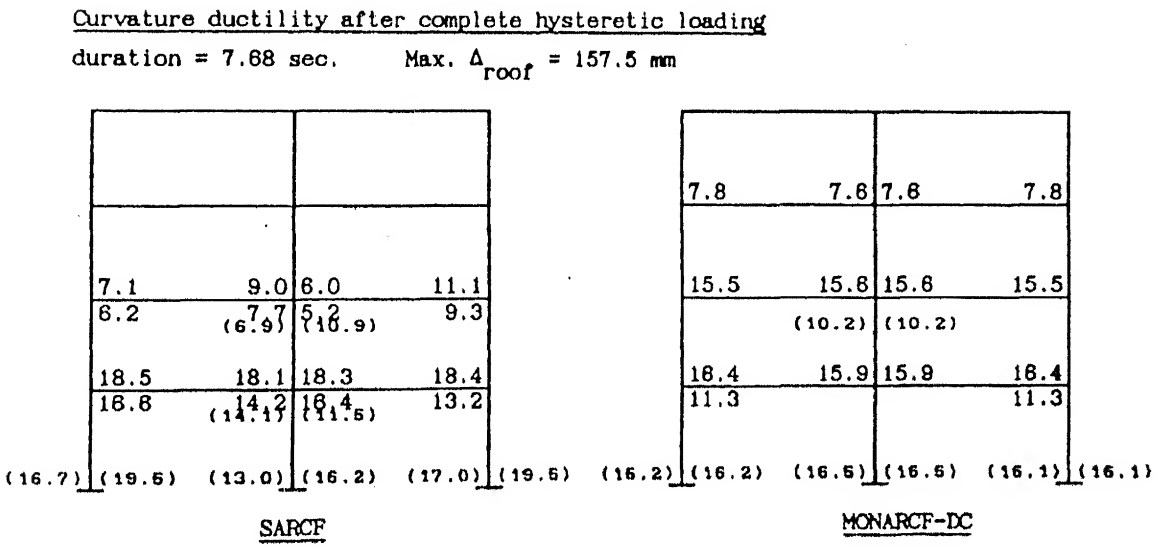

Fig 5.21 Comparison of curvature ductility for example EC4* subjected to 1 × El Centro accelerogram.

CHAPTER VI

ILLUSTRATIVE EXAMPLE

6.1 EXAMPLE PROBLEM

In this chapter, the application of DDBDP in earthquake-resistant design of RC buildings is demonstrated through an example. The example consists of a 3-storey reinforced concrete building with a base dimension of 18.0 m × 12.0 m and a height of 11.40 m (Fig. 6.1). The structure consists of three frames in the longitudinal direction with equal spacing, and four frames in the transverse direction with unequal spacing. The building has 150 mm thick solid slab at floor levels. The size of all columns is 450 mm × 450 mm. All beams, except the beams of 8.0 m span, are 300 mm × 500 mm, while 8 m span beams are 300 mm × 600 mm. The internal partitions and the exterior infill walls consist of precast light concrete panels connected with the upper and lower floors with flexible joints. The building is assumed to be in seismic zone 4 specified by the UBC-1991. The soil profile is considered stiff and the entire building is supported on a raft foundation. Concrete grade is M25 (i.e., characteristic cube strength, f_{ck}, = 25 N/mm^2; the cylinder strength, f_c', $\cong$ 20.0 N/mm^2). Steel is of grade 415 (f_y = 415 N/mm^2). The building is detailed as per the ACI-318 (1989). The DDBDP is demonstrated on the intermediate frame in the longitudinal direction (frame B).

6.2 DESIGN BASIS PARAMETERS

The DDBDP is based on two linear elastic design spectra corresponding to SLS and ULS. Here, the elastic design force at SLS (P_w)

has been taken same as the lateral design base shear force recommended by the UBC-1991 for seismic zone 4. The elastic design force at ULS (P) is assumed to be 12 times the elastic design force at SLS. The design parameters, for calculating the seismic design force as per UBC-1991, are as follows:

1. The seismic zone factor (Z) for zone 4 is 0.4.
2. The importance factor (I) is 1.0.
3. The site factor (S) is 1.0.
4. The response reduction factor (R_w) for special-moment resisting concrete frames is 12.

For ductility and drift design, the following constraints are imposed:

1. The minimum required overall structural displacement ductility ($\mu_{s(min)}$) is 2.5. The maximum usable displacement ductility ($\mu_{s(max)}$) is 4.
2. At SLS, the roof displacement (Δ_w) and inter-storey drift (ISD_w) shall not exceed 0.003 times the building height (h) and the storey height, respectively.
3. At ULS, the maximum allowable roof displacement ($\Delta_{max(n.l.)}$) and inter-story drift (ISD_{max}) are 0.0125 times the building height (h) and the storey height, respectively.

6.3 PRELIMINARY DESIGN

The frame is first designed for the force corresponding to SLS (P_w) and detailed as per codal procedures. Thus, strength requirements at SLS are automatically satisfied.

The seismic weight (W) at floor levels is 1980 kN at roof, 2250 kN at 2^{nd} floor, and 2490 kN at 1^{st} floor. Hence, the total seismic weight

of the entire building is 6720 kN. The approximate fundamental period of the building (T_a) is calculated according to UBC-1991 as

$$T_a = C_t(h)^{0.75} \tag{6.1}$$

where h is the total building height in feet, and C_t = 0.03. Thus,

$$T_a = 0.03\ (11.4/0.3048)^{0.75} = 0.45 \text{ sec} \tag{6.2}$$

The design base shear force at SLS (P_w) for the entire building in a given direction is calculated as follows (UBC-1991):

$$C = \frac{1.25\ S}{T_a^{2/3}} = \frac{1.25 \times 1.0}{0.45^{2/3}} = 2.12 \tag{6.3}$$

$$P_w = \frac{Z\ I\ C}{R_w}\ W = \frac{0.4 \times 1.0 \times 2.12}{12.0} \times 6720 = 475 \text{ kN} \tag{6.4}$$

The total design base force (P_w) is distributed over the height as specified by the UBC-1991; 209 kN at roof, 159 kN at second floor, and 107 kN at first floor. Since the building consists of three identical frames at equal spacing and the slab is acting as rigid floor diaphragm, the total lateral load in the x-direction is equally distributed on the three frames. Therefore, the design lateral load at SLS (P_w) on frame B is:

$$P_w = \frac{475}{3} = 158 \text{ kN} \tag{6.5}$$

Structural analysis of the building has been carried out by modelling it as a three-dimensional bare frame, using the computer program SUPER-ETABS (Maison and Neuss, 1983). In the analysis, the axial deformations are ignored, and the floors are assumed rigid in their own plane. The structure has been designed for the following nine load combinations as per ACI-318 (1989):

a- 1.4 DL + 1.7 LL

b- 1.05 DL + 1.28 LL + 1.4 EQ_x

c- 1.05 DL + 1.28 LL - 1.4 EQ_x

d- 1.05 DL + 1.28 LL + 1.4 EQ_y

e- 1.05 DL + 1.28 LL - 1.4 EQ_y

f- 0.9 DL + 1.43 EQ_x

g- 0.9 DL - 1.43 EQ_x

h- 0.9 DL + 1.43 EQ_y

i- 0.9 DL - 1.43 EQ_y

where DL is the dead load; LL is the live load; EQ_x is the earthquake load in x-direction; and EQ_y is the earthquake load in y-direction.

Design and detailing of members has been done satisfying the detailing requirements of ACI-318 (1989) for frames located in high seismic risk, except that the strong column - weak girder requirement has not been satisfied. The columns are designed for biaxial bending. The reinforcement details for frame B are given in Table 6.1.

6.4 DRIFT ANALYSIS AT SLS

As explained earlier, the initial lateral stiffness obtained from the non-linear analysis tends to be unusually low since it is based on cracked sections of the members. For instance, as will be seen in the next section, the analysis based on cracked sections gives the fundamental period of this building as 1.1 sec; this is much higher than what one would realistically expect a three-storey building to have. Hence, if one were to satisfy drift requirements based on the cracked sections, it will be very much conservative. Instead, an effort may be made to make a more realistic assessment of the stiffness. Further, such assessment should be bench-marked with empirical expressions based on experimental values. For instance, the code-specified approximate fundamental period (= 0.45 sec for this example building) may be taken as the lower bound on period which will

be used for stiffness criteria.

A linear static analysis of the structure has been carried out to estimate its lateral stiffness in the elastic range. The moment of inertia for beam and column elements is based on gross moments of inertia of the sections (the contribution of reinforcement is neglected). The beams are treated as T- or L-beams with effective width of slab taken as per ACI-318. The modulus of elasticity of concrete is taken as the secant modulus (E_c), as per ACI-318; it is equal to 4700 $\sqrt{f'_c}$ (MPa). Since the infill panels are attached to the frame with flexible joints, lateral stiffness contribution of infill panels is small and has been neglected in the analysis. The fundamental period is obtained as 0.70 sec; this model gives stiffness lower than the bench-mark stiffness (with T = 0.45 sec) and hence can be used for checking the drift requirements.

The lateral storey deformations in x-direction under the gravity load plus the seismic load at SLS (P_w) (in positive and negative directions) as obtained from the analysis are shown in Fig. 6.2. The maximum value of roof displacement (Δ_w) is 9.9 mm which is 0.09% of the building height as against the allowable value of 0.3%. The maximum inter-storey drift (ISD_w) is the largest in the first storey with a value of 0.11% of storey height as against 0.3% that is allowed. Therefore, the lateral displacements at SLS are within the acceptable limits.

6.5 NON-LINEAR QUASI-STATIC ANALYSIS

To consider the adequacy of design at the ultimate limit state (ULS), base shear - roof displacement relationship of the frame has been obtained using the MONARCF-DC program. The curve has been obtained for a

roof displacement of about 3% of the building height; the maximum roof displacement expected at the ULS is likely to fall within this limit. Since the frame is unsymmetric, the non-linear analysis has been carried out in both positive and negative directions.

Response of the frame obtained from this analysis is shown in Fig. 6.3. Since the initial stiffness in the non-linear analysis is based on the cracked sections, the fundamental period obtained is 1.1 sec which is quite high. As summarized in Table 6.2, the frame exhibits an overstrength ($\Omega = P_y / P_w$) of 3.6 to 3.8. Therefore, to satisfy the strength requirements at the ULS, the frame requires a ductility reduction factor ($R_\mu = \frac{P}{P_w \Omega}$) of about 3.3. One needs to then work out the required overall structural ductility (μ_r) which would provide this much ductility reduction factor. Therefore, according to the expressions given by Riddell et al. (1989) (Fig. 2.3), the structure should have a ductility of at least 3.3; this is within the overall ductility of about 3.8 exhibited by the structure in Fig. 6.3 (the actual ductility of the building will be still higher because the quasi-static analysis was stopped arbitrarily at roof displacement of about 350 mm). Moreover, the building possesses overall ductility greater than $\mu_{s(min)}$ (= 2.5), and the ductility (= 3.3) being used to satisfy ULS requirements is less than the maximum usable displacement ductility ($\mu_{s(max)}$) (= 4.0). Hence, the structure satisfies the overall ductility requirements.

Considering the drift requirements at the ULS, the roof displacement of 300 mm (2.6% of building height), and the corresponding inter-storey drift (190 mm in the first storey, or 3.8% of storey height), obtained by the non-linear analysis are well beyond the acceptable limits. However, as discussed in Section 3.4, it will be highly conservative to satisfy the drift requirements on the basis of

the non-linear analysis because such an analysis is based on an unduly flexible model. Hence, one could apply the stiffness correction based on a more realistic assessment of the initial stiffness. In this case, the initial stiffness calculation from linear analysis (T = 0.7 sec) appears quite reasonable and adequately conservative. On this basis, it is obvious that the building which experiences a roof displacement of 9.9 mm at the SLS loading, will at the ULS experience a roof displacement of $(9.9 \Omega \mu_r)$ = 119 mm. This is about 1% of the building height which is within the acceptable limit of 1.25%. Now a more realistic assessment of the inter-storey drift for first storey can be obtained by prorating the displacements, i.e., 190 mm x $\frac{119}{300}$ = 75.3 mm; this is 1.5% of the storey height which is more than the maximum allowable inter-storey drift of 1.25%. Hence, the design may be revised by increasing the lateral stiffness of the building, for instance, by increasing the member sizes. In the present example, the design has not been revised considering that the stiffness of infills, if considered with T = 0.45, would fulfill the ISD criteria.

The sequence of plastic hinge formation during the loading in both the directions, and the corresponding base shear and roof displacement values, are presented in Table 6.3. It is observed that upto the maximum roof displacement corresponding to the required displacement ductility, all four columns in the first storey yield at both top and bottom ends. This is the reason for inter-storey drift in the first-storey being high as compared to that in the upper storeys.

Tables 6.4 and 6.5 compare the values of member ductility provided (δ_p) with the higher values of ductility demand (δ_m) in the members at the roof displacement of 298 mm or -300 mm corresponding to the overall structural ductility of 3.28 or 3.17, respectively. The ductility

provided (δ_p) for beam elements ranges from 2.5 to 11.4 times the ductility demand (δ_m) (except at node 14(h)-b7, where it is 20.8 times). The ratio of the ductility provided to ductility demand of column elements ranges from 2.3 to 7.6 (except at node 16(l)-c12, where the ratio is 12.7). The parametric study in Section 5.5 indicates that these values of ratio ($\frac{\delta_p}{\delta_m}$) are adequate to account for higher ductility demand due to the hysteretic behaviour. Tables 6.4 and 6.5 also show that the ratio of the member ductility provided to the average required displacement ductility ($\mu_{r(a)}$) ranges from 18.8 to 34.2 in beam elements and from 18.8 to 25.8 in column elements; again the parametric study discussed in Section 5.5 indicates that all the members have adequate curvature ductility vis-a-vis the required displacement ductility. Therefore, the present detailing provides adequate curvature ductility to the members.

Table 6.1 Details of Beam and Column Reinforcements

1. Beams

Beam	Size mm		Longitudinal Reinforcement			Conf. Stirrup at Element End
			Left End	Mid Span	Right End	
b1 & b4	300 × 500	T	4 - 25ϕ_d	4 - 25ϕ_d	4 - 25ϕ_d	8ϕ_d @ 110 m
		B	4 - 18ϕ_d	4 - 18ϕ_d	4 - 18ϕ_d	
b2 & b5	300 × 500	T	4 - 25ϕ_d	4 - 25ϕ_d	4 - 28ϕ_d	8ϕ_d @ 110 m
		B	4 - 22ϕ_d	4 - 22ϕ_d	4 - 22ϕ_d	
b3 & b6	300 × 600	T	4 - 28ϕ_d	4 - 28ϕ_d	4 - 28ϕ_d	8ϕ_d @ 125 m
		B	4 - 25ϕ_d	4 - 25ϕ_d	4 - 25ϕ_d	
b7	300 × 500	T	4 - 18ϕ_d	4 - 18ϕ_d	4 - 18ϕ_d	8ϕ_d @ 110 m
		B	4 - 18ϕ_d	4 - 18ϕ_d	4 - 18ϕ_d	
b8	300 × 500	T	4 - 18ϕ_d	4 - 18ϕ_d	4 - 25ϕ_d	8ϕ_d @ 110 m
		B	4 - 18ϕ_d	4 - 18ϕ_d	4 - 18ϕ_d	
b9	300 × 600	T	4 - 25ϕ_d	4 - 25ϕ_d	4 - 25ϕ_d	8ϕ_d @ 125 m
		B	4 - 25ϕ_d	4 - 25ϕ_d	4 - 25ϕ_d	

T = Top reinforcement B = Bottom reinforcement

2. Columns

Column	Size mm	Longitudinal Reinforcement	Conf. Stirrups at Element Ends
c1, c2, c3, c4, c5, c6	450 × 450	8 - 22ϕ_d	8ϕ_d @ 100 mm
c7, c8, c9, c10, c11, c12	450 × 450	8 - 25ϕ_d	8ϕ_d @ 100 mm

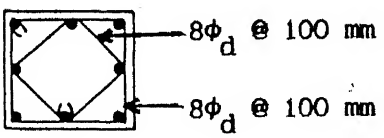

Column Section

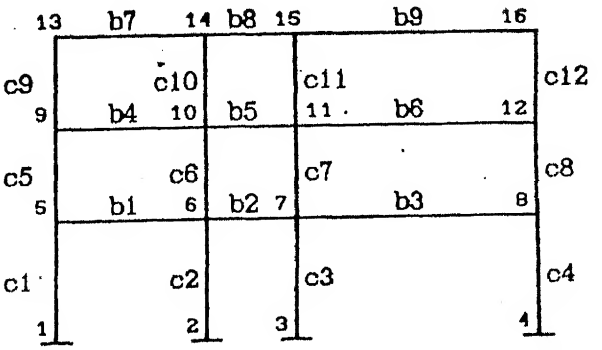

Table 6.2 The Design Parameters for Drift Analysis

Design Level			+ve direction	-ve direction
1. SLS		P_w	158 kN	-158 kN
		Δ_w (*)	9.6 mm	-9.9 mm
		Δ_w /h % (*)	0.084%	0.087%
		ISD_w %	0.112% h_1	0.114% h_1
2. ULS		P	1898 kN	-1898 kN
		Δ_y (**)	90.9 mm	-94.5 mm
		P_y (**)	580.0 mm	-600.0 mm
		Ω (= P_y/ P_w)	3.66	3.79
		R_μ (= $\frac{P}{P_w \Omega}$)	3.28	3.17
		μ_r	3.28	3.17
	a	$\Delta_{max(n.l.)}$	298 mm	-300 mm
		$\Delta_{max(n.l.)}$/h %	2.6%	2.6%
		ISD_{max}	185# mm	-190# mm
		ISD_{max} %	3.7% h_1	3.8% h_1
	b	$\Delta_{max(n.l.)}$	114 mm	-119 mm
		$\Delta_{max(n.l.)}$/h %	1.0%	1.04%
		ISD_{max}	71.5# mm	-75.3# mm
		ISD_{max} %	1.43% h_1	1.50% h_1

(*) = obtained from the linear static analysis
(**) = obtained fron the non-linear quasi-static analysis
h = total height of the building (11.4 m)
h_1 = height of first storey (5.0 m)
a = drift analysis without stiffness correction
b = drift analysis using stiffness correction
# = maximum inter-storey is the largest in first storey

Table 6.3 Sequence of Plastic Hinge Occurrence

Loading in +ve direction		
Δ (mm)	P (kN)	P. Hinge Location
73.6	460.7	8-b3
78.6	488.7	2-c2
		4-c4
88.6	524.7	1-c1
93.6	537.7	6-b2
		3-c3
		16-c12
98.6	543.7	6-b1
		7-b2
		10-c6
103.6	548.7	6-c2
108.6	553.7	5-b1
113.6	557.7	12-b6
138.6	577.1	14-c10
148.6	585.2	12-c8
153.6	589.3	7-c3
163.6	596.3	14-b7
		8-c4
		11-c7
168.6	598.6	10-c10
198.6	611.1	11-b5
238.6	625.7	9-b4
253.6	631.7	5-c1
263.6	633.7	7-c7
318.6	645.4	7-b3
338.6	649.2	10-b5
		15-c11

Loading in +ve direction		
Δ (mm)	P (kN)	P. Hinge Location
-71.4	-434.5	15-c11
-76.4	-465.4	7-b3
-81.4	-494.3	3-c3
		2-c2
		1-c1
-86.4	-509.8	6-b2
		11-c7
-91.4	-522.1	5-b1
-96.4	-533.3	4-c4
-106.4	-545.0	7-b2
		7-c3
		7-c7
-116.4	-553.9	11-c11
-136.4	-571.4	13-b7
-141.4	-575.8	6-b1
		10-c6
-146.4	-580.2	6-c2
-151.4	-583.9	9-b4
-161.4	-591.0	10-b5
-186.4	-608.1	11-b6
-191.4	-611.1	5-c1
-201.4	-617.4	8-b3
		8-c4
-208.4	-618.9	14-b8
-236.4	-626.3	9-c5
-296.4	-638.8	12-c8
-321.4	-643.7	14-c10
		10-b4

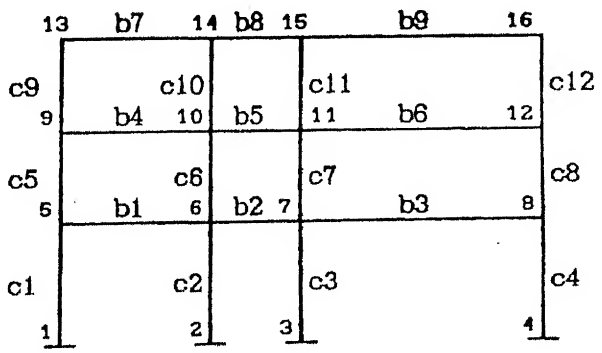

Table 6.4 Ductility of Beam Elements

Beam No	Node	$\delta_p = \frac{\phi_f}{\phi_y}$	δ_m from MONARCF-DC	$\frac{\delta_p}{\delta_m}$	$\frac{\delta_p}{\mu_{r(a)}}$
b1	5 (h)	60.6	16.0	3.79	18.8
	5 (s)	110.4	40.1	2.75	34.2
	6 (h)	60.6	14.0	4.32	18.8
	6 (s)	110.4	33.5	3.30	34.2
b2	6 (h)	72.3	24.1	3.00	22.4
	6 (s)	90.0	35.4	2.54	27.8
	7 (h)	62.5	13.7	4.56	19.4
	7 (s)	95.8	18.7	5.13	30.0
b3	7 (h)	72.0	18.7	3.85	22.3
	7 (s)	88.3	.....	.....	27.3
	8 (h)	72.0	20.6	3.50	22.3
	8 (s)	88.3	.....	.....	27.3
b4	9 (h)	60.6	9.9	6.12	18.8
	9 (s)	110.4	18.2	6.07	34.2
	10(h)	60.6	.....	.....	18.8
	10(s)	110.4	.....	.....	34.2
b5	10(h)	72.3	9.8	7.38	22.4
	10(s)	90.0	.....	.....	27.8
	11(h)	62.5	7.0	8.93	19.4
	11(s)	95.8	.....	.....	30.0
b6	11(h)	72.0	6.3	11.4	22.3
	11(s)	88.3	.....	.....	27.3
	12(h)	72.0	11.1	6.49	22.3
	12(s)	88.3	.....	.....	27.3

Cont'd

b7	13(h)	77.0	12.8	6.01	23.8
	13(s)	77.0	.....	.....	23.8
	14(h)	77.0	3.7	20.8	23.8
	14(s)	77.0	.....	.....	23.8
b8	14(h)	77.0	7.6	10.1	23.8
	14(s)	77.0	.....	.....	23.8
	15(h)	60.7	.....	.....	18.8
	15(s)	110.4	.....	.....	34.2
b9	15(h)	82.2	.....	.....	25.5
	15(s)	82.2	.....	.....	25.5
	16(h)	82.2	.....	.....	25.5
	16(s)	82.2	.....	.....	25.5

(h) = hogging (s) = sagging

δ_p = ductility provided δ_m = ductility demand

$\mu_{r(a)}$ = average displacement ductility required from +ve and -ve directions [0.5(3.28+3.17) = 3.23]

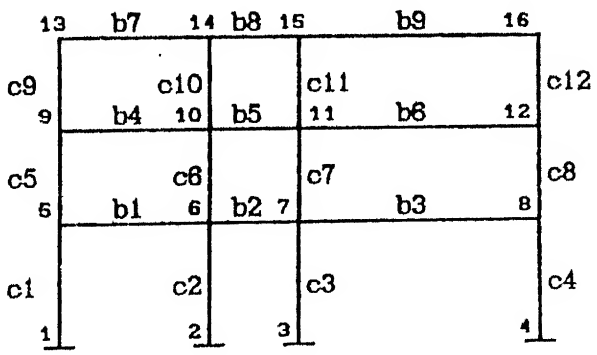

Table 6.5 Ductility for Column Elements

Col. No	Node	$\delta_p = \frac{\phi_f}{\phi_y}$	δ_m from MONARCF-DC	$\frac{\delta_p}{\delta_m}$	$\frac{\delta_p}{\mu_{r(a)}}$
C1	1 (l)	71.8	30.3	2.36	22.2
	1 (r)	71.8	30.6	2.34	22.2
	5 (l)	71.8	15.2	4.72	22.2
	5 (r)	71.8	11.9	6.03	22.2
C2	2 (l)	66.0	24.4	2.71	20.4
	2 (r)	66.0	25.3	2.61	20.4
	6 (l)	66.0	15.2	4.34	20.4
	6 (r)	66.0	16.7	3.95	20.4
C3	3 (l)	60.6	23.4	2.60	18.8
	3 (r)	60.6	22.0	2.75	18.8
	7 (l)	60.6	15.6	3.89	18.8
	7 (r)	60.6	16.8	3.61	18.8
C4	4 (l)	65.6	25.3	2.60	20.3
	4 (r)	65.6	25.0	2.63	20.3
	8 (l)	65.6	12.7	5.16	20.3
	8 (r)	65.6	14.7	4.46	20.3
C5	5 (l)	75.2	.....	.....	23.3
	5 (r)	75.2	9.4	8.0	23.3
	9 (l)	75.2	.....	.....	23.3
	9 (r)	75.2	.....	.....	23.3
C6	6 (l)	71.8	24.0	3.0	22.2
	6 (r)	71.8	.....	.....	22.2
	10(l)	71.8	15.9	4.51	22.2
	10(r)	71.8	.....	.....	22.2
C7	7 (l)	68.5	11.5	5.96	21.2
	7 (r)	68.5	9.0	7.61	21.2
	11(l)	68.5	24.0	2.85	21.2
	11(r)	68.5	18.4	3.72	21.2

Cont'd

C8	8 (l)	71.5	.....	.....	22.1
	8 (r)	71.5	.....	.....	22.1
	12(l)	71.5	.....	.....	22.1
	12(r)	71.5	17.6	4.06	22.1
C9	9 (l)	83.4	.....	.....	25.8
	9 (r)	83.4	.....	.....	25.8
	13(l)	83.4	.....	.....	25.8
	13(r)	83.4	.....	.....	25.8
C10	10(l)	79.0	15.7	5.03	24.5
	10(r)	79.0	.....	.....	24.5
	14(l)	79.0	.....	.....	24.5
	14(r)	79.0	19.1	4.13	24.5
C11	11(l)	79.0	.....	.....	24.5
	11(r)	79.0	19.6	4.03	24.5
	15(l)	79.0	23.9	3.30	24.5
	15(r)	79.0	.....	.....	24.5
C12	12(l)	79.2	17.6	4.5	24.5
	12(r)	79.2	.....	.....	24.5
	16(l)	79.2	6.6	12.7	24.5
	16(r)	79.2	.....	.....	24.5

(l) = tension on left face (r) = tension on right face

δ_p = ductility provided δ_m = ductility demand

$\mu_{r(a)}$ = average displacement ductility required from +ve and -ve directions (0.5(3.28+3.17) = 3.23)

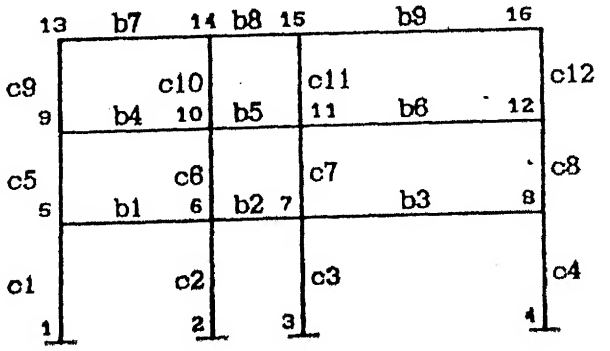

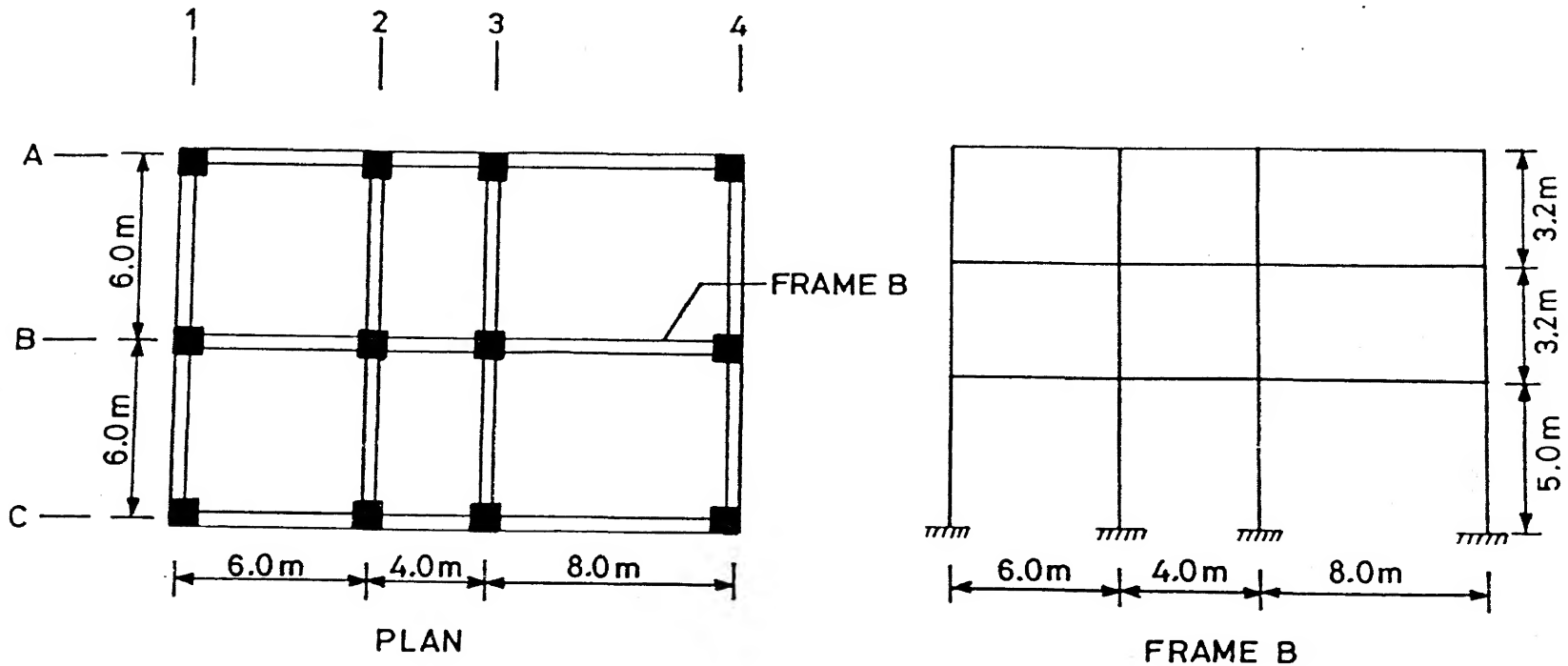

Fig. 6.1 Layout of the example building.

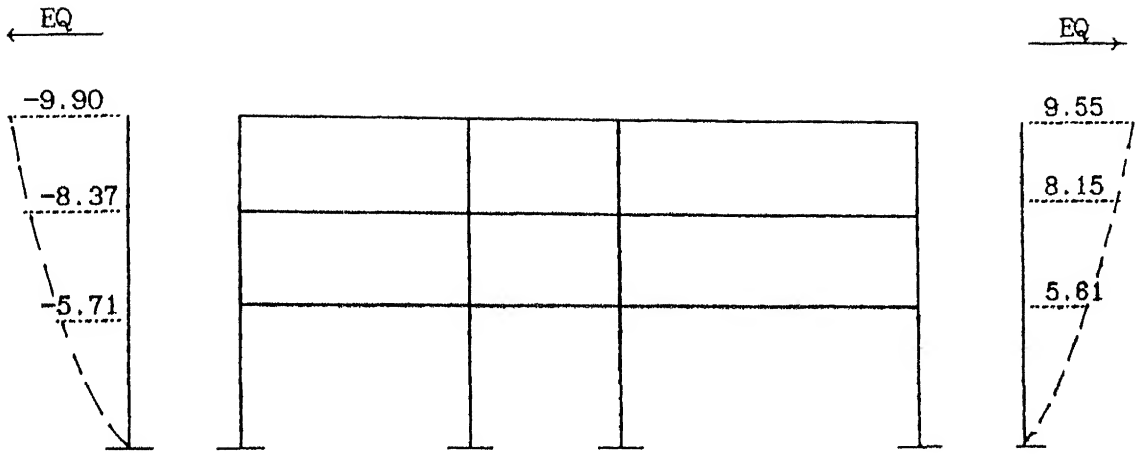

Fig. 6.2 Lateral displacement at floor levels (in mm) under gravity load plus seismic load at SLS (P_w).

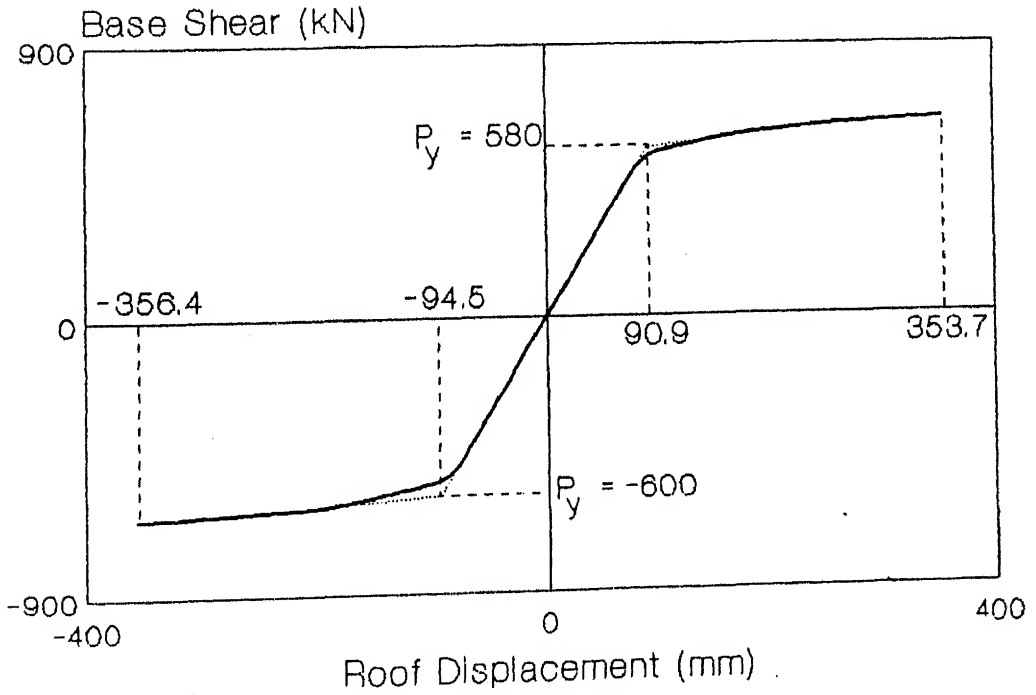

Fig. 6.3 Base shear - roof displacement response.

CHAPTER VII

SUMMARY AND CONCLUSIONS

The seismic performance of a structure is basically governed by its structural configuration, stiffness, strength, and ductility. The current seismic codes generally emphasize the lateral strength in design; issues regarding configuration are addressed through general recommendations in the code, sufficient ductility is sought to be provided through detailing procedures, and adequate stiffness is ensured through checks on drift. The design lateral force is often obtained by dividing the maximum expected elastic force by a response reduction factor, which depends on the type of structure and the ductility it is expected to have. The response reduction factor accounts for ductility (i.e., the post-yield behaviour), and overstrength (i.e., the ratio of lateral force at yield condition to the design lateral load). However, overstrength in a building varies with its configuration, and the relative dominance of gravity loads vis-a-vis seismic loads in design; the latter depends on seismic zone, number of storeys in the building, and the design live load. The present design procedures do not explicitly account for variations in overstrength and ductility.

In the recent years, greater emphasis is being placed on ensuring adequate lateral stiffness in the building structures for good seismic performance, considering the fact that more flexible structures invariably suffer more damage during earthquake shaking. Suggestions have been made in the literature for adopting a displacement-based design approach (Moehle, 1992a) as an alternative to the present ductility-based design procedure.

A structure is expected to resist minor, moderate, and severe ground shaking with different performance criteria. For instance, while in case of minor shaking the structure should not suffer any damage, in the event of severe shaking it is expected to be damaged but must not collapse. Most seismic codes only implicitly incorporate the three levels of performance criteria (limit states) in the design procedures. However, in recent years, some codes require consideration of at least two limit states, e.g., serviceability limit state (SLS) and ultimate limit state (ULS) as in BSL-1984 or damageability limit state (DLS) and ULS as in Tri-Services Manual, 1986.

Since the structure is expected to behave inelastically during a severe ground motion, a non-linear analysis is considered desirable whenever feasible. Such an analysis usually consists of either a non-linear time-history analysis or a non-linear static analysis (quasi-static). The non-linear time history analysis, besides being computationally intensive, can be very sensitive to the structural modelling (particularly with regard to initial stiffness and hence the time period) and to the strong motion record used in analysis. For instance, it is difficult to model reinforced concrete buildings accurately to provide a realistic time period even in the linear range of response. In quasi-static non-linear analysis, lateral loads are applied to the structure in small increments; the profile of these loads with height is often kept similar to the code-specified loads. This method cannot account for the hysteretic behaviour. Besides, it has limitations that (a) it cannot provide softening part of the load-displacement relationship of the structure, and (b) the profile of applied loads may differ substantially from the actual one. The actual seismic force profile on a structure not only depends on its configuration, but also

changes as yielding progresses in it.

Non-linear time-history analysis by the computer program SARCF has been carried out on four example frames (3-storey 1-bay, 3-storey 2-bay, 4-storey 1-bay, and 4-storey 2-bay) for two recorded ground motions. From the obtained responses, it is seen that 1) the structure has a somewhat unique upper bound envelope for the base shear - roof displacement relationship; 2) plastic hinges in the structure form when the base shear - roof displacement response lies on the upper bound envelope of the structure; 3) the sequence of plastic hinge formation may not significantly vary from one ground motion to another; 4) in the linear range, the lateral displacement profile is close to first mode shape during loading and reloading but takes different shape during unloading; and 5) in the non-linear range, along the upper bound envelope, the lateral displacement profile along the height is close to the first mode shape. Thus, it appears that response along the upper bound envelope can give most of the important information about inelastic response of structure; also along the upper bound envelope the deflection profile of building is close to the first mode shape.

A displacement-control non-linear quasi-static method of analysis for reinforced concrete frames has been proposed. The analysis is carried out by imposing in small increments a lateral displacement profile on the structure; the profile is proportional to the first mode shape. As the yielding starts, the increments in the displacement profile are chosen as a function of the normalized incremental displacement profile of the previous stage and first mode shape of the "yielding" structure at that stage. A computer program, named MONARCF-DC (MOnotonic Non-linear Analysis of Reinforced Concrete Frames - Displacement-Control method), has been developed to carry out this analysis.

Also, a procedure has been developed for seismic design of reinforced concrete frames which integrates strength, ductility and displacement requirements. This design approach, named Ductility and Displacement Based Design Procedure (DDBDP), explicitly considers the overstrength in a structure and it is particularly suitable for buildings with irregular configurations. The procedure considers two limit states, namely SLS and ULS. To obtain a realistic base shear - roof displacement relationship of the structure, which is needed for assessing the ductility requirements, the proposed displacement-control non-linear quasi-static monotonic analysis is used.

In the DDBDP, the design ground motions are specified through two linear elastic design spectra, one corresponding to each limit state. The structure is first designed and detailed for forces induced by SLS spectrum as per the usual code procedures. The requirements on overall displacement and inter-storey drift at SLS are checked; if these are not satisfied, the lateral stiffness of the structure must be increased. The base shear - roof displacement relationship of the structure is used to obtain the seismic overstrength (Ω) which is the ratio of the actual yield strength of the structure (P_y) to the design seismic force (P_w). Also, the required ductility reduction factor (R_μ) is computed by dividing the elastic design force at ULS (P) by P_y. The required displacement ductility (μ_r) is then obtained using empirical expressions which relate μ_r to R_μ. To satisfy strength requirements at the ULS the structure should be able to provide the required ductility. The overall displacement and inter-storey drift requirements at ULS are then checked for deformations corresponding to the ductility μ_r. Considering that non-linear analysis usually underestimates the initial lateral stiffness by a significant amount, a procedure has been suggested to scale down the

deflections at ULS through lateral stiffness obtained by a more realistic linear analysis. Also, at the ULS deflection, the hinge locations are studied with a view to avoid undesirable collapse mechanisms and ductility demand for different members are compared with the section ductility available.

A parametric study has been conducted to assess the accuracy of the displacement-control quasi-static non-linear procedure (MONARCF-DC). The responses of the four example frames, for the two recorded motions, are compared with those obtained by MONARCF-DC as well as the force-control quasi-static analysis regarding the upper bound envelope of the base shear - roof displacement relationship and the sequence of plastic hinge formations. The base shear - roof displacement plot and its parameters (e.g., elastic stiffness, and yield point of the structure), obtained by MONARCF-DC are quite comparable to the outer envelope of base shear - roof displacement plots obtained by SARCF. The response obtained from the displacement-control method algorithm compares much better than that from force-control algorithm. The displacement-control analysis allows one to obtain the envelope curve upto a larger value of roof displacement than does the force-control method. It is seen that for the first significant inelastic load excursion, the sequence of plastic hinge formation obtained by MONARCF-DC is close to that obtained by SARCF. During the subsequent hysteretic loading, most of the plastic hinges which formed in the SARCF analysis also form by MONARCF-DC analysis. However, a number of hinges which form in SARCF, particularly those located at the top of columns, do not form in MONARCF-DC.

In the linear range and during the first significant non-linear excursion of load, the joint rotations obtained by MONARCF-DC were found close to those from SARCF. Under subsequent excursions of loading and

unloading, with moderate damage to the structure, the joint rotations obtained by SARCF are higher than those obtained by MONARCF-DC by upto 33%. For one significant excursion of loading, MONARCF-DC gave reasonable estimates of the curvature ductility demand for beams but overestimated the curvature ductility demand of columns. For moderate damage situations, the curvature ductility demand for beams and columns obtained by MONARCF-DC is not very much different from that obtained after several hysteretic excursion of loads by using the time-history analysis. In severe damage situations, the effects of hysteretic behaviour become more pronounced and hence the quasi-static analysis procedure underestimates the ductility demand.

The proposed procedure has been illustrated on a two-dimensional frame but can readily be extended to three-dimensional frames. Buildings with shear walls can also be similarly treated. However, more research is required to arrive at performance criteria, in terms of acceptable displacements and ductility, to be used in the DDBDP. The issue of modelling lateral stiffness of buildings needs more research efforts; the problem assumes greater significance in view of concern for controlling deflections for limiting damage in the earthquake event. In view of difficulties that remain on this account, the pseudo-static non-linear analysis has a lot of potential for design applications. To account for hysteretic behaviour, when using quasi-static analysis, extensive parametric studies are needed to better understand magnitude of hysteresis effects.

REFERENCES

Abrams, D. P., 1987, Axial Force Influence on Flexural Behavior of Reinforced Concrete Columns, ACI Structural Journal, Vol.84, No. 3, 246-254.

ACI-318, 1989, Building Code Requirements for Reinforced Concrete, American Concrete Institute, Detroit, Michigan, USA.

ACI SP-84, 1984, Earthquakes Effects on Reinforced Concrete Structures: US - Japan Research, American Concrete Institute, Detroit, Michigan, USA.

Anagnostopoulous, S.A., Haviland, R.W., and Biggs, J.M., 1978, Use of Inelastic Spectra in Aseismic Design, Journal of the Structural Division, ASCE, Vol. 104, No. ST1, pp. 95-109.

Anagnostopoulous, S.A., and Nikolaou, D. A., 1992, Behavior Versus Ductility Factors in Earthquake Resistant Design, Proceedings of the Tenth World Conference on Earthquake Engineering, Madrid, Spain, Vol. VII, pp. 3727-3732.

Anderson, J. C., and Bertero, V. V., 1969, Seismic Behavior of Multistory Frames Designed by Different Philosophies, Report No. EERC 69-11, Earthquake Engineering Research Centre, University of California, Berkeley, California, USA.

Assaf, A. F., 1989, Evaluation of Structural Overstrength in Steel Building Systems, Thesis for the Degree of Master of Science, Northeastern University, at Boston, Mass., USA

Allan Porush, Dames and Moore, 1989, The New 1988 Blue Book and UBC Perspective and Overview of Lateral Force Section, 1988 UBC SEAOC New Seismic Design Criteria, California, USA.

ATC 3-06, 1978, Tentative Provisions for the Development of Seismic Regulations, Applied Technology Council, Palo, Alto, California, USA.

Bathe, K. J., 1982, Finite Element Procedures in Engineering Analysis, Prentice-Hall, Englewood Cliffs, NJ.

Bertero, V. V., and Bresler, B., 1977, Panel Paper: Failure Criteria (Limit States), Proceedings, Sixth World Conference on Earthquake Engineering, New Delhi, India, Vol. I, pp. 77-87.

Bertero, V. V., Aktan, A. E., Charney, F. A., and Sause, R., 1984, Earthquake Simulation Tests and Associated Studies on a 1/5th - Scale Model of a 7-Storey R/C Frame-Wall Test Structure, Report No. UCB/EERC-84/05, Earthquake Engineering Research Centre, University of California, Berkeley, California, USA.

Bertero, V. V., 1986, Lessons Learned from Recent Earthquakes and

Research and Implications for Earthquake-Resistant Design of Building Structures in the United States, Earthquake Spectra, Vol. 2, No. 4, pp. 825-858.

Bertero, V. V., Anderson, J. C., Krawinkler, H., Miranda, E., and the CUREe and the Kajima Research Teams, 1991, Design Guidelines for Ductility and Drift Limits: Review of State-of-the-Practice and the State-of-the-Art in Ductility and Drift-Based Earthquake-Resistant Design of Buildings, Report No. UCB/EERC-91/15, Earthquake Engineering Research Center, University of California at Berkeley, USA.

Blume, J. A., 1977, Allowable Stresses and Earthquake Performance, Proceedings of the Sixth World Conference on Earthquake Engineering, New Delhi, India, pp. 165-174.

Boneli, P., and Tobar, R., 1992, Experimental Analysis of One-Tenth Scale Reinforced Concrete Model of a Ten Storey Building, Proceedings of the Tenth World Conference on Earthquake Engineering, Madrid, Spain, Vol. V, pp. 2701-2705.

BSL-1984, (Japan Building Standard Code), IAEE, Earthquake Resistant Regulations - A World List - 1992, International Association for Earthquake Engineering, Japan, July 1992.

Briseghella, L., Zaccaria, P. L., and Giuffre A., 1982, Inelastic Response Spectra, Proceedings of the Seventh Symposium on Earthquake Engineering, University of Roorkee, India, Vol.I, pp. 159 -162.

Casciati, F., and Faravelli, L., 1984, Plastic Zone Spread and Seismic Reliability of RC Frames, Proceedings of the Eighth World Conference on Earthquake Engineering, San Francisco, USA, Vol. IV, pp. 567-574.

Cassis, J.H., and Bonelli, P., 1992, Lessons Learned from the March 3, 1985 Chile Earthquake and Related Research, Proceedings of the Tenth World Conference on Earthquake Engineering, Madrid, Spain, Vol. X, pp. 5675-5680.

Chung, Y. S., Meyer, C., and Shinozuka, M., 1987, Seismic Damage Assessment of Reinforced Concrete Members, Technical Report NCEER-87-0022, National Centre for Earthquake Engineering Research, State University of New York at Buffalo.

Chung, Y. S., Meyer, C., and Shinozuka, M., 1988, SARCF User's Guide Seismic Analysis of Reinforced Concrete Frames, Technical Report NCEER-88-0044, National Centre for Earthquake Engineering Research, State University of New York at Buffalo.

Clough, R. W., Benuska, K. L., and Wilson, E. L., 1965, Inelastic Earthquake Response of Tall Buildings, Proceedings of the Third World Conference on Earthquake Engineering, Auckland, New Zealand, Vol. II pp. 68-69.

Derecho, A. T., Fintel, M., and Ghosh, S. K., 1986, Handbook of Concrete

Engineering, Chapter 12, Van Norstrand Reinhold Co., New York, USA.

Deshpande, M. R., and Jain, A. K., 1983, Inelastic Response of Concrete Frames, Master's Thesis, Civil Engineering Department, University of Roorkee, Roorkee, India.

Fajfar, P., and Fischinger, M., 1987, Non-linear Seismic Analysis of RC Buildings: Implications of a Case Study, Journal of European Earthquake Engineering, Vol. 1, pp. 31-43.

Ferguson, P. M., Breen, J. E., and Jirsa, J. O., 1988, Reinforced Concrete Fundamentals, John Wiley & Sons, New York.

Fintel, M., 1973, Resistance to Earthquakes - Philosophy, Ductility, and Details, Response of Multistory Concretes Structures to Lateral Forces, (SP-36), American Concrete Institute, Detroit, Michigan, USA, pp. 75-95.

Foutch, D. A., Goel, S. C., and Roeder, C. W., 1987, Seismic Testing of Full-Scale Steel Buildings - Parts I and II, Journal of Structural Engineering, ASCE, Vol. 113, No. 11, pp. 2111-2145.

Freeman, S. A., Czarnecki, R. M., and Honda, K. K., 1980, Significance of Stiffness Assumptions on Lateral Force Criteria, Reinforced Concrete Structure Subjected to Wind and Earthquake Forces, (SP-63), American Concrete Institute, Detroit, Michigan, Detroit,USA.

Giberson, M. F., 1967, The Response of Nonlinear Multi-Story Structures Subjected to Earthquake Excitation, Earthquake Engineering Research Laboratory, California Institute of Technology, Pasadena, California, USA.

Ghosh, S. K., 1991, "Seismic Design of Reinforcing Concrete Structures Considering Inelasticity", Earthquake-Resistant Concrete Structures Inelastic Response and Design, SP-127, American Concrete Institute, Detroit, Michigan, pp. 1-20.

Goel, S. C., 1969, P-Δ and Axial Column Deformation in Aseismic Frames, Journal of Structural Engineering, Paper No. 6738, August 1969.

Hwang, H. H. M., and Jaw, J. W., 1989, Statistical Evaluation of Response Modification Factors For Reinforced Concrete Structures, Technical Report NCEER-89-0002, National Center For Earthquake Engineering Research, State University of New York at Buffalo.

IS:456-1978, Indian Standard Code of Practice for Plain and Reinforced Concrete, Bureau of Indian Standards, New Delhi.

IS:1893-1984, Indian Standard Criteria for Earthquake Resistant Design of Structures, Bureau of Indian Standards, New Delhi.

Jennings, P. C., 1969, Spectrum Techniques for Tall Buildings, Proceedings of the Fourth World Conference on Earthquake Engineering, Santiago De Chile, A-3, pp. 61-74.

Kaminosono, T., Watabe, M., Okamoto, S., Nakata, S., and Yoshimura, M., 1984, U.S. - Japan Cooperative Research on R/C Full-Scale Building Test (Part 1: Single-Degree-of-Freedom Pseudo-Dynamic Test), Proceedings of the Eighth World Conference on Earthquake Engineering, San Francisco, California, Vol. VI, pp. 595-602.

Kanaan, A. E., and Powell, G. H., 1973, DRAIN-2D, A General Purpose Computer Program for Dynamic Analysis of Planar Structures, UCB/EERC Report 73-6, University of California, Berkeley, 1973.

Klingner , R. E., and Bertero, V. V., 1976, Infilled Frames in Earthquake Resistant Construction, Report No. 76-32, Earthquake Engineering Research Centre, University of California, Berkeley, California, December 1976.

Krawinkler, H. and Rahnama, M., 1992, Effects of Soft Soils on Design Spectra, Proceedings of the Tenth World Conference on Earthquake Engineering, Madrid, Spain, Vol. X, pp. 5841-5846.

Lai, S. P., and Biggs, J. M., 1980, Inelastic Response Spectra for Aseismic Building Design, Journal of the Structural Division, ASCE, Vol. 106, No. ST6, pp. 1295-1310.

Lin, J., and Mahin, S. A., 1985, Effects of Inelastic Behaviour on the Analysis and Design of Earthquake Resistant Structures, Report No. UCB/EERC-85-08, Earthquake Engineering Research Centre, University of California, Berkeley, California.

Mahin, S. A., and Bertero, V. V., 1976, Problems in Establishing and Predicting Ductility in Structural Design, Proceedings of the International Symposium on Earthquake Structural Engineering, St. Louis, Mo., Vol. I, pp. 613-580.

Mahin, S. A., and Bertero, V. V., 1981, An explanation of Inelastic Seismic Design Spectra, Journal of the Structural Division, ASCE, Vol. 107, No. ST9, pp. 1777-1795.

Maison, B.F., and Neuss, C.F., (1983), "SUPER-ETABS - An Enhanced Version of the ETABS Program", J.G. Bouwkamp, Inc., Berkeley, California, USA, 52 pp.

Meli, R., 1992, Code-Prescribed Seismic Actions and Performance of Buildings, Proceedings of the Tenth World Conference on Earthquake Engineering, Madrid, Spain, Vol. X, pp. 5783-5788.

Meyer, C., 1991, Computation of Inelastic Response, Earthquake-Resistant Concrete Structures Inelastic Response and Design, SP-127, American Concrete Institute, Detroit, Michigan 48219, pp. 199-238.

Midorikawa, M., and Kitagawa, Y., 1984, U.S.-Japan Cooperative Research on R/C Full-Scale Building Test (Part 4: Ultimate Moment-Resistance Capacity), Proceedings of the Eighth World Conference on Earthquake Engineering, San Francisco, California, Vol. VI, pp. 619-626.

Miranda, M., and Bertero, V. V., 1989, The Mexico Earthquake of September 19, 1985 — Performance of Low-Rise Buildings in Mexico

City, Earthquake Spectra, Vol. 5, No. 1, pp. 121-143.

Miranda, E., 1992, Nonlinear Response Spectra for Earthquake Resistant Design, Proceedings of the tenth World Conference on Earthquake Engineering, Madrid, Spain, Vol. X, pp. 5835-5840.

Miyama, T., Kanda, J., and Iwasaki, R., 1988, Inelastic Response Spectra for Typical Hysteresis Systems Calculated from Elastic Response Spectra, Proceedings of the Ninth World Conference on Earthquake Engineering, Tokyo-Kyoto, Japan, Vol. V, pp. 153-158.

Moazami, S., and Bertero, V. V., 1987, US-Japan Cooperative Earthquake Research Program: Three-Dimensional Inelastic Analysis of Reinforced Concrete Frame-Wall Structures, Report No. UCB/EERC-87/05, Earthquake Engineering Research Center, University of California at Berkeley, USA.

Moehle, J. P., 1984, Strong Motion Drift Estimates for R/C Structures, Journal of Structural Engineering, ASCE, Vol. 110, No. 9, pp. 1988-1989.

Moehle, J. P., 1992a, Displacement_based Design of RC Structures Subjected to Earthquakes, Earthquake Spectra, Vol. 8, No. 3, August 1992, pp. 403-427.

Moehle, J. P., 1992b, Displacement Based Design of RC Structures, Proceedings of the Tenth World Conference on Earthquake Engineering, Madrid, Spain, pp. 4297-4302.

Montgomery, C. J., 1981, Influence of P-Delta Effects on Seismic Design, Canadian Journal of Civil Engineering, Vol. 8, pp. 31-43.

Moss, P. J., and Carr, A. J., 1980, The Effects of Large Displacements on the Earthquake Response of Tall Concrete Frame Structures, Bulletin of the New Zealand National Society for Earthquake Engineering, Vol. 13, No.4, pp. 317-328.

Murakami, M., and Penzien, J., 1977, NonLinear Response Spectra for Probabilistic Seismic Design, of Reinforced Concrete structures, Proceedings of the Sixth World Conference on Earthquake Engineering, New Delhi, India, Vol. II, pp. 1046-1051.

Nassar, A. A., Osteraas, J. D., and Krawinkler, H., 1992, Seismic Design Based on Strength and Ductility Demands, Proceedings of the Tenth World Conference on Earthquake Engineering, Madrid, Spain, Vol. 10, pp. 5861-5866.

Navin, R., and Jain, S. K., 1993, Assessment of Seismic Overstrength in Reinforced Concrete Frames, Research Report, Indian Institute of Technology Kanpur, India.

NEHRP-1991, Recommended Provisions for the Development of Seismic Regulations for New Buildings, Building Seismic Safety Council, Washington, D.C., USA.

Neville, A. M., 1981, Properties of Concrete, 3/e, Pitman, London.

Newmark, N. N., and Hall, W. J., 1973, Procedure and Criteria for Earthquake Resistant Design, Building Practices for Disaster Mitigation, Building Science Series 46, U.S. Department of Commerce, National Bureau of Standards, Washington, DC, February 1973.

Newmark, N. N., and Riddell, R., 1980, Inelastic Spectra for Seismic Design, Proceedings of the Seventh World Conference on Earthquake Engineering, Istanbul, Turkey, Vol. IV, pp. 129-136.

Newmark, N. M., and Hall, W. J., 1982, Earthquake Spectra and Design, Earthquake Engineering Research Institute, El Cerrito, California.

NZS 4203: 1992 (draft), IAEE, Earthquake Resistant Regulations- A World List -1992, International Association for Earthquake Engineering, Japan, July 1992.

Otani, S., Okada, T., Kubo, T., and Nomura, S., 1992, Outline of AIJ Design Guidelines for RC Buildings, Proceedings of the Tenth World Conference on Earthquake Engineering, Madrid, Spain, Vol. 10, pp. 5623-5628.

Pal, S., Daraka, S. S., and Jain A. K., 1987, Inelastic Response Spectra, Computers and Structures, Vol. 25, No. 3, pp. 335-344.

Palazzo, B. and Siano, F., 1992, A New Proposal for a Structural Reduction Factor Formulation, Proceedings of the 10th World Conference on Earthquake Engineering, Madrid, Spain, Vol. 10, pp. 5897-5902.

Park, R, and Paulay, T., 1975, Reinforced Concrete Structures, John Wiley & Sons, New York.

Park, R., 1988, Ductility Evaluation from Laboratory and Analytical Testing, State-of the-Art-Report, Proceedings of the Ninth World Conference on Earthquake Engineering, Tokyo-Kyoto, Japan, Vol. VIII, pp. 605 -616.

Park, Y. J., Reinborn, A. M., and Kunnath, S. K., 1987, IDARC: Inelastic Damage Analysis of Reinforced Concrete Frame - Shear-Wall Structures, Technical Report NCEER-87-0008, National Centre for Earthquake Engineering Research, State University of New York at Buffalo.

Paulay, T., and Priestly, J. N., 1992, Seismic Design of Reinforced Concrete and Masonry Buildings, John Wiley & Sons, New York.

Powell, G. H., and Row, D. G., 1976, Influence of Analysis and Design Assumptions on Computed Elastic Response of Moderately Tall Frames, Report EERC-76-11, Earthquake Engineering Research Center, University of California, Berkeley, USA.

Priestly, M. J. N., and Park, R., 1987, Bridge Columns under Seismic Loading, ACI Structural Journal, Vol. 84-S8, pp. 61-76.

Qi, X., and Moehle, J. P., 1991, Displacement Design Approach for Reinforced Concrete Structures Subjected to Earthquakes, Report No. UCB/EERC-91/02, University of California at Berkeley.

Rashad, G. E., and Jain, S. K., 1991, Ductility of Reinforced Concrete Flexure Members for Unconfined and Confined Concrete, Proceedings of the 16th Conference on Our World in Concrete & Structures, Singapore, pp. 191-196.

Riddell, R., and Newmark, N. M., 1979, Statistical Analysis of the Response of Nonlinear Systems Subjected to Earthquakes, Structural Research Series No. 468, University of Illinois, Urbana, Illinois.

Riddell, R., and Vásquez, J., 1988, Analysis of Response Spectra for Records in the Epicentral Region of the March 3, 1985 Earthquake in Chile, Proceedings of the Ninth World Conference on Earthquake Engineering, Tokyo-Kyoto, Japan, Vol. II, pp. 295-300.

Riddell,, R., Hidalgo, P., and Cruz, E., 1989, Response Modification Factors for Earthquake Resistant Design of Short Period Buildings, Earthquake Spectra, Vol. 5, No. 3, pp. 571-590.

Roufaiel, M. S. L., and Meyer, C., 1987, Analytical Modeling of Hysteretic Behavior of R/C Frames, Journal of Structural Engineering, ASCE, Vol. 113, No. 3, pp. 429-444.

Saatcioglu, M., 1991, "Modeling Hysteretic Force-Deformation Relationships for Reinforced Concrete Elements", Earthquake-Resistant Concrete Structures Inelastic Response and Design, SP-127, American Concrete Institute, Detroit, Michigan 48219, pp. 153-198.

Saiful, M. I., Ellingwood, B., and Corotis, R. B., 1990, Dynamic Response of Tall Buildings to Stochastic Wind Load, Journal of Structural Engineering, ASCE, Vol. 116, No. 11, pp. 2982-3002.

Saiidi, M., and Sozen, M. A., 1979, Simple and Complex Models for Nonlinear Seismic Response of Reinforced Concrete Structures, Structural Research Series No. 465, University of Illinois, Urbana, Illinois, USA.

SEAOC-1973, Recommended Lateral Force Requirements and Commentary, Structural Engineers Association of California, San Francisco, California, USA.

SEAOC-1990, Recommended Lateral Force Requirements and Commentary, Structural Engineers Association of California, San Francisco, California, USA.

Shahrooz, B. M., and Moehle, J. P., 1990, Evaluation of Seismic Performance of Reinforced Concrete Frames, Journal of Structural Engineering, ASCE, Vol.116, No. 5, pp. 1403-1422.

Shing, P. B., and Mahin, S. A., 1985, Computational Aspects of a Seismic Performance Test Method Using On-Line Computer Control, Earthquake Engineering and Structural Dynamics, Vol. 13, pp. 507-526.

Sozen, M. A., 1981, Review of Earthquake Response of Reinforced Concrete Buildings with a View to Drift Control, State-of-the-Art in Earthquake Engineering - 1981, Ankara, pp. 383-418.

Sugano, S., 1989, Study of the Seismic Behavior of Retrofitted Reinforced Concrete Buildings, Seismic Engineering Research and Practice, ASCE, pp. 669-678.

Takada, T., Hwang, H. H. M., Shinozuka, M., 1988, Response Modification Factor for Multiple-Degree-of-Freedom Systems, Proceedings of the Ninth World Conference on Earthquake Engineering, Tokyo-Kyoto, Japan, Vol. V, pp. 129-134.

Takayanagi, T., and Schnobrich, W. C., 1976, Computed Behavior of Reinforced Concrete Coupled Shear Walls, Structural Research Series No. 434, Civil Engineering Studies, University of Illinois, Urbana, Illinois, USA.

Takeda,T., Sozen, M. A., and Nielsen, N. N., 1970, Reinforced Concrete Response to Simulated Earthquakes, Journal of the Structural Division, ASCE, Vol. 96, No ST12, USA, pp. 2557-2573.

Tri-Services Manual, 1986, Seismic Design Guidelines for Essential Buildings, Departments of the Army, the Navy, and the Air Force, Washington, D.C., 1986.

Uang, C. M., and Bertero, V. V., 1986, Earthquake Simulation Tests and Associated Studies of a 0.3-Scale Model of a 6-Storey Concentrically Braced Steel Structure, Report No. UCB/EERC-86/10, Earthquake Engineering Research Centre, University of California, Berkeley, California, December 1986.

Uang, C. M., 1991, Establishing R (or R_w) and C_d factors for Building Seismic Provisions, Journal of Structural Engineering ASCE, Vol. 117, No 1, pp. 19-29.

Uang, C. M., 1993, An Evaluation of Two-Level Seismic Design Procedure, Earthquake Spectra, Vol. 9, No.1, pp. 121-135.

UBC-1985, Uniform Building Code, International Conference of Building Officials, Whittier, California, USA.

UBC-1991, Uniform Building Code, International Conference of Building Officials, Whittier, California, USA.

Whittakar, A. S., Uang, C. M., and Bertero, V. V., 1987, Earthquake Simulation Tests and Associated Studies of a 0.3-Scale Model of a 6-Storey Eccentrically Braced Steel Structure, Report No. UCB/EERC-87/02, Earthquake Engineering Research Centre, University of California, Berkeley, California, June 1987.

Whittakar, A. S., Uang, C. M., and Bertero, V. V., 1989, Experimental Behaviour of a Dual Steel System", Journal of Structural Engineering, ASCE, Vol. 115, No. 1, pp. 183-200.

Zhu, T. J., Tso, W. K., Heidebrecht, A. C., 1992, Seismic Performance of Reinforced Concrete Ductile Moment-Resisting Frame Buildings Located in Different Seismic Regions, Canadian Journal of Civil Engineering, Vol. 19, pp. 688-710.